University of Alberta

In vitro and *in vivo* targeting of immunoliposomal doxorubicin to hematological B cell lymphomas and multiple myeloma

By

Daniel E. Lopes de Menezes

©

A thesis submitted to the Faculty of Graduate Studies and Research in partial fulfillment of the requirements of the requirements for the degree of Doctor of Philosophy

Department of Pharmacology

Edmonton, Alberta

Fall 1998

National Library of Canada
Acquisitions and Bibliographic Services
395 Wellington Street
Ottawa ON K1A 0N4
Canada

Bibliothèque nationale du Canada
Acquisitions et services bibliographiques
395, rue Wellington
Ottawa ON K1A 0N4
Canada

Your file Votre référence

Our file Notre référence

The author has granted a non-exclusive licence allowing the National Library of Canada to reproduce, loan, distribute or sell copies of this thesis in microform, paper or electronic formats.

L'auteur a accordé une licence non exclusive permettant à la Bibliothèque nationale du Canada de reproduire, prêter, distribuer ou vendre des copies de cette thèse sous la forme de microfiche/film, de reproduction sur papier ou sur format électronique.

The author retains ownership of the copyright in this thesis. Neither the thesis nor substantial extracts from it may be printed or otherwise reproduced without the author's permission.

L'auteur conserve la propriété du droit d'auteur qui protège cette thèse. Ni la thèse ni des extraits substantiels de celle-ci ne doivent être imprimés ou autrement reproduits sans son autorisation.

0-612-34804-0

Canada

University of Alberta

Library Release Form

Name of Author:	Daniel E. Lopes de Menezes
Title of Thesis:	*In vitro* and *in vivo* targeting of immunoliposomal doxorubicin to hematological B cell lymphomas and multiple myeloma
Degree:	Doctor of Philosophy
Year this Degree Granted:	1998

Permission is hereby granted to the University of Alberta Library to reproduce single copies of this thesis and to lend or sell such copies for private, scholarly, or scientific research purposes only.

The author reserves all other publication and other rights in the association with the copyright in the thesis, and except as hereinbefore provided, neither the thesis nor any substantial portion thereof may be printed or otherwise reproduced in any material form whatever without the author's prior written permission.

3A-9203 112 Street,
Edmonton, Alberta
Canada T6G 2C5

Sept. 25, 1998

University of Alberta

Faculty of Graduate Studies and Research

The undersigned certify that they have read, and recommend to the Faculty of Graduate Studies and Research for acceptance, a thesis entitled *In vitro* and *in vivo* targeting of immunoliposomal doxorubicin to hematological B cell lymphomas and multiple myeloma submitted by Daniel E. Lopes de Menezes in partial fulfillment of the requirements of the degree of Doctor of Philosophy.

Dr. T.M. Allen, Supervisor

Dr. L.M. Pilarski, Committee member

Dr. A.S. Clanachan, Committee member

Dr. F. Jamali, Examiner

Dr. G. Storm, External Examiner

Sept 21. 1998

ABSTRACT

Antibody-mediated targeting of liposomal anticancer drugs to specific antigens expressed on malignant cells could improve the therapeutic effectiveness of the liposomal preparations as well as reduce adverse side effects associated with chemotherapy. Liposomes (SL) were composed of either high phase transition hydrogenated soy phosphatidylcholine, HSPC, or low phase transition partially hydrogenated soy phosphatidylcholine, PC40, in combination with cholesterol, and were sterically stabilized with lipid derivatives of polyethylene glycol (PEG). Monoclonal antibodies (mAbs) were attached to the terminus of the PEG, creating sterically stabilized immunoliposomes (SIL). SIL containing entrapped anticancer drug, doxorubicin (DXR) are predicted to be useful in the treatment of hematological malignancies such human B-cell lymphomas or multiple myeloma, where diseased cells are present within the vasculature.

The specific *in vitro* binding and antineoplastic activity of DXR encapsulated in SIL, prepared by coupling liposomes to the mAb anti-CD19, were investigated against $CD19^+$ B lymphoma cell line (Namalwa) and a $CD19^+$ multiple myeloma cell line (ARH77). Binding experiments showed a two- to three-fold higher association of the SIL[anti-CD19] compared to SL (no mAb) or isotype-matched control NSIL[IgG2a] for both cell lines, and was commensurate with the expression of CD19 on target cells. The selectivity of fluorescent-labeled SIL[anti-CD19] to B cells was demonstrated in a heterogenous mixture of cells composed of peripheral blood mononuclear cells from MM patients. Internalization of SIL[anti-CD19] into a low pH compartment, likely endosomes or lysosomes, was observed for both Namalwa and ARH77 cells using a pH-sensitive probe, 1-hydroxypyrene-3,6,8-trisulfonic acid (HPTS). The endocytosis and intracellular

fate of liposomal DXR formulations were also studied using confocal microscopy. At early times (1 h), the drug appeared mainly at the cell surface with some DXR sequestered within vesicular structures within cells (probably endosomes). The cellular levels of DXR-SIL[anti-CD19] increased appreciably after longer incubation periods, resulting in substantial nuclear staining, and this could be inhibited by metabolic inhibitors of endocytosis. The ability of DXR-SIL[anti-CD19] to target the nucleus was demonstrated using an *in vitro* proliferation assay and by measuring the DNA content in cells by flow cytometry. The targeted DXR-SIL[anti-CD19] displayed a significantly higher cytotoxicity to B cells relative to DXR entrapped in non-targeted SL.

Therapeutic experiments in SCID mice implanted with Namalwa cells by the i.v. or i.p. routes resulted in significantly greater therapeutic effectiveness of DXR-SIL[anti-CD19] compared to similar amounts of free DXR, DXR-SL (no mAb) or DXR-NSIL[IgG2a]. Single doses of 3 mg/kg DXR given as DXR-SIL[anti-CD19] administered i.v. resulted in significantly improved therapeutic benefit, including some long-term survivors. Monoclonal antibody treatments, when given in conjunction with free DXR and various liposomal DXR formulations, were found to be additive with the drug treatments in therapeutic effectiveness. The observed therapeutic effect was found to depend on a number of factors including: the drug formulation (free or liposomal drug, etc.), tumour burden, and dosing schedule.

Our results indicate that antibody-mediated targeting approach using DXR-SIL[anti-CD19] targeted against the internalizing CD19 antigen may be an effective strategy for selective targeting of malignant $CD19^+$ B lymphocytes in B-cell malignancies (i.e., leukemias, lymphomas and multiple myeloma).

ACKNOWLEDGEMENTS

I am extremely grateful to my supervisor, Dr. T.M. Allen, for her support, guidance and encouragement through my research, writing of papers and putting together of this thesis

I wish to thank my supervisory committee members, Drs. L.M. Pilarski and A.S. Clanachan, for their knowledgeable advice, suggestions and constructive criticism.

I would like to thank Dr. Andy Belch for helpful discussion and provision of human multiple myeloma patient samples. Also, I would like to thank Dr. Vera Chlumecky, Dorota Rutkowski, and Juanita Wizniak for suggestions, and instruction in confocal laser scanning imaging and flow cytometry. I extend my gratitude to members of Dr. Pilarski's lab, especially Dr. Anna Masellis-Smith, Darlene Paine and Eva Pruski for monoclonal antibodies, experimental protocols, cell lines and purified human blood cells. The help provided by Dr. Nick Nation with gross histopathological examination of mice is gratefully acknowledged. I would like to acknowledge the provision of human H9 cells by Dr. Lung-Ji Chang, Department of Medical Microbiology and Immunology.

I extend my gratitude to every "Lipozoid" who has been a part of the Allen laboratory from 1993-98, for their sincere friendship and help with lab work: Christian Hansen, Grace Kao, Elaine Moase, Susan Cubitt, Cheryl Santos, Renee LeClerc, Felicity Wang, Marc Kirchmeier, Tatsuhiro Ishida, Darrin Stuart, Fatehia Saleh, Faisal Rahman, Greg Charrois, Joao Moreira, George Wardle, Jeff Gagne, Zsolt Gabos, Yulun Ho, Jie Ma, Weimin Qi, Jihan Marjan, Pravin Bhatnagar, Sarah Halleran, Jennifer Szydlowski, Christien Oussoren, Gerben Koning, Kami Makar and John Cesarz. A special thanks to Elaine, Susan, Marc and Darrin for critical reading of sections of this thesis.

Finally, I would like to thank my family, friends and fellow graduate students for their support and encouragement during the last five years.

Financial support from the Alberta Heritage Foundation for Medical Research is gratefully acknowledged.

TABLE OF CONTENTS

CHAPTER 1 Introduction and hypothesis 1

1.1 INTRODUCTION 2

1.1.1 Liposomal drug delivery systems 4

1.1.2 Types of liposomes and methods of preparation. 5

1.1.3 Association of drugs with liposomes. 8

1.1.4 Advantages of liposomes as a drug delivery systems. 11

1.1.5 Applications of liposomes. 13

1.1.6 Interaction of liposomes with plasma proteins and the mononuclear phagocyte system (MPS). 13

1.1.7 *In vivo* fate of liposomes after intravenous administration. 16

1.1.8 Interaction of liposomes with cells. 18

1.1.9 Classical liposomes (CL). 21

1.1.10 Development of long circulating liposomes 22

1.1.11 Pharmacokinetics of liposomal anthracyclines. 25

1.1.12 Targeted liposomal drugs. 31

1.1.13 Targeted liposomal systems. 39

1.1.14 *In vivo* therapeutics in experimental models. 41

1.1.15 Hematological malignancies: B-cell lymphomas and multiple myeloma. 45

1.2 HYPOTHESIS AND OBJECTIVES 54

CHAPTER 2 *In vitro* and *in vivo* targeting of immunoliposomal doxorubicin to human B-cell lymphoma 57

2.1 ABSTRACT 58

2.2 INTRODUCTION 59

2.3 MATERIALS AND METHODS 62

2.3.1 Materials. 62

2.3.2 Mice. 62

2.3.3 Cell lines and antibodies. 63
2.3.4 Preparation of liposomes. 64
2.3.5 *In vitro* cell binding/uptake experiments. 66
2.3.6 *In vitro* cytotoxicity experiments. 67
2.3.7 Pharmacokinetic and biodistribution of liposomes in CD1(ICR)BR (outbred) *versus* SCID mice implanted with $CD19^+$ Namalwa cells. 68
2.3.8 *In vivo* therapeutic experiments. 69
2.3.9 Statistical analysis. 70
2.4 RESULTS 71
2.4.1 *In vitro* recognition experiments. 71
2.4.2 Specific recognition of immunoliposomes SIL[anti-CD19] to B cells in a mix of B and T cells. 73
2.4.3 *In vitro* cytotoxicity of SIL[anti-CD19]. 75
2.4.4 Tumour model of Namalwa cells implanted in SCID mice. 79
2.4.5 Pharmacokinetics of SIL[anti-CD19] in CD1(ICR) outbred mice *versus* SCID mice implanted with $CD19^+$ Namalwa cells. 82
2.4.6 *In vivo* experiments in SCID mice innoculated with Namalwa cells. 87
2.5 DISCUSSION 94

CHAPTER 3 Cellular trafficking and cytotoxicity of anti-CD19-targeted liposomal doxorubicin for a human B lymphoma cell line (Namalwa) *in vitro* 101
3.1 ABSTRACT 102
3.2 INTRODUCTION 103
3.3 MATERIALS AND METHODS 105
3.3.1 Chemicals. 105
3.3.2 Antibodies and human cell lines. 106
3.3.3 Immunophenotyping of Namalwa cell line. 107
3.3.4 Preparation of liposomes. 108

3.3.5 Loading of doxorubicin (DXR). 109
3.3.6 Hydrazide method for coupling mAb anti-CD19 to liposomes. 109
3.3.7 Leakage of DXR from liposomes. 110
3.3.8 *In vitro* binding experiments using fluorescent liposomes. 111
3.3.9 Uptake of doxorubicin (DXR) by Namalwa cells using flow cytometry. 111
3.3.10 Analysis of liposomal DXR associated with Namalwa cells using HPLC. 112
3.3.11 Internalization experiments using the pH-sensitive fluorophore HPTS. 113
3.3.12 Intracellular distribution of liposomal DXR using confocal laser scanning microscopy. 113
3.3.13 Quantitation of DXR-induced cytotoxicity on cell lines using propidium iodide. 114
3.3.14 Cytotoxicity assays. 114
3.3.15 Statistical analyses. 116
3.4. RESULTS 116
3.4.1 Immunophenotyping of Namalwa cells using flow cytometry. 116
3.4.2 Leakage of doxorubicin (DXR) from liposomes. 116
3.4.3 Binding of immunoliposomes to Namalwa cells. 119
3.4.4 Quantitation of DXR association with Namalwa cells as a function of time and DXR concentration. 122
3.4.5 *In vitro* cytotoxicity of SIL[anti-CD19]. 124
3.4.6 Measurement of internalization of immunoliposomes using liposome-encapsulated HPTS 128
3.4.7 Internalization of liposomes visualized using confocal microscopy. 130
3.4.8 Measurement of doxorubicin-induced apoptosis. 145
3.5 DISCUSSION 147

CHAPTER 4 Selective targeting of immunoliposomal doxorubicin against human multiple myeloma *in vitro* and *ex vivo* 155
4.1 ABSTRACT 156
4.2 INTRODUCTION 157
4.3 MATERIALS AND METHODS 160
4.3.1 Chemicals. 160
4.3.2 Antibodies, human cells and cell lines. 161
4.3.3 Mice. 162
4.3.4 Immunophenotyping of the ARH77 cell line. 163
4.3.5 Preparation of liposomes. 163
4.3.6 *In vitro* cell binding/recognition experiments. 165
4.3.7 Uptake of DXR by ARH77 cells using flow cytometry. 166
4.3.8 Internalization experiments using the pH-sensitive fluorophore HPTS. 166
4.3.9 Intracellular distribution of liposomes using confocal laser scanning microscopy. 167
4.3.10 *In vitro* cytotoxicity experiments. 168
4.3.11 *In vitro* cytotoxicity using DNA content analysis. 168
4.3.12 Therapeutic experiments. 169
4.3.13 Statistical analyses. 170
4.4 RESULTS 171
4.4.1 Phenotyping of ARH77 multiple myeloma cell line using flow cytometry. 171
4.4.2 Binding of immunoliposomes to ARH77 cells. 171
4.4.3 Association of free doxorubicin (DXR) or liposomal DXR with ARH77 cells *in vitro* using flow cytometry. 177
4.4.4 Spectrofluorimetric measurement of immunoliposomal internalization using liposome-encapsulated HPTS. 179

4.4.5 Interaction of liposomes with ARH77 cells by confocal microscopy. 179
4.4.6 *In vitro* cytotoxicity of SIL[anti-CD19] to ARH77 cells. 186
4.4.7 Specific binding, and recognition of immunoliposomes to PBMC from MM patients. 188
4.4.8 Confocal microscopy of uptake of DXR-SIL[anti-CD19] by PBMC. 192
4.4.9 Cytotoxicity of DXR-SIL[anti-CD19] to B cells in PBMC from MM patients. 193
4.4.10 *In vivo* therapeutics of ARH77 cells in SCID-beige mice. 203
4.5 DISCUSSION 205

CHAPTER 5
Summarizing discussion and conclusions 215

REFERENCES 229

LIST OF TABLES

Table 1.1. Transition temperatures of common phospholipids. 5

Table 1.2. A list of some liposomal and lipid-based drugs in clinical development. 14

Table 1.3. A comparison of pharmacokinetic parameters of free anthracyclines (doxorubicin (DXR) and daunorubicin (DNR)), and liposomal formulations of DXR and DNR that are in clinical use in humans. 29

Table 2.1. Cytotoxicity data (IC_{50} μM) for free anti-CD19, isotype-matched control mAb, empty immunoliposomes (SIL), free DXR and liposomal DXR formulations (with or without anti-CD19) determined on $CD19^+$ B-cells (Namalwa) and $CD19^-$ T-lymphoma (H9) cell lines by the MTT tetrazolium dye assay. 76

Table 2.2. Summary of tumour dissemination of human B-cell lymphoma (Namalwa) after i.p. and i.v. implantation in SCID mice. 80

Table 2.3. Comparison of the pharmacokinetic parameters of SIL[anti-CD19] and SL (no Ab) in CD1(ICR)BR outbred mice or tumour-bearing SCID mice implanted (i.p.) with $CD19^+$ B lymphoma cell line (Namalwa). 84

Table 2.4. Summary of mean survival times of SCID mice after immunoliposomal treatment. 88

Table 3.1. Immunophenotyping of Namalwa cell line using flow cytometry. 117

Table 3.2. Cytotoxicity data (IC_{50}, μM) against Namalwa cells for free DXR, and various liposome-encapsulated doxorubicin formulations. 126

Table 3.3. Internalization of liposomes by $CD19^+$ Namalwa cells studied using a pH-sensitive fluorophore (HPTS). 129

Table 4.1. Immunophenotyping of ARH77 cell line using flow cytometry. 172

Table 4.2. Cytotoxicity data (IC_{50}, μM) for free mAbs, doxorubicin (DXR), or various liposome-encapsulated DXR formulations against ARH77 cells. 187

Table 4.3. Specific binding of liposomes to either B or T cells in a heterogenous mixture of PBMC from multiple myeloma patients. 190

Table 4.4. Cytotoxicity of free DXR or various formulations of liposomal DXR on PBMC from MM patients. 200

LIST OF FIGURES

Figure 1.1. Structure of classical liposomes. 6

Figure 1.2. Chemical structures of commonly used phospholipids. 7

Figure 1.3. Classification of liposomes. 9

Figure 1.4. Possible interactions of drugs with liposomes. 10

Figure 1.5. Remote loading of DXR using an ammonium sulphate gradient 12

Figure 1.6. Schematic for the interaction of liposomes with cells. 19

Figure 1.7. Structural formulae of some anthracylines that are currently in clinical use. 26

Figure 1.8. Strategies for the formation of targeted liposomes (CIL and SIL). 33

Figure 1.9. Binding of immunoliposomes to target cells. 34

Figure 1.10. Schematics of various strategies for coupling antibodies or ligands to SL. 35

Figure 1.11. Stages of B- and T-lymphocyte differentiation. 46

Figure 2.1. Binding/uptake of [^{3}H]CHE-labelled liposomes by B and T cells as a function of liposome concentration. 72

Figure 2.2. Two-colour flow cytometry for selective recognition of fluorescent NBD-labelled liposomes by CD19$^+$ B lymphoma cells (Namalwa) 74

Figure 2.3. Two-colour flow cytometry to determine the degree of implantation in various tissues of Namalwa cells after i.v. implantation in SCID mice. 81

Figure 2.4. Blood clearance of SL (no mAb), SIL[anti-CD19] and NSIL[IgG2a]. 83

Figure 3.1. *In vitro* release of doxorubicin (DXR) from liposomes. 118

Figure 3.2. *In vitro* binding of fluorescent NBD-labelled liposomes to CD19$^+$ Namalwa cells and control CD19$^-$ H9 cells using flow cytometry. 120

Figure 3.3. Uptake of doxorubicin (DXR) by Namalwa cells using flow cytometry. . . 123

Figure 3.4. Quantitation of doxorubicin (DXR) associated with Namalwa *in vitro*. . . 125

Figure 3.5. Confocal laser scanning micrographs of Namalwa cells treated with free doxorubicin or various formulations of liposome-encapsulated doxorubicin. . . 131

Figure 3.6. Confocal laser scanning micrographs of heterogenous mixture of $CD4^+$ H9 cells and $CD19^+$ Namalwa cells treated with free doxorubicin or various formulations of liposome-encapsulated doxorubicin. 133

Figure 3.7. Confocal laser scanning micrographs of Namalwa cells treated with free doxorubicin or various formulations of liposome-encapsulated doxorubicin in the presence of a cation exchange resin Dowex-50W. 138

Figure 3.8. Confocal laser scanning micrographs of Namalwa cells treated with free propidium iodide or liposomal propidium iodide. 140

Figure 3.9. Intracellular localization of DXR-SL compared to DXR-SIL[anti-CD19] as a function of time using confocal imaging microscopy. 143

Figure 3.10. Cytotoxicity of liposomal doxorubicin to Namalwa cells compared to H9 cells. 146

Figure 4.1. Binding of [^{3}H]CHE-labelled liposomes by ARH77 cells as a function of liposome concentration. 173

Figure 4.2. *In vitro* binding of fluorescent NBD-labelled liposomes to ARH77 cells using flow cytometry. 176

Figure 4.3. Flow cytometric analyses for the association of free DXR or liposome-encapsulated DXR with ARH77 cells. 178

Figure 4.4. Internalization of liposomes by $CD19^+$ multiple myeloma cell line ARH77 using a pH-sensitive fluorophore, HPTS. 180

Figure 4.5. Confocal laser scanning micrographs of ARH77 cells treated with free DXR or various formulations of liposomal doxorubicin. 182

Figure 4.6. Confocal laser scanning micrographs of ARH77 cells treated with liposomal propidium iodide. 184

Figure 4.7. Two-colour flow cytometry of the binding of immunoliposomes by B cells in PBMC from a representative multiple myeloma patient. 191

Figure 4.8. Confocal microscopy of the interaction of liposome-encapsulated DXR with PBMC from MM patients. 194

Figure 4.9. *In vitro* cytotoxicity assay of free DXR or various liposomal DXR formulations on PBMC obtained from a MM patient using the DAPI assay. . . 198

Figure 4.10. Two-colour flow cytometry to examine the expression of CD19 on ARH77 cells after i.p. implantation in SCID-beige mice. 206
Figure 4.11. *In vivo* therapeutics of free DXR and various liposomal DXR in SCID-beige mice. 207
Figure 5.1. Proposed mechanism of action of immunoliposomes 219
Figure 5.2. Schematic illustrating the interaction of targeted and non-targeted liposomes *in vivo*. 224

LIST OF ABBREVIATIONS

Ab	antibody
Ara-C	cytosine arabinoside
AUC	area under the concentration-time curve
BM	bone marrow
CD19	epitope expressed at the surface of cells of B-cell lineage
CHOL	cholesterol
CL	conventional liposomes
DAPI	4,6-diamidino-2-phenylindole
DMSO	dimethyl sulfoxide
DPPC	dipalmitoyl phosphatidylcholine
DSPE	distearoylphosphatidylethanolamine
DXR	doxorubicin
DXR-SIL[anti-CD19]	doxorubicin encapsulated in sterically stabilized immunoliposomes coupled to mAb anti-CD19
DXR-SL	doxorubicin encapsulated in sterically stabilized liposomes
FACS	fluorescence activated cell sorting/ flow cytometry
FBS	fetal bovine serum
FITC	fluorescein isothiocyanate
g	gram
h	hour
[^{3}H]CHE	[1,2(N)-^{3}H]-cholesteryl hexadecylether
HEPES	4-(2-hydroxyethyl)-1-piperazineethanesulphonic acid
HPLC	high pressure liquid chromatography
HPTS	1-hydroxypyrene-3,6,8-trisulfonic acid
HSPC	hydrogenated soy phosphatidylcholine
Hz-PEG-DSPE	hydrazide-derivatized poly(ethyleneglycol) (molecular weight 2000) covalently linked to distearoylphosphatidylethanolamine

IC_{50}	concentration of drug inhibiting 50% cell growth
IF	immunofluorescence buffer
Ig	immunoglobulin
ILS	increased life span
i.p.	intraperitoneal
i.v.	intravenous
kg	kilogram
LN	lymph node
LTS	long-term survivors
LUV	large unilamellar vesicles
MAb	monoclonal antibody
M	molar
MFI	mean fluorescence intensity
mg	milligram
µg	microgram
min	minute
ml	millilitre
MLV	multilamellar vesicles
µm	micrometers
MM	multiple myeloma
MRT	mean residence time
MST	mean survival time
MTD	maximum tolerated dose
MTT	3-(4,5-dimethylthiazol-2-yl)-2,5-diphenyltetrazolium bromide
Mw	molecular weight
nm	nanometers
PBMC	peripheral blood mononuclear cells
PC40	partially hydrogenated soy phosphatidylcholine, iodine number 40

PEG	poly(ethyleneglycol)
PhE	phycoerythrin
PL	phospholipid
P_{oct}	octanol/water partition coefficient
r^2	correlation coefficient
s.c.	subcutaneous
SCID	severely compromised immunodeficient
S.D.	standard deviation
SDS	sodium dodecyl sulfate
sec	second
SL	sterically stabilized liposomes (Stealth^R)
SIL	sterically stabilized (Stealth^R) immunoliposomes
SUV	small unilamellar vesicles
$t_{1/2}$	half life
Tc	gel to liquid crystalline transition temperature
UV	ultraviolet
v/v	volume/volume
w/v	weight/volume

CHAPTER 1

Introduction and hypothesis

1.1 INTRODUCTION

Cancer is the second leading cause of death in North America, responsible for approximately 25% of all deaths in Canada and the United States. At present, chemotherapy, surgery, radiation therapy, or a combination of these therapies are the most common interventions in cancer. In spite of the wide variety of treatment options, a majority of malignancies are still incurable. Chemotherapeutic agents are widely used in anticancer therapy, but these agents have poor target specificity leading to adverse drug effects and dose-limiting toxicities. Some selectivity of a few anticancer drugs against cancer cells comes from their activity against actively dividing cells, hence, drugs that are cytotoxic to cancer cells also exhibit cytotoxicities to normal proliferating cells of the body. Serious bone marrow depression, alopecia, gastrointestinal toxicity, mucositis, cardiotoxicity, hepatic, and renal damage are some common effects of chemotherapy that limit the number of therapeutic cycles which can be administered to patients. The utilization of anticancer drugs, is therefore, dependent upon the critical balance between effective patient therapy and overall quality of life. The design of a drug delivery system that could alleviate some of the adverse drug effects, as well as impart some specificity to the therapeutic agent, would radically improve the future of cancer treatment.

The concept of drug targeting was first proposed by Ehrlich in the early 1900's (1). He conceptualized the "magic bullet", in which therapy was targeted to the desired site of action of the drug, with no involvement of normal host tissues (1). One of the first demonstrations of targeting was from work by Korngold and Pressman in 1954 that described the first radiolabelled polyclonal antibody as an imaging agent in rat

lymphosarcoma tumours *in vivo* (2). More recently, the development of monoclonal antibody technology has revolutionized the area of targeted drug delivery (3). The high specificity of antibodies (or ligands) for epitopes expressed on select tissues confers the potential of target selectively for drugs to diseased cells, thus sparing normal tissues (4, 5). Several strategies have employed antibodies or other ligands to impart specificity to the intended therapeutic: radiolabelled Abs, Ab-drug conjugates, Ab-polymer conjugates, Ab-targeted liposomes (immunoliposomes) are just a few systems that have generated interest over the last decade (5-16). Although there have been important advances in this area of research, there is no targeted therapeutic agent that is currently approved for clinical use in humans.

With recent advances in drug development, several new drug entities with novel mechanisms of biological activity are being generated at an accelerated rate. Some of these drugs, although extremely effective *in vitro*, cannot be administered *in vivo* due to several formulation problems, short biological half-lives, and/or adverse drug reactions. As a result, research has been focussed on ways to deliver these drugs *in vivo*. One intensively researched area is the use of drug carriers. An ideal drug carrier would direct drug specifically to the site of action, increase its therapeutic response, and prevent indiscriminate toxicities, i.e., it would increase the therapeutic index of the drug, defined as the ratio of the drug's effective dose to its toxic dose.

A number of particulate or colloidal systems have been investigated as drug carriers including: liposomes, polymeric delivery systems (e.g., microparticles, nanoparticles, microspheres, hydrogels), polymer-drug conjugates, micellar systems (non-

ionic surfactant vesicles), macromolecule complexes, enzyme-drug conjugates, ligand-conjugated delivery systems. Biocompatibility, biodegradability, and toxicity profiles are important factors in the choice of a drug carrier system. Physiological compatibility of liposomes has led to their extensive investigation as drug carriers and they are the first drug carrier to be approved for clinical use.

1.1.1 Liposomal drug delivery systems.

Liposomes were first described by Alec Bangham and colleagues in 1965 (17). Upon hydration, amphiphilic molecules like phospholipids (PL) in aqueous media spontaneously assemble into highly organized, closed concentric membrane bilayers enclosing aqueous compartments (Fig. 1.1). Liposomes can be prepared with a variety of phospholipids of natural and synthetic sources (Table 1.1, Fig. 1.2).

Phospholipids exhibit a characteristic phase transition behaviour, i.e., molecules in the "solid-state" (or "gel-state") undergo a phase transition to a disorganized fluid "liquid-crystalline" state above the phase transition temperature of the phospholipid (Tc) (18) (Table 1.1). This thermotropic behaviour of liposomes results in increased mobility of the phospholipid molecules above the Tc, and as a consequence influences the stability of the bilayer and the rate of drug release (19). In addition to the phospholipids, cholesterol (CHOL) is often present as a "stabilizing" lipid (Fig. 1.1) (20). The inclusion of cholesterol in fluid-state bilayers rigidifies the bilayer by increasing the degree of phospholipid acyl chain packing, making the vesicles less permeable to solutes, i.e., reducing the rate of drug release in part by decreasing adsorption of serum proteins that play a role in the destabilisation of liposomes (21, 22).

Table 1.1. Transition temperatures of common phospholipids.

Phospholipid	Acyl chains	Transition temperature (°C)
Dimyristoyl phosphatidylcholine	14:0	24°C
Dipalmitoyl phosphatidylcholine	16:0	41°C
Distearoyl phosphatidylcholine, HSPC	18:0	56°C
Partially hydrogenated soy phosphatidylcholine, PC40	16:0, 18:1,18:2	< 0°C

1.1.2 Types of liposomes and methods of preparation.

Liposomes having a variety of physico-chemical properties can be formed by manipulating the lipid composition, phospholipid headgroup, fatty acyl chain length, and method of preparation (reviewed in (23)).

Various methods have been used to prepare liposomes of a variety of sizes (0.03 to 10 μm in diameter), and number of bilayer lamellae (Fig. 1.3). Liposomes are classified in terms of their size and number of bilayers, as either small or large unilamellar vesicles (SUV or LUV), or multilamellar vesicles (MLV) (Fig. 1.3). MLVs form spontaneously upon hydration of dried phospholipid films (17, 24) and are heterogenous in size (300-2000 nm in diameter) (Fig. 1.3). The aqueous trapped volumes of MLVs are relatively low (approximately 0.5 μl entrapped aqueous contents/μmol lipid) due to close packing of the concentric bilayers (25). In some cases, incorporation of charged lipids, may significantly increase intralamellar spacing and the resulting trapped volumes up to 10 μL/μmol due to electrostatic repulsion between lamellae (25).

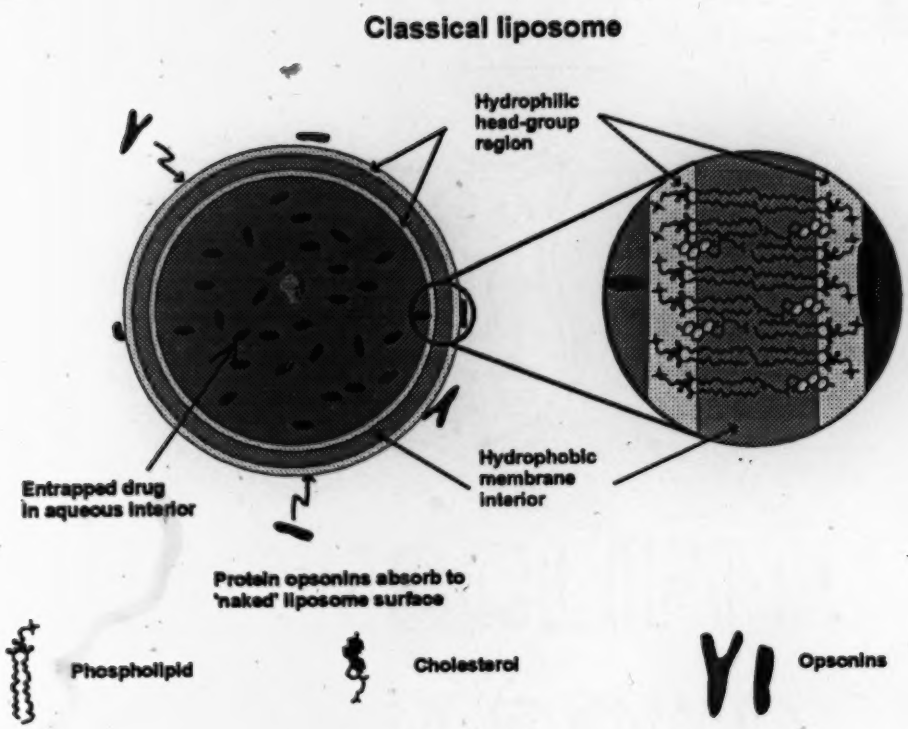

Figure 1.1. Structure of classical liposomes.
Phospholipid and cholesterol form lipid bilayers, where the hydrophilic polar head groups of the phospholipids orient towards the aqueous media, and the non-polar fatty acid tails orient towards the membrane interior.

Structures of some phospholipids

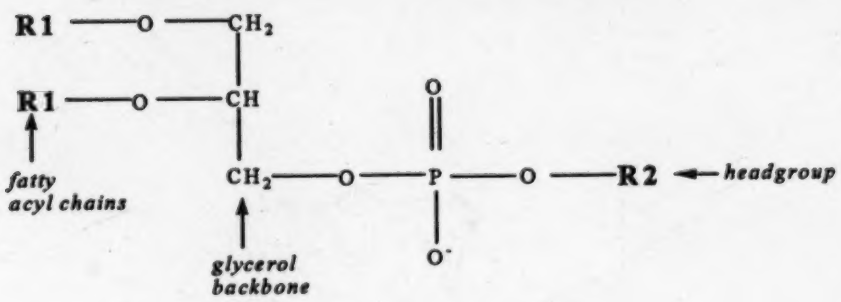

R1

saturated fatty acids

Lauric	$CH_3(CH_2)_{10}COOH$
Myristic	$CH_3(CH_2)_{12}COOH$
Palmitic	$CH_3(CH_2)_{14}COOH$
Stearic	$CH_3(CH_2)_{16}COOH$

unsaturated fatty acids

Palmitoleic	$CH_3(CH_2)_5CH=CH(CH_2)_7COOH$
Oleic	$CH_3(CH_2)_7CH=CH(CH_2)_7COOH$
Linoleic	$CH_3(CH_2)_5CH=CHCH_2CH=CH-(CH_2)_7COOH$
Linolenic	$CH_3CH_2CH=CHCH_2CH=CH-CH_2CH=CH(CH_2)_7COOH$
Arachidonic	$CH_3(CH_2)_4(CH=CHCH_2)_3CH=CH-(CH_2)_3COOH$

R2

Neutral phospholipids

choline $-CH_2CH_2N^+(CH_3)_3$
(phosphatidylcholine)

ethanolamine $-CH_2CH_2NH_3^+$
(phosphatidylethanolamine)

Negative phospholipids

serine $-CH_2CH(COO^-)-NH_3^+$
(phosphatidylserine)

glycerol $-CH_2CH(OH)CH_2OH$
(phosphatidylglycerol)

inositol
(phosphatidylinositol)

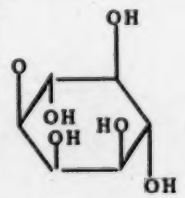

Figure 1.2. Chemical structures of commonly used phospholipids.
The basic chemical structure of PLs combines a polar head group with two non-polar fatty acid chains within a single molecule. The type of polar head group, length of the fatty acid chain, and the degree of unsaturation can influence the physicochemical properties of liposome bilayers. The presence of positive, negative, or neutral lipids can control the net membrane surface charge of the resulting liposome.

Small unilamellar liposomes (25-50 nm) (Fig. 1.3) have been prepared by ethanol injection (26) or from MLVs by mechanical-disruptive procedures like high-sheer homogenization (27), french press (28), or ultrasonication (29). Vesicles of this size typically exhibit excess lipid in the outer monolayer compared with the inner monolayer due to their low radius of curvature and have extremely low trapped volumes (approximately 0.2 µl/µmol lipid) (28, 29). The low radius of curvature and the surface free energy associated with such small vesicles can sometimes lead to instability problems resulting in spontaneous aggregation to form larger vesicles, and/or premature release of drug.

Large unilamellar liposomes (LUV, 50-300 nm) (Fig. 1.3) are usually prepared by reverse-phase evaporation (30), detergent dialysis (31) or by freeze-thawing of MLVs (32). Sequential extrusion through membrane filters of defined pore sizes is one of the most common methods to produce LUVs of monodisperse, narrow particle size distribution LUVs (33, 34). These liposomes are characterized by their large trapped volumes, i.e., for 100 nm LUV, trapped volumes of as high as 3 µl/µmol lipid have been achieved (35).

1.1.3 Association of drugs with liposomes.

Since the first realization that drugs could be trapped in liposomes, they have generated enormous interest in their potential as a drug carrier systems (36). Drugs can interact with liposomes in several different ways (Fig. 1.4). The ease of association of drug molecules with liposomes depends upon the drug solubility characteristics, i.e., their octanol/water partition coefficients (P_{oct}) (37). Hydrophilic drugs, like ara-C are

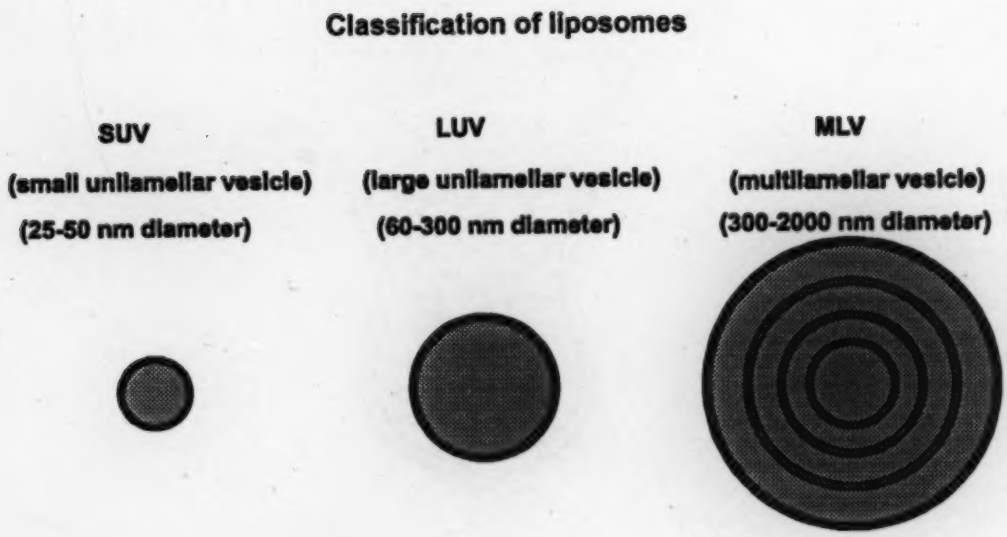

Figure 1.3. Classification of liposomes.
Liposomes have been classified depending based on their size and bilayer lamellarity, as either small unilamellar (SUV), large unilamellar (LUV) or multi-lamellar (MLV) vesicles.

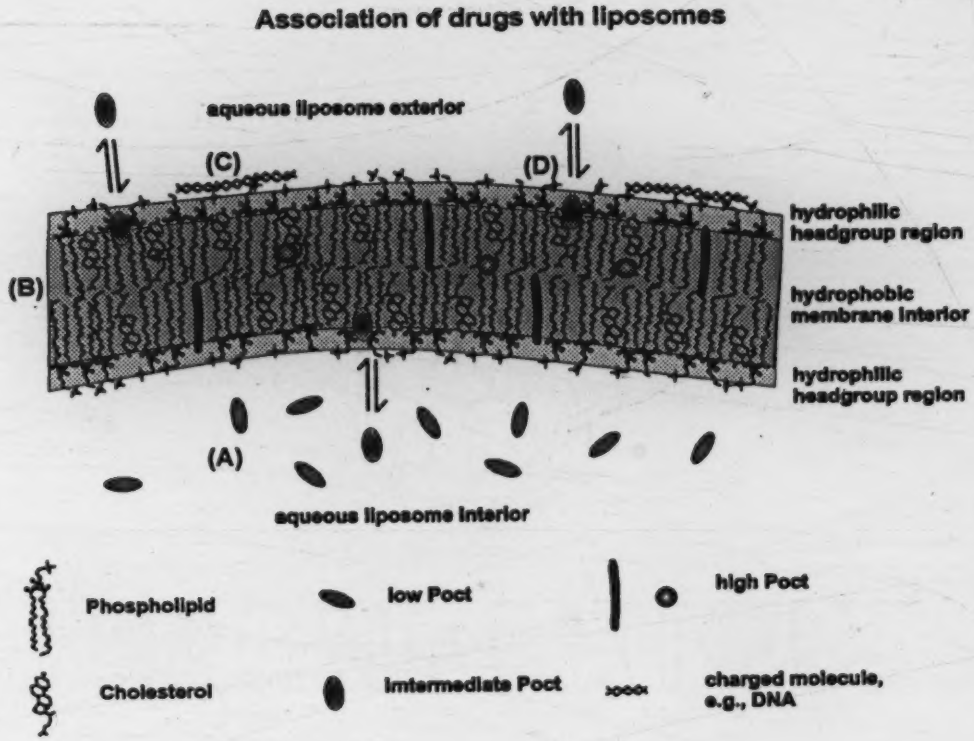

Figure 1.4. Possible interactions of drugs with liposomes.
Most hydrophilic drugs with low P_{oct} do not interact with bilayer lipids and are encapsulated in the aqueous compartment(s) **(A)**. Drug molecules can be accommodated in bilayer interior, depending on their hydrophobicity (high P_{oct}) and the strength of drug-lipid interactions within the bilayer **(B)**. Charged molecules, e.g. DNA associate with the bilayer surface through Van de Waal's interactions **(C)**. Molecules with intermediate P_{oct} will be in equilibrium between the membrane interior and exterior and will not easily form a stable association with liposomes **(D)**. (adapted from T.M. Allen).

physically entrapped in the aqueous interior of liposomes (38), whereas, hydrophobic molecules with low aqueous solubility, e.g. corticosteroids, taxol, or lipophilic drugs like hydrophobic analogues of cisplatinun are incorporated into the hydrophobic bilayers of liposomes (39) (Fig. 1.4).

There are two basic techniques for the encapsulation of drugs into liposomes, passive or active entrapment. Passive encapsulation is a physical process where water soluble drugs are dissolved in the aqueous media and entrapped during vesicle formation or lipid soluble drugs are included in the organic solvent and spontaneously associate with the lipid bilayer. The active encapsulation procedure, on the other hand, requires the ability of certain molecules, e.g., amphiphilic weak amines, to distribute across bilayers of preformed liposomes having a chemical/or ion gradients (40, 41). Uncharged drug molecules freely cross the bilayer into the liposome interior, where they acquire a net charge (usually protonated) and are unable to traverse back across the membrane. This procedure has been widely used for drugs like doxorubicin (DXR) (40, 42), daunorubicin (43) and vincristine (44, 45). A schematic of the ammonium sulphate loading method (41, 42) is illustrated in Fig. 1.5.

1.1.4 Advantages of liposomes as a drug delivery systems.

Liposomes can carry large numbers of drug molecules, relative to, e.g. drug-polymer conjugates, and can have high drug to lipid ratios. Liposomes with a variety of well defined physicochemical characteristics can be prepared by altering the bilayer components of liposomes, e.g., formulations of rigid or fluid lipids, fusogenic components, etc. (46)). The resulting effect may be either modulation of drug release from

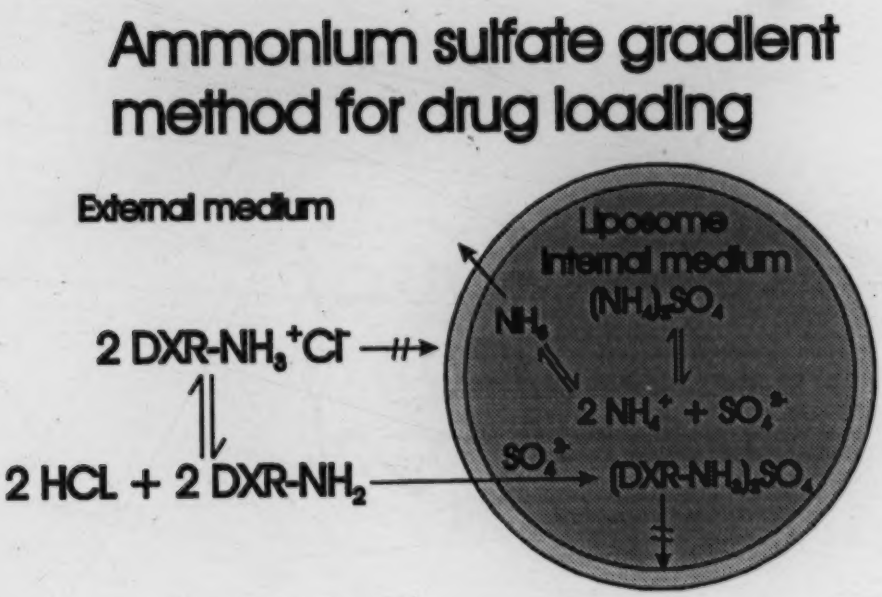

Figure 1.5. Remote loading of DXR using an ammonium sulphate gradient. The liposomes contain ammonium sulfate in the liposome interior. Uncharged DXR molecules cross the liposome membrane and are protonated in the liposome interior and form a highly insoluble doxorubicin-sulphate precipitate (42). This procedure allows preferential accumulation of the drug DXR within the liposomes permitting encapsulation efficiencies as high as 100% (42, 53) (adapted from (42))

liposomes or enhanced interaction with cells. Liposomal encapsulation will protect drugs from the external environment and will retard the degradation of drugs that may be, e.g., photolabile or sensitive to enzymatic degradation (38). Liposomes can alter the pharmacokinetics of entrapped agents, often increasing the drug's area under the concentration time curve (AUC), and hence its therapeutic availability (38). Examples include liposomal doxorubicin (DXR) (47), daunorubicin (DNR) (48), vincristine (45) or cytosine arabinoside (Ara-C) (38). Alteration in the biodistribution of drugs can result in decreases in toxicities, e.g., reduction in the cardiotoxicity of DXR (49) or decreased nephrotoxicity of amphotericin B (50). Furthermore, encapsulated drugs have been shown to accumulate passively at sites of increased capillary permeability like tumours, sites of inflammation, or areas of infections (51, 52).

1.1.5 Applications of liposomes.

Liposomal drug delivery systems have been used in a broad range of pharmaceutical applications including, cancer (39, 48, 54-57); infections (52, 58-61); as antigen presenting systems for modifying an immune response (62); for the delivery of genes (63); as imaging agents (64); for topical formulations of drugs (65-68); for pulmonary delivery (69); and in cosmetic creams and lotions (70). Research in some these areas has led to a number of liposomal therapies that are in clinical trials or approved for clinical use in humans (Table 1.2).

1.1.6 Interaction of liposomes with plasma proteins and the mononuclear phagocyte system (MPS).

After i.v. administration, liposomes are distributed mainly in the blood

Table 1.2. A list of some liposomal and lipid-based drugs in clinical development.

Liposomal drug	Clinical indication	Investigational status	Company
1. Liposomal amphotericin B (AmBisome^{R})	Systemic fungal infections	Approved (Europe Mexico, USA)	NeXstar Pharmaceuticals, CO.
2. Amphotericin B-lipid complex (ABLC^{R})	Systemic fungal infections	Approved (Europe, USA)	The Liposome Co., N.J.
3. Amphotericin B colloidal dispersion (Amphocil^{R})	Systemic fungal infections	Approved (Europe, USA)	Sequus Pharmaceuticals, CA.
4. Liposomal nystatin Nyotran-Aronex	Systemic fungal infections	Phase II/III (USA) Phase III	NeXstar Pharmaceuticals, CO Aronex Pharmaceuticals, TX
5. Liposomal amikacin (MiKasome)	Bacterial infections	Phase II (Europe)	NeXstar Pharmaceuticals, CO.
6. Liposomal prostaglandin- E1 (Ventus)	Inflammatory diseases	Phase III (USA)	The Liposome Co., N.J.
7. Liposomal HepB antigen	Hepatitis B	Approved (Europe)	Swiss Serum Inst., Bern
8. Liposomal hexadecyl PC	topical cancer	Approved (Germany)	AstaMedica/ Degussa
9. Liposomal annamycin	Advanced breast cancer	Phase I /II (USA)	Aronex Pharmaceuticals, TX
10. Liposomal *trans*-retinoic acid (Atragen)	Kaposi's sarcoma	Phase II/III (USA)	Aronex Pharmaceuticals, TX
11. Liposomal vincristine	Non-Hodgkin's lymphoma, pancreatic cancer	Phase II (Canada)	Inex Pharmaceuticals, BC.
12. Liposomal muramyl tripeptide	Relapsed osteosarcoma	Phase III (USA)	Ciba-Geigy

13. Liposomal daunorubicin (Daunosome^{R})	Kaposi's sarcoma Leukemia, lymphoma, breast, lung cancer	Approved (USA) Phase II (USA)	NeXstar Pharmaceuticals, CA
14. Liposomal doxorubicin (TLC Dox-99)	Advanced lung, breast cancer Soft tissue sarcomas in combination with GM-CSF)	Phase III (USA) Phase II (USA)	The Liposome Co., N.J.
15. Long circulating liposomal doxorubicin (Doxil^{R} or Caelyx^{R})	Kaposi's sarcoma Advanced breast, ovarian, lung cancer	Approved (Europe and USA) Phase III (USA, Canada)	Sequus Pharmaceuticals, CA.
16. Liposomal cisplatin (SPI-77)	Lung cancer	Phase I (USA)	Sequus Pharmaceuticals, CA.

compartment and to the mononuclear phagocyte system (MPS) (71). In the blood stream, liposomes interact with several blood components, and/or the cells of the immune system which eventually lead to their removal from circulation and to the release of their contents (22, 72). After i.v. injection, the rate of liposome clearance from circulation and the rate of contents release both affect the overall drug therapeutic availability, and consequently the amount of drug reaching the target cells.

In the circulation, liposomes may interact with a variety of lipoproteins and other opsonins that can mediate their removal from blood. The mechanisms of liposome opsonization and its relationship to clearance may involve complex processes. In brief, clearance mechanisms are believed to be due to activation of complement *via* the classical pathway, involving the binding of various serum opsonins (73, 74). The most important

opsonin being complement activation fragment of C3, C3b (74-76).

Serum proteins can lead to the release of encapsulated components by contributing to the disintegration of the liposomes (77, 78). High density lipoprotein (HDL), apolipoprotein A-1, can rapidly exchange with the phospholipids in the liposome bilayer (78) causing liposome breakdown. Complement proteins or protein components that are capable of activating complement, have been implicated in the formation of complement complexes on the surface of liposomes. The formation of this complex can be followed by complement-mediated lysis of liposomes.

Macrophages have an important role to play in the clearance of liposomes and other particulate matter from circulation. These may be either the resident macrophages in the liver (Kupffer cells), spleen, lung, gut, skin, bone marrow or circulating monocytes in blood (collectively called the mononuclear phagocyte system, MPS). These specialized cells, work by processing and presenting antigens, secreting cytokines that regulate action of other cells, or by recognizing foreign particulate material, including liposomes, and mediating their removal from circulation. Macrophages contain an array of receptors, specific for glycoproteins, lipids, and Fc fragments of immunoglobulins. Adsorption of specific proteins (known as opsonins) on liposomes, in particular, complement proteins (C1q, C3, C3b), fibronectin, IgG or IgM, leads to their binding to and their removal from circulation by specific macrophage receptors (79). Liposomes are phagocytosed by the macrophages and subsequently degraded in the lysosomes.

1.1.7 *In vivo* distribution of liposomes after intravenous administration.

After parenteral administration, most particulate carriers are restricted in their

distribution. Their biodistribution depends to some extent on the size of the carrier. Large particles, like multilamellar liposome vesicles MLVs with diameters in the micron range are rapidly filtered by the first capillary bed they encounter, usually in the lung. Smaller liposomes avoid this filtering mesh and circulate until removed into the MPS. The ability of drug delivery systems to extravasate from blood to an extravascular site largely depends upon the capillary structure of the site. Capillaries in most tissues like heart or muscle, are continuous. Here the endothelial cells are tightly aligned, with an uninterrupted basement membrane. As a result, these capillaries are impermeable to large macromolecules and colloidal particles, including liposomes. In tissues such as renal glomeruli or gastrointestinal tract, fenestrations exists in capillaries where the endothelial cells are separated by gaps as large as 40-80 nm, but these gaps are likely too small to allow the passage of liposomes. The endothelial cells lining the capillaries of organs like liver, spleen or bone marrow are largely discontinuous. These blood vessels have openings that range from 100-1000 nm, with the basal lamina either fragmented (bone marrow, spleen) or totally absent (liver). Clearly these capillaries would provide routes for the escape of small liposomes and other particles from circulation should they escape the specialized MPS cells lining the capillaries in the liver (Kupffer cells) and spleen.

Solid tumours, as they grow, recruit new blood vessels in a process known as angiogenesis. Angiogenesis is accompanied by increased vascular permeability (80, 81). Hence, angiogenic tumours are permeable to a variety of macromolecules, including small liposomes less than approximately 200 nm in diameter (82). Certain pathological conditions like infection and inflammation can also enhance the permeability of blood

vessels in areas of disease and results in increased liposome uptake into these tissues (81-83). Factors capable of increasing the permeability of the vascular endothelia, can also increase the localization of liposomes into these tissues (84). Thus, a number of mechanisms exist which allow liposomes to escape from circulation and to passively accumulate in tissues. This process is strongly dependent on the ability of the liposomes to maintain long circulation times and a direct correlation between long circulation times and increased distribution of liposomes into solid tumours has been shown in tumour models of C-26 colon carcinoma, J6456 lymphoma, M-109 lung carcinoma, metastatic mammary carcinomas and ovarian tumours (85-89).

1.1.8 Interaction of liposomes with cells.

At the cellular level, there are several possible mechanisms for liposomes and their associated drugs to interact with target cells, as illustrated in the schematic (Fig. 1.6). These mechanisms depend upon the composition (i.e., fluidity, fusogenicity), size (large versus small) or charge of the liposomes, the cell type, e.g., macrophage, lymphocyte etc., and the presence of specific cell receptors or liposomes surface ligands (18, 90, 91).

Random, non-specific association of liposomes with the cell surface is the most common mechanism of liposome-cell interaction. Non-specific interactions with cells are mediated through Van der Waal's forces of between liposomal lipid and cell surface components (Fig. 1.6A). This results in the liposomal contents being brought in close proximity to the cell, with the possibility of release of the encapsulated material and cellular uptake occurring as a function of time *via* diffusion. Another mechanism of liposome-cell interaction involves the transfer and/or exchange of lipid components

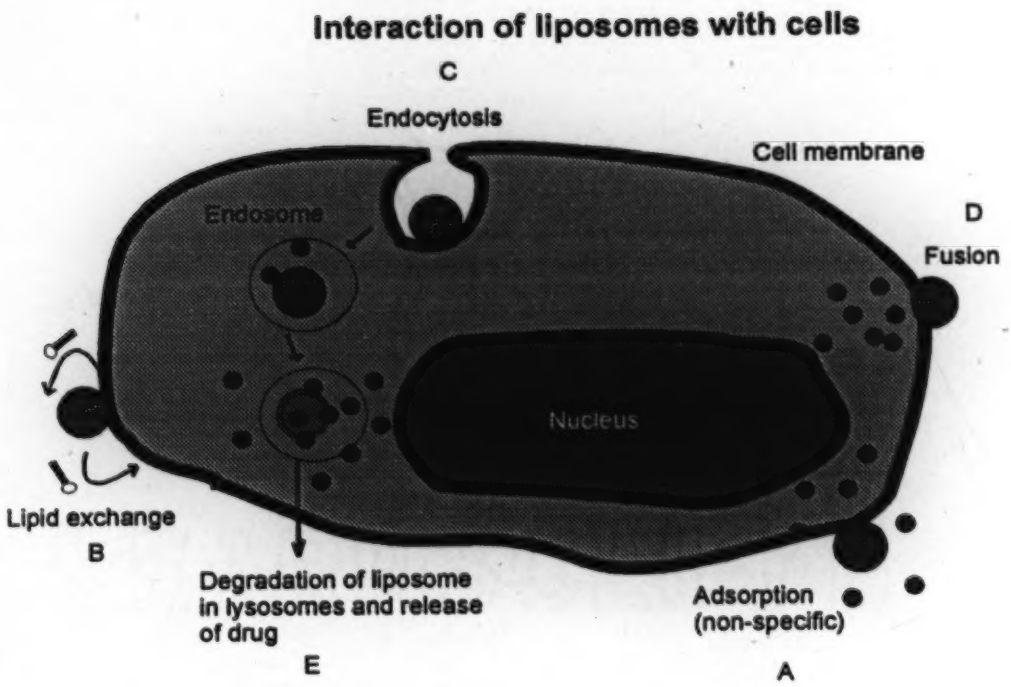

Figure 1.6. Schematic for the interaction of liposomes with cells.
A. Liposomes adsorb to the cell surface, resulting in the drug released locally at the cell surface; B. Exchange of lipids or hydrophobic drugs with the cell membrane; C. Endocytosis of liposomes into endosome and/or lysosomes, result dismantling of liposomes within these compartments to release the drug intracellularly; D. Fusion of liposomes with the cell plasma membrane, resulting in delivery of the contents directly into the cytoplasm. Adapted from (18, 91).

or hydrophobic drugs from the liposomal membrane to the cell membrane (72) (Fig. 1.6B). This mechanism however, does not allow transfer of drugs from the aqueous compartment of liposomes, but may help induce drug leakage by destabilizing the liposome membrane (92).

Adsorption of liposomes to the cell surface may, for some types of cells (e.g. phagocytic cells like macrophages), result in endocytosis (Fig. 1.6C). This mechanism involves internalization of the liposomes and delivery of the liposomal drug package to the endosomes. This can also be triggered in non-phagocytic cells, through the coupling to the liposome surface of ligands triggering receptor-mediated endocytosis. Early endosomes undergo intracellular processing ultimately leading to the formation of lysosomes. The processing of liposomes within acid environment of the enzyme-enriched lysosomes may eventually lead to the release of drugs from the liposomes. Whether or not this leads to a therapeutic effect depends on the stability of the liposomes and the ability of the drug to withstand lysosomal degradation. Acid-labile drugs or those degraded by lysosomal enzymes, e.g., phospholipases, proteases, etc., may be destroyed in the lysosomes. Drugs that are chemically resistant in the acid milieu of the lysosomes (like DXR[1]) may remain in the lysosomes until they are released into the cytoplasm.

Fusion of the liposomal bilayer with the cell membrane (Fig. 1.6D), with direct introduction of the contents into the cytoplasm, is another mechanism of liposome-cell interactions. These liposomes usually contain a fusogenic component like a viral surface

---

[1] Storm, G., Regts, J., Beijnen, J.F., Roerdink, F.H. Processing of doxorubicin-containing liposomes by liver macrophages *in vitro*. J. Liposome Res. *1*: 195-210, 1989.

protein (virosomes) or membrane-destabilizing lipids like DOPE reconstituted into the liposomal bilayer. The attractiveness of this interaction is that liposomal contents introduced directly into the cytoplasm of the cell bypass the acid/enzyme environment of the endocytotic machinery. Fusion between liposomes, lacking fusogenic components, and cells is thought to occur rarely, if ever.

1.1.9 Classical liposomes (CL).

Liposomes composed of phospholipids and (usually) cholesterol, lacking engrafted glycolipids, polymers or other sterically stabilizing components (*vide infra*) are generally referred to as "conventional or classical" liposomes (CL). The normal route of clearance of CL is by recognition and uptake by phagocytic cells of the mononuclear phagocyte system MPS, also known as the reticuloendothelial system, subsequent to their opsonization by plasma proteins (93, 94). At low doses of neutral CL (120 nm in diameter), approximately 80 % of CL are cleared by the Kupffer cells of the liver and fixed macrophages of the spleen within minutes of i.v. injection (71). Thus, CL have short circulation times, and non-linear, dose-dependent pharmacokinetics (71, 95, 96), occurring as a result of their rapid uptake by the MPS. The pharmacokinetics of CL, is affected by a number of factors, including, route of administration, dose, size, or liposome composition, e.g., the inclusion of cholesterol, rigid lipids and/or charged components (97-99).

The rapid uptake of most formulations of CL by the MPS cells has been the basis of numerous applications involving infections within the MPS, e.g., in the treatment of leishmanaisis (60, 100) or as a means of boosting macrophage function with immune stimulants encapsulated into liposomes (101).

It was realized that if liposomes could circulate for longer times in blood, they would be able to reach a variety of cells other than those of the MPS. Prior to the development of long circulating (sterically stabilized) liposomes (described later), attempts to reduce MPS uptake of liposomes led to the development of small, rigid, neutral liposomes. Increasing the rigidity of CL by incorporating high phase transition temperature lipids (e.g. DSPC) can decrease their extent of distribution to the MPS. Thus rigid CL of small size, such as DSPC:CHOL, 100 nm in diameter, have circulation half-lives of several hours, compared to formulations of more fluid CL showing half-lives on the order of minutes (96). This observation led to the development of liposomal daunorubicin and vincristine (56, 102).

1.1.10 Development of long circulating liposomes.

Prior to the advent of long circulating liposomes, a number of attempts were made to reduce the uptake of liposomes by the MPS, i.e., to increase their circulation times in blood. It was hypothesized that this would result in liposomes gaining improved access to sites outside the MPS.

Some of the first attempts were aimed at saturating MPS uptake, achieved by pre-dosing with large doses of empty conventional liposomes (CL) (96). The resulting effect was a spill-over of liposomes into circulation (96). Along similar lines, administration of a MPS-blocking substances like colloidal carbon or dextran sulphate 500 were shown to moderately increase circulation times of liposomes (103). MPS blockade, in certain instances, can be achieved by cytotoxic drugs like doxorubicin encapsulated in CL which are toxic to MPS cells (104). However, with such attempts, major complications may

arise as a result of MPS blockade (105, 106)

In the development of long-circulating liposomes, there were three distinct stages, a) decreasing liposomal size, b) increasing bilayer rigidity, and c) modification of liposomes by surface grafting of polysaccharides, glycolipids or polymers (reviewed in (107)). Previous work showed a direct relationship between the liposomal size and the rate of removal of liposomes from circulation. The smaller the diameter, the slower the clearance from circulation (108, 109). After i.v. administration, large MLV's composed of PC/CHOL demonstrated circulation half lives of 10 min, which is approximately 4-fold faster clearance than liposomes of mean diameter of 80 nm (108).

Formulations of liposomes from high phase transition temperature phospholipids, e.g., saturated DSPC, and rigid lipids like sphingomyelins (99, 110) and the inclusion of cholesterol in the bilayer both increase circulation times of liposomes as a result of their ability to decrease bilayer fluidity and lipid exchange (111, 112).

Addition of sterically stabilizing components to the surface of liposomes has an interesting history (reviewed by (107)). Several years ago it was observed that some negatively charged lipids, particularly GM_1, sulfogalactosylceramide (sulphatides) and phosphatidylinositol (PI) (113, 114) and recently, N-glutaryl/adipyl derivatives of DOPE (115) were able to prolong blood circulation times of liposomes after i.v. administration. However, most negatively-charged liposomes PG, PS, PA, were cleared at faster rates from circulation compared to neutral PC-containing liposomes (99, 108, 113, 114, 116). The decreased rate of clearance of GM_1- and PI-liposomes has been attributed to the decreased opsonization of liposomes by plasma proteins, resulting from increased

hydrophilicity of the liposomal surface imparted by the sugar moieties present in these molecules, and the "shielding" of the negative charge by the conformation of the sugars (117).

Interestingly, the work with glycolipids came about through attempts to mimic the outer membrane of red blood cells, which have a surface membrane enriched with glycoproteins and glycolipids with terminal sialic acid residues (118). In early experiments, ganglioside GM_1 was shown to increase circulation times of PC/CHOL liposomes by 4-fold, compared to conventional PC/CHOL liposomes (113, 114, 119). The increase in circulation times was even more pronounced for rigid liposomes composed of sphingomyelin (113) or distearoylphosphatidylcholine (114).

Surface modification of liposomes by inclusion of hydrophilic PEG, covalently attached to a lipid anchor significantly prolonged the circulation times of liposomes *in vivo*, as a result of their decreased uptake by the MPS (71, 120-125). Some of the earliest work on the use of hydrophilic polymers was with polymer-coated particles, e.g., bovine serum albumin coated with methoxypolyethylene glycol (126) and microspheres coated with non-ionic surfactant block co-polymer polyoxamer 388 (103, 127). These experiments were the first to describe the ability of hydrophilic molecules to increase circulation times of particles (103, 127). Later, carbohydrates like dextran, pullalan and other hydrophilic polysaccharides were used to coat liposomes and were found to have reduced MPS uptake (128, 129).

The addition of polyethylene glycol (Mw 2000) at the liposome surface results in sterically stabilized liposomes (SL). The hydrated, flexible polymer acts by hindering

adsorption of plasma proteins (opsonins) at the surface of liposomes (22, 121, 130-132). This in turn reduces the rate of removal of liposomes from circulation by the MPS, leading to prolonged times in blood. Another advantage that occurred from this approach was the conversion of the pharmacokinetics from dose-dependent to dose-independent pharmacokinetics (71, 86).

A number of studies, comparing different PEG derivatives of different molecular weights (Mw 120-5000), and varying compositions, have established that PEG of Mw 2000 incorporated into liposomes at 5 mol% of phospholipids is optimal for long circulation times. More recently new hydrophilic and flexible polymers have been described including poly(acrylamide) and poly(vinyl pyrrolidone) (133), poly(oxazolines) (134), and poly(glycerols) (135), which, when incorporated into liposomes, result in circulation times approaching or equivalent to PEG-liposomes.

1.1.11 Pharmacokinetics of liposomal anthracyclines.

Doxorubicin (DXR) is the most widely used drug of the anthracycline family (Fig. 1.7). DXR is classified as an antitumour antibiotic and was first isolated from strains of *Streptomyces peucetius*. The basic chemical structure of the molecule consists of a tetracyclic ring, the aglycone, of which one ring is a quinone (Fig. 1.7) . This part of the molecule is water insoluble, and is a chromophore which has the ability to fluoresce upon excitation. In addition to the aglycone backbone, the molecule contains an amino-sugar moiety, which is responsible for imparting a hydrophilic character to the drug (136).

DXR has a broad spectrum of antitumour activity, and is active against a range of malignancies including carcinomas of the breast, ovaries, lung, thyroid, and

Chemical structures of anthracylines

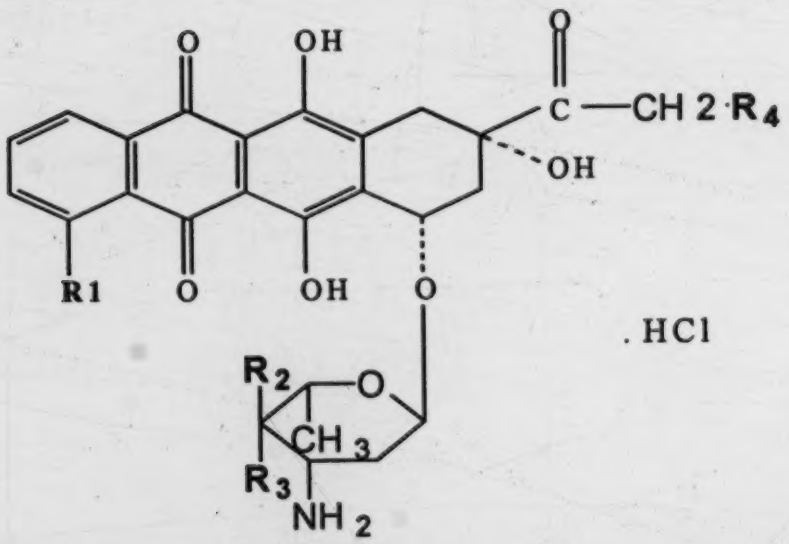

	Doxorubicin	Daunorubicin	Epirubicin	Idarubicin
R1 =	OCH_3	OCH_3	OCH_3	H
R2 =	H	H	OH	H
R3 =	OH	OH	H	OH
R4 =	OH	H	OH	H

Figure 1.7. Structural formulae of some anthracylines that are currently in clinical use.

gastrointestinal tract, as well as tumours of mesenchymal origin such as acute lymphocytic and myelogenous leukemias, lymphomas, myelomas, and sarcomas (137).

Some of the common adverse effects of DXR are nausea, vomiting, bone marrow suppression, mucositis, alopecia, cardiac toxicities, and extravasation injuries leading to tissue necrosis. Of these side effects, cardiac toxicities are the most serious. DXR exhibits both acute and chronic forms of cardiotoxicities (136). The acute version can be elicited within minutes of i.v. administration of DXR, and is commonly detected as cardiac arrhythmias, contractile defects, and conduction abnormalities. The dose limiting toxicities of a single dose of DXR are myelosuppression and stomatitis (MTD for a single dose is approximately 60 mg/m^2) (136). Delayed cardiotoxicity, including, late cardiomyopathies and congestive heart failure, can be fatal and is the dose limiting toxicity. The onset of delayed toxicities usually occurs at cumulative doses of approximately 550 mg/m^2 DXR (136).

DXR crosses liposomal membranes or enters cells *via* passive diffusion. The drug exists in equilibrium between a neutral and an ionized form. Only drug molecules in the unionized form are able to cross cell membranes. The amino group on the sugar moiety is protonated at acid pH, and due to the low membrane permeability of the protonated species, the charged form of the drug is unable to cross cell membranes. In addition to the diffusion of the drug into cells, DXR can also undergo active efflux from cells expressing a transmembrane transport pump, P-glycoprotein (P-gp).

The exact cytotoxic mechanism of the anthracyclines is still unclear. One of the proposed mechanisms is intercalation of the anthracycline with adjacent base pairs of

nucleic acids (both DNA and RNA), leading to inhibition of DNA and RNA polymerases, and inhibition of protein synthesis (138). Alternate pathways for cellular cytotoxicity include the induction of topoisomerase II-mediated strand breaks. Free radical generation, anthracycline-mediated chelation of iron, and bioreductive activation (by one or two electron reduction) to superoxide and/or peroxide anions has also been implicated in widespread damage to DNA and cell membranes.

DXR is one of the most commonly used liposomal drugs. The pharmacokinetics of both the liposomal drug and the free drug are well understood (Table 1.3). Free DXR, when administered i.v. is rapidly cleared from plasma in a biexponential manner with initial distribution half-life ($t_{½}\alpha$) in humans of 0.06 h (51) and in mice of 0.08 h (47). DXR has a slow terminal elimination phase with a half-life ($t_{½}\beta$) in humans of 10 h (51), and in mice of 8.6 h (47). Like most anthracyclines, DXR has a high apparent volume of distribution, V_D, of 365 L, as result of extensive drug distribution into tissues. Doxorubicinol, a cytotoxic metabolite is the primary breakdown product of DXR upon its biotransformation by liver NADPH-dependent aldo-ketoreductase. Two additional inactive aglycone metabolites, namely the 7-deoxy- and 7-hydroxy-aglycones are products of reductases and hydrolases. A large fraction of DXR is excreted *via* the bile, both as the parent drug, metabolites or their glucuronides- and sulphated-conjugates. Renal excretion accounts for a small (<10 %) proportion of the drug.

Encapsulation of DXR in liposomes changes its pharmacokinetic profile substantially (Table 1.3). When entrapped in SL the liposome-associated drug exhibits a primarily monoexponential clearance pattern, indistinguishable from that of the carrier

Table 1.3. A comparison of pharmacokinetic parameters of free anthracyclines (doxorubicin (DXR) and daunorubicin (DNR)), and liposomal formulations of DXR and DNR that are in clinical use in humans.

Treatment	i.v. dose (mg/m^2)	$t_{1/2}\alpha$ (h)	$t_{1/2}\beta$ (h)	AUC (μg.h/ml)	C_{max} (μg/ml)	CL (ml/min)	V_D (l)	Ref.
Free DXR	25 50	0.07 0.06	8.7 10.4	1.0 3.5	3.3 5.9	755 422	254 365	(51)
Caelyx[R a]	25 50	3.2 1.4	45.2 45.9	609 902	12.6 21.2	1.3 1.5	4.1 5.9	(51)
TLC-D99[R b]	25 90	0.29 0.45	6.7 13.5	19.7 14.4	1.3 4.1	388 363	18.8 14.6	(55)
Free DNR	80	0.77	55.4	10.33	0.4	233	1055	(48)
DaunoXome[R c]	20 80	- -	3.8 5.2	57.2 375.3	8.2 43.6	14.3 6.6	4.1 2.9	(48)

$t_{1/2}\alpha$, initial half-life; $t_{1/2}\beta$, terminal half-life; AUC, area under the concentration time curve; C_{max}, peak concentration; CL, clearance; V_D, volume of distribution.

[a] liposome composition: HSPC:CHOL:PEG2000-DSPE:α-tocopherol, 56.2:38.3:5.3:0.2 molar ratio, 100 nm in diameter.

[b] liposome composition: egg PC:CHOL, 55:45 molar ratio, 180 nm in diameter.

[c] liposome composition: DSPC:CHOL, 2:1 molar ratio, 45 nm in diameter.

(Adapted from (139)).

and free drug *in vivo*. Pharmacokinetic studies of DXR-SL (HSPC:CHOL:PEG_{2000}-DSPE or HSPC:CHOL:hydrogenated PI) in rodents and dogs show that the bulk of the drug was eliminated with half -lives ($t_{½}$) ranging from approximately 15 to 30 h (47, 140). V_D was close to the estimated plasma volume, suggesting that DXR is confined largely to the central compartment. In humans, the circulation half-life was found to be even longer with $t_{½}$ of approximately 2 days and V_D of 6 L. A substantial increase in circulation times of DXR-SL was observed compared to solid formulations of DXR-CL (HSPC:CHOL:PG) which had a $t_{½}$ approximately 1 h or fluid DXR-CL (eggPC:CHOL) which had a $t_{½}$ of 0.3 h. The AUC in mice was higher for DXR-HPI-SL (1099 µg·h/ml), compared to 58.5 µg·h/ml for DXR-CL and 3.9 µg·h/ml for free DXR. There was also a decrease in clearance of the drug by more than 200-fold for DXR-SL (0.2 ml/h for DXR-HPI-SL) compared to free DXR (51.3 ml/h). The altered kinetics resulted in a 3-fold reduction of the concentration of DXR in the heart, which is useful in eliminating some of the dose-limiting toxicities associated with the free drug. Similar reductions in the peak levels of DXR in heart was also reported for DXR-SL in rats (141). These results suggest that DXR-SL may allow greater cumulative doses of DXR to be administered clinically before cardiac toxicities appear.

Altering the lipid composition and the drug content of liposomes has been shown to produce marked changes in the plasma levels of liposomal DXR. High doses (20 mg/kg DXR) of small neutral CL (DSPC:CHOL), 100 nm in diameter when injected into mice were able to retain as much as 80 % of the injected dose in circulation after 24 h (104). This effect was partly due to the toxicity of DXR to cells of the MPS subsequent to its

delivery to the MPS *via* DXR-CL. Mice injected with DXR encapsulated in either HSPC:CHOL, 10:8 (DXR-CL); HSPC:CHOL:HPI, 9:8:1 (DXR-HPI-SL) or HSPC:CHOL:PEG_{2000}-DSPE (DXR-SL) resulted in plasma DXR levels after 24 h of 3.6, 12.5 and 34.8 μg DXR/ml, respectively. However, altering the phospholipid in DXR-SL, from HSPC to either DPPC or eggPC, resulted in either a 2-fold or 50-fold reduction in the plasma concentrations of DXR, respectively. The change in drug levels was attributed mainly to lower vesicle stability and increased membrane permeability of the liposomal bilayer to DXR when lower phase transition phospholipids were present in SL.

Phase I, II and III clinical studies have been conducted in cancer patients to compare the pharmacokinetics of free DXR, DXR-CL (HSPC:CHOL:PG) and DXR-SL (HSPC:CHOL:PEG_{2000}-DSPE) at two doses of 25 and 50 mg/m^2 (51, 54, 142). Free DXR is characterized by rapid distribution ($t_{½}$ < 5 min), short elimination $t_{½}$ (approximately 10 h) and its significantly greater clearance and V_d compared to DXR-SL. For DXR-SL, a minor portion (<5%) of the injected dose is distributed with a $t_{½}$ of approximately 1-3 h, and, the remainder (95%) was cleared with a $t_{½}$ approximately 45 h. Compared to free DXR or DXR-CL in humans DXR-SL had a decreased volume of distribution V_d, decreased clearance and a greater mean residence time, all contributing to increased therapeutic availability of the drug (Table 1.3).

1.1.12 Targeted liposomal drugs.

The liposomes which have currently received clinical approval rely on "passive" targeting for their increased uptake into solid tumours or regions of inflammation. This "passive" targeting strategy is not expected to increase targeting of liposomes within the

vasculature, as these liposomes have low recognition to target cells, e.g., to circulating cells from hematological malignancies, nor would there be any targeting to micrometastatic tumours prior to angiogenesis. Increasing the site-specific delivery of drugs in these instances requires a new approach. The next generation of liposomes relies on a strategy of "active" or ligand-mediated targeting. In this approach, antibodies or ligands which recognize cell surface-associated antigens are attached at the surface of liposomes containing associated therapeutics. Binding of the liposomal drug package to its appropriate antigen will result in the selective delivery of drug to the target cells. These targeted liposomes are called "immunoliposomes" or "ligand-liposomes". As outlined below, a number of chemical coupling techniques have been developed for the attachment of antibodies at the cell surface.

Monoclonal antibodies have been widely used in liposomal targeting. A number of coupling strategies have been developed to attach antibodies or ligands to liposomes and have been used for targeted applications (reviewed in (15)). This has been made possible by the development of several cross linking reagents that allow covalent coupling of the targeting moieties to either the surface of the liposomes, anchored to phospholipid headgroups, or to the termini of PEG chains (Fig. 1.8 and 1.10). Ideally the coupling method should be simple, rapid and combine a high coupling efficiency, with retention of the binding affinity of the Ab. There have been several covalent methods and one non-covalent method used to attach antibodies to liposomes (Fig. 1.8 and 1.10).

The non-covalent method takes advantage of the strong affinity of avidin (or streptavidin) for biotin (143). In this approach, biotinylated antibodies are conjugated

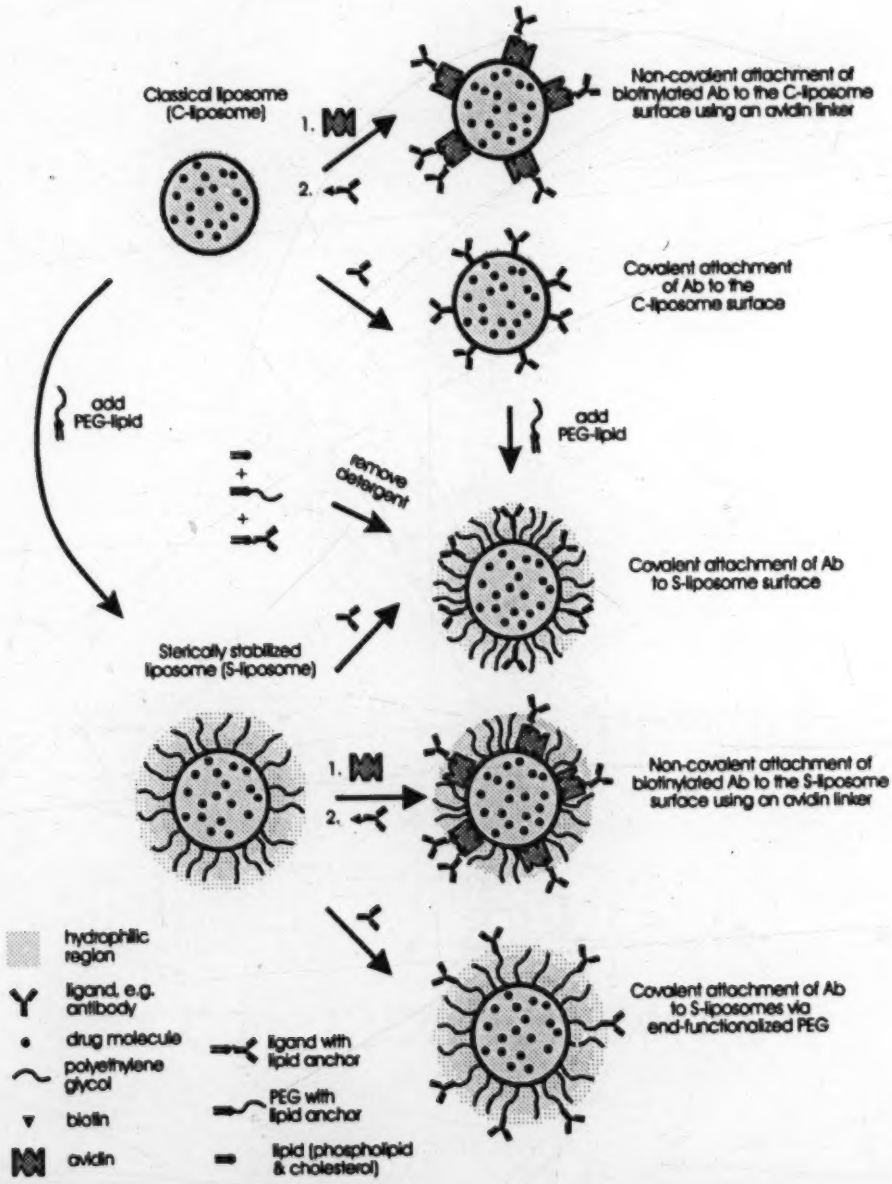

Figure 1.8. Strategies for the formation of targeted liposomes (CIL and SIL). Ligands can be linked covalently the surface of CL or SL, or linked non-covalently through avidin / biotin. For SIL, ligands can be attached to the terminus of PEG *via* end-group functionalised PEGs. SIL can also be created from SL, SL from CL or SIL from CIL, by transfer of polymers in the form of micelles, which spontaneously incorporate into the liposomes (adapted from (15))

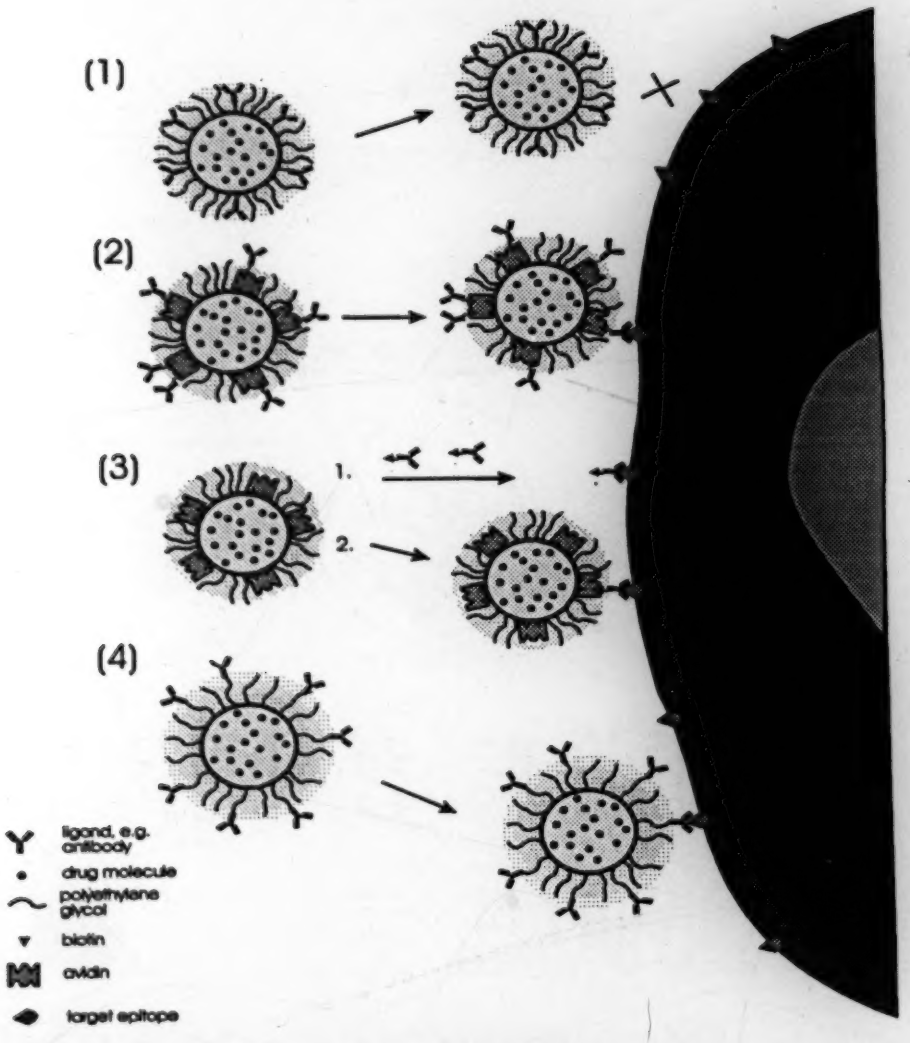

Figure 1.9. Binding of immunoliposomes to target cells.
Ligands attached to the surface of immunoliposomes containing PEG are sterically inhibited from binding to target epitopes on the cell surface at low mAb/PEG molar ratios (1). Ligands can be conjugated to liposomes *via* a spacer molecule (e.g., avidin) and in this case, cell binding can proceeds unhindered by PEG (2). However, initial ligand coupling efficiency may be reduced by the presence of PEG on the liposomes. Two-step method of cell binding of ligand-liposomes has been achieved by biotin-labelled liposomes to chase streptavidin conjugated Abs (3). Ligands can be conjugated at the distal end of a spacer endgroup functionalised molecules (e.g., functionalised PEG-lipid derivatives) and cell binding proceeds unhindered by PEG. Adapted from (15).

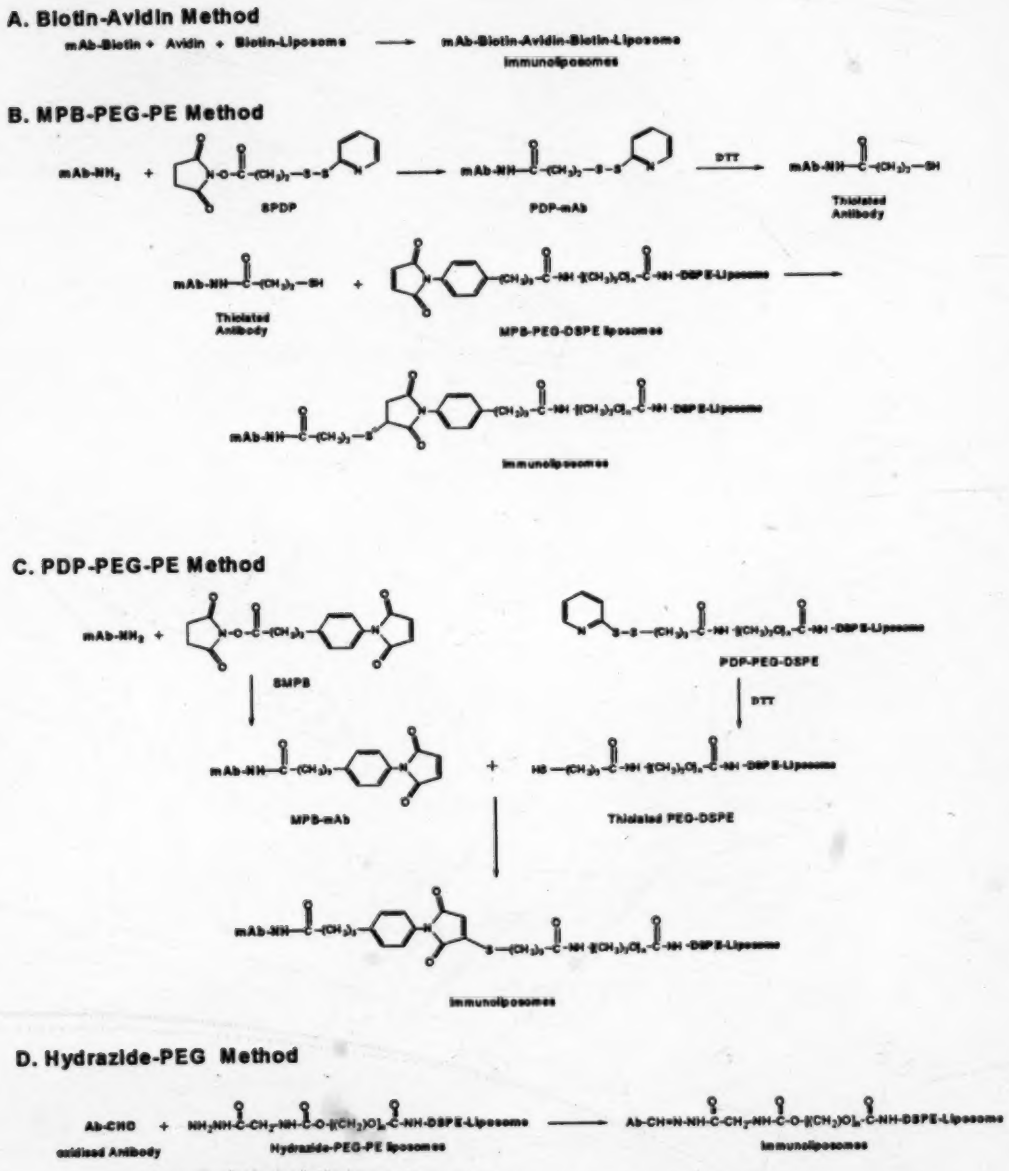

Figure 1.10. Schematics of various strategies for coupling antibodies or ligands to SL.
(Adapted from (53))

to biotinylated liposomes *via* an avidin or streptavidin bridge (144-150) (Fig. 1.8, 1.10). A variation on this is the two-step approach. In this case, a biotinylated antibody or ligand is first allowed to bind to the receptor, and subsequently is chased with streptavidin-liposomes (Fig. 1.9) (151, 152). Although this non-covalent approach appears to be simple, it has low coupling efficiency, is prone to liposome aggregation, and avidin and streptavidin are potentially immunogenic. Hence the applicability of the non-covalent methodologies for human use may be limited.

There are three main covalent methods for the attachment of ligands or antibodies to liposomes and they are illustrated in Figures 8-10 with their variations. Prior to the development of polymer-grafted long circulating liposomes, most of the coupling procedures involved the attachment of the ligands directly to the surface of preformed liposomes by conjugating the antibodies to the polar head groups of phospholipids (53, 153-156). Symmetric bifunctional cross-linking agents like glutyraldehyde, suberimidate, and carbodiimide allow coupling between the amine group of PE and amino groups on antibodies. However, these bifunctional cross-linking reagents often result in the aggregation of the proteins or liposomes. As a result, heterobifunctional cross-linkers were developed and were able to minimize some of these problems as the two functional ends of the reagent have different cross-linking entities (53).

Most heterobifunctional coupling reagents modify an amino group on the headgroup of phosphatidylethanolamine (PE) (53), and usually relies on the formation of a thiolether bond between the ligands, antibody or antibody fragments and pre-formed liposomes (Fig. 1.9). Liposomes containing N-pyridyldithiopropionyl-PE (PDP-PE) can

be reduced to give free thiol groups and can be coupled *via* thiol-ether linkages to maleimide groups introduced onto proteins, using a heterobifunctional cross linker such as N-succinimidyl-4-(p-maleimidophenyl)butyrate (SMPB) (153, 157). The reaction can also be reversed, presenting the maleimide groups on the liposomes and the thiol groups on the proteins (158) (Fig. 1.9).

Another approach covalently links the antibody to a phospholipid anchor, usually a derivative of PE prior to the formation of the liposomes (159). This method involves carbodiimide activation of ligands followed by coupling to carboxyl groups on the lipid anchor N-glutaryl-PE activated with N-hydroxysulfosuccinimide (159-164). Immunoliposomes using this method were prepared by either direct hydration of these Ab-lipid conjugates or by solubilizing the Ab-lipid conjugates in detergent in the presence of phospholipids and cholesterol, and forming immunoliposomes by dialyzing away the detergent (159-161). The major disadvantage of this approach is the orientation of an unknown portion of the Ab to the liposomes interior, where they are unavailable for binding.

With the development of polymer-grafted liposomes, alternative strategies have evolved to attach the antibodies to the distal ends of functionalised PEG-lipid conjugates (53, 165). The dynamic movement of PEG polymer chains on the surface of liposomes, was found to sterically hinder the approach of Ab to the phospholipid headgroup region of the liposomes surface and resulted in low coupling efficiencies for PEG-liposomes (53). As a result, new strategies are being developed to form PEG-immunoliposomes, where ligands could first coupled to the liposome surface or attached to PEG, as previously

described, and in a subsequent step, PEG in micellar form could then transferred into these immunoliposomes (166) (Fig. 1.8) . Alternatively, thiolated antibodies could be coupled to maleimidophenyl butyrate-PE (MPB-PE)-containing liposomes, followed by the chemical conjugation of PEG at the liposome surface. Although both methods were able to introduce antibodies to the outer surface of liposomes, the PEG chains on liposomes were found to sterically hinder target binding of the Ab (Fig. 1.8).

The most successful strategies have involved direct attachment of antibodies to the terminus of PEG using functionalised PEG-lipid conjugates. The lipid-PEG-ligand conjugate may be either incorporated either before or after liposomes preparation. Thiol, amino-succinimidyl-, carboxyl- and hydrazide groups have been introduced onto the PEG terminus. As described earlier, reactive thiols on antibodies or liposomes, form stable thiol-ether linkages with maleimide residues introduced on liposomes or antibodies, respectively.

Two commonly used functionalised PEGs are PDP-PEG-PE, which react with maleimide derivatized Abs to form immunoliposomes, and MPB-PEG-PE, which reacts with thiol-derivatized Abs (Fig. 1.9). In a different approach, proteins activated by carbodiimide have been attached to the carboxyl-derivatized PEG (167). Immunoliposomes have also been prepared by incorporating hydrazide-derivatized PEG into liposomes during their preparation (53, 168-171). This method involves the oxidation of the antibody at carbohydrate residues on the antibody Fc regions (168). The reactive aldehydes generated during oxidation are capable of condensation with the hydrazides on the distal ends of PEG forming stable hydrazone linkages. This is a relatively simple

procedure which immobilizes the antibody through the Fc region, exposing the binding regions. The hydrazide functional group has a pKa of 3.0, so it is stable at physiological pH and dissociates at low pH (172).

1.1.13 Targeted liposomal systems.

Several parameters determine the overall effectiveness of antibody-targeted liposomal therapeutics. Among these factors, are the binding affinities of the targeting molecule to its antigen, the rate of dissociation of this complex, and the density of the antigen at the cell surface. Ideally, the target antigen would be expressed only by tumour tissues, and not by normal tissues, which would improve the selectivity of targeting. While tumour-specific antigens are not wide-spread, several cancers overexpress antigens, e.g., HER2 (165), or express modified normal antigens, e.g., mucin-I (173). This provides a window of opportunity to target tumour cells to a greater extent than normal tissues.

Problems associated with antibody-based therapies include: tumour cell heterogeneity and down-regulation or loss of epitopes during tumour growth and lack of access of the Ab-particulates into the tumour interior (174). Some tumours shed antigens into the blood. This is useful as a diagnostic tool but creates problems for drug targeting (175). Circulating antigens will bind to antibody-targeted delivery systems triggering their removal from circulation and preventing them from reaching their desired targets. One strategy to handle this would be the depletion, or inactivation of the soluble antigen by pre-injecting a sufficient quantity of free antibody prior to the targeted liposomal therapy. Additional problems arises when attempting to treat large solid tumours with Ab-based therapies. The penetrability of immunoliposomes into solid tumours may be restricted by

the "binding site barrier" (174). In this case, it is hypothesized that immunoliposomes would bind the first target cells they encounter, usually at the tumour exterior, restricting the penetration of the targeted liposomes into the inner tumour mass.

A major concern with the use of antibody-based therapies is the potential of generating a host immune response to the foreign protein (4, 176-178). Most antibodies are currently of murine origin, and murine antibodies when administered to humans, have been shown to elicit a human anti-mouse antibody response (HAMA) (4, 176, 179, 180). This results in part through the recognition of the Fc region of the antibody by the cells of the immune system, particularly macrophages which have Fc receptors (181, 182). This problem can be addressed in several ways. Recent advances in the production of chimerized or humanized Abs reduces the potential for HAMA, but does not eliminate it completely (4, 176). The use of antibody fragments, such as $F(ab)_2$, Fab' (165), single chain (Sv) fragments (183) or humanized antibodies (184) may have decreased immunogenic potential, but this remains to be tested. Alternatively, one could eliminate the potential for HAMA completely through the use of various endogenously ligands as targeting molecules, e.g., growth factors, folate, transferrin, asialofetiun, peptide sequences to adhesion receptors, carbohydrates, glycoproteins or apolipoproteins. The potential problems with this last approach is that these ligand receptors, although often overexpressed on tumours, are also expressed on normal tissues. Therefore, some non-specific activity against normal cells may occur.

Over the years, the area of antibody-targeted liposomes has attracted increasing interest. Many different targeting moieties directed to a variety of targeting sites have

been attached to liposomes. Monoclonal antibodies have been the most widely used molecules for liposome targeting, however, numerous other ligands have also been investigated to target various cell antigens and receptors (151, 160, 167, 178, 185-203) or tumour associated antigens (162, 204-207). These include, peptides (170), proteins and lipoproteins (208, 209), carbohydrates (210-212), glycoproteins (185, 213, 214), growth factors and vitamins (196, 215) (and reviewed in (15, 16, 175, 216)).

1.1.14 *In vivo* therapeutics in experimental models.

The first demonstration of *in vivo* targeting of long-circulating immunoliposomes was from Maruyama et al. (159). They demonstrated that as much as 50% of an injected dose of GM_1-immunoliposomes conjugated to a monoclonal antibody (34A) against a anticoagulant glycoprotein thrombomodulin expressed on capillary lung endothelial cells was shown to localize into lungs (159). The targeted liposomes demonstrated significantly increased binding and retention of liposomes in lung compared to immunoliposomes lacking the targeting antibody. Similarly, PEG-immunoliposomes conjugated to the same antibody 34A, were able to show increased recognition of liposomes for rat lung endothelial tissue.

Torchilin et al., have described successful *in vivo* targeting of PEG immunoliposomes to infarcted rabbit heart. Experimentally induced-cardiac infarcts, were treated with PEG-immunoliposomes coupled to antimyosin Fab' fragments. Significantly increased numbers of immunoliposomes bound to myosin, exposed as a result of cellular hypoxic damage in the infarcted hearts (162, 217). In another experiment, binding of anti-myosin immunoliposomes to a cytoskeletal antigen of rat embryonic cardiocytes were

shown to increase cell-viability compared to untreated controls, presumably by sealing the sites where the cell membranes had been ruptured as a result of ischemic damage (218). On similar lines, oxidative injury in fetal lungs as a result of oxygen supplementation, is another interesting applications where targeted liposomes have been utilized in experimentally-induced conditions (219). pH-sensitive liposomes containing surfactant protein-A were able to deliver five-fold higher enzyme superoxide dismutase to fetal rat lung distal epithelial cells under oxidative stress, compared to non-targeted liposomes (219).

There are very few models where the therapeutic effectiveness of immunoliposomes have actually been studied. The first successful therapy with immunoliposomes was in a murine model of lung squamous cell carcinoma cell line (KLN-205) (146, 147). Ahmad and Allen demonstrated that KLN-205 cells, seeded into the mouse lung following i.v. injection, could be effectively targeted at day 3 after cell implantation with immunoliposomal DXR coupled to mAb 174H.64 (146). A significant improvement in therapeutic effectiveness, with some long-term survivors was observed for the immunoliposomes compared to free drug or antibody-free SL (146, 185). However, when mice were treated one to three weeks following cell implantation, the immunoliposomes lost their effectiveness (185). These results may reflect the restricted ability of the immunoliposomes to penetrate into some types of large solid tumours due to the "binding site barrier", described earlier.

Bankert et al. showed that liposomes loaded with Ara-C and bearing anti-idiotypic Abs to an idiotype specific for an Ig receptor on the surface of a murine B-cell tumour,

2C3, was able to suppress the growth of tumour in the spleen of mice, but did not affect the growth of the same tumour in the peritoneum (220). In other experiments, human ovarian carcinoma cells (OVCAR-3) were found to specifically bind immunoliposomes *in vitro* but did not demonstrate any improved therapy with the targeted liposomes in i.p. xenografts of the ascitic tumour in nude mice (207, 324). Lack of internalization of the antibody-targeted liposomes after target-cell binding, along with leaky drug formulations was suggested as an explanation. The drug released at the cell surface *in vivo* from the leaky formulations would rapidly redistribute away from target cells.

EMT-6 mouse mammary carcinoma cells, which seed into murine lungs after i.v. injection, were targeted with GM_1-immunoliposomes bearing the antibody 34A, which bind to lung endothelial cells, and carrying the lipophilic prodrug 3',5'-o-dipalmitoyl-5-fluoro-2'-deoxyuridine (dpFUdR) (201). In this case, the prodrug, released in close proximity to the target EMT-6 cells, demonstrated a significant effect (165% T/C) when the treatments were initiated one and three days post inoculation of tumour cells, and the immunoliposomes were superior to non-targeted liposomes or free drug (201). In this model, the physiological characteristics of lung capillaries permitted drug molecules to be retained in close proximity to the site of implantation of tumour cells, with the bound liposomes acting as depots for sustained drug release in the lungs (201). As this targeting approach does not directly target tumour cells but normal cells in the vicinity of the tumour, clearly toxicities to the normal tissue would be expected.

In other studies, Caov.3 ovarian xenografts implanted s.c. in nude mice were treated in an advanced stage of tumour development with immunoliposomal doxorubicin

coupled to mAb B43.13 by the i.v. route (185). Treatment with immunoliposomal DXR was less effective than the non-targeted liposomal DXR (185). This may reflect the greater penetrability of the non-targeted *versus* the targeted liposomes into these larger tumours.

Some promising recent targeting results have been obtained with $HER2^{neu}$-overexpressing breast tumour xenografts in nude mice (16). DXR delivered *via* humanized anti-HER2-Fab' antibody fragments coupled to liposomes significantly increased the antitumour activity and the immunoliposomal drug resulted in improved cytotoxicity compared to either the free drug or non-targeted liposomes in this solid tumour model (16, 165, 206). The penetration of immunoliposomes in this solid tumour model was not affected by the occurrence of the "binding-site" barrier (described earlier). These results may be explained by the inherent physiology of this breast tumour xenografts, i.e., extent of vascularization and presence of interstitial spaces, that may allow greater percolation of liposomes into the tumour. In this model, the breast cancer cells expressed a high density of the targeted antigen, there was a high binding affinity of the anti-HER2-Fab'-immunoliposomes, and the binding resulted in internalization of the liposome-drug package, all of which probably contribute to the observed results (165, 206).

With the exception of the results with the anti-HER2-immunoliposomes, the above results suggested that immunoliposomes performed better when they had unrestricted access to their target cell, e.g., very small tumours, or sites accessible from the vasculature like damaged heart cells or lung endothelial cells. A consideration of the

results to date suggest that hematological malignancies, where immunoliposomes have unrestricted access to single cells in blood, may result in successful therapy with immunoliposomes.

1.1.15 Hematological malignancies: B-cell lymphomas and multiple myeloma.

The majority of hematological cancers are B and T cell malignancies (221). Circulating populations of B and T lymphocytes originate from pluripotent stem cells at sites of hematopoiesis such as fetal liver and bone marrow (222, 223) (Fig. 1.11). Prior to their differentiation into either B or T cells, lymphocytic precursors enter a highly regulated program of lymphocyte maturation. B cells in the bone marrow and T cells in the thymus undergo stages of selection that removes lymphocytes that are defective or possess self-reactive antigen receptors (224, 225). Both cell types use similar mechanisms for their immune receptor assembly, and they activate similar, but not identical, pathways upon antigen-receptor and coreceptor stimulation. In the peripheral system, B and T cells act on different cells, and have different functions. While T cells are primarily involved in mediating cellular immunity, B cells are involved in the host humoral immune response.

T cells mature in the thymus, and develop specific antigen receptors, T-cell receptors (TCR) that allow them to recognise specific endogenous antigens. Unlike the immunoglobulin (Ig) molecules, TCR do not recognize soluble antigens (223). TCR molecules are associated with a variety of surface receptors, namely, CD2, CD3, CD4, CD8, CD45, or CD28 (226, 227). Engagement of the receptors or coreceptors with complementary molecules forming receptor-complexes has been shown to be necessary for a complete response of T cells to recognized antigens. Different T lymphocyte

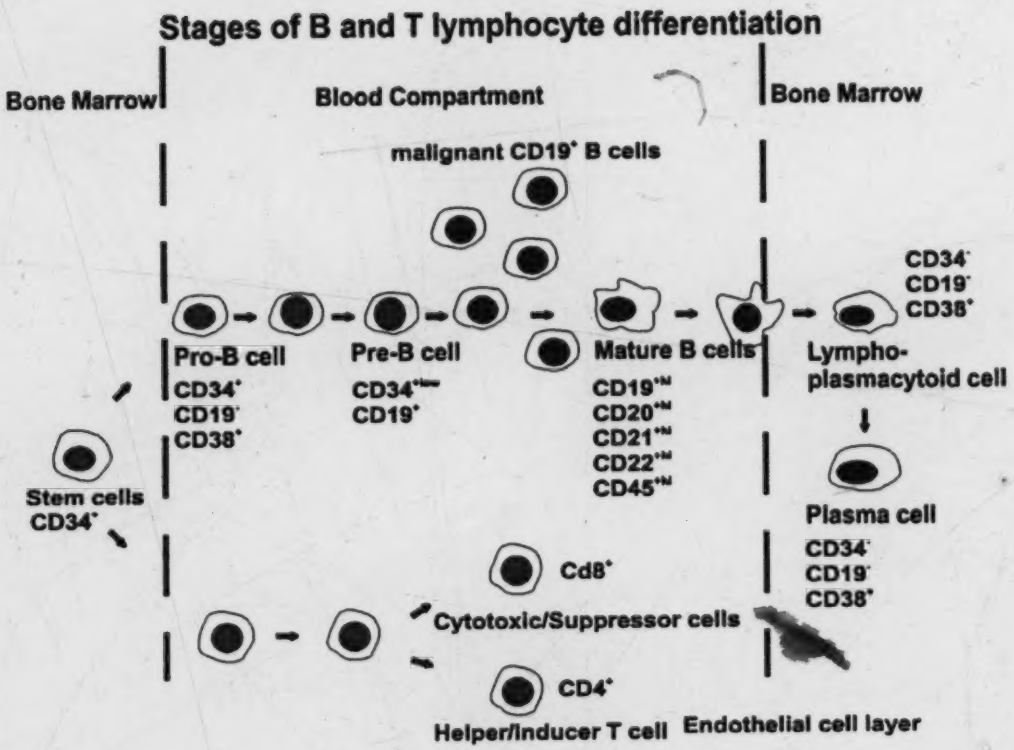

Figure 1.11. Stages of B- and T-lymphocyte differentiation.
B and T cells originate from the pluripotent stem cells in the bone marrow and mature through a series of differentiation and maturation events as illustrated. B-cell lymphomas and MM are characterized by a regenerative, malignant lineage of B cells, which may derive from any of the B-cell subsets. In MM, malignant B cells are suggested to continuously differentiate into plasma cells which populate the bone marrow to cause overt symptoms of MM.

subpopulations exist with different effector functions, mainly T-helper (CD4) and T-cytotoxic (CD8) cells (226) (Fig. 1.11). T cells interact with specific antigens presented on the surface of special antigen-presentation cells *via* the major histocompatibility complex, MHC, displaying either class II MHC ($CD4^+$ T cells) (228) or class I MHC molecules ($CD8^+$ T cells) (229, 230). $CD8^+$ T cells mediate a variety of cytotoxic functions, like destruction of virus-infected cells, and are referred to as cytotoxic T cells. In contrast, $CD4^+$ helper T cells are involved in the secretion of lymphokines, they support antigen-dependent differentiation and the expansion of cytotoxic T cells (223).

B cells are the major cell type involved in humoral immunity (222, 231). Early B cell development starts in the fetal liver and then continues in the bone marrow (232) (Fig. 1.11). The first cell type derived from the pluripotent stem cell which is committed towards B-lineage is the "pro-B cell" (232). Cells of the B lineage expand in the lymphoid organs and in the bone marrow. In these tissues, the presence of soluble mediators like cytokines and growth factors may be needed for early B-cell development. During maturation these cells migrate towards the centre of the bone marrow, and exit into the circulation *via* the capillary sinuses. B cells initially reside in the bone marrow, migrate into blood and finally the bone marrow where they mature into plasma cells (225, 232) (Fig. 1.11).

B-effector cells, and particularly plasma cells which are end-stage differentiated B cells, produce immunoglobulins that are capable of binding to soluble or cell-surface antigens (231). Naive B cells carry membrane receptors on their cell surface that are necessary for cellular activation and differentiation during B-cell maturation. During B

lymphocyte development, the assembly of the multiple variable (V), diversity (D) and joining (J) regions of the gene is directed by DNA rearrangements at the immunoglobulin loci to form exons encoding the heavy and light chains of the Ab molecule (233). The patterns of heavy and light chain immunoglobulin (Ig) gene rearrangements, and Ig protein expression, either surface or cytoplasmic, are associated with different stages of B cell development (233, 234). Some of the distinct phenotypes expressed on B cells during maturation are illustrated in Fig. 1.11 (222, 225, 235). B cells are capable of internalizing a variety of antigens, and further processing them for presentation to T cells (228).

Most B cells express surface IgM and IgD, but rarely other Ig isotypes. Membrane-associated Ig have structural homologies to secreted Ig. Immunoglobulins present on B cells are usually associated with CD79 molecules and have potential signal transduction functions (225). Membrane Igs form a part of a B-cell receptor complex with coreceptors such as CD19, CD21, CD22 (222, 225, 236). Activation of these molecules usually modulates antigen-receptor signalling in B cells which determines the B-cell response to the antigen (225, 237). At present there are several accessory molecules known to bind coreceptors on B cells, namely, the CD19/CD21 complex, CD20, CD22, CD24, CD40, CD45 (225, 236-240).

CD19 and CD21 noncovalently associate to form a multimeric complex on the B cell surface (236, 237). CD19 is a 95 kD Ig superfamily of glycoprotein expressed from early stages of B cell development until the late B cell stage (237). Not much is known about the function of CD19 on B cells. However, activation of CD19 *in vitro* has been implicated in increased tyrosine phosphorylation, activation of phospholipase C, inositol

(IP3) turnover, calcium mobilization, and stimulation of serine-specific protein kinases (234, 241, 242).

Human malignancies involving the cells of the B-lineage are usually classified according to their stages of B-lymphocyte differentiation. Clonal expansion of B cells may be restricted to blood or may involve tissues through which these cells transit, particularly the lymph nodes. These include malignancies of either early precursors (i.e., pre-B cells, or pro-B cells), B cells or plasma cells[2]. Immunophenotypically, B-cell lymphomas and leukemias express B cell differentiation antigens, in particular CD19, CD20 and CD22, monotypic surface immunoglobulin (usually IgM heavy chain) and μ and λ light chains[2].

B-cell lymphomas comprise a diverse group of cancers that range from relatively indolent low grade diseases to extremely aggressive forms (243, 244). Historically, malignant lymphomas were divided into Hodgkin's and non-Hodgkin's lymphoma, based on differences in histology and disease progression. Many malignant B-cell lymphomas are characterised by genetic abnormalities, where chromosomal translocations (or rearrangement) lead to oncogenic mutations. At the molecular level, several translocations, i.e., t9 (2;8) (q12; q24) and t(8;22) (q24; q11 or q12) in lymphomas have been described[2], and have been suggested to play a role in the pathogenesis of B-cell malignancies. The progression and transformation of a B-cell clone into a malignant form is usually accomplished by a variety of pathways, namely, activation of oncogenes (MYC, LAZ3), and/or deletion and mutation of tumour suppressor genes (p53). In addition,

---

[2] Canellos, G.P., Lister, T.A., and Sklar, J.L. (eds.), The lymphomas, W.B. Saunders Co., Philadelphia, 1998.

Epstein-Barr Virus (EBV), a lymphotropic herpes virus, is presently the best known viral contributor in the development of human lymphomas and is associated with increasing numbers of patients with human B-cell malignancies.

Most B cell malignancies are sensitive to chemotherapy and radiotherapy. Patients with low or intermediate grade disease may undergo remission after first line chemotherapy, however, patients with high grade disease are usually not curable with standard chemotherapy. Current chemotherapeutic protocols usually consists of a combination of anticancer drugs, including cyclophosphamide (C), doxorubicin (A), methotrexate (M), prednisone (P), bleomycin (B), dexamethasone (D) or vincristine (V) (245, 246). The most common regimens include: CAVP, MBACVD or MACVBP. High-dose chemotherapy and autologous bone marrow transplants has established itself as a salvage therapy for several patients with refractory or relapsed B-cell lymphoma. More recently several biological therapeutic approaches are under clinical investigation for B-cell lymphoma. These include utilization of inteferons (IFN), monoclonal antibody-based approaches, cytokines and growth factor therapy.

Multiple myeloma is the most common of the plasma cell dyscrasias, and is characterized by bone marrow infiltration of the terminally differentiated neoplastic plasma cells (247-249). The disease is manifested by severe bone destruction, hypercalcemia, elevated blood protein spikes (M-protein), Bence Jones proteinuria and ensuing kidney stress (248). The incidence of myeloma has been increasing in recent years with nearly 13,000 people diagnosed every year in the USA alone (250, 251). The current incidence stands at approximately 3 in 100,000 people (250). In MM, mortality rates are very

similar to the incidence rates, because almost all of the people who develop the disease eventually succumb to the disease within 2.5-3.5 years after diagnosis or onset of treatment (247-249, 251)

Plasma cells are the end-effector cells of the B lymphocyte lineage that produce and secrete antigen-specific antibodies (252). They originate from hematopoietic stem cells in the bone marrow, and then maturate to B cells and consequently to plasma cells through a series of activation, proliferation, and differentiation stages (231). Historically, considered a malignancy of the plasma cells (249), the identity of malignant stem cells in MM is still under debate (253-257). Recent evidence implicates a circulating population of malignant B lymphocytes in the pathogenesis of MM (258, 259). Patients with MM have been shown to have abnormal numbers of B cells in peripheral blood. Continuously differentiating, monoclonal B cells have been reported, with extensive DNA aneuploidy (255, 259). The fact that MM B cells display characteristics consistent with invasive progenitors of plasma cells, i.e. expression of cellular differentiation antigens and adhesion receptors for binding and extravasation, led to speculation that this population of malignant B cells may be involved in the pathogenesis of MM (255, 257, 260-263).

Conventional chemotherapy is the usual treatment for MM patients. Aggressive chemotherapy in MM usually involves a combination of drugs, containing one or more of the following anticancer drugs: doxorubicin (adriamycin, A), vincristine (V), nitrosureas (BCNU, B), melphalan (M), dexamethasone (D), prednisolone (P) and cyclophosphamide (C). Combination chemotherapies for MM include: ABCM, VAD, BCP, MP, and VBAD (264). In addition, MM is radiosensitive cancer and hence radiotherapy remains an

important adjunct to chemotherapy for local lesions. However, with conventional chemotherapy and/or radiotherapy, complete remissions are very rare (264). Patients that initially respond to either or both treatments, in nearly all cases fatally relapse within a couple of years.

Recent therapeutic approaches for MM have moderately improved the outlook for MM patients. Interferons (IFN), display potent inhibitory effects on cell growth by interfering with one or more cellular biochemical processes, including, alteration of expression of several genes, namely, c-myc, c-fos etc. (265). High-risk patients with MM treated with IFN therapy display improved response with this new approach (266). High-dose chemotherapy and whole body irradiation, alone or in conjunction with a bone marrow (BM) transplant has been shown to improve relapse-free intervals (264, 267). The rationale behind BM transplantation is that BM ablative therapy may have the potential to eradicate the malignant disease, which after BM transplantation, would have the potential to regenerate the immune system after cessation of treatment.

Resistance to chemotherapy is a common problem in myeloma and at least 30% of patients are resistant to primary chemotherapy (264). In many cases, drug resistance is associated with the expression of the multidrug resistant (MDR) phenotype. A 170 kDa glycoprotein, called P-glycoprotein (P-gp) is a product of the MDR gene known to be overexpressed on resistant cells (268, 269). The P-gp transporter functions by modulating drug efflux from cells, and is a substrate for a variety of structurally dissimilar chemotherapeutics including, doxorubicin (269). The extent of overexpression of Pgp on malignant B cells in MM has been correlated with resistance to chemotherapeutics (258,

270-273). Efforts to overcome drug resistance include the use of high dose chemotherapy and combination treatments with drugs which are not substrates for MDR transport (264). More recently, several drugs including cyclosporine and verapamil have been shown to reverse drug resistance *in vitro*, and based on the positive results *in vitro*, clinical trials are currently underway in patients with refractory disease and undergoing VAD therapy (273-275).

In spite of these recent advances in treatments for B-cell lymphomas and multiple myeloma, complete remissions can only be achieved in patients with low or intermediate grade B-cell lymphomas. In the case of high grade B-cell lymphomas or MM, standard chemotherapy is generally ineffective and eventually almost all patients relapse and become refractory to further treatment. Both these diseases are still largely incurable, and hence there remains a need for the development of new drug treatment alternatives for these cancers. One new approach is the subject of this thesis.

1.2 HYPOTHESIS AND OBJECTIVES

Most anticancer agents, including doxorubicin, are limited in their clinical use due to severe dose-limiting toxicities. Encapsulation of drugs within drug delivery systems like liposomes may decrease some of the harmful side effects and improve patient response. This is related to liposome-mediated changes in the pharmacokinetics in general and distribution of entrapped anticancer drugs in particular. The selective targeting of liposomal anticancer drugs *via* specific antibodies (resulting in immunoliposomes) against antigens expressed on malignant cells could improve the therapeutic effectiveness of liposomal preparations as well as reduce some of the adverse side effects associated with conventional chemotherapy.

The applicability of immunoliposomes in the treatment of human B-cell diseases including multiple myeloma (MM) and B-cell lymphoma has not yet been explored. Clonal expansion of malignant B cells resident in blood of B-cell lymphoma or MM patients may be unique targets for immunoliposomal therapy. Long-circulating liposomes (SL) containing the anticancer drug doxorubicin (DXR), and coupled to the monoclonal antibody anti-CD19 (SIL[anti-CD19]) may be useful in the treatment of hematological B-cell cancers, where the SIL[anti-CD19] may have unrestricted access to the malignant B cells in blood. Specific binding and internalization of the DXR-SIL[anti-CD19] drug package *via* the internalizing CD19 leucocyte differentiation antigen could deliver higher drug levels to cells leading to improved cytotoxicity, compared to non-targeted DXR-SL or free drug. This strategy may allow selective targeting and eradication of malignant B cells from blood of B-cell lymphoma or MM patients, improving patient survival. This

approach may have an additional advantage of preventing non-specific toxicities to other cells, in particular T lymphocytes, preserving T-cell-mediated immunity in patients.

The research objectives of this thesis were to evaluate the application of immunoliposomal therapy in B-cell cancers. In order for immunoliposomes to be clinically useful, they must be able to satisfy certain criteria. This thesis examines several of these criteria, namely, formulation of immunoliposomal preparations, coupling of antibodies to liposomes, *in vitro* binding characteristic of immunoliposomes, cytotoxicity of immunoliposomal drugs, *in vivo* pharmacokinetics and therapeutic effectiveness in xenograft models of human B-cell cancers in severely compromised immunodeficient (SCID) mice. This thesis describes some of the first liposome targeting results to $CD19^+$ human B cell cancers.

Chapter 3 deals with *in vitro* and *in vivo* targeting of human B-cell lymphoma (Namalwa cell line). An animal model of human B-lymphoma has been developed in SCID mice. The application of DXR-SIL[anti-CD19] in targeting and therapeutic studies has been examined. *In vivo* pharmacokinetics were conducted in both naive outbred mice and tumour-bearing SCID mice. The circulation time of immunoliposomes in outbred mice and their ability to target Namalwa cells in tumour-bearing mice was studied. To test the effectiveness of the targeted liposomes *in vivo*, therapeutic experiments were done to compare the targeted liposomal drug *versus* free drug or various non-targeted liposomal drug formulations in SCID mice xenografts of the B-cell lymphoma. Parameters studied included: different drug formulations, routes of tumour cell implantation, routes of treatments, tumour-cell burden, dose and dosing schedule.

In Chapter 4, the cellular trafficking and internalization of DXR-SIL[anti-CD19] by Namalwa cells *in vitro* was examined. Recognition of immunoliposomes by Namalwa cells was studied with fluorescent liposomes and flow cytometry. The drug uptake into cells was quantified using HPLC and attempts were made to correlate this with cellular cytotoxicity using various cytotoxicity assays. Two independent *in vitro* assays were used to examine the mechanisms for the intracellular handling of liposomes by Namalwa cells: a fluorimetric method to monitor the intracellular pH using a pH-sensitive pyranine probe encapsulated into liposomes, and direct visualization of the intracellular distribution of liposomes using confocal imaging microscopy.

In Chapter 5, we evaluated the applicability of immunoliposomes in the treatment of human multiple myeloma using similar assays to those described above. This chapter incorporates work done on the targeting of DXR-SIL[anti-CD19] to human peripheral blood mononuclear cells from MM patients.

CHAPTER 2

In vitro and *in vivo* targeting of immunoliposomal doxorubicin to human B-cell lymphoma

(Cancer Res. *58*: 3320-3330, 1998)

2.1 ABSTRACT

The ability to selectively target liposomal anticancer drugs *via* specific ligands against antigens expressed on malignant cells could improve the therapeutic effectiveness of the liposomal preparations as well as reduce adverse side effects associated with chemotherapy. Long-circulating formulations of liposomes containing lipid derivatives of poly(ethyleneglycol) (PEG) (sterically stabilized liposomes, SL) have been described previously and new techniques have recently been developed for coupling monoclonal antibodies (mAb) at the PEG terminus of these liposomes. Antibody-targeted SL (immunoliposomes, SIL) containing entrapped anticancer drugs are predicted to be useful in the treatment of hematological malignancies such as B-cell lymphomas or multiple myeloma (MM) where the target cells are present in the vasculature.

The specific binding, *in vitro* cytotoxicity and *in vivo* antineoplastic activity of doxorubicin (DXR) encapsulated in SIL coupled to the mAb anti-CD19 (SIL[anti-CD19]) was investigated against malignant B cells expressing CD19 surface antigens. Binding experiments with SIL[anti-CD19] resulted in a three-fold higher association of the SIL with a human $CD19^+$ B lymphoma cell line (Namalwa) in comparison with non-targeted SL. Using flow cytometry, fluorescently-labelled SIL[anti-CD19] bound to B cells, with no recognition of T cells in a mixture of B and T cells in culture. Non-targeted SL demonstrated significantly lower recognition of either B or T cells. Targeted DXR-SIL[anti-CD19] displayed a higher cytotoxicity to B cells relative to DXR entrapped in non-targeted SL.

Therapeutic experiments in SCID mice implanted with Namalwa cells by the i.v. or

i.p. routes, resulted in significantly increased effectiveness of DXR-SIL[anti-CD19] compared to similar amounts of free DXR, DXR-SL (no Ab) or isotype-matched non-specific antibodies attached to DXR-SL. Single doses (3 mg/kg) DXR-SIL[anti-CD19] administered i.v. resulted in a significantly improved therapeutic benefit, including some long-term survivors. From our results, we infer that targeted anti-CD19 liposomes containing the anticancer drug DXR may be selectively cytotoxic for B cells, and may be useful in the selective elimination of circulating malignant B cells *in vivo*.

2.2 INTRODUCTION

B-cell malignancies (B-cell leukemias/lymphomas and multiple myeloma (MM)) remain a major group of human hematological cancers and are still largely incurable (247, 257, 276, 277). Their immunological features, and clinical prognosis are dependent on the malignant expansion of a clonal B-cell phenotype, and the diseased cells are confined mainly in the vascular compartment. Most patients initially respond to conventional chemotherapy and/or radiotherapy, but in nearly all cases the disease recurs and becomes refractory to further treatment.

Recent therapeutic approaches to cancer have focussed on developing novel delivery systems to increase the therapeutic indices of anticancer agents by targeting drugs to diseased cells and away from normal tissues (12). One approach utilizes the expression of cell-surface epitopes as unique targets for the selective delivery of antibody-based therapies (i.e. immunoconjugates, radiolabelled antibodies, Ab-polymer conjugates or immunoliposomes) (4, 7, 11, 13, 14, 185, 216, 278, 279). Liposome encapsulation of

anticancer drugs can alter their pharmacokinetics and biodistribution resulting in increased efficacy and/or decreased toxicity (47, 51, 86, 280, 281). Long-circulating, dose-independent liposome formulations containing engrafted poly(ethyleneglycol) (PEG) on their surface (sterically stabilized or Stealth^{R} liposomes, SL) have been developed (71, 121, 123, 163, 282) and doxorubicin (DXR)-containing SL (Doxil^{R}) has been approved in a number of countries for treatment of Kaposi's sarcoma (142).

With the recent development of methods for coupling specific ligands to the PEG terminus of SL (53, 165, 167, 168, 283, 284), new opportunities exist for use of immunoliposomes as homing devices for selective targeting of anticancer drugs to diseased cells (146, 147, 185, 202, 216, 217, 285). A few studies have shown that sterically stabilized immunoliposomes (SIL) have significantly increased target cell binding *in vitro* (53, 147, 202, 284, 285) and result in improved therapeutic efficacy *in vivo* in the treatment of early (micrometastatic) solid tumours (146, 185). However, SIL appear to lose their advantage in treating more advanced solid tumours (185), likely because the "binding site barrier" restricts penetration of the SIL into the tumour interior (174, 286).

Targeting of immunoliposomes within the vasculature, where the SIL should have unrestricted access to malignant cells, is a feasible strategy for the treatment of hematological diseases (e.g. B or T cell malignancies and MM). In particular, this strategy may allow selective eradication of the malignant B cell population from the blood of B-cell lymphoma (or MM) patients. Selective targeting of the malignant B cells may have the additional advantage of preventing non-specific toxicity to T cells, preserving T cell mediated immune responses in patients. A further advantage might come from the

ability of the SIL to overcome multidrug resistance (MDR) in B cells (258, 270, 271). Targeting an internalizing CD19 epitope, may result in enhanced delivery of the liposome-drug package to the cell interior *via* the lysosomes, bypassing the plasma membrane MDR pump mechanism.

The CD19 receptors are exclusively expressed on most B-lineage malignancies, and are absent on haematopoietic stem cells in the bone marrow (287, 288). This approach allows targeting to the malignant cells, leaving the progenitor population intact. The free anti-CD19 antibody, by itself, has cytotoxic effects and is currently in preclinical and clinical trials for the therapy of B-cell leukemias and lymphomas, conjugated to toxins or as targeted radiotherapy (9, 288-293).

In this study, we selectively targeted $CD19^+$ malignant B cells *in vitro* and *in vivo* with DXR-containing SIL, coupled with a mAb anti-CD19 (DXR-SIL[anti-CD19]). A $CD19^+$ human B-cell lymphoma (Namalwa cell line) which grows readily in SCID mice was chosen as a model system to examine liposome targeting. In these experiments, we demonstrate increased targeting and specific cytotoxicity to Namalwa cells by DXR-SIL[anti-CD19] relative to DXR-SL or free DXR. In addition, *in vivo* pharmacokinetics and survival experiments were performed in SCID mice xenografts of the Namalwa cell line. Our results demonstrate that targeted immunoliposomal therapy compared to either DXR-SL, free DXR, or free antibody can result in a significantly improved therapeutic benefit in mice implanted with the B-cell tumour.

2.3 MATERIALS AND METHODS

2.3.1 Materials.

Hydrogenated soy phosphatidylcholine (HSPC), poly(ethyleneglycol) (molecular weight 2000) covalently linked to distearoylphosphatidylethanolamine (PEG_{2000}-DSPE) and hydrazide-derivatized PEG (Hz-PEG-DSPE) were generous gifts from SEQUUS Pharmaceuticals, Inc. (Menlo Park, CA) and have been described elsewhere (123, 168). Cholesterol (CHOL) and 12-[N-(nitrobenz-2-oxa-1,3-diazol-4-yl)amino]dodecanoyl phosphatidylethanolamine (NBD-PE) were purchased from Avanti Polar Lipids (Alabaster, AL). N-acetyl-methionine (NAM), Sephadex G50, Sepharose CL-4B, sodium periodate, and 3-[4,5-dimethylthiazol-2-yl]-2,5,-diphenyltetrazolium bromide (MTT) were purchased from Sigma Chemical Co. (St. Louis, MO). Doxorubicin (DXR, Adriamycin RDF) was obtained from Adria Laboratories Inc. (Mississauga, ON). RPMI 1640 media and fetal bovine serum (FBS) was purchased from Gibco BRL (Burlington, ON). Cholesteryl-[1,2- ^{3}H-(N)]-hexadecyl ether ([^{3}H]CHE), 1.48-2.22 TBq/mmol, was purchased from New England Nuclear (Mississauga, ON). Iodobeads were from Pierce Chemical Co. (Rockford, IL). Tyraminylinulin synthesis and preparation of [^{125}I]tyraminylinulin ([^{125}I]TI) has been previously described (294). All other chemicals were of analytical grade purity.

2.3.2 Mice.

Female CD1(ICR)BR outbred mice were obtained from Charles River (St. Constant, Quebec) and kept in standard housing. Female C.B.-17/Icr-Tac-SCID mice 4-6 weeks of age, weighing 18-20 g, were purchased from Taconic Farms (German Town,

NY). The SCID mice were housed and maintained in sterile enclosures under specific virus and antigen-free conditions. SCID mice were maintained on a specified diet with trimethoprim-sulphamethoxazole in their drinking water. Mice were used when they were 7-10 weeks old. All experiments were approved by the Health Sciences Animal Welfare Committee (University of Alberta).

2.3.3 Cell lines and antibodies.

Murine mAb anti-CD19 (from FMC-63 murine CD19 hybridoma) and isotype-matched control IgG2a (IAG.11) were obtained from Dr. H. Zola (Child Health Research Institute, North Adelaide, Australia) (295). The concentration of all mAb were determined by spectrophotometry (λ=280 nm) and the identification of mAb and purity of some batches was assessed by SDS-PAGE. All mAb reactivities were checked prior to use by indirect immunofluorescence using fluorescein isothiocyanate (FITC)-labelled goat anti-mouse IgG and fluorescence activated cell sorting (FACS) (Becton Dickinson, San Jose, CA) against appropriate cell lines. In FACS experiments, to discriminate individual populations of B and T cells, the following mAb-fluorescent conjugates were used: FMC63-FITC (anti-CD19-FITC conjugate), B1RD1 (anti-CD20-phycoerythrin (PhE)-conjugate) (Coulter, Hialiah, FL), and Leu-3-PhE (anti-CD4-PhE conjugate) (Becton Dickinson, San Jose, CA) along with the appropriate FITC or PhE-conjugated isotype-matched controls. Anti-CD45-PhE was mAb 17G10 from Dr. J. Wilkins, Univ. of Manitoba.

For iodination of mAb, 2 mg mAb in 300 µl 25 mM N-2-hydroxyethyl piperazine-N'-2-ethanesulphonic acid (HEPES), 140 mM NaCl (pH 7.4) was treated with 185 MBq

$Na^{125}I$ and 5 iodobeads in a 2 ml reaction vial at 22°C for 1 h. The resulting [^{125}I]mAb was desalted over a Sephadex G25 column in the same HEPES buffer to remove unreacted free ^{125}I. The specific activity of the [^{125}I]mAb radiolabel was determined from its γ counts.

The human B cell lymphoma line, Namalwa (ATCC CRL 1432) was obtained from American Type Culture Collection (Rockville, MD). A human T-lymphoma cell line (H9) (ATTC HTB 176) was a gift from Dr. L. Chang (Department of Medical Microbiology and Immunology, University of Alberta). All cell lines were grown as suspension cultures in RPMI1640 supplemented with 10 % heat-inactivated FBS and maintained at 37°C in a humidified incubator (90 % humidity) containing 5 % CO_2.

2.3.4 Preparation of liposomes.

Liposomes were composed of either HSPC:CHOL:mPEG$_{2000}$-DSPE at a 2:1:0.1 molar ratio of phospholipids (PL), or HSPC:CHOL:Hz-PEG$_{2000}$-DSPE (2:1:0.1 molar ratio). For fluorescently- labelled liposomes, NBD-PE (1 mol %) was incorporated into the lipid mixture. For [^{125}I]TI-loaded liposomes, the aqueous space label was added during liposome hydration. In some experiments, [^{3}H]CHE was added into the liposome composition during preparation, and is a non-metabolized, non-exchangeable lipid tracer (296, 297). Each of these markers did not affect the physical stability, i.e., size of liposomes. Briefly, dried lipid films were hydrated in 25 mM HEPES, 140 mM NaCl buffer (pH 7.4) and sequentially extruded (Lipex Biomembranes Extruder, Vancouver, BC) through a series of polycarbonate filters (Nuclepore Corp., Pleasanton, CA) of pore size ranging from 0.4 down to 0.08 μm. This extrusion procedure has been shown to

produce primarily small unilamellar vesicles (33, 34). The mean diameter of liposomes was determined by dynamic light scattering using a Brookhaven B190 submicron particle size analyser (Brookhaven Instruments Corp., Holtsville, NY). The diameters of extruded liposomes were in the range of 110 ± 10 nm.

For DXR-loaded liposomes, the drug was encapsulated by remote loading using an ammonium sulphate gradient (42). Briefly, liposomes were hydrated in 155 mM ammonium sulphate (pH 5.5) and the external buffer was exchanged by eluting through Sephadex G-50 column equilibrated with 123 mM sodium citrate (pH 5.5). DXR was added to the liposomes at a PL:DXR ratio of 1:0.2 w/w and incubated for 1 h at 65°C. The liposome-encapsulated DXR was separated from the free DXR over a Sephadex G-50 column eluted with 123 mM sodium citrate (pH 5.5). The concentration of the liposome-entrapped DXR was determined by spectrophotometry (λ= 490 nm) and phospholipid concentrations were determined using the Bartlett colorimetric assay (298). The loading efficiency of DXR was greater than 95 % and liposomes routinely contained DXR at a concentration of 140-160 µg DXR/µmol PL (0.24-0.28 µmol DXR/µmol PL).

Immunoliposomes (SIL) were prepared by the hydrazide coupling method (53). Briefly, mAb was oxidized with sodium periodate (10 mM in distilled water) for 1 h at 22°C. The excess periodate was quenched with 50 mM NAM and oxidized mAb was incubated with Hz-PEG-liposomes (overnight at 5°C) at an Ab:PL molar ratio of 1:1000. This mAb:PL coupling ratio resulted in mAb densities on SIL of approximately 40-60 µg mAb/µmol PL, which is considered optimal for maintaining long-circulation times of liposomes *in vivo* (53). Finally, the immunoliposomes were separated from the free mAb

over a Sephadex CL-4B column equilibrated with 25 mM HEPES buffer (pH 7.4). The efficiency of coupling was determined from the amount of [^{125}I]-labelled mAb bound to the surface of liposomes, expressed as μg mAb/μmol PL. All mAb coupling densities on liposomes (HSPC:CHOL:Hz-PEG$_{2000}$-DSPE, 2:1:0.1 molar ratio, 100 nm diameter) were routinely in the range of 40-60 μg anti-CD19/μmol PL (2.6-3.9 x10^{-4} μmol mAb/μmol PL).

2.3.5 *In vitro* cell binding/uptake experiments.

Cell binding and uptake experiments were performed with Namalwa cells and H9 cells. Cells were plated at 1x10^6 cells/100 μl RPMI1640 supplemented with 10 % FBS in 48-well tissue culture plates. Various formulations of [^{3}H]-CHE-labelled liposomes, with or without coupled anti-CD19, were added to each well (50-1600 nmol/ml) and maintained either at 4°C or 37°C in a humidified atmosphere containing 5 % CO_2 in air in a total volume of 200 μl. In competition experiments, liposome binding was conducted in the presence of 6 to 200-fold excess free antibody (6.4 x 10^{-4} μmol free anti-CD19) which was added 15 min prior to the addition of SIL[anti-CD19]. After 1 h incubation, the cells were washed three times with cold phosphate buffered saline (PBS) (pH 7.4) and the amount of [^{3}H]CHE-liposomes associated with the cells was determined by scintillation counting (ACS scintillation fluid) in a Beckmann LS-6800 counter. The amount of liposomes bound (in nmol PL) was calculated from the initial specific activity of [^{3}H]-CHE-liposomes.

In some experiments, immunoliposomes were labelled with a green fluorescent lipid marker, NBD-PE (0.1 mol %), and liposome-cell recognition was determined using

FACS. Various formulations of NBD-PE-labelled liposomes were incubated with a mix of B and T lymphoma cells ($1x10^6$ cells/well) at a final PL concentration of 400 nmol/ml for 1 h at 37°C in a humidified incubator containing 5 % CO_2. Cells were washed three times with immunofluorescence (IF) buffer (IF buffer: PBS containing 0.1 % FBS and 0.02 % sodium azide) and fixed with 1 % formaldehyde prior to analysis on the flow cytometer. Cell debris were excluded by appropriate gating on forward *versus* side angle scatter profiles. Files were collected of 10000-20000 events and later analysed using the LYSIS II software program (Becton Dickinson, San Jose, CA). For two-colour immunofluorescence experiments with mix of B and T lymphoma cells, cells were labelled with red-labelled anti-CD20-PhE (B cell marker) or anti-CD4-PhE (T cell marker) to identify the individual cell populations, in addition to the green-labelled liposomes. Appropriate fluorescent isotype-matched control Abs were used to ascertain specific labelling and identification of appropriate cell types.

2.3.6 *In vitro* cytotoxicity experiments.

A comparison of the *in vitro* cytotoxicity of free drug and various liposomal formulations, were performed on $CD19^+$ Namalwa cells and a $CD19^-$ T lymphoma cell line (H9) with an *in vitro* proliferation assay utilizing the tetrazolium dye (MTT) (299). Briefly, $5x10^5$ cells were plated in 96-well plates and were incubated with either free DXR or various formulations of DXR encapsulated in long-circulating liposomes with or without antibody. Groups included free anti-CD19, free isotype-matched IgG2a, free DXR; DXR-SL; DXR-SL conjugated to either anti-CD19 (DXR-SIL[anti-CD19]) or isotype-matched control mAb IgG2a (DXR-NSIL[IgG2a]. DXR-SL and DXR-SIL were

used alone, or in conjunction with free anti-CD19, 10 μg/10^6 cells. Additional experiment groups included non-specific, isotype-matched IgG2a mAb (DXR-NSIL[IgG2a]), or empty (no DXR) SIL[anti-CD19]. Cells were incubated for 1, 24 or 48 h at 37°C in an atmosphere of 95 % humidity and 5 % CO_2. For the 1 and 24 h time points, cells were washed twice prior to replacing with fresh media, and were incubated for an additional 47 and 24 h, respectively. All plates were incubated for a total 48 h. At the end of the incubation time, tetrazolium dye was added and the plates were read on a Titertek Multiskan Plus (Flow Laboratories Inc., Mississauga, Ont.) at dual wavelengths 570 and 650 nm. The absorbance reading from each well was proportional to the cell viability and results were expressed as percent cell viability of test compared to untreated controls. The IC_{50} of the test was defined as the concentration of the test drug that produced a 50 % reduction in cell viability compared to untreated controls.

2.3.7 Pharmacokinetic and biodistribution of liposomes in CD1(ICR)BR (outbred) *versus* SCID mice implanted with CD19$^+$ Namalwa cells.

Female CD1(ICR)BR (outbred) mice or SCID mice bearing i.p. Namalwa cells in the weight range of 20-30 g were injected *via* the tail vein with a single bolus dose of 0.2 ml liposomes (0.5 μmol PL/mouse). Liposomes were composed of HSPC:CHOL:Hz-PEG_{2000}-DSPE (2:1:0.1 molar ratio, 100 nm in diameter), with or without coupled anti-CD19 (or isotype-matched IgG2a), and contained approximately 2-4x10^5 cpm of aqueous space label [^{125}I]TI (113, 294). Free [^{125}I]TI is rapidly excreted after i.v. administration, and has a high latency when encapsulated in liposomes (71, 113). At selected time points (0.5, 1, 2, 4, 6, 12, 24 or 48 h) post-injection, mice (3/group) were anesthetized with

halothane and sacrificed by cervical dislocation. A blood sample (100 µl) was collected by heart puncture and major organs namely, liver, spleen, lung, heart, kidney were excised. For tumour-bearing SCID mice, in addition, the mesenteric lymph nodes were isolated. All organs were counted for the [^{125}I]- label in a Beckmann 8000 gamma counter. Blood correction factors were applied to all samples (300). Pharmacokinetic parameters were calculated using polyexponential curve stripping and least squares parameter estimation program PKAnalyst (Micromath, Salt Lake City, USA).

2.3.8 *In vivo* therapeutic experiments.

Namalwa cells were passaged i.p. in SCID mice to develop a more virulent strain with reproducible tumour takes. The pre-adapted cell line was grown in tissue culture and cells were harvested in sterile PBS. Cell viability was assessed by dye exclusion using eosin staining prior to implantation. SCID mice were injected with pre-adapted cells in 0.2 ml sterile PBS either i.p. ($5x10^7$ cells) or i.v. *via* the tail vein ($5x10^6$ cells). Mice injected i.p. developed ascitic tumours and had a mean survival time (MST) of 23 days. Mice injected i.v. had a MST of approximately 20 days and mice were terminated when they showed signs of hind-leg paralysis. From some mice, blood samples were taken by tail vein bleeding and the blood lymphocytes were separated using Ficoll-Paque gradients. Diseased animals were subjected to a gross histopathological examination to detect tumour dissemination. In order to detect tumour cells in the tissues, samples of liver, spleen, lung, heart, kidney, bone marrow and solid tumours were dissociated with pronase-collagenase treatment, followed by labelling with both anti-CD19-FITC and anti-CD45-PhE, and analysed by FACS.

For therapeutic experiments, mice (5/group), implanted with i.v. (5×10^6 or 1×10^5 cells) or i.p. (5×10^6 or 5×10^7) cells, were treated at either 1 or 24 h post-implantation, with single doses or three weekly doses of 3 mg/kg DXR (i.v. or i.p.) as either free DXR, DXR-SL (no Ab), DXR-SIL[anti-CD19] or DXR-NSIL[IgG2a]. The dose of 3 mg/kg DXR was close to the MTD in SCID mice, and at this dose mice did not develop any DXR-induced toxicities. Free mAb treatments (anti-CD19 or isotype-matched control IgG2a) were also investigated at doses of 10 μg/mouse. The contribution to the therapeutic results of the free mAb, anti-CD19, was investigated in conjunction with either free DXR, DXR-SL (no Ab), DXR-SIL[anti-CD19]. Treatments were given either as a single dose or three weekly treatments at a dose of 3 mg/kg DXR. Mice were monitored routinely for weight loss and survival times were noted.

2.3.9 Statistical analysis.

All linear regression analyses were done using Quattro Pro 4.0 (Borland Inc., Scotts Valley, CA). Unless otherwise stated, Student's t-test was used to measure statistical significance between two treatment pairs. For multiple comparisons of groups in the cytotoxic assays, or mean survival times of various treatment groups within the same experiment were performed using one-way analysis of variance (ANOVA) with INSTAT (GraphPAD software, version 1.11a). Post-tests comparing the different treatment means were done using Bonferroni's test. Comparisons of two means between groups of different experiments were done using Student's t-test. Data was considered significant for p values < 0.05.

2.4 RESULTS

2.4.1 *In vitro* recognition experiments.

To examine if immunoliposomes (SIL[anti-CD9]) could specifically target $CD19^+$ B cells, *in vitro* binding studies were conducted at 4 and 37°C with the Namalwa cell line and a control $CD19^-$ T cell line (H9) (Fig. 2.1A-C). Binding was quantified from the specific activity of [^{3}H] counts associated with cells. To discriminate the processes of cell binding and uptake, the experiments were conducted at 4 and 37°C. The association (binding + uptake) of SIL[anti-CD19] or SL (no mAb) by $1x10^6$ Namalwa cells after 1 h incubation at 37°C is shown in Fig. 2.1A. There was a 3-fold increase in association of SIL[anti-CD19] to Namalwa cells compared to Ab-free liposomes (Fig. 2.1A). Binding/uptake of the SIL[anti-CD19] increased log-linearly with incubated lipid concentrations (in a concentration from 50-200 nmol PL/ml) and appeared to saturate at concentrations greater than 400 nmol PL/ml (Fig. 2.1A). Association of SIL[anti-CD19] with Namalwa cells could be competitively inhibited by the addition of excess free anti-CD19, indicating that the association was mediated through the CD19 surface epitope on B cells (Fig. 2.1A). Non-specific binding/uptake of SL (no Ab) was also observed, but was significantly lower than specific binding (Fig. 2.1A).

From the binding plots, the dissociation constant (K_D) and the maximum number of liposomes bound per cell were determined (B_{max}) using non-linear regression methods. The number of liposomes/μmol PL was estimated to be 7.7×10^{12} liposomes/μmol PL (calculated from the literature values for bilayer thickness, molecular areas of PL, CHOL and PEG, with the assumptions that liposomes were spherical, 100 nm in diameter,

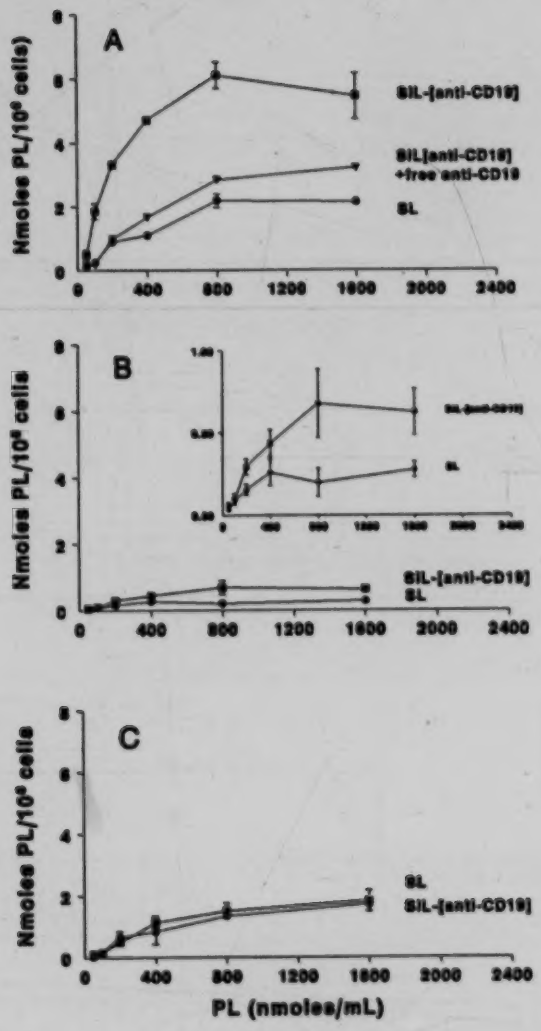

Figure 2.1. Binding/uptake of [^{3}H]CHE-labelled liposomes by B and T cells as a function of liposome concentration.
Liposomes were composed of HSPC:CHOL:PEG_{2000}-DSPE, 2:1:0.1 (100 nm in diameter) ± mAb anti-CD19. SL or SIL[anti-CD19] were incubated with $1x10^6$ Namalwa cells at either 4°C or 37°C. In competition experiments, the binding of SIL[anti-CD19] was conducted in the presence of excess free anti-CD19. (A) Namalwa cells, 37°C, (B) Namalwa cells, 4°C (including insert) and (C) H9 cells, 37°C. Data are expressed as nmol PL ± SD per 10^6 cells (n=3).

monodisperse, and contained unilamellar bilayers) (301-305). This translates into approximately 48,000 total binding sites for $CD19^+$ Namalwa cells by SIL[anti-CD19] (*versus* 15,000 SL non-specifically bound) at saturated concentrations of PL. Therefore, there are 33,000 specific binding sites for SIL[anti-CD19] on Namalwa cells. The dissociation constant, K_D, for the SIL[anti-CD19] was 160 μM phospholipid, which was 2.5-fold greater than that seen for the SL.

The binding/uptake of SIL[anti-CD19] by the $CD19^-$ T cell line, H9, was significantly lower than for the $CD19^+$ B cells and no significant differences were observed in comparison with control Ab-free liposomes (Fig. 2.1C). Binding/uptake of SIL[anti-CD19] to Namalwa cells at 37°C was significantly higher than the binding at 4°C (Fig. 2.1A *vs.* B), suggesting a requirement for metabolic processes in the uptake of SIL[anti-CD19] by the target cell (306).

2.4.2 Specific recognition of immunoliposomes SIL[anti-CD19] to B cells in a mix of B and T cells.

Using flow cytometry (FACS) and green fluorescent NBD-liposomes, specific labelling to human B cell lymphoma (Namalwa cell line) was evaluated in a mix of $CD19,20^+$ Namalwa and $CD4^+CD19^-$ T cell lines (Fig. 2.2). Fig. 2.2A shows cells stained with isotype-matched control antibodies. In Fig. 2.2B, following staining with fluorescent mAb anti-CD19-FITC (B cells) and anti-CD4-PhE (T cells), the mixture of cells, could be resolved into two populations containing 44 % of the $CD19^+$ B cells and 47 % of the $CD4^+$ T cells, respectively. Treatment with non-targeted SLs showed no appreciable association of the NBD green fluorescence to either the $CD20^+$ B cells (Fig. 2.2C) or the

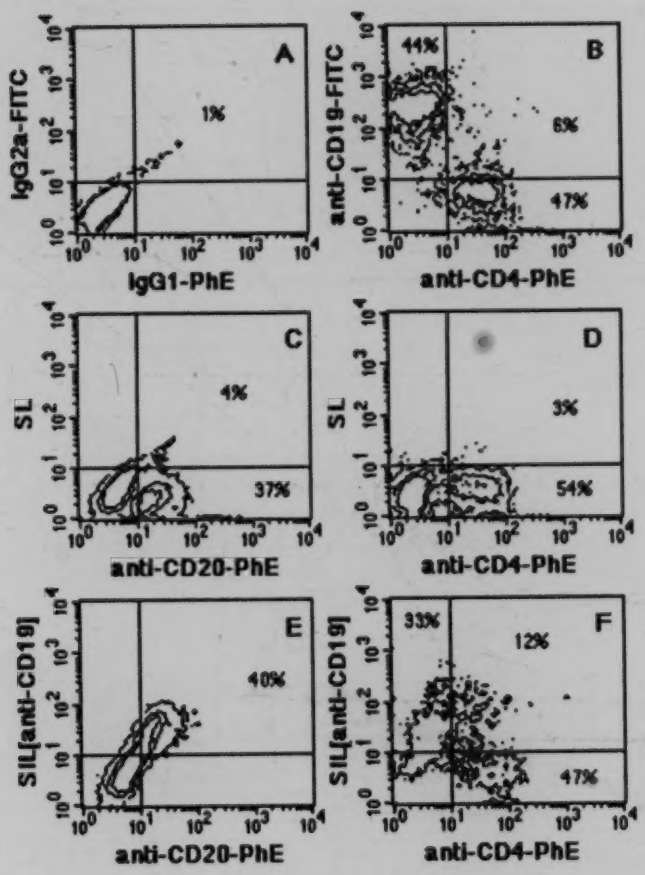

Figure 2.2. Two-colour flow cytometry for selective recognition of fluorescent NBD-labelled liposomes by CD19$^+$ B lymphoma cells (Namalwa).
NBD-labelled (0.1 mol %) liposomes were composed of HSPC:CHOL:PEG_{2000}-DSPE (2:1:0.1 molar ratio, 100 nm) ± mAb anti-CD19. A mixture of CD19,20$^+$ B and CD4$^+$, CD19$^-$ T cells were incubated with either SIL[anti-CD19] or SL, and stained with either anti-CD20-PhE (B1RD1, B cell marker) or anti-CD4-PhE (T cell marker). (A) Cells stained with appropriate fluorescent isotype-matched control Abs, (B) Mabs anti-CD19-FITC and anti-CD4-PhE, (C) SL and anti-CD20-PhE, (D) SL and anti-CD4-PhE, (E) SIL[anti-CD19] and anti-CD20-PhE, (F) SIL[anti-CD19] and anti-CD4-PhE.

$CD4^+$ T cell population (Fig. 2.2D). On the other hand, SIL[anti-CD19] selectively bound B cells (Fig. 2.2E), with 40 % of the cells dual-labelled with SIL[anti-CD19] (green fluorescence) and CD20-PhE (red fluorescence), as seen in the upper right quadrant of Fig. 2.2E, with the rest of the cells almost exclusively unstained (presumably $CD20^-$ T cells). To confirm the identity of this unstained population (presumably T cells), cells were stained with the T cell marker, anti-CD4-PhE following treatment with SIL[anti-CD19] (Fig. 2.2F). In this case, the cell mixture was again separated into two distinct populations (Fig. 2.2F). Cells (47 %) were either exclusively, CD4-PhE^+ (Fig. 2.2F, lower right panel) with low NBD fluorescence (i.e. no association of targeted liposomes with T cells) or $CD4^-$ cells g. 2D). On the other hand, SIL[anti-CD19] selectively bound B cells (Fig. 2.2E) where 40 % of the cells were dual labelled with SIL[anti-CD19] (green fluorescence) and CD20-PhE (red fluorescence) as seen in the upper right hand quadrant of panel E, that were labelled (33 %) SIL[anti-CD19] (Fig. 2.2F, upper left panel) (i.e. $CD4^-$ B cells). Only a small proportion of cells (12 % or less) appeared dual-labelled with both NBD and CD4-PhE seen in the upper right hand quadrant). In comparison, SL did not bind any of the cells (Fig. 2.2C,D).

2.4.3 *In vitro* cytotoxicity of SIL[anti-CD19].

The cytotoxicity of DXR-SIL[anti-CD19], DXR-SL, free DXR, free mAb and drug-free controls were compared, as a function of time. As seen in Table 2.1, the IC_{50} of free DXR, DXR-SL or DXR-NSIL[IgG2a] significantly decreased ($p<0.001$) as the exposure of cells to drug increased from 1 h to 48 h. The IC_{50} of DXR-SIL[anti-CD19] was significantly lowered after 24 h incubation (1 h *vs.* 24 h, $p<0.001$), but was not further

Table 2.1. Cytotoxicity data (IC_{50} μM) for free anti-CD19, isotype-matched control mAb, empty immunoliposomes (SIL), free DXR and liposomal DXR formulations (with or without anti-CD19) determined on $CD19^+$ B-cells (Namalwa) and $CD19^-$ T-lymphoma (H9) cell lines by the MTT tetrazolium dye assay.

Time (h)	$CD19^+$ B lymphoma cell line (Namalwa)										IC_{50} ratio
	Free mAb anti-CD19 (μM)	Free mAb isotype-matched IgG2a (μM)	Drug-free SIL[anti-CD19] (μM PL)	Free DXR (μM DXR)	anti-CD19 + Free DXR (μM DXR)	DXR-SL (μM DXR)	anti-CD19 + DXR-SL (μM DXR)	DXR-NSIL[IgG2a] (μM DXR)	DXR-SIL[anti-CD19] (μM DXR)	anti-CD19 + DXR-SIL[anti-CD19] (μM DXR)	DXR-SL:DXR-SIL[anti-CD19]
1	1.00±0.04	>2.6	>1500	1.30±0.6	0.79±0.10	78.1±14.0	139.7±21.2	67.1±11.2	13.5±9.8	55.9±13.3	5.8:1
24	0.43±0.10	>2.6	230±30	0.28±0.1	0.22±0.05	5.1±1.4	1.4±0.4	10.9± 3.1	1.4±1.2	3.32±0.86	3.6:1
48	-	-	-	0.07±0.01	-	4.4±0.4	-	5.0±0.6	1.2±0.1	-	3.7:1
			$CD19^-$ T lymphoma cell line (H9)								
1	-	-	-	3.2±1.0	-	30.5±8.0	-	-	38.5±22.4	-	0.8:1
24	-	-	-	0.76±0.6	-	1.5±0.7	-	-	1.9±0.9	-	0.8:1

$5x10^5$ cells were plated in 96-well plates and were incubated with either free DXR or various formulations of DXR encapsulated in long- circulating liposomes with or without antibody. Groups included free anti-CD19, isotype-matched control mAb IgG2a, free DXR; DXR-SL; DXR-SL conjugated to either anti-CD19 (DXR-SIL[anti-CD19]) (alone or in conjunction with free anti-CD19, 10 μg/10^6 cells) or non-specific, isotype-matched IgG2a mAb (DXR-NSIL[IgG2a]), and drug-free SIL[anti-CD19]. Antibody coupling, *via* the PEG-Hz method, was 40-50 μg mAb/μmol PL ($2.6\text{-}3.9x10^{-4}$ μmol mAb/μmol PL) and DXR-loading was 140-160 μg DXR/μmol PL (0.24-0.28 μmol DXR/μmol PL). Cells were incubated for 1 or 24 h at 37°C in an atmosphere of 95 % humidity and 5 % CO_2. At the end of each incubation period, cells were washed twice prior to replacing with fresh media. Plates were incubated for a total 48 h, tetrazolium dye (50) was added and the plates were read at dual wavelengths 570 and 650 nm. Cytotoxicity data are expressed as mean IC_{50} ± SD (n=2-7).

reduced after 48 h exposure to cells (24 h *vs.* 48 h, $p>0.05$). After 1 h incubation, targeted DXR-SIL[anti-CD19] were 6-fold more cytotoxic than non-targeted liposomes ($p<0.001$) or isotype-matched liposomes DXR-NSIL[IgG2a] ($p<0.001$) for the Namalwa cell line. While DXR-SIL[anti-CD19] displayed a cytotoxicity approaching that of the free DXR ($p>0.05$), both non-targeted liposomal formulations were significantly less cytotoxic than the free DXR *in vitro* ($p<0.001$).

Free DXR (free or leaked) may adsorb to the plastic wells during the incubation with cells[3], and under this experimental setup, it possible that free DXR may desorb and be present in the media for the continued incubation period of 24 h or 47 h. The relatively low levels of DXR may lead to some cytotoxicity to cells and hence, underestimate the IC_{50}.

With incubations of 24 h and 48 h, the difference in cytotoxicity between DXR-SL and DXR-SIL[anti-CD19] was 4-fold decreased ($p<0.01$) (Table 2.1). This likely results from the gradual release of the encapsulated drug from the DXR-SL with uptake of the released drug with longer incubation times. When the cytotoxicities were done on the $CD19^-$ H9 T cell line, no significant differences were observed in the IC_{50} of DXR-SIL[anti-CD19] compared to non-targeted DXR-SL both at 1 and 24 h ($p>0.05$), suggesting the requirement of CD19 receptors in mediating cytotoxicity of targeted DXR-SIL[anti-CD19]. Free DXR demonstrated a three-fold greater cytotoxicity to B cells (Namalwa), compared to the T cell line (H9) ($p<0.05$) (Table 2.1). The cytotoxic effects

---

[3] Storm, G., Steerenberg, P.A., Van Borssum-Waalkes, M., Emmen, F., Crommelin, D.J.A. Potential pitfalls *in vitro* antitumor testing of free and liposome-encapsulated doxorubicin. J. Pharm. Sci. *77*: 823-830, 1988.

of the liposomal formulations to T cells (*versus* B cells) were however, reversed. The liposomal DXR formulations were 1.5 to 2-fold less cytotoxic to B cells in comparison to T cells ($p<0.01$) at 1 and 24 h incubation (Table 2.1). Since cytotoxicity is mediated by doxorubicin released from liposomes, this suggests that the T-cell preparations may increase leakage of drug from DXR-SL.

Control experiments were done to rule out the possibility that the cytotoxic effect may arise from either the lipid, mAb or a combination of both. Free mAb (anti-CD19) molecules were, on a molar basis, equivalent in cytotoxicity to free DXR molecules ($p>0.05$) (Table 2.1). The isotype-matched control IgG2a was not cytotoxic in the concentration range tested (Table 2.1). Drug-free liposomes, which contain approximately, 3.2×10^{-4} μmol Ab/μmol PL, did not appear to have significant cytotoxicity (Table 2.1).

Co-incubation of free anti-CD19, at concentrations found on the mAb-coupled liposomes, with free DXR did not significantly alter the IC_{50} of the free drug ($p>0.05$), and hence low concentrations of anti-CD19 do not appear to sensitize Namalwa cells to free drug *in vitro*. Anti-CD19 incubated with DXR-SL had minimal effects on cytotoxicity at 1 h or 24 h ($p<0.05$). Free anti-CD19 competed with DXR-SIL[anti-CD19] and increased the IC_{50} of the targeted liposomes by 4-fold after 1 h incubation ($p<0.01$), giving an IC_{50} which was not significantly different from non-targeted DXR-SL or DXR-NSIL[IgG2a] ($p>0.05$). No competition effect of free anti-CD19 for DXR-SIL[anti-CD19] was observed at 24 h (Table 2.1).

2.4.4 Tumour model of Namalwa cells implanted in SCID mice.

Following i.p. injection, mice implanted with Namalwa cells developed an ascitic tumour accompanied by an approximately 30 % gain in body weight. At necropsy, the tumour was found to have invaded blood and lymph nodes (particularly the mesenteric lymph nodes and serosal surfaces) with disseminated involvement of liver, spleen, diaphragm, anterior thoracic cavity, lungs, ovaries and heart (pericardium) (Table 2.2).

After i.v. injection of cells, the primary tissues of infiltration were lymph nodes, bone marrow, spleen, lung, liver and renal capsule (Table 2.2). In contrast to the i.p. model, there were no significant numbers of tumour cells found circulating in blood at 24 h post-inoculation when treatment began. When hind-leg paralysis was observed after i.v. implantation as a result of cells infiltrating the vertebrae and compressing the spinal cord, the mice were euthanised.

Cell surface expression of CD19 was examined in SCID mice implanted with Namalwa cells. FACS analysis demonstrated that the *in vivo* transplantation of these cells did not result in a significant variation of CD19 surface antigen expression in tissues (fig. 2.3). Compared with cells in culture, CD19 expression appeared slightly depressed in solid tumours, particularly in lymph nodes. Cells isolated from solid tumours regained surface expression of CD19 when they were returned to culture. To examine the tumour dissemination after i.p. or i.v. implantation, dissociated cells from excised tissues were retrieved and stained with both anti-CD19 and anti-CD45. The additional staining with anti-CD45 was done to identify human leucocytes, in order to discriminate implanted cells that may have down-regulated the expression of CD19. The highest levels of tumour

Table 2.2. Summary of tumour dissemination of human B-cell lymphoma (Namalwa) after i.p. and i.v. implantation in SCID mice.

Model	Route of implantation of Namalwa cells	
	i.p. ($5x10^7$ cells)	i.v. ($5x10^6$ cells)
Mean survival time	23.4±2.7 days	20.4 ± 1.6 days
End point	ascitic tumour	hind-leg paralysis
Blood	++	-
Ascites development	+++	-
Liver	++	++
Spleen	++	++
Lung	+	++
Solid tumours in lymph nodes	+++	++
Bone marrow	-	+++
Hind-leg paralysis	-	+++

Relative levels of implantation of cells in mice after histological examination, scored as +++,high; ++, intermediate, +, low or -, no cells identified in tissue sections.

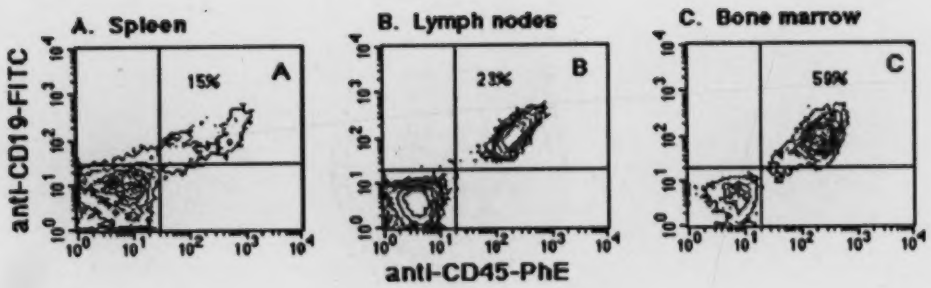

Figure 2.3. Two-colour flow cytometry to determine the degree of implantation in various tissues of Namalwa cells after i.v. implantation in SCID mice.
Dissociated cells from excised tissues were stained with both anti-CD19-FITC (human B cell marker) and human anti-CD45-PhE (common leucocyte antigen marker). (A) spleen, (B) lymph nodes, and (C) bone marrow.

cells were observed in spleen, bone marrow and lymph nodes (Fig. 2.3), but tumour cells were also found in liver, lung, heart and kidney after gross histological examination.

2.4.5 Pharmacokinetics of SIL[anti-CD19] in CD1(ICR) outbred mice *versus* SCID mice implanted with CD19$^+$ Namalwa cells.

The pharmacokinetics of SL and SIL[anti-CD19] were examined in CD1(ICR)BR mice (Fig. 2.4, Table 2.3). In these studies, [^{125}I]tyraminylinulin (TI) was utilized as a liposomal aqueous-space radioactive marker. At Ab-coupling densities of 40-60 μg Ab/μmol PL, the distribution profiles of both SIL[anti-CD19] and SL from blood over time were log-linear (Fig. 2.4) with mean residence times (MRT) of 16.4 and 15.4 h, respectively (Table 2.3). SL were cleared from blood in a log-linear single-exponential process (Fig. 2.4, Table 2.3), while SIL[anti-CD19] displayed a biexponential clearance process characterized by distribution and elimination half-lives, $t_{1/2}\alpha$ and $t_{1/2}\beta$, respectively (Fig. 2.4). The blood kinetics of SL, NSIL[IgG2a] or SIL[anti-CD19] in tumour-free mice were strongly dominated by the elimination phase (ß), and >90 % of the liposome formulations were predominantly eliminated by this slow process. The area under the curve (AUC) observed for SIL (1244 nmol·h/ml) was slightly lower than that seen for SL (1407 nmol·h/ml) (Table 2.3).

A comparison of the pharmacokinetics of SL *versus* SIL[anti-CD19] were then examined in SCID mice implanted with the CD19$^+$ B-cell lymphoma cell line (Namalwa). SCID mice were injected with $5x10^7$ Namalwa cells i.p., and the pharmacokinetic studies were initiated when mice showed signs of ascitic tumour development (day 22), and corresponded with a population of Namalwa cells in blood. Figure 2.4 illustrates the more

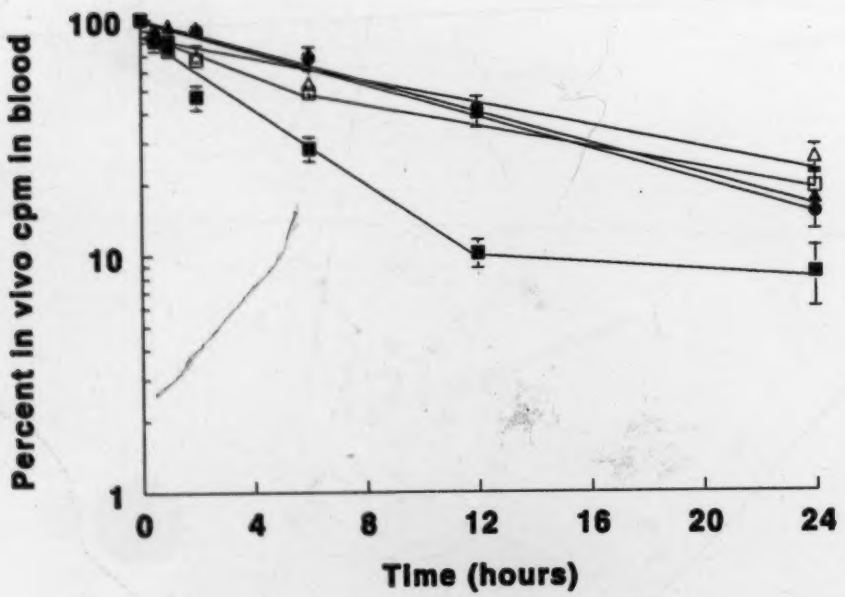

Figure 2.4. Blood clearance of SL (no mAb), SIL[anti-CD19] and NSIL[IgG2a]. Blood clearance kinetics of SL (△,▲), SIL[anti-CD19] (□,■) and NSIL[IgG2a] (●) in either CD1(ICR)BR outbred mice (open symbols) or SCID mice (filled symbols) implanted i.p. with CD19$^+$ B-lymphoma cell line (Namalwa). Liposomes were composed of HSPC:CHOL:PEG_{2000}-DSPE (2:1:0.1 molar ratio, 100 nm) ± mAb anti-CD19, containing the aqueous space label [^{125}I]TI. Either SIL[anti-CD19] or SL were injected i.v. *via* the tail vein (0.5 μmol PL/mouse, 30 μg mAb) and blood/tissues were isolated at various time points post-injection and counted for ^{125}I. Results are expressed as the amount of label in blood/tissues as a percentage of the of the label remaining in the body at various times post-injection of liposomes (mean ± SD, n=3).

Table 2.3. Comparison of the pharmacokinetic parameters of SIL[anti-CD19] and SL (no Ab) in CD1(ICR)BR outbred mice or tumour-bearing SCID mice implanted (i.p.) with CD19$^+$ B lymphoma cell line (Namalwa).

	Liposome composition	MRT[a] (h)	$AUC_{t=0\ -\infty}$[b] (nmol*h/ml)	k_{10}[c] (h^{-1})	$t_{½}\alpha$ (h)	$t_{½}\beta$ (h)	Cl_T[d] (ml/h)
CD1 (ICR)-BR mice	SIL[anti-CD19]	16.4	1244.6	0.08	0.36	11.48	0.40
	SL (no Ab)	15.4	1407.3	0.06	-	10.70	0.36
Tumour-bearing SCID mice	SIL[anti-CD19]	11.4	621.2	0.16	0.85	8.78	0.80
	NSIL[IgG2a]	14.3	1412.5	0.07	-	9.93	0.35
	SL (no Ab)	14.0	1436.2	0.07	-	9.70	0.34

[a]Mean residence time (MRT); [b]Area under the blood concentration *versus* time curve ($AUC_{t=0\ -\infty}$); [c]Elimination rate constant from the central compartment (k_{10}); [d] Clearance.

CD1(ICR)BR mice or tumour-bearing SCID mice were injected i.v. *via* the tail vein with a single bolus dose (0.5 µmol PL/mouse) of HSPC:CHOL:Hz-PEG_{2000}-DSPE liposomes, 2:1:0.1 molar ratio (100 nm in diameter), labelled with [^{125}I]tyraminylinulin. MAb anti-CD19 was coupled to the liposomes at an Ab:PL molar ratio of 1:1000 and mice received 20 µg mAb. Pharmacokinetic parameters were calculated using either a one-compartment (single exponential curve fit) or two-compartment (biexponential-α and β) open model with bolus input and first-order output and least squares parameter estimation program PKAnalyst (Micromath Scientific Software, Salt Lake City, UT).

rapid clearance of SIL[anti-CD19] compared to SL or non-specific isotype-matched control NSIL[IgG2a] in tumour-bearing mice. The pharmacokinetic profiles of SL and NSIL[IgG2a] were similar (Table 2.3, Fig. 2.4). The MRT of SL and NSIL[IgG2a] were approximately the same, and was slightly higher than that observed for SIL[anti-CD19] (Table 2.3). There was a substantial decrease in AUC for the targeted SIL[anti-CD19] *versus* the non-targeted SL or NSIL[IgG2a] formulations. Furthermore, an increase in elimination rate constant k_{10} (from the central compartment) and a decreased $t_{1/2}\beta$ (Table 2.3) was obtained for the targeted formulation. The rapid clearance of SIL[anti-CD19] from blood (Fig. 2.4) resulted in these liposomes accumulating predominantly into the liver, spleen, and carcass. This may reflect, in part, the binding of SIL[anti-CD19] to tumour cells present in blood, increasing their clearance from blood (307). This may be due to a "target-cell dragging effect"[4], where tumour cells bound to SIL[anti-CD19] may be taken up by the liver and spleen macrophages.. Accumulation of SIL[anti-CD19] into the liver, spleen and carcass may also be a result of liposomes binding the large $CD19^+$ tumour-cell population in these organs, where micrometastatic tumours could be demonstrated from tissue analysis (Fig. 2.3).

We also compared the amount of liposomes distributed in solid tumours excised from mesenteric lymph nodes (normalized as cpm/mg tissue) (Fig. 2.5), one of the sites of infiltration of the B lymphoma cells (Fig. 2.3). The targeted liposomes distributed quickly

---

[4] Peeters, P.A.M., Bruninck, B.G., Eling, W.M., Crommelin, D.J.A. Therapeutic effect of chloroquine (CQ)-containing liposomes in rats infected with Plasmodium Berghei parasitized mouse red blood cells: comparison with combination of antibodies and CQ or liposomal CQ. Biochim. Biophys. Acta. *981*:269-276. 1989.

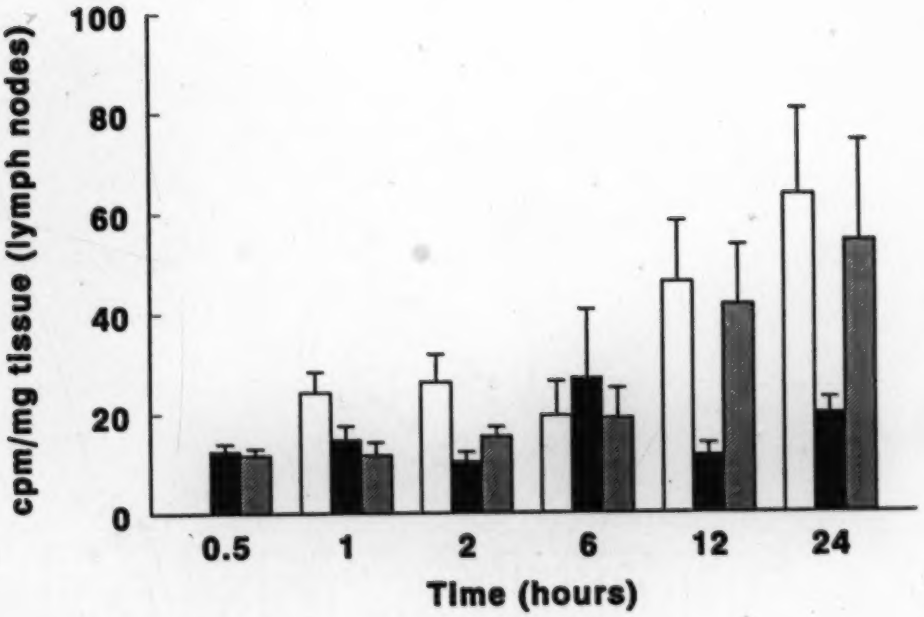

Figure 2.5. Comparison of lymph node (mesenteric lymph node solid tumours) levels of SL (open bars), SIL[anti-CD19] (solid bars) and NSIL[IgG2a] (hatched bars) in SCID mice implanted with CD19$^+$ B lymphoma cell line (Namalwa).
Liposomes were composed of HSPC:CHOL:PEG_{2000}-DSPE (2:1:0.1 molar ratio, 100 nm) ± mAb anti-CD19 coupled by the hydrazide method and containing the aqueous space label [^{125}I]TI. Either SL or SIL[anti-CD19] were injected i.v. *via* the tail vein (0.5 µmol PL/mouse, 30 µg mAb) and the mesenteric lymph nodes solid tumours were isolated at various time points post-injection and counted for ^{125}I. Results are normalized as the amount of label in lymph nodes (cpm/mg tissue) at various times post-injection of liposomes (mean ± SD, n=3).

into the lymph nodes and accumulated only slowly thereafter (Fig. 2.5). By contrast, SL or NSIL[IgG2a] accumulated more slowly in lymph nodes but achieved a 4-5- fold greater localization by 24 h, likely due to a passive targeting effect (47, 51). The reduced accumulation of SIL[anti-CD19] in the tumour-containing lymph nodes may be due, in part, to the lower AUC of these liposomes compared to SL or NSIL.

2.4.6 *In vivo* experiments in SCID mice innoculated with Namalwa cells.

In initial experiments, to test the effectiveness of the targeted DXR-SIL[anti-CD19] $5x10^7$ Namalwa cells were implanted i.p. in SCID mice, with treatments also given i.p. Results of the therapeutic experiments comparing free DXR, DXR-SIL[anti-CD19] and DXR-SL (no Ab) are summarized in Table 2.4 A.1-2. Mice receiving 3 mg/kg of DXR-SIL[anti- CD19] at 24 h post-inoculation of cells had a statistically significant improvement ($p<0.001$) in their MST compared with either control mice, or mice treated with DXR-SL or free DXR treatments (Table 2.4 A.1). There was no significant difference in mean survival times of mice treated with either free DXR or DXR-SL ($p>0.05$), however each of these treatment groups were better than untreated controls ($p<0.001$) (Table 2.4 A.1). Lowering the i.p. implanted tumour burdens, (i.e., 5×10^6 cells) resulted in significantly improved effect for DXR-SIL[anti-CD19] with 2/5 long-term survivors (Table 2.4 A.2), compared to free DXR, DXR-SL or isotype-matched control DXR-NSIL[IgG2a] ($p<0.001$). At necropsy, mice treated with DXR-SIL[anti-CD19] showed no apparent ascitic tumour development, unlike those treated with DXR-SL or free DXR, but instead developed isolated solid tumours in the lower abdomen.

As B-cell malignancies (leukemias, lymphomas and MM) have malignant cells in

Table 2.4. Summary of mean survival times of SCID mice after immunoliposomal treatment. Mice were injected with either 5 x 10^6 or 5 x 10^7 Namalwa (human B-lymphoma) cells i.p., or 1x10^5 - 1.5 x 10^7 cells i.v., on day 0 and treated 1 or 24 h post-cells with the following treatments.

Group	Treatment	Route of cells	Route of DXR	Dosing Schedule	Dose of DXR	MST[a] (median) ± SD (days)	ILS[b] (%)	LTS[c](>250 days)
A	Namalwa cells (either 5x10^7 or 5 x 10^6 cells) were injected i.p. and following treatments were initiated i.p., 24 h post-implantation of cells (i.p. - i.p. model).							
1	Controls (PBS)	i.p. 5x10^7	i.p.	day 1	1 x 3 mg/kg	23.4(23) ± 2.7		0/5
	Free DXR					30.6(32) ± 2.8	39	0/5
	DXR-SL					32.8(33) ± 1.3	43	0/5
	DXR-SIL[anti-CD19]					41.4(42) ± 2.1	83	0/5
2	Controls (PBS	i.p. 5x10^6	i.p.	day 1	1 x 3 mg/kg	27.8(28) ± 0.4		0/5
	Free DXR					31.2(31) ± 2.4	11	0/5
	DXR-SL					31.4(30) ± 3.2	7	0/5
	DXR-NSIL[IgG2a]					35.8(36) ± 4.0	29	0/5
	DXR-SIL[anti-CD19]					47.7(58) ± 9.0	107	2/5

Group	Treatment	Route of cells	Route of DXR	Dosing Schedule	Dose of DXR	MST[a] (median) ± SD (days)	ILS[b] (%)	LTS[c](>250 days)
B	Namalwa cells (either $5x10^6$ or $1.5 x 10^7$ cells) were injected i.v. on day 0 and the following treatments (as single or three multiple treatments) were initiated either 1 h or 24 h post-inoculation of cells (i.v.-i.v. model).							
3	Controls	i.v. $5x10^6$	i.v.	day 1	1 x 3 mg/kg	19.6(20) ± 0.5		0/5
	Free DXR					22.0(22) ± 1.0	10	0/5
	DXR-SL					23.0(23) ± 1.0	15	0/5
	DXR-NSIL[IgG2a]					22.2(22) ± 0.5	10	0/5
	DXR-SIL[anti-CD19]					30.6(32) ± 3.2	60	0/5
	DXR-SIL[anti-CD19]	i.v. $5x10^6$	i.v.	1 h	1 x 3 mg/kg	39.6(39) ± 3.0	95	0/5
4	Controls	i.v. $1.5x10^7$	i.v.	1 h	1 x 3 mg/kg	19.3(20) ± 0.9		0/10
	Free DXR					23.2(23) ± 0.8	15	0/5
	DXR-SL					26.8(27) ± 0.8	35	0/5
	DXR-SIL[anti-CD19]					30.8(31) ± 2.1	55	0/10
5	Controls	i.v. $1x10^5$	i.v.	1 h	1 x 3 mg/kg	33.2(32) ± 2.8		0/12
	Free DXR					36.7(33) ± 7.9	11	0/10
	DXR-SL					35.0(34) ± 3.8	5	0/10
	DXR-NSIL[IgG2a]					34.4(36) ± 2.3	4	0/5
	DXR-SIL[anti-CD19]					51.6(57) ± 7.0	55	4/9

Group	Treatment	Route of cells	Route of DXR	Dosing Schedule	Dose of DXR	MST[a] (median) ± SD (days)	ILS[b] (%)	LTS[c](>250 days)
6	Controls	i.v. $5x10^6$	i.v.	days 1,8,15	3 x 3 mg/kg	19.6(20) ± 2.0		0/9
	Free DXR					24.2(25) ± 1.6	25	0/5
	DXR-SL					24.4(25) ± 2.6	25	0/10
	DXR-SIL[anti-CD19]					33.5(34) ± 2.6	70	0/10
	Drug-free SIL[anti-CD19]					23.7(23) ± 1.2	15	0/5

Group	Treatment	Route of cells	Route of DXR	Dosing Schedule	Dose of DXR	MST[a] (median) ± SD (days)	ILS[b] (%)	LTS[c](>250 days)
C	**Effect of mAb anti-CD19 alone or in conjunction with liposomal DXR treatments. Namalwa cells ($5x10^6$ or $1.5 x 10^7$) were injected i.v. on day 0, and the following treatments were initiated 24 h post-inoculation of cells.**							
7	Controls	i.v. $5x10^6$	i.v.	day 1	1 x (10 µg anti-CD19+ 3 mg/kg DXR)	21.4(22) ± 0.9		0/5
	Free mAb anti-CD19					25.8(26) ± 2.3	18	0/5
	Isotype mAb IgG2a					21.2(21) ± 1.5	0	0/5
	anti-CD19 + free DXR					29.8(30) ± 1.3	35	0/4
	anti-CD19 + DXR-SL					29.6(31) ± 2.8	41	0/5
	anti-CD19 + DXR-SIL[anti-CD19]					54.4(43) ± 21.3	95	0/5
	anti-CD19 + DXR-SIL[anti-CD19]	i.v. $1.5x10^7$	i.v.	1 h	1 x (10 µg anti-CD19+ 3 mg/kg DXR)	35.7(36) ± 5.4	80	0/10
	anti-CD19 + drug free-SIL[anti-CD19]					25.0(25) ± 1.0	25	0/5
8	Controls	i.v. $5x10^6$	i.v.	days 1,8,15	3 x (10 µg anti-CD19+ 3 mg/kg DXR)	20.0(20) ± 2.3		0/5
	Free mAb anti-CD19					27.6(28) ± 1.5	40	0/5
	anti-CD19 + free DXR					28.4(28) ± 1.7	40	0/5
	anti-CD19 + DXR-SL					37.6(37) ± 1.8	85	0/5
	anti-CD19 + DXR-SIL[anti-CD19]					39.6(39) ± 6.4	95	0/5

[a] MST, mean survival time (not including long-term survivors); [b] ILS, Increased life span (from median survival time of controls); [c] LTS, Long-term survivors.

the vasculature, we also treated an i.v. model of the disease. Mice were inoculated by the i.v. route (5 x 10^6 Namalwa cells), and various therapies were commenced 24 h post injection of cells (Table 2.4 B.3), a time when tumour cells were no longer detectable in blood (Table 2.2). Treatment with DXR-SIL[anti-CD19] resulted in a significant increase in survival of mice ($p<0.001$) compared with non-treated controls, free DXR, DXR-SL or DXR-NSIL[IgG2a] (non-specific controls). There were no significant differences ($p>0.05$) between the mean survival times of the mice receiving 3 mg/kg of either free DXR, DXR-SL or DXR-NSIL[IgG2a], although all three groups had a significantly longer life span ($p<0.01$) than non-treated controls. However, in the same experiment, if the treatment with DXR-SIL[anti-CD19] was initiated 1 h post injection of cells, when a significant number of the tumour cells remained in the circulation, a further increase in life span was observed compared to treatment at 24 h ($p<0.01$).

As early treatment schedule (i.e. 1 h after implantation of Namalwa cells in SCID) appeared to be more successful than treating mice at 24 h, we then repeated the experiment comparing the various therapies at 1 h post implantation of cells (Table 2.4B.4). We normalized the implanted tumour dose to 1.5x10^7 Namalwa cells, equivalent to the tumour burden when the treatments were initiated 24 h using a doubling time of 16 h. Treatment with targeted DXR-SIL[anti-CD19] was able to significantly improve the MST of mice, compared to either free DXR, or DXR-SL ($p<0.001$) (Table 2.4 B.4). In addition, both free drug ($p<0.001$) and DXR-SL ($p<0.001$) were able to increase MST of mice compared to untreated controls, and DXR-SL therapy was also significantly better than free DXR ($p<0.01$).

To test the therapeutic effect of DXR-SIL[anti-CD19] at lower tumour-cell burdens, Namalwa cells ($1x10^5$ cells, i.v.) were inoculated in SCID mice and treatments were initiated 1 h post cell implantation (Table 2.4B.5). Targeted DXR-SIL[anti-CD19] given at 3 mg/kg was able to improve survival times of mice and was by far the most successful treatment resulting in 4/9 long-term survivors. However, no significant differences were observed between the mean survival times of mice given 3 mg/kg of either free DXR, or DXR-SL compared with controls ($p>0.05$).

Multiple treatment schedules of DXR-SIL[anti-CD19] (i.e. three i.v. treatments given 1/week of 3 mg/kg DXR) commenced 24 h post implantation of cells was able to improve significantly the MST of mice compared to either free DXR ($p<0.001$), DXR-SL ($p<0.01$), drug-free SIL[anti-CD19] ($p<0.001$), or untreated controls ($p<0.001$) (Table 2.4 B.6). There was no therapeutic difference observed between either free DXR, DXR-SL or drug-free SIL[anti-CD19] (dosed at an equivalent phospholipid concentration), $p>0.05$. However, the survival times of mice given three treatments were modestly improved compared to a single treatment (Table 2.4 B.6 *vs.* 4 B.3).

The therapeutic effect of free anti-CD19, and free anti-CD19 in conjunction with the various liposomal DXR formulations were examined (Table 2.4 C.7-8). Single doses of free anti-CD19 (10 μg) were able to modestly improve survival time of mice compared to untreated controls ($p<0.05$), or mice given the isotype-matched IgG2a control (10 μg) ($p<0.05$). There was no significant difference between the mean survival time of isotype-matched IgG2a-dosed mice and that of controls ($p>0.05$). The inclusion of anti-CD19 (10 μg) with either free DXR, DXR-SL or DXR-SIL[anti-CD19] increased survival time of

mice in an additive manner (Table 2.4 C.7 *vs.* 4 B.3). Treatment at 1 h with anti-CD19 plus DXR-SIL[anti-CD19] was more effective than anti-CD19 plus drug-free SIL[anti-CD19] controls ($p<0.001$) (Table 2.4 C.7).

Multiple doses of mAb anti-CD19 resulted in significantly increased mean survival times of mice compared to single treatments with mAb (Table 2.4 C.7 *vs.* 4C.8). MAb anti-CD19 was as effective by itself in multiple doses, as it was in combination with free DXR. Addition of free mAb to DXR-SL or DXR-SIL[anti-CD19] showed a significantly improved therapeutic benefit ($p<0.001$) (Table 2.4 B.6 *vs.* 4 C.8).

2.5 DISCUSSION

In these experiments we have shown that DXR-SIL[anti-CD19] can be selectively targeted to, and have preferential cytotoxicity for $CD19^+$ B cells *in vitro*. *In vivo* experiments in $CD19^+$ B-lymphoma (Namalwa cell line) xenografts established in SCID mice show that treatment with a long-circulating formulation of DXR-SIL[anti-CD19] can inhibit the growth of tumour resulting in an increased mean survival time of treated mice, compared to mice treated with non-targeted liposomes or free drug. The results for the DXR-SIL[anti-CD19] were additive with those of the free mAb anti-CD19.

Targeting immunoliposomal anticancer drugs to the highly expressed leucocyte differentiation antigen CD19, an internalizing epitope (287, 288, 308-310), may lead to efficient entry of drug into the target cells, and may explain the increased therapeutic effects seen for DXR-SIL[anti-CD19] compared to other treatment groups. We hypothesize that gradual breakdown of the drug package within the endocytotic apparatus

of the cell and subsequent release of drug into the cytoplasm results in the observed cytotoxicity. In the case of free drug DXR, its large volume of distribution, and rapid redistribution quickly lowers the plasma drug levels, resulting in exposure of circulating B cells to only low drug levels (47, 51, 281). In contrast, DXR-SL is capable of maintaining the entrapped drug in circulation for several hours (the volume of distribution of DXR-SL is roughly equivalent to the blood volume), allowing a sustained release of DXR over a prolonged period (47). However, because these liposomes do not attach to the vascular target cells, the uptake of the released drug will be low, as released drug will rapidly redistribute *in vivo*. If liposomes became attached to vascular target cells by non-specific adsorption or *via* a non-internalizing epitope, high local concentrations of DXR might be achieved at the outer surface of the target cell. However, only a fraction of the released drug might actually be delivered into the target cell, depending upon both the rate of drug release from liposomes and/or rate of diffusion of released drug away from the cell surface. Thus targeting to an internalizing epitope appears to be a more successful strategy for cells in the vasculature.

At present it is not known to what extent DXR-SIL[anti-CD19] will be able to access tumour cells which have extravasated and are growing as solid tumours. The pharmacokinetic data in tumour-bearing *versus* tumour-free mice suggests that SIL[anti-CD19] are binding to $CD19^+$ tumour cells in blood, liver, spleen and carcass. It is known that passive targeting of long-circulating liposomes such as DXR-SL to solid tumours can achieve increased tumour accumulation of drug as a result of the increased vascular permeability of tumours during angiogenesis (47, 51). It is reasonable to hypothesize that

DXR-SIL are also able to accumulate to some extent in solid tumours, although passive accumulation of DXR-SL over time appears to be greater than that of DXR-SIL in tumour-bearing lymph nodes (Fig. 2.5).

We observed no apparent ascitic tumour development in mice with i.p. treatments of DXR-SIL[anti-CD19], after the tumour cells were inoculated i.p. However, the appearance of solid tumours in the peritoneum of treated mice suggests that the ability of SIL to kill cells which extravasate and lodge in the peritoneum is somewhat limited. Although malignant cells could be found in the blood of untreated i.p.-inoculated mice, no malignant cells could be found in the blood of mice treated i.p. with DXR-SIL[anti-CD19]. This suggests that the SIL treatment was able to eliminate tumour cells from the peritoneal cavity before they could migrate into blood. Alternatively, the SIL may be capable of crossing from the peritoneal cavity into the blood (311), perhaps by the same route as the cells, or in association with the cells, resulting in subsequent tumour cell kill in blood (307).

When the mice were inoculated i.v. with tumour, very few B cells could be detected in blood at 24 h post-implantation. Yet a single DXR-SIL[anti-CD19] treatment, given at 24 h, resulted in significantly increased survival times over the other treatment groups (Table 2.4 B.3). This suggests that the SIL were able to access at least some of the malignant B cells soon after they had extravasated into lymph nodes, spleen or bone marrow. Multiple weekly treatments (i.v.) modestly improved the survival times of mice, i.e., two additional treatments resulted in only a marginal therapeutic benefit (Table 2.4 B.6). This suggests that target cells may be relatively inaccessible one week or more after

extravasation, or have grown to a size which hinders penetration of subsequent DXR-SIL treatments. Treatment effectiveness was dependent on both the dose of implanted tumour, and time of initiation of the therapeutic protocol. Early intervention (i.e. 1 h post-cells) and lower tumour burdens resulted in the most successful therapy, yielding some cures in mice implanted with the B-cell tumour (Table 2.4B.5). The success of this schedule, indicated that the SIL[anti-CD19] were readily able to target and destroy tumour cells which were still circulating in blood.

Free mAb anti-CD19 is a signalling molecule, and binding of anti-CD19 to $CD19^+$ B cells has been suggested to trigger a series of second messages ultimately leading to cell cycle arrest in B cells (4, 289, 312). In our study, the anti-CD19 alone was cytotoxic *in vitro* and *in vivo*. Combination treatment of anti-CD19 with either free DXR, DXR-SL or DXR-SIL[anti-CD19] was superior than each of the treatments given alone, with the improvements appearing to be due to an additive effect between low levels of the mAb and DXR-treatments. This observation may provide a means for improving therapy while keeping levels of mAb low, thus reducing the potential for immune reactions against the antibody.

Our results suggest that DXR-SIL[anti-CD19] readily targets and destroys individual cells in the blood or ascites, and perhaps single or small groups of cells newly extravasated into lymph nodes, but is unable to prevent the growth of these cells once they establish themselves as multicellular solid tumours. These observations may provide additional evidence for the 'binding site barrier' in solid tumours (174), which states that targeted therapies bind to the first recognized target antigen, generally at the outer limits

of tumours, preventing the therapeutic agent from penetrating to a significant extent into the tumour interior.

At the Ab densities at which our studies were done (40-60 μg Ab/μmol PL), the SIL retained long circulation times ($t_{1/2}$ in blood of 7-9 h), sufficient to bind to target cells. Previous studies have shown that high Ab densities on liposomes (>140 μg/μmol PL) induces rapid clearance from plasma ($t_{1/2}$<1 h), so Ab densities in a lower range mediate more effective *in vivo* targeting (284). For the coupling method used here, the linkage occurs *via* an oxidised carbohydrate on the Fc portion of the mAb, coupled to the terminus of Hz-PEG-DSPE *via* a hydrazone bond (53, 168, 169). This orientation of the Ab appears to expose the Fab binding domain (53, 169) allowing it to recognize the CD19 epitope on B cells.

The affinity constant, K_a and number of binding sites this anti-CD19 on Daudi cells (another $CD19^+$ B cell line) have been reported as 4.2×10^9 M^{-1} (dissociation constant, K_D of 2.4×10^{-4} μM mAb) and 32,000 sites per cell, respectively (313). In comparison, the K_D for SIL[anti-CD19] was significantly lower (K_D of 160 μM phospholipid or 4.0×10^{-2} μM mAb, at an mAb density of 40 μg/μmol PL), but the number of specific sites were similar (33,000 *vs.* 32,000). This is comparable to the number of binding sites reported for Namalwa cells (18,000 to 40,000) (312, 314). We have calculated that each liposome contains approximately 25 molecules of mAb. Assuming an interaction of one mAb/liposome/receptor binding site, then only 4 % of the mAbs on each liposome are binding. The K_D of the mAb which bind then can be calculated as 1.6×10^{-3} μM. Thus, the K_D of antibody was higher than the free mAb after coupling of anti-CD19 on the

terminus of the PEG chains. This may be a result of damage to the mAb during the oxidation step of the coupling reaction and/or immobilization of mAb coupled *via* the Fc domain reducing rotational freedom of the mAb to bind CD19 receptors. Several steric factors, i.e., relative size of mAb to liposome-mAb conjugate, and dynamic movement of PEG polymers chains (315) may also be responsible in part for the reduced affinity of SIL[anti-CD19].

A possible clinical application of DXR-SIL[anti-CD19] is in the treatment of B-cell malignancies (i.e. B-cell leukemias/lymphomas, MM). To date, these cancers still remain largely incurable. For example in the case of MM, the presumptive ability of circulating malignant B cells to repopulate the bone marrow and contribute to patient relapse poses a problem for curing this disease, as does the development of multidrug resistant B cell variants (258, 270, 271). The use of long-circulating immunoliposomes in eliminating the circulating B cells may help to prevent patient relapse. A possible concern might be the depletion of normal B cells as well as the malignant clone. Myeloma patients have been shown to have severely depressed numbers of normal B cells (316), probably making this concern of minimal significance. It is known that the CD19 is B-lineage specific, is present on B cells from the pre-B until the late B stage, but is absent from some progenitor stem cells, non-haematopoietic organs, blood cells (myeloid and erythroid) and in particular T cells (287, 288). As a result, immunoliposomal therapy with DXR-SIL[anti-CD19] should deplete B-lineage cells but spare early stem cells allowing regeneration of normal B cells post-therapy. In addition, upon internalization immunoliposomes can deliver high levels of drug into the cytoplasm, potentially bypassing

the P-gp and MRP transporters (269, 317) which have been implicated in the drug resistance of multiple myeloma (258), thus providing a means of overcoming MDR.

In summary, targeting of anticancer drugs by means of liposomes coupled to an antibody against an internalizing epitope appears to be an effective strategy for the treatment of hematological malignancies, particularly when the target cell is resident primarily within the vasculature. We have shown selective targeting and cytotoxicity of doxorubicin entrapped in a liposome coupled to anti-CD19 against a human lymphoma cell line *in vitro* and *in vivo*. This strategy may be generally applicable in the treatment of many blood dyscrasias of both B cell and T cell origin, and in addition may be helpful in overcoming MDR in the target cells.

CHAPTER 3

Cellular trafficking and cytotoxicity of anti-CD19-targeted liposomal doxorubicin for a human B lymphoma cell line (Namalwa) *in vitro*

3.1 ABSTRACT

We have examined cellular trafficking of doxorubicin in human B lymphoma (Namalwa) cells in the form of free drug (DXR), non-targeted liposomal drug (DXR-SL) or drug delivered *via* liposomes targeted against an internalizing CD19 receptor expressed at the cell surface (anti-CD19 immunoliposomal DXR, DXR-SIL[anti-CD19]). Liposomes (SL) were sterically stabilized with lipid derivatives of polyethylene glycol (PEG) to which monoclonal antibody was attached, and were composed of either high-phase transition (HSPC) or low phase transition phosphatidylcholine (PC40) in combination with cholesterol. *In vitro* binding experiments using fluorescent liposomes and flow cytometry demonstrated selective affinity of SIL[anti-CD19] for $CD19^+$ Namalwa cells, but not control $CD19^-$ T cells. Internalization of SIL[anti-CD19] into a low pH compartment, i.e., endosomes or lysosomes, could be demonstrated using a pH-sensitive probe, HPTS, encapsulated in liposomes. Time-dependent studies using flow cytometry revealed that free DXR accumulated rapidly in cells, DXR-SIL[anti-CD19] accumulated less rapidly and DXR presented in non-targeted control liposomes was taken up by cells only very slowly. The cellular levels of DXR were similar for both high and low phase transition formulations of DXR-SIL[anti-CD19], and were several-fold higher than for non-targeted controls. The endocytosis and intracellular fate of DXR-loaded liposomes were also studied using confocal microscopy. At early times (1 h), the drug appeared mainly at the cell surface with some DXR sequestered within vesicular structures (likely endosomes) in cells. The cellular levels of DXR-SIL[anti-CD19] increased appreciably after longer incubation periods, and this could be abolished by metabolic

inhibitors of endocytosis. Namalwa cells incubated with DXR-SIL[anti-CD19] for 48 hours demonstrated substantial nuclear staining. This suggests that lysosomal processing of targeted liposomes may traffic the drug from the endosomes and/or lysosomes to the target site of action (i.e., the nucleus). Supporting this, was the observation that cytotoxicity of DXR-SIL[anti-CD19] was 5-fold higher than that observed for non-targeted controls. The targeted formulations were shown to be selectively apoptotic to $CD19^+$ cells compared to a $CD19^-$ cells.

We suggest that an antibody-mediated targeting approach using liposomal doxorubicin against the internalizing CD19 antigen may be an effective therapy for the selective destruction of malignant $CD19^+$ B cells in B-cell malignancies.

3.2 INTRODUCTION

One approach to increasing the selective toxicity of anticancer drugs against their target cells is the association of the drugs with targetable carrier devices, i.e., antibodies or ligands, polymers, microcapsules, microspheres or liposomes (7, 12, 13, 185, 318). Over the last decade, new formulations of long-circulating sterically stabilized liposomes (SL) have been described, having polyethylene glycol (PEG) grafted at the liposome surface (71, 122, 319). It has been shown that encapsulation of doxorubicin (DXR) in SL can improve tumour localization and reduce toxicities associated with the free drug therapy (15, 51, 86, 142, 320). This occurs primarily as a result of liposome-mediated changes in the pharmacokinetics and biodistribution of the drug (45, 86, 119, 280, 281, 321).

The development of coupling technologies for attaching antibodies or ligands to

the surface of SL, creating long circulating immunoliposomes (SIL), provides opportunities for further increasing the selective toxicity of liposomal anticancer drugs (156, 165, 284, 322). Immunoliposomes have been shown to increase target-cell recognition (147, 202, 283) and cytotoxicity in a number of tumour models *in vitro* and *in vivo* (162, 165, 323, 324). However, most studies to date have utilized immunoliposomes in the treatment of solid tumours (16, 185, 324), where penetration of liposomes into the tumour mass may be restricted (174).

In hematological malignancies, large numbers of clonal, phenotypically aberrant, diseased cells are present within the circulatory system (257, 259), presenting a readily accessible target for immunoliposomal anticancer drugs. Malignant B and T cells express a variety of surface antigens, many of which demonstrate receptor-mediated internalization following binding of the appropriate antibody (4, 16, 278, 279). Attachment of antibodies like anti-CD19 or anti-CD22 to SL may enhance the uptake of liposomal anticancer drugs by malignant B cells in the blood, resulting in selective toxicity. To test this hypothesis, we analyzed the binding, internalization, intracellular trafficking, and cytotoxicity of DXR-SIL[anti-CD19] against Namalwa cells *in vitro*.

In our study we have targeted a human B cell lymphoma (the Namalwa cell line) with an antibody directed against the human lymphocyte differentiation antigen CD19. The targeted antigen CD19 is highly expressed on the cell surface, and is exclusive to B lymphocytes (287, 288). CD19 is known to be an internalizing receptor and has been implicated in a number of signaling functions, leading to differentiation events, cell-cycle arrest or apoptosis (309, 310). Hence, binding of DXR-SIL[anti-CD19] to CD19 is

expected to result in endocytosis of the liposomal- drug package. The trafficking of liposomal DXR from lysosomes or endosomes to its nuclear site of action has not been well studied. Also, relatively little work has been done to compare drug trafficking for drug presented in targeted *versus* non-targeted liposomes. Two formulations of DXR-SIL[anti-CD19] were assessed, a high phase transition temperature formulation and a more leaky, low phase transition formulation, to test the hypothesis that a leakier formulation may enhance the release of drug after endocytosis and improve its trafficking to the nucleus.

3.3 MATERIALS AND METHODS

3.3.1 Chemicals.

Hydrogenated soy phosphatidylcholine (HSPC), partially hydrogenated egg phosphatidylcholine (PC40) iodine value 40 (325), methoxy poly(ethyleneglycol) (molecular weight 2000) covalently linked to distearoylphosphatidylethanolamine ($mPEG_{2000}$-DSPE) and hydrazide-derivatized PEG (Hz-PEG-DSPE) were generous gifts from SEQUUS Pharmaceuticals, Inc. (Menlo Park, CA) and have been described elsewhere (123, 168). Cholesterol (CHOL) and 12-[N-(nitrobenz-2-oxa-1,3-diazol-4-yl)amino]dodecanoyl phosphatidylethanolamine (NBD-PE) were purchased from Avanti Polar Lipids (Alabaster, AL). 1-hydroxypyrene-3,6,8-trisulfonic acid (HPTS) was obtained from Molecular Probes (Eugene, OR). N-acetyl-methionine (NAM), sodium periodate, propidium iodide (PI), 3-[4,5-dimethylthiazol-2-yl]-2,5,-diphenyltetrazolium bromide (MTT) and Dowex-50W were purchased from Sigma Chemical Co. (St. Louis,

MO). 4-(2-hydroxyethyl)-1-piperazine ethanesulphonic acid (HEPES) was acquired from BDH (Toronto, ON). Doxorubicin (DXR, Adriamycin RDF) was obtained from Adria Laboratories Inc. (Mississauga, ON). RPMI 1640 media (without phenol red), penicillin-streptomycin, and fetal bovine serum (FBS) were purchased from Gibco BRL (Burlington, ON). Sephadex G50 and Sepharose CL-4B were from Pharmacia (Dorval, QC). Cholesteryl-[1,2- ^{3}H-(N)]-hexadecyl ether ([^{3}H]CHE), 1.48-2.22 TBq/mmol, was purchased from New England Nuclear (Mississauga, ON). Iodobeads^{R} were from Pierce Chemical Co. (Rockford, IL). Scintillation fluor/ aqueous counting scintillant (ACS) was from Amersham Canada Ltd. (Oakville, ON). Polycarbonate filtration membranes, Nuclepore^{R} (pore sizes: 0.4 μm, 0.2 μm, 0.1 μm and 0.08 μm), were obtained from Corning Costar (Kennebunk, ME). All other chemicals were of analytical grade purity.

3.3.2 Antibodies and human cell lines.

Murine monoclonal antibody (mAb) anti-CD19 (IgG2a) (from FMC63 murine CD19 hybridoma) and isotype-matched control IgG2a (IAG.11) were obtained from Dr. H. Zola (Adelaide, Australia) (295). The concentrations of all mAbs were determined by spectrophotometry (λ= 280 nm) and BioRad protein assays, and the purity was assessed by SDS-PAGE. Anti-CD45-phycoerythrin (PhE) was mAb 17G10 from Dr. J. Wilkins, University of Manitoba. MAbs anti-CD19 (IgG1, HD37) , anti-CD22 (IgG1, RF-B4-B3) and isotype matched control (IgG1, 3F12) were obtained from Dr. E. Vitetta (University of Texas Southwestern Medical Centre, Dallas). Mouse monoclonal antibodies specific for human leukocyte differentiation antigens: CD4, CD8, CD20, CD21, CD22, CD24, CD34, CD38, PCA-1, CD45 were either prepared in one of our laboratories, or were

purchased from Coulter (Hialiah, FL) or Becton Dickinson (San Jose, CA). All mAb reactivities were checked prior to use by indirect immunofluorescence using fluorescein isothiocyanate (FITC)-labelled goat anti-mouse IgG and fluorescence activated cell sorting (FACS) (Becton Dickinson, San Jose, CA) against appropriate cell lines. All comparisons were made with FITC or PhE staining against appropriate isotype-matched controls.

The human B-cell lymphoma line, Namalwa (ATCC CRL 1432) was obtained from American Type Culture Collection (Rockville, MD). A human T-lymphoma cell line (H9) (ATTC HTB 176) was a gift from Dr. L-J. Chang (Department of Medical Microbiology and Infectious Disease, University of Alberta). All cell lines were grown as suspension cultures in RPMI 1640, without phenol red, supplemented with 10 % heat-inactivated FBS and maintained at 37°C in a humidified incubator (90 % humidity) containing 5 % CO_2. All experiments were performed on mycoplasma-free cell lines. For *in vitro* experiments, only cells in the exponential growth phase were utilized (i.e., cell concentration in flasks of approximately 0.5 - 1 x 10^6 cells/ml) and cell concentrations in culture wells were adjusted according to the *in vitro* cell doubling times of each cell line, to assure exponential growth in assays.

3.3.3 Immunophenotyping of Namalwa cell line.

The Namalwa human B-cell lymphoma cell line was phenotyped with antibodies against the following lymphocyte differentiation antigens CD19, CD20, CD21, CD22, CD24, CD34, CD38, CD45 using flow cytometry. Cell surface markers were examined by immunostaining with specific Abs, by direct or indirect immunostaining methods. Antibodies were either unlabelled, or labelled with fluorescein isothiocyanate (FITC) or

phycoerythrin (PhE). Namalwa cells ($1x10^6$ cells) were incubated in the dark with 10 µg mAb at 4°C for 30 min in a total volume of 50 µl, adjusted with phosphate buffered saline (PBS). After incubation, cells were washed three times with immunofluorescence buffer containing PBS supplemented with 0.1 % FBS and 0.1 % sodium azide (IF buffer) and run on the flow cytometer. For the indirect staining protocol, after staining with the primary Ab, cells were incubated with 50 µl of a 1:20 dilution of goat anti-mouse-FITC IgG (Sigma) in PBS at 4°C for 30 min. In some cases, cells were fixed with 1 % paraformaldehyde and run at a later time, but no longer than 24 h after fixation. Cell-associated fluorescence was analysed on a Becton Dickinson FACScan using Lysis II software (Becton Dickinson, San Jose, CA). FITC- and PhE-fluorescent markers were excited with an argon laser (488 nm) and the emitted fluorescence was detected using 530 nm or 560 nm band pass filters for FITC or PhE, respectively.

3.3.4 Preparation of liposomes.

Liposomes were composed of either HSPC or PC40 together with CHOL and $mPEG_{2000}$-DSPE at a 2:1:0.1 molar ratio. When mAb was to be coupled to the liposomes the composition was either HSPC or PC40 with CHOL and Hz-PEG_{2000}-DSPE (2:1:0.1 molar ratio). For fluorescent-labelled liposomes, NBD-PE (1 mol%) was incorporated into the lipid mixture. In some preparations, [^{3}H]CHE was added as a non-exchangeable, non-metabolizable lipid tracer (296, 297). Dried lipid films were hydrated in 25 mM HEPES, 140 mM NaCl buffer (pH 7.4) and the hydrated liposomes (MLV) were sequentially extruded (Lipex Biomembranes Extruder, Vancouver, BC) through a series of polycarbonate filters of pore size ranging from 0.4 µm down to 0.08 µm. The

temperature of extrusion was maintained slightly above the transition temperature of the phospholipid, i.e., 65°C for HSPC- or 40°C for PC40-containing liposomes. This extrusion procedure has been shown to produce primarily unilamellar vesicles (34). Liposomal size was characterized by dynamic light scattering using a Brookhaven B190 submicron particle size analyser (Brookhaven Instruments Corp., Holtsville, NY). The mean liposomal diameters of extruded liposomes were in the range of 95 - 110 nm. Phospholipid concentrations were determined from either the specific activity counts of [^{3}H]CHE tracer or by the Bartlett colorimetric assay (298).

3.3.5 Loading of doxorubicin (DXR).

DXR was encapsulated into liposomes by remote loading using an ammonium sulphate gradient (42). Lipid films were hydrated in 250 mM ammonium sulphate (pH 5.5) and the external buffer was exchanged by eluting through a Sephadex G-50 column equilibrated with 123 mM sodium citrate (pH 5.5). DXR was added to the liposomes at a phospholipid:DXR ratio of 1:0.2 w/w and incubated for 1 h at 65°C. The liposome-encapsulated DXR was separated from the free DXR over a Sephadex G-50 column eluted with 123 mM sodium citrate (pH 5.5). The concentration of the liposome-entrapped DXR was determined by spectrophotometry (λ= 480 nm). The amount of DXR loaded in liposomes was 150 µg DXR/µmol PL (0.26 µmol DXR/µmol PL), with an encapsulation efficiency of greater than 95 %.

3.3.6 Hydrazide method for coupling mAb anti-CD19 to liposomes.

Antibodies were coupled to the terminus of PEG *via* the hydrazide coupling method (53, 169). Carbohydrate in the Fc region of the mAb was oxidized for 1 h at

22°C with 10 mM sodium periodate in 250 mM citrate buffer, pH 5.5. To determine the efficiency of coupling, in some experiments a trace amount of ^{125}I-labelled mAb was added. To terminate the oxidation reaction, excess periodate was quenched with 50 mM NAM in distilled water, for approximately 5 min. The oxidized Ab was then incubated overnight at 5°C with Hz-PEG-liposomes at an Ab:PL molar ratio of 1:1000. Finally, the immunoliposomes were separated from the free mAb over a Sephadex CL-4B column equilibrated with 25 mM HEPES, 140 mM NaCl buffer, pH 7.4. The efficiency of coupling was determined from the amount of ^{125}I-labelled mAb bound to the surface of liposomes. The coupling efficiency was approximately 32 %, with 40 - 60 μg mAb/μmol PL (or 0.32 nmol mAb/μmol PL) attached at the liposome surface.

3.3.7 Leakage of DXR from liposomes.

Leakage experiments were performed on DXR-loaded liposomes composed of either HSPC:CHOL:Hz-PEG-DSPE or PC40:CHOL:Hz-PEG-DSPE (2:1:0.1 molar ratio). All liposome preparations were freshly prepared and free DXR, when present, was separated by eluting over a Sephadex G-50 column. Liposomes were incubated with either phosphate buffered saline (PBS) or human plasma in 24-well plates at a final DXR concentration of 10 μg/ml. The plates were incubated at 37°C with constant agitation for 24 h using a plate shaker. The fluorescence of anthracyclines is quenched at high concentrations, or when encapsulated in liposomes (350). DXR-leakage from liposomes was followed by measuring the fluorescence-dequenching of DXR at selected time points (0 - 24 h) using fluorimetry (CytoFlour 2350™, Millipore, Bedford, MA). Complete release (100 % dequenching) of DXR was obtained by treating liposomes with 5 μl of 10

% Triton X-100 in distilled water. Percent DXR released was determined from fluorescence intensity of wells relative to 100 % dequenching.

3.3.8 *In vitro* binding experiments using fluorescent liposomes.

Immunoliposomes were labelled with a fluorescent lipid marker, NBD-PE (1 mol %), and binding of liposomes to cells was examined using FACS. Various formulations of NBD-PE-labelled liposomes were incubated with 1 x 10^6 B or T lymphoma cells at a final PL concentration of 400 nmol/ml for 1, 4 and 24 h at 37°C in a humidified incubator containing 5 % CO_2. In competition experiments, targeted NBD-SIL[anti-CD19] liposomes were incubated with 25-fold excess free anti-CD19 (6.4 x 10^{-4} µmol anti-CD19). Cells were washed three times with IF buffer and fixed with 1 % formalin prior to analysis on the flow cytometer. Cell debris were excluded by appropriate gating on forward *versus* side angle scatter profiles. Files were collected of 5000 - 20000 events and later analysed using the LYSIS II software program (Becton Dickinson, San Jose, CA).

3.3.9 Uptake of doxorubicin (DXR) by Namalwa cells using flow cytometry.

The characteristic fluorescence spectra of DXR (excitation 480 nm, emission peak 580 nm) was used to determine the association of DXR with Namalwa cells, using flow cytometry. Namalwa cells were incubated with either free DXR or various liposomal formulations of DXR at concentrations of drug ranging from 0.1 - 100 µg/ml for 1, 4 or 24 h at 37°C. Post-incubation, cells were washed with cold IF buffer and immediately run on a Becton Dickinson FACScan (Becton Dickinson, San Jose, CA). DXR molecules associated with cells were excited with an argon laser (488 nm) and the emitted

fluorescence could be detected through 560 nm (FL2) band pass filters. Files were collected of 10,000 ungated events and were later analysed using the LYSIS II software. Cell debris were excluded by appropriate gating on forward *versus* side angle scatter profiles during analysis, taking into account that DXR-treated cells may be apoptotic.

3.3.10 Analysis of liposomal DXR associated with Namalwa cells using HPLC.

The amount of DXR associated with Namalwa cells was measured using HPLC (326-328). Namalwa cells (1 x 10^6 cells/well) were incubated with free DXR, low or high phase transition DXR-SL, or low or high phase transition DXR-SIL[anti-CD19] at concentrations from 0.1 µg DXR/ml to 100 µg DXR/ml. Post-incubation, cells were washed three times with cold PBS, lysed with cold distilled water, then extracted with a mixture of chloroform and acidified (0.4 N sulphurc acid) isopropanol (1:1 v/v). After mixing at room temperature, the organic extract as collected, solvent evaporated, and the residue was reconstituted in methanol. The recovered compounds were analysed on a Beckman HPLC (Beckman Instruments Inc., Fullerton, CA), using a Supelcosil LC-18 reverse phase column after a pre-column filter and a Supelcosil LC-18 guard column. Compounds were eluted at room temperature at a flow rate of 1 ml/min for 30 min with a linear gradient from 30 % acetonitrile in water containing 0.05 % trifluoroacetic acid to 90 % acetonitrile in water. DXR and its primary metabolite were detected by fluorimetry (excitation 480 nm, emission 580 nm) using a Shimadzu spectrofluorimetric detector (Shimadzu Scientific Instruments Inc., Japan). DXR was quantitated by measuring relative peak area ratios against an internal daunorubicin standard.

3.3.11 Internalization experiments using the pH-sensitive fluorophore HPTS.

Internalization of liposomes by Namalwa cells was studied using an encapsulated pH-sensitive fluorescent probe HPTS as described elsewhere (329, 330). The dye displays two complementary pH-dependent peaks at 403 and 450 nm and a pH-independent peak at 413 nm (isobestic point). Briefly, 1 x 10^6 cells were incubated with liposomal HPTS at a final PL concentration of 400 nmol/ml for 1 h at 37°C. After incubation, cells were washed with PBS, and the cell-associated fluorescence determined by scanning the excitation spectra from 320 to 500 nm, keeping the emission wavelength fixed at 510 nm. The ratios of the excitation peaks at 403 nm and 450 nm to the isobestic point at 413 nm, were measured and the pH environment of the HPTS was determined from a previously prepared standard curve of HPTS in the pH range 4 - 9.

3.3.12 Intracellular distribution of liposomal DXR using confocal laser scanning microscopy.

Namalwa cells, control cells ($CD19^-$ T cells), or a heterogenous mixture of Namalwa and T cells (1:1), were incubated at 1 x 10^6 cells/well in a total volume of 100 µl RPMI 1640 supplemented with 10 % FBS. Free DXR, or liposomal formulations of DXR (20 µg DXR/ml, in a total volume of 500 µl media) was incubated with cells for 1, 24 or 48 h at 4°C or 37°C. In some experiments, cells were treated with 0.1 % sodium azide, a metabolic inhibitor. Cells were then washed with cold PBS and stained for 30 min with appropriate cell surface markers, i.e., anti-CD19-FITC (or anti-CD19 + goat anti-mouse FITC-IgG) (B cells) or anti-CD4-FITC (or anti-CD4 + goat anti-mouse FITC-IgG) (T cells). Cells were allowed to adhere onto poly-L-lysine-coated slides prior to mounting

with PermaFluor (Lipshaw Immunon, Pittsburgh, PA.). Cells were then visualized on the confocal laser scanning microscope system consisting of a Leitz Aristoplan Fluorescence Microscope illuminated by a 100W HBO mercury burner (for direct observation) and an argon-krypton laser with emissions at 488, 568, and 647 nm for scanning. Cells were optically sectioned and images (512 x 512 pixel) were stored on optical disks for further analyses using Leica Lasertechnick GmbH (Heidelberg, Germany) software. All instrumental parameters pertaining to fluorescence illumination, detection, and image analyses were held constant to allow sample comparison.

3.3.13 Quantitation of DXR-induced cytotoxicity on cell lines using propidium iodide.

Cytotoxicity of DXR or liposomal DXR to Namalwa cells was evaluated using the DNA-binding dye propidium iodide (PI). Namalwa cells (1×10^6) were incubated with either DXR or different formulations of liposomal DXR for 24 h at 37°C. After 24 h, cells were washed and allowed to grow for an additional 24 h in drug-free media. At the end of the incubation period, cells were washed, permeabilized with 70 % ethanol at 4°C, RNAase-treated, and stained with 0.2 ml of 50 µg/ml propidium iodide. Samples were stored for 30 min on ice, prior to running on the flow cytometer. Files of 20,000 ungated events were collected and analysed by Cellquest software (Becton Dickinson, San Jose, CA). The position of the diploid peak was set on a linear fluorescence scale and appropriate markers were set to detect diploid, hypodiploid or apoptotic cells.

3.3.14 Cytotoxicity assays.

Comparisons of the cytotoxicity of various liposomal formulations of DXR were

performed on Namalwa cells with an *in vitro* proliferation assay utilizing tetrazolium dye MTT (299). Briefly, 5 x 10^5 cells were plated in 96-well plates, with or without Dowex-50W (331, 332), and were allowed to incubate for 1h at 37°C. Dowex-50W efficiently adsorbs free DXR or DXR released from liposomes. The amount of Dowex-50W used in these experiments was limited to levels which showed minimal inhibition of cell growth in the absence of drug treatments.

Cells were incubated with either free DXR, DXR-SL, DXR-SIL[anti-CD19] or liposomes coupled to an isotype-matched control antibody (DXR-NSIL[IgG2a]). Approximately 5 to 6 replicate microcultures were prepared at each drug concentration. Cells were incubated for 1 or 24 h at 37°C in an atmosphere of 95 % humidity and 5 % CO_2. Cells were washed twice prior to replacing with fresh media. Plates were incubated for a total 48 h. At 48 h, the plates were then centrifuged for 10 minutes at 800 rpm and the supernatant was carefully aspirated. MTT (25 μg/well) was added to each well and the plates were further incubated for 4 h at 37°C in a CO_2 incubator, protected from light. Following this, the colored formazan product was dissolved using 100 μl of acid-isopropanol and the plates were read on a Titertek Multiskan Plus (Flow Laboratories Inc., Mississauga, Ont.) at a test wavelength λ= 570 nm against a reference, λ= 650 nm. The absorbance reading from each well was proportional to the cell viability and results were expressed as % cell viability in test wells compared to controls measured in the absence of test drug, mAbs or liposomes. The IC_{50} of the test was defined as the concentration of test agents that produced a 50 % reduction in cell viability compared to drug-free control.

3.3.15 Statistical analyses.

All linear regression analyses were done using Quattro Pro 4.0 (Borland Inc., Scotts valley, CA). Unless otherwise stated, Student's t-test was used to measure statistical significance between two treatment pairs. Multiple comparisons of various groups in cytotoxic assays were evaluated using one-way analysis of variance performed on INSTAT (GraphPAD software, version 1.11a), and post-tests comparing the different treatment means were done using Bonferroni's test. Data were considered statistically significant at p values < 0.05. Data were reported as mean ± standard deviation (S.D.).

3.4. RESULTS

3.4.1 Immunophenotyping of Namalwa cells using flow cytometry.

Phenotyping of the Namalwa cells demonstrated that this cell line had a high expression of B-cell differentiation antigens: CD19, CD20, CD22, CD24. Expression of the antigens were ranked in terms of their mean fluorescent intensity, in Table 3.1. The levels of expression of the B-cell epitopes tested ranked as CD19 > CD24 > CD20 = CD22 > CD21 (Table 3.1). The B cell antigens were found to have no cross reactivities with the control $CD4^+$ T cell line (H9).

3.4.2 Leakage of doxorubicin (DXR) from liposomes.

Leakage experiments were performed on liposome-encapsulated DXR composed of HSPC(or PC40):CHOL:Hz-PEG-DSPE (2:1:0.1 molar ratio) (Fig. 3.1). All liposome preparations showed minimal leakage in PBS, retaining >90 % of the encapsulated DXR

Table 3.1. Immunophenotyping of Namalwa cell line using flow cytometry.

Marker	Expression[1]
CD4	-
CD8	-
CD19 IgG2a (FMC63)	++½
CD19 IgG1 (HD37)	++½
CD20	++
CD21	+
CD22 (RF-B4-B3)	++
CD24	+++
CD29 (β)	+++
CD34	-
CD38	+++½
CD45	++½
CD45RA	++
CD45RO	+++
PCA-1	+++½
IgG1-3F12	+
IgG1(control)	-
IgG2a (control)	-

Namalwa cells were incubated with an appropriate mAb (10 μg mAb/10^6 cells) at 4°C for 30 min. Cell surface markers were examined for immunostaining with specific Abs, by either direct or indirect immunofluorescent staining methods. Cells were washed with IF buffer prior to running on the flow cytometer. Cell-associated fluorescence was analysed on a Becton Dickinson FACScan.

[1] The reactivities of mAbs are presented in terms of relative mean logarithmic intensity of fluorescence (MFI) staining on Namalwa cells. ++++ MFI 10^4 (very high); +++ MFI 10^3 (high); ++ MFI 10^2 (moderate); + MFI 10^1 (dim/low); +/- MFI $10^{0.5}$-10^1 (very low); - MFI $<10^{0.5}$ (negative).

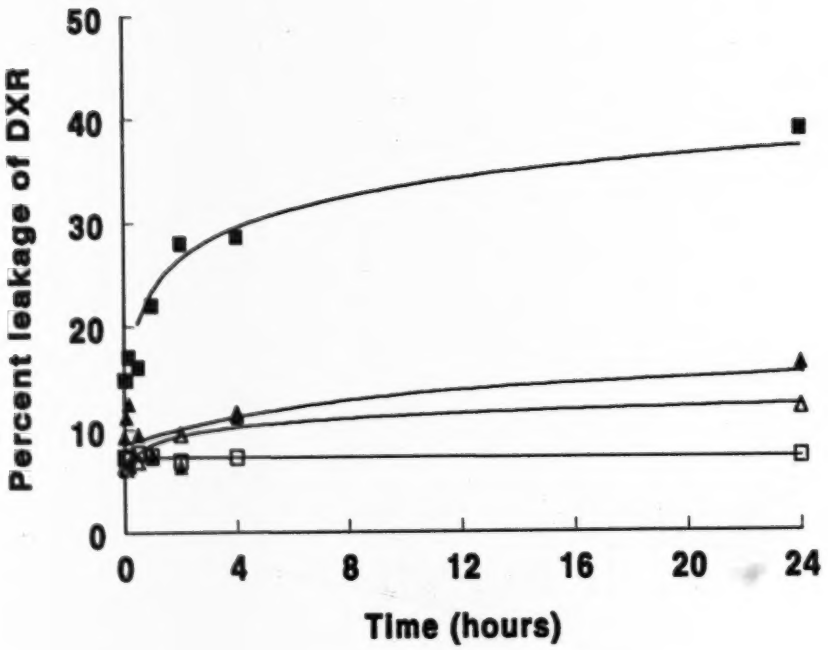

Figure 3.1. ***In vitro*** **release of doxorubicin (DXR) from liposomes.**
Liposomes were incubated in either phosphate buffered saline (open symbols) or 25 % human plasma (solid symbols) at a final DXR concentration of 10 μg/ml. The leakage of DXR was measured by fluorescence dequenching. Liposomes were composed of either HSPC:CHOL:Hz-PEG-DSPE (△,▲) or PC40:CHOL:Hz-PEG-DSPE.(□,■) containing encapsulated DXR.

after 24 h incubation. When the leakage experiments were conducted in 25 % human plasma, liposomes containing the high phase transition phospholipid, HSPC, showed a modest increase in DXR-leakage (16 %) at 24 h. The leakage rate was higher for the more fluid PC40 liposomes (Fig. 3.1) with approximately 40 % drug leaking out of the liposomes after 24 h (Fig. 3.1). This was likely due to release of any drug adsorbed at the liposome surface and enhanced leakage across the more fluid bilayers, perhaps induced in the presence of serum.

3.4.3 Binding of immunoliposomes to Namalwa cells.

Binding of NBD-labelled SIL[anti-CD19] or free anti-CD19-FITC by Namalwa cells was studied using flow cytometry (Fig. 3.2A). Namalwa cells stained with anti-CD19-FITC displayed a high surface expression of target antigen CD19, in comparison to untreated cells or cells treated with a isotype-matched control antibody IgG2a-FITC (Fig. 3.2A-a). NBD-SL (no Ab) or isotype-matched control liposomes NBD-NSIL[IgG2a] displayed minimal recognition by Namalwa cells, and were not different from the autofluoresence associated with untreated cells (Fig. 3.2A-b *vs.* a). NBD-SIL[anti-CD19] displayed a 1.5 log-fold increase in mean fluorescence intensity and was significantly higher than non-targeted controls (Fig. 3.2A-c *vs.* b). This specific association of SIL[anti-CD19] with Namalwa cells could be competively inhibited in the presence of excess free anti-CD19 (Fig. 3.2A-c).

The experiments in Fig. 3.2A were repeated using a control $CD4^+$H9 cell line, which does not express CD19 (Fig. 3.2B-a,b). As expected, no binding to the H9 cell line was observed for NBD-SL, NBD-NSIL[IgG2a] or NBD-SIL[anti-CD19] (Fig. 3.2B-c).

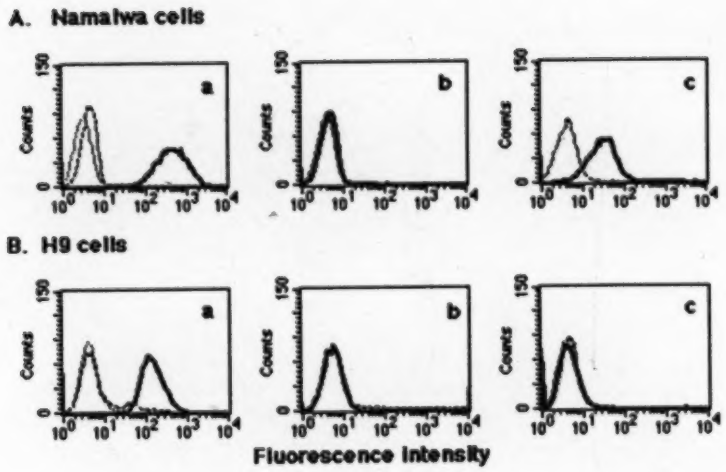

Figure 3.2. ***In vitro*** **binding of fluorescent NBD-labeled liposomes to CD19$^+$ Namalwa cells and control CD19$^-$ H9 cells using flow cytometry.**
NBD-labelled liposomes (0.1 mol%)were composed of HSPC or PC40:CHOL:Hz-PEG-DSPE, 2:1:0.1 molar ratio (105 nm in diameter) ± mAb anti-CD19. Namalwa cells were incubated with liposomes at a final lipid concentration of 400 nmol/ml for 1 h at 37°C. Panels illustrate: **A. Namalwa cells: a.** Untreated cells (dotted), irrelevant mAb IgG2a-FITC (dashed) and anti-CD19-FITC (bold line); **b**. NBD-SL (dashed) and NBD-NSIL[IgG2a] (bold line); **c**. Free anti-CD19 + NBD-SIL[anti-CD19] (dashed) and NBD-SIL[anti-CD19] (bold line); **B. H9 cells: a.** Untreated cells (dotted), control mAb IgG1-FITC, and anti-CD4-FITC (bold line); **b**. Control IgG2a-FITC (dashed) and anti-CD19-FITC (bold line); **c**. NBD-SL (dotted), NBD-NSIL[IgG2a] (dashed), or NBD-SIL[anti-CD19]. **C. Namalwa cells: a.** HSPC-SL at 1h (dashed) and 24 h (bold line); **b.** PC40-SL at 1h (dashed) and 24 h (bold line); **c.** HSPC-SIL[anti-CD19] at 1h (dashed) and 24 h (bold line); **d.** PC40-SIL[anti-CD19] at 1h (dashed) and 24 h (bold line).

C

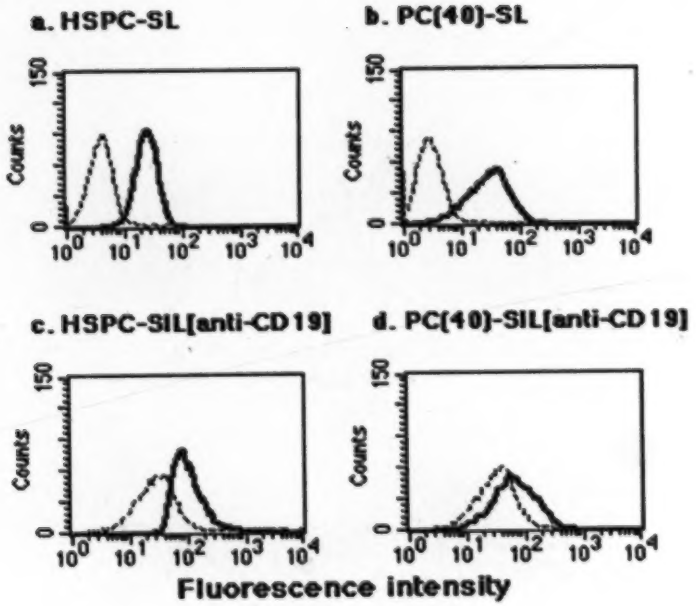
a. HSPC-SL
b. PC(40)-SL
c. HSPC-SIL[anti-CD19]
d. PC(40)-SIL[anti-CD19]
Counts
150
0
10^0 10^1 10^2 10^3 10^4
Fluorescence intensity

The time course for the association of SL, SIL[anti-CD19] and NSIL[IgG2a] with Namalwa cells was studied at 1 and 24 h. In these experiments, two formulations of NBD-liposomes were tested, HSPC-SL or PC40-SL, together with their targeted counterparts (Fig. 3.2C). NBD-labelled HSPC-SIL[anti-CD19] and PC40-SIL[anti-CD19] bound equally to Namalwa cells (Fig. 3.2C-c *vs.* d) and both targeted formulations exhibited higher binding to Namalwa cells at 1 and 24 h compared to non-targeted SL (Fig. 3.2C-c *vs.* a, and d *vs.* b). The association of all formulations with cells increased with time (Fig. 3.2C, 1 h *vs.* 24 h).

3.4.4 Quantitation of DXR association with Namalwa cells as a function of time and DXR concentration.

The term 'association' is used to indicate a combination of surface absorption of the liposomal DXR, internalization of the liposome together with its contents into Namalwa cells, and diffusion of free drug into the cells.

The diffusion of free drug into Namalwa cells was rapid and was essentially complete within 1 h (Fig. 3.3b). Association of free DXR with cells was significantly higher than that seen for either targeted or non-targeted liposomes at both 1 and 24 h (Fig. 3.3-b *vs.* c-f). Rigid (Fig. 3.3-e) and fluid (Fig. 3.3-f) DXR-SIL[anti-CD19] both bound specifically to Namalwa cells, and the amount of DXR associated with the Namalwa cells was 4-8 fold higher than for non-targeted DXR-SL (Fig. 3.3-c) or DXR-HSPC-NSIL[IgG2a] (Fig. 3.3-d). The specific association of DXR-SIL[anti-CD19] with Namalwa cells could be competitively inhibited with the addition of free anti-CD19 (see Table 2.1). At 24 h, the levels of rigid or fluid DXR-SIL[anti-CD19] associated with

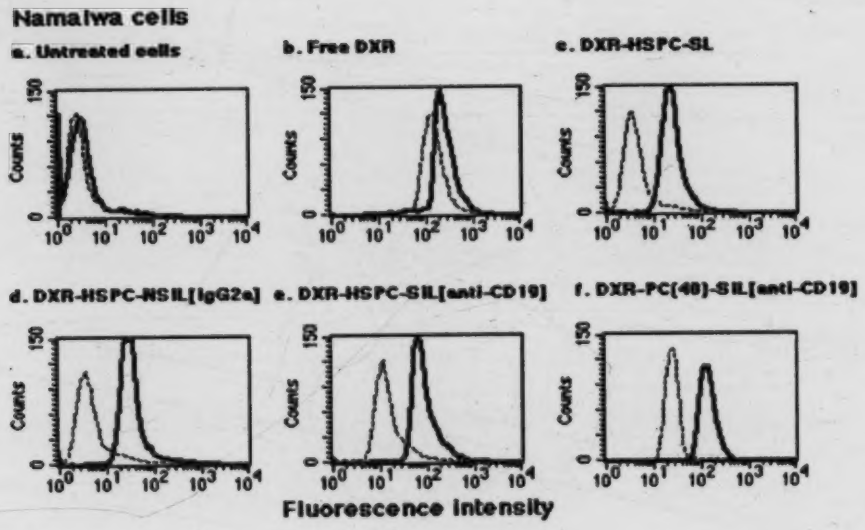

Figure 3.3. Uptake of doxorubicin (DXR) by Namalwa cells using flow cytometry. Namalwa cells ($1x10^6$ cells/well) were incubated with either free DXR or various formulations of liposomes at a final DXR concentration of 20 μg/ml for 1 h (dashed line) or 24 h (bold line), at 37°C. Cells were washed and cell-associated DXR was evaluated using flow cytometry. **a.** Untreated control cells; **b.** Free DXR; **c.** DXR-SL (no mAb); **d.** DXR-NSIL[IgG2a]; **e.** DXR-HSPC-SIL[anti-CD19]; **f.** DXR-PC40-SIL[anti-CD19].

cells approached those seen for free DXR (Fig. 3.3-e,f *vs.* b), though the fluid formulation gave somewhat higher DXR levels possibly resulting from leakage and uptake of free drug (Fig. 3.1).

Results of the HPLC experiments are shown in Fig. 3.4. The cellular levels of free DXR increased with increasing concentrations of DXR. At low concentrations of drug less than 10 μg DXR/ml, the levels of free DXR associated with Namalwa cells were not significantly different from that of either fluid DXR-SIL[anti-CD19] ($p>0.05$). At concentrations of DXR of 20 to 100 μg/ml the cellular accumulation of free DXR increased significantly ($p<0.001$) relative to the liposomal formulations. No difference between the accumulation of drug from fluid *versus* rigid targeted formulations were apparent ($p>0.05$) (Fig. 3.4). Both DXR-SIL[anti-CD19] preparations showed a 3 to 15-fold higher accumulation of DXR compared to that seen for the non-targeted DXR-SL (no mAb) preparations, consistent with the flow cytometry data (Fig. 3.3).

3.4.5 *In vitro* cytotoxicity of SIL[anti-CD19].

We have reported in Chapter 2 that targeted DXR-SIL[anti-CD19] is more cytotoxic to Namalwa cells than is non-targeted DXR-SL. In our current experiments (Table 3.2), we compared the cytotoxicity of liposomes prepared with either a high (HSPC) or low (PC40) phase transition phospholipid. After 1 h incubation, targeted DXR-HSPC-SIL[anti-CD19] were more cytotoxic to the Namalwa cell line than were non-targeted DXR-SL ($p<0.001$) or isotype-matched DXR-HSPC-NSIL[IgG2a] ($p<0.05$) (Table 3.2). There was no difference between the cytotoxicities of targeted DXR-PC40-SIL[anti-CD19] and non-targeted DXR-PC40-SL ($p>0.05$).

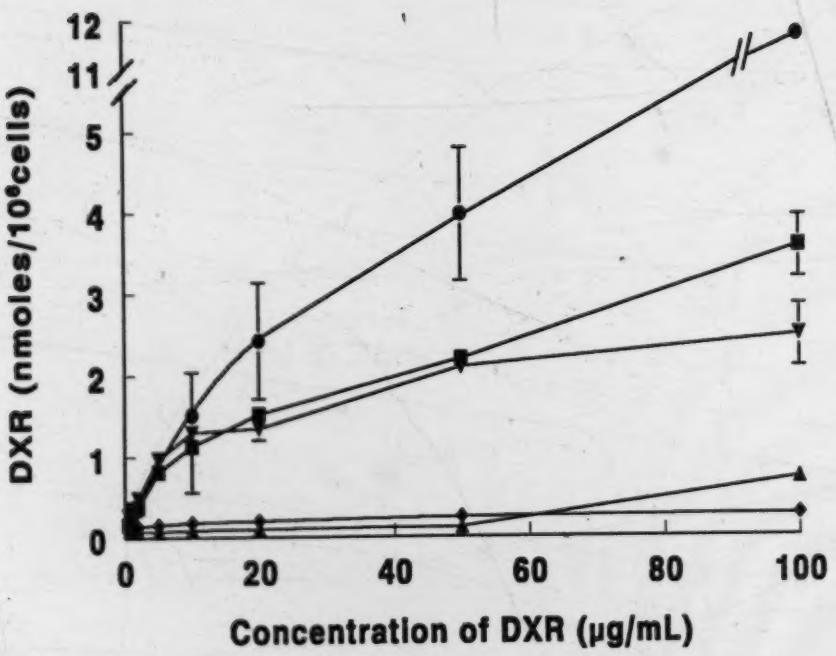

Figure 3.4. Quantitation of doxorubicin (DXR) associated with Namalwa *in vitro*. Namalwa cells (1 x 10^6 cells/well) were incubated with free DXR (●), DXR-HSPC-SL (▲), DXR-PC40-SL (◆), DXR-HSPC-SIL[anti-CD19] (■) or DXR-PC40-SIL[anti-CD19] (▼) for 1 h at 37°C. After incubation, cells were washed and lysed prior to DXR extraction. The amount of DXR associated with cells was determined using HPLC. Figure illustrates the amount of DXR associated with cells (pmol DXR/10^6 cells) *versus* the incubated DXR concentration (µg/ml), n=3.

Table 3.2. Cytotoxicity data (IC_{50}, μM) against Namalwa cells for free DXR, and various liposome-encapsulated doxorubicin formulations.

Time (h)	IC_{50} μM DXR against $CD19^+$ B lymphoma cell line (Namalwa)								
	Free DXR		HSPC-DXR-SL		HSPC-DXR-SIL[anti-CD19]		PC40-DXR-SL	PC40-DXR-SIL[anti-CD19]	HSPC-DXR-NSIL[IgG2a]
	-Dowex	+Dowex	-Dowex	+Dowex	-Dowex	+Dowex	-Dowex	-Dowex	-Dowex
1	1.6 ± 0.2	28.4 ± 8.6	149.8 ± 8.8	>689.7	20.7 ± 3.4	39.2 ± 4.3	0.71 ± 0.21	0.45 ± 0.10	150.5 ± 30.8
24	0.2 ± 0.2	-	4.8 ± 0.3	-	1.7 ± 1.0	-	0.07 ± 0.01	0.09 ± 0.02	14.1 ± 1.9

Namalwa cells ($5x10^5$ /well) were incubated with either free DXR or various formulations of DXR encapsulated in long-circulating liposomes with or without the antibody. Cells were incubated for 1 or 24 h at 37°C in an atmosphere of 95 % humidity and 5 % CO_2. At the time points indicated, cells were washed and each well replaced with fresh media. At 48 h, the plates were then centrifuged, supernatants removed, the tetrazolium dye MTT solution (25 μg/well) was added to each well and the plates were further incubated for 4 h at 37°C. The colored formazan product was dissolved using 100 μl of acid-isopropanol and the plates were read on a Titertek Multiskan Plus (Flow Laboratories Inc., Mississauga, Ont.) at dual wavelengths 570 and 650 nm (n= 3 - 6).

Both DXR-PC40-SL ($p<0.001$) and DXR-PC40-SIL[anti-CD19] ($p<0.05$) were more cytotoxic than comparable HSPC counterparts (Table 3.2) and displayed cytotoxicities comparable with the free DXR ($p>0.05$). DXR-HSPC-SIL[anti-CD19] ($p<0.01$) was more cytotoxic than DXR-HSPC-SL ($p<0.001$), but both were significantly less cytotoxic than the free drug. The cytotoxicity of the targeted HSPC-SIL[anti-CD19] could be competitively inhibited by co-incubation with excess free anti-CD19 antibody, suggesting that binding of targeted DXR-SIL[anti-CD19] was responsible for its cytotoxic action (Chapter 2).

With incubations of 24 h, the IC_{50}'s of all formulations were significantly lower ($p<0.01$) (Table 3.2). At 24 h, DXR-SIL[anti-CD19] was significantly more cytotoxic than DXR-SL ($p<0.001$) or DXR-HSPC-NSIL[IgG2a] ($p<0.001$), but not different from free DXR ($p>0.05$). Both DXR-PC40-SL and DXR-PC40-SIL[anti-CD19] displayed similar cytotoxicities ($p>0.05$) and were both more cytotoxic than free DXR ($p<0.001$). At the longer incubation times, release of encapsulated drug from the fluid liposomes followed by uptake of released drug, combined with the uptake of the liposomal drug by endocytosis, may account for the differences in cytotoxicities (Fig. 3.1, Table 3.2).

To test if a portion of the cytotoxicity was due to free drug released from liposomes, we performed additional control experiments incubating liposomes and cells in the presence of a strong cation exchange resin Dowex-50W (Table 3.2). Any free drug released into the medium from liposomes would be rapidly taken up by the Dowex beads. This would thus discriminate between the cytotoxicity due to endocytosis of the liposomal drug by cells, *versus* the uptake of released drug in the media or at the liposome surface.

Dowex treatment increased the IC_{50} of the free drug 18-fold ($p<0.01$). It was apparently not possible to absorb all free DXR from the media at higher DXR concentrations before some was taken up by cells. In comparison to the free drug, the IC_{50} of the non-targeted DXR-SL was increased by only approximately 5-fold by Dowex (Table 3.3). This may be due to the low leakage rate of DXR-SL where only a small fraction (<10 %) of drug is released from the liposomes into the media (Fig. 3.1). Inclusion of Dowex with DXR-SIL[anti-CD19], and Namalwa cells gave only a 2-fold increase in IC_{50} ($p<0.01$), indicating that DXR-SIL[anti-CD19] cytotoxicity was primarily due to internalized liposomes, with approximately half the contribution of drug cytotoxicity due to leakage of DXR from liposomes. This suggests that the cytotoxicity of these liposomes may be due to a combination of drug release and endocytosis.

3.4.6 Measurement of internalization of immunoliposomes using liposome-encapsulated HPTS.

To examine receptor-mediated internalization of liposomes by Namalwa cells, experiments were performed utilizing a pH sensitive probe 1-hydroxypyrene-3,6,8-trisulfonic acid (HPTS), encapsulated within liposomes (329, 330). This procedure allowed the quantitation of the liposomes (i.e., encapsulated HPTS) endocytosed into the acid environment of the endosomes and/or lysosomes.

Both rigid and fluid formulations of targeted HPTS-SIL[anti-CD19] liposomes, when incubated with Namalwa cells (for 1 or 24 h) produced a decrease in the fluorescence excitation peak at 450 nm, and therefore a decrease in I_{450}/I_{413} ratio, indicative of a reduction in pH from 7.4 to pH 6.5 ($p<0.01$) (Table 3.3). This is

Table 3.3. Internalization of liposomes by CD19$^+$ Namalwa cells studied using a pH-sensitive fluorophore (HPTS).

Liposome formulations (composition, molar ratio)	pH (HPTS-liposomes)			
	4°C, 1 h	37°C, 1 h	37°C, 4 h	37°C, 1 h (cells pretreated with sodium azide)
SL	7.4 ± 0.1	7.3 ± 0.1	7.3 ± 0.2	7.5 ± 0.1
HSPC-SIL[anti-CD19]	7.2 ± 0.2	6.6 ± 0.2	6.1 ± 0.3	7.4 ± 0.2
PC40-SIL[anti-CD19]	7.2 ± 0.1	6.5 ± 0.2	6.1 ± 0.2	7.4 ± 0.1

Liposomes were composed of either rigid HSPC or fluid PC40:CHOL:Hz-PEG-DSPE (2:1:0.1 molar ratio) ± coupled mAb anti-CD19 (PL: mAb= 1:0.001 molar ratio, 104 - 109 nm in diameter) and contained the pH-sensitive dye HPTS. Cells were plated in 48-well plates (1 x 10^6 cells/well) and were incubated with liposome-encapsulated HPTS at 4°C or 37°C, for time periods of 1 or 4 h, respectively. An additional control involved pretreating cells with metabolic inactivator sodium azide. At the end of the incubation, cells were washed with cold PBS and the fluorescence excitation spectra was scanned (from λ= 325 - 500 nm) keeping the emission wavelength fixed at λ= 510 nm. By measuring the ratio of the excitation peaks, 450/413 nm, the pH environment of the liposomes was determined (n= 3).

compatible with the accumulation of the liposomes in the acidic milieu of the endosomes and/or lysosomal compartment. In comparison, non-targeted liposomes HPTS-SL (no mAb) or isotype-matched HPTS-NSIL[IgG2a] incubated with Namalwa cells displayed HPTS spectra similar to seen at physiological pH, i.e., pH 7.4 ($p>0.05$) (Table 3.3). HPTS-SIL[anti-CD19] were not internalized by the control $CD19^-$ T cell line, H9. These results are consistent with the binding data, suggesting that non-targeted liposomes do not internalize, and are possibly non-specifically associated with the outer cell membrane. As controls, targeted SIL[anti-CD19] incubated with sodium azide-treated cells, or cells incubated at 4°C, experienced no pH drop, consistent with the energy requirement for receptor-mediated internalization (Table 3.3).

3.4.7 Internalization of liposomes visualized using confocal microscopy.

DXR is naturally fluorescent red when excited at 488 nm. To confirm that DXR-SIL[anti-CD19] internalizes by Namalwa cells, this was investigated using two-color fluorescent confocal imaging. The localization of DXR in the cell could be determined by the pattern of red fluorescence. The cell surface was visualized by the green staining of the surface antigens by either anti-CD4-FITC (T cells) or anti-CD19-FITC (B cells). Free DXR, DXR-SL, DXR-NSIL[IgG2a], or DXR-SIL[anti-CD19] composed of either HSPC or PC40 lipids were incubated with Namalwa cells at 37°C for 1 h (Fig. 3.5).

During the 1 h incubation, the free DXR rapidly diffused into Namalwa (Fig. 3.5A). DXR fluorescence was observed in both the cytoplasm and the nucleus (Fig. 3.5A). Non-targeted DXR-HSPC-SL or DXR-HSPC-NSIL[IgG2a] displayed minimal, diffuse DXR staining (Fig. 3.5B,C), probably resulting from low levels of DXR released

Figure 3.5. Confocal laser scanning micrographs of Namalwa cells treated with free doxorubicin or various formulations of liposome-encapsulated doxorubicin. Namalwa cells ($1x10^6$ cells/well) were incubated with either free DXR or various formulations of liposomes at a final DXR concentration of 20 μg/ml, for 1 h at 37°C. After incubation, cells were stained with anti-CD19-FITC (or anti-CD19 + goat anti-mouse FITC-IgG), washed and adhered on glass slides. Specimens were visualized on the confocal microscopy and optically sectioned. These panels illustrate images acquired on an equatorial plane over a random field of adhered cells. **Panels: A**. Free DXR; **B**. DXR-HSPC-SL; **C**. DXR-HSPC-NSIL[IgG2a]; **D**. DXR-HSPC-SIL[anti-CD19]; **E**. DXR-PC40-SIL[anti-CD19]; **F**. DXR-HSPC-SIL[anti-CD19] + excess free anti-CD19.

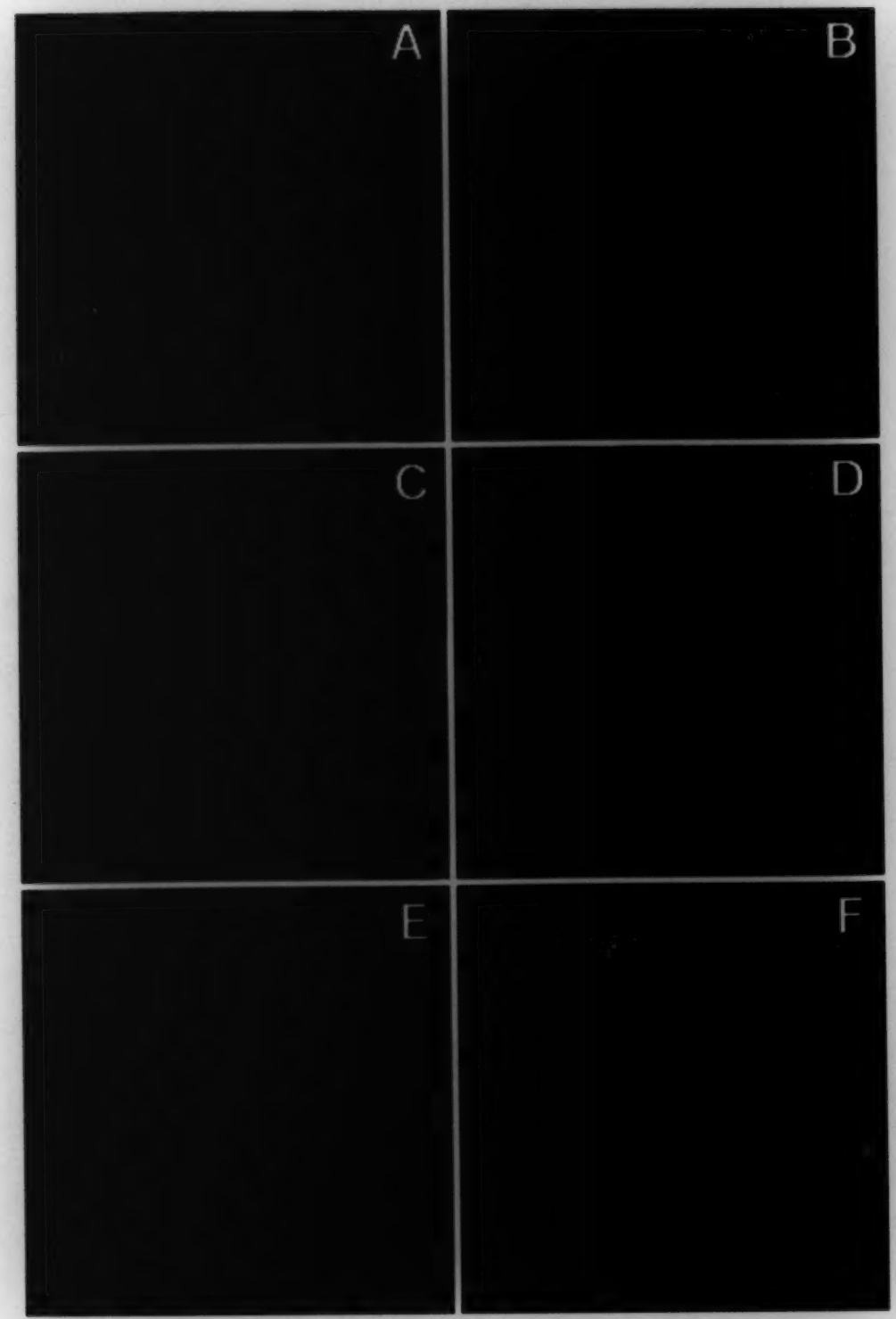
A
B
C
D
E
F

Figure 3.6. Confocal laser scanning micrographs of heterogenous mixture of $CD4^+$ H9 cells and $CD19^+$ Namalwa cells treated with free doxorubicin or various formulations of liposome-encapsulated doxorubicin.

Mixtures of Namalwa and H9 cells ($1x10^6$ cells/well) were incubated with either free DXR or various formulations of liposomes, at a final DXR concentration of 20 μg/ml, for 1 h at 37°C. Post incubation of liposomes, H9 cells were surface stained with anti-CD4-FITC and Namalwa cells were surface stained with anti-CD19-FITC. Cells were washed and adhered on glass slides. Specimens were visualized by confocal microscopy and optically sectioned. These panels illustrate images acquired on an equatorial plane over a random field of adhered cells. **A**. Free DXR + anti-CD4-FITC; **B**. Free DXR + anti-CD19-FITC; **C.** DXR-SL + anti-CD4-FITC; **D**. DXR-SL + anti-CD19-FITC; **E.** DXR-HSPC-DXR-NSIL[IgG2a] + anti-CD4-FITC; **F.** DXR-HSPC-NSIL[IgG2a] + anti-CD19-FITC; **G.** DXR-HSPC-DXR-SIL[anti-CD19] + anti-CD4-FITC; **H.** DXR-HSPC-SIL[anti-CD19] + anti-CD19-FITC.

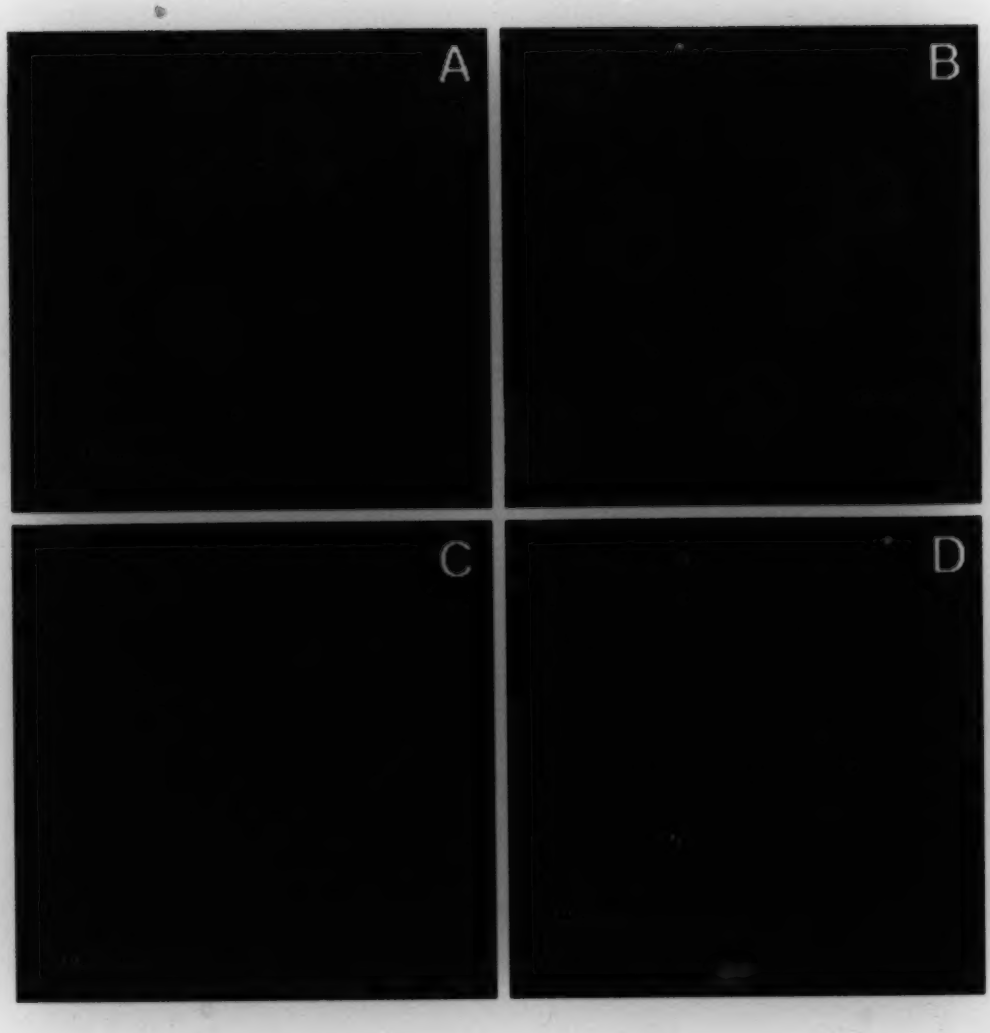
A
B
C
D

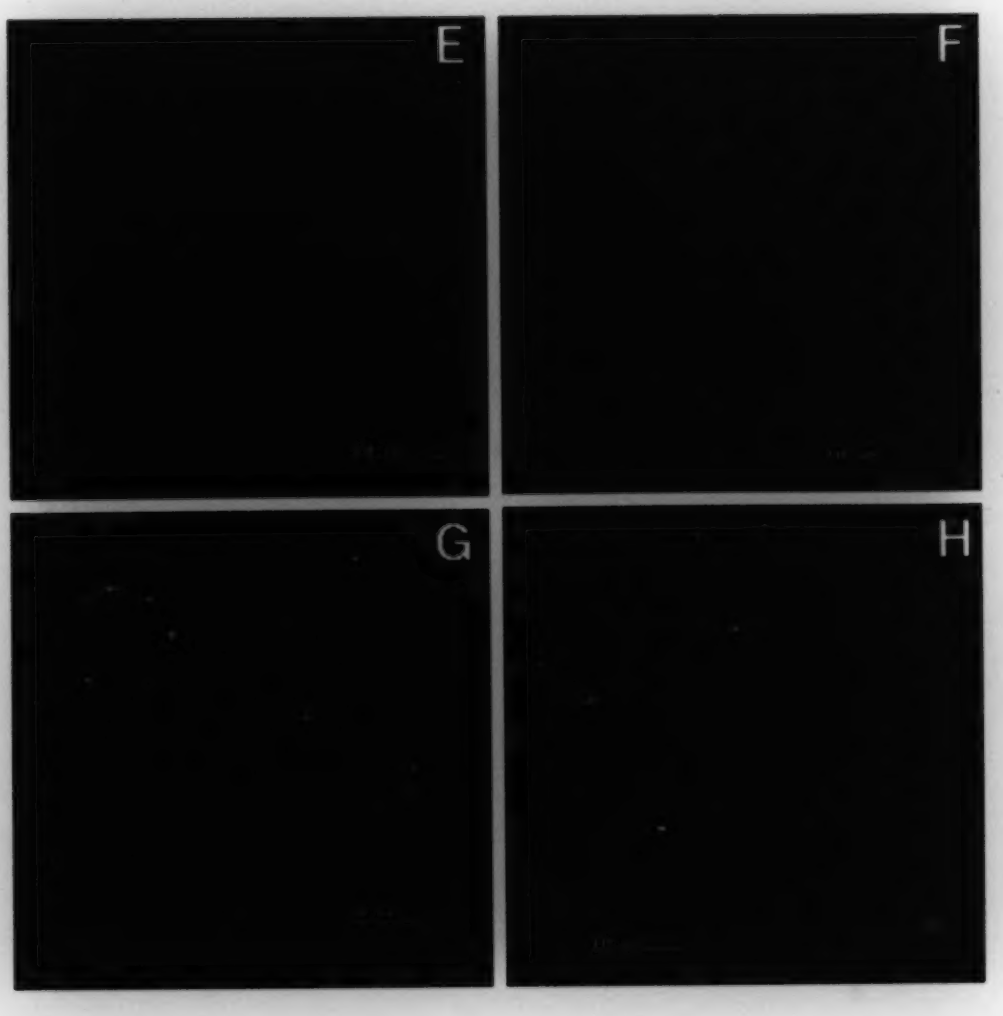
E
F
G
H

from the liposomes (Fig. 3.5B,C). Both HSPC and PC40 formulations of DXR-SIL[anti-CD19] demonstrated a higher binding, internalization and accumulation of DXR-SIL[anti-CD19] into Namalwa cells, compared to non-targeted DXR-SL or DXR-NSIL[IgG2a] (Fig. 3.5D,E *vs.* 5B,C). The internal DXR fluorescence was, however, less intense than that observed for the free drug (Fig. 3.5A). The red DXR fluorescence was associated with both the cell surface and the cytoplasm, the cytoplasm showing both punctate and diffuse DXR fluorescence (Fig. 3.5D,E). Fluid DXR-PC40-SIL[anti-CD19] appeared to have a higher intensity of DXR within cells compared to the rigid DXR-HSPC-SIL[anti-CD19]) (Fig. 3.5D *vs.* E). The fluorescence of DXR-PC40-SIL[anti-CD19] in cells appeared less punctate, and more cytoplasmic, compared to DXR-HSPC-SIL[anti-CD19] (Fig. 3.5D *vs* E). Treatment with the metabolic inhibitor sodium azide resulted in the accumulation of liposomes predominantly on the cell surface with minimal DXR-SIL[anti-CD19] staining observed in the cytoplasm. The specificity of DXR-SIL[anti-CD19] binding and internalization was confirmed by co-incubation of cells in the presence of excess free anti-CD19, which competitively inhibited the binding of DXR-SIL[anti-CD19] (Fig. 3.5F).

Confocal experiments were done using a heterogenous mixture of Namalwa and H9 cells to confirm specificity of DXR-SIL[anti-CD19] for the B cells (Fig. 3.6). B or T cells were identified with appropriate FITC-conjugated free mAbs, i.e., anti-CD19 for Namalwa and anti-CD4 for H9 cells. Accumulation of free DXR was rapid in both Namalwa and H9 cells (Fig. 3.6A,B). Minimal DXR was associated with either cell line when incubated with non-targeted DXR-SL (Fig. 3.6C,D) or DXR-NSIL[IgG2a] (Fig.

3.6E,F). Incubation of a H9/Namalwa cell mixture with DXR-SIL[anti-CD19] appeared to label only Namalwa cells and not H9 cells (Fig. 3.6G,H). As seen in Fig. 3.6G, H9 cells, identified by staining with anti-CD4-FITC, displayed no association of DXR-SIL[anti-CD19]. The DXR fluorescence was exclusively in cells that lacked CD4, i.e., Namalwa cells (Fig. 3.6G). The co-localization of the red and green fluorescence to the cells labelled with anti-CD19-FITC in the heterogenous mix of Namalwa and H9 cells confirmed the specificity of binding of the DXR-SIL[anti-CD19] to Namalwa cells (Fig. 3.6H).

In addition, we used confocal imaging to corroborate the cytotoxicity experiments conducted in the presence of Dowex (Fig. 3.7). The amount of cation exchange resin used was unable to completely expunge DXR from the media. The diffusion of free drug into cells in the presence of Dowex was, however, reduced and was significantly lower than that seen for cells treated with DXR in the absence of Dowex (Fig. 3.7A *vs.* Fig. 3.5A). Non-targeted DXR-SL (Fig. 3.7B) had little or no DXR fluorescence associated with cells. Targeted DXR-SIL[anti-CD19] showed a small accumulation of DXR within cells, compared to either DXR-SL or DXR-NSIL[IgG2a] (Fig. 3.7C). The association of DXR with the Namalwa cells incubated with DXR-SIL[anti-CD19] appeared to be lower than that seen with cells not treated with Dowex (Fig. 3.5D *vs.* 3.7C). This suggests that a portion of the drug fluorescence in cells may be due to uptake of free drug released from liposomes.

Evidence from the Dowex and HPTS studies suggest that endocytosis of SIL[anti-CD19] is occurring with release of contents within the cell. To further study this

Figure 3.7. Confocal laser scanning micrographs of Namalwa cells treated with free doxorubicin or various formulations of liposome-encapsulated doxorubicin in the presence of a cation exchange resin Dowex-50W.
Namalwa cells ($1x10^6$ cells/well) were incubated with either free DXR or various formulations of liposomes, at a final DXR concentration of 20 μg/ml, in the presence of Dowex for 1 h at 37°C. Post incubation of liposomes, cells were washed and stained with anti-CD19-FITC, prior to adhering on glass slides. Specimens were visualized by confocal microscopy and optically sectioned. These panels illustrate images acquired on an equatorial plane over a random field of adhered cells. **A**. Free DXR + Dowex; **B**. DXR-SL + Dowex; **C**. HSPC-DXR-SIL[anti-CD19] + Dowex.

A
B
C

Figure 3.8. Confocal laser scanning micrographs of Namalwa cells treated with free propidium iodide or liposomal propidium iodide.
Namalwa cells ($1x10^6$ cells/well) were incubated with free propidium iodide or liposomal propidium iodide for 1 or 24 h at 37°C as indicated. Post incubation of liposomes, cells were washed and stained with anti-CD19-FITC, prior to adhering on glass slides. Specimens were visualized by confocal microscopy and optically sectioned. These panels illustrate images acquired on an equatorial plane over a random field of adhered cells. **A**. Free propidium iodide (1 μg/ml), 1 h; **B**. Namalwa cells permeabilized with 70 % ethanol + free propidium iodide (1 μg/ml), 1 h; **C**. Namalwa cells + propidium iodide-SL, 24 h; **D**. Namalwa cells + propidium iodide-SIL[anti-CD19], 24 h.

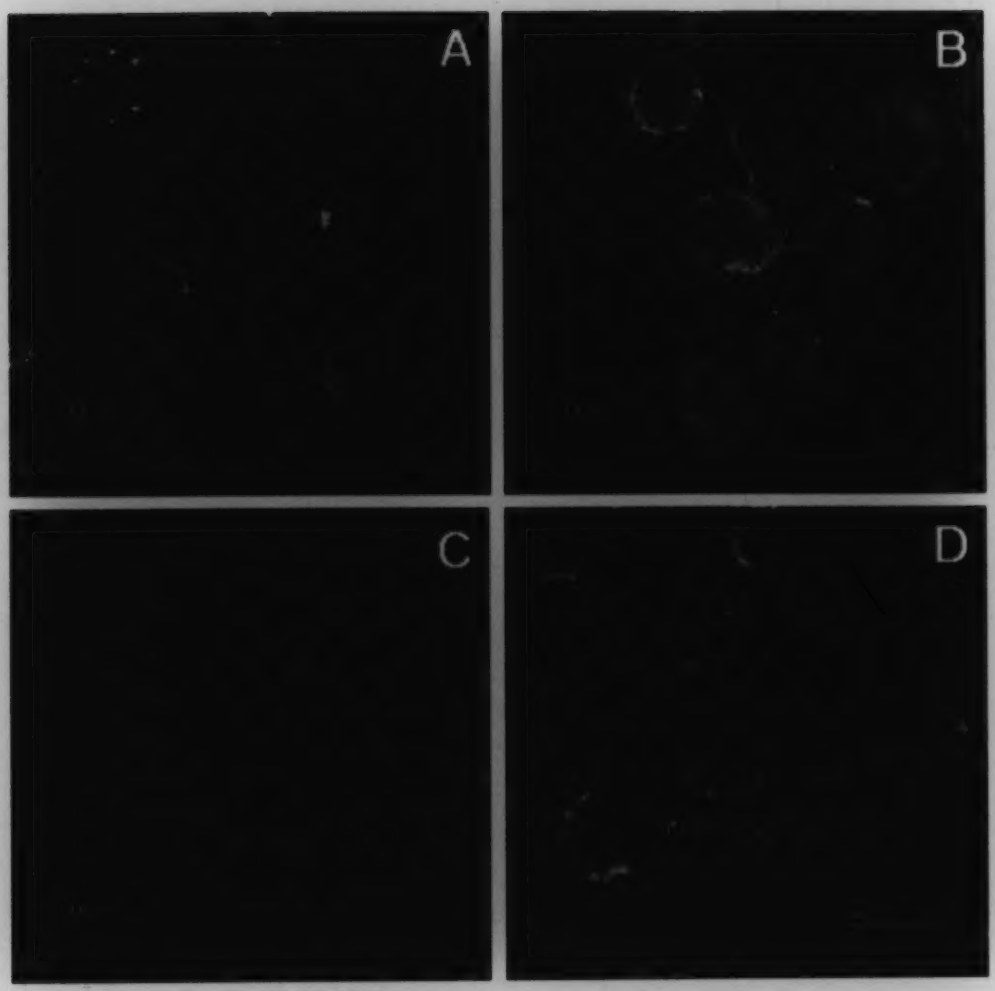
A
B
C
D

phenomenon, confocal experiments were performed on Namalwa cells treated with liposomes encapsulating an aqueous DNA-intercalating dye, propidium iodide (Fig. 3.8). Intact cell membranes are impermeable to free propidium iodide (Fig. 3.8A), which only stains the nucleus of permeabilized cells (Fig. 3.8B). In these studies, we hypothesized that internalization of propidium iodide liposomes would result in nuclear fluorescence only if the liposomes were endocytosed, and the dye released from the lysosomes into the cytoplasm. One hour incubation at 37°C of propidium iodide liposomes with Namalwa cells resulted in a slightly higher intracellular fluorescence for the targeted liposomes compared to non-targeted liposomes. The fluorescence appeared to be vesicular, suggesting that the dye was sequestered within the endosomes and/or lysosomes. No nuclear staining was observed. Even with 24 h incubation periods, no cytoplasmic or nuclear staining was observed with the propidium iodide liposomes (Fig. 3.8C,D).

For endocytosed liposomal DXR to exert its cytotoxic effects, it is necessary for the drug to move from the endosomes or lysosomes through the cytoplasm into the nucleus. As doxorubicin exerts its major cytotoxic effect by intercalating with nuclear DNA, we attempted to follow these events by visualizing the intracellular trafficking of DXR, from both DXR-SL and DXR-SIL[anti-CD19], from 1 to 48 h at either 4°C or 37°C (Fig. 3.9). After 1 h incubation at 4°C, we observed minimal DXR fluorescence in Namalwa cells (Fig. 3.9A,B). Even after 48 h at 4°C, drug was associated with the cell periphery with no accumulation of DXR-SL or DXR-SIL[anti-CD19] within cells (Fig. 3.9E,F and I,J). The cell-associated levels of DXR resulting from the targeted treatment were higher than that seen for the non-targeted DXR-SL (Fig. 3.9B,F,J *vs.* A,E,I).

Figure 3.9. Intracellular localization of DXR-SL compared to DXR-SIL[anti-CD19] as a function of time using confocal imaging microscopy.
Namalwa cells ($1x10^6$ cells/well) were incubated with either HSPC-DXR-SL or HSPC-DXR-SIL[anti-CD19] at a final DXR concentration of 20 μg/ml, for 1, 24 or 48 h at 37°C. At the respective time points, cells were washed and stained with anti-CD19-FITC. Cells were then adhered to glass slides and imaged on the confocal microscope. Panels: DXR-SL at 4°C, treated for 1, 24, 48 h **(A, E, I)**; DXR-SIL[anti-CD19] at 4°C, treated for 1, 24, 48 h **(B, F, J)**; DXR-SL at 37°C, treated for 1, 24, 48 h **(C, G, K)**; and DXR-SIL[anti-CD19] at 37°C, treated for 1, 24, 48 h **(D, H, L)**.

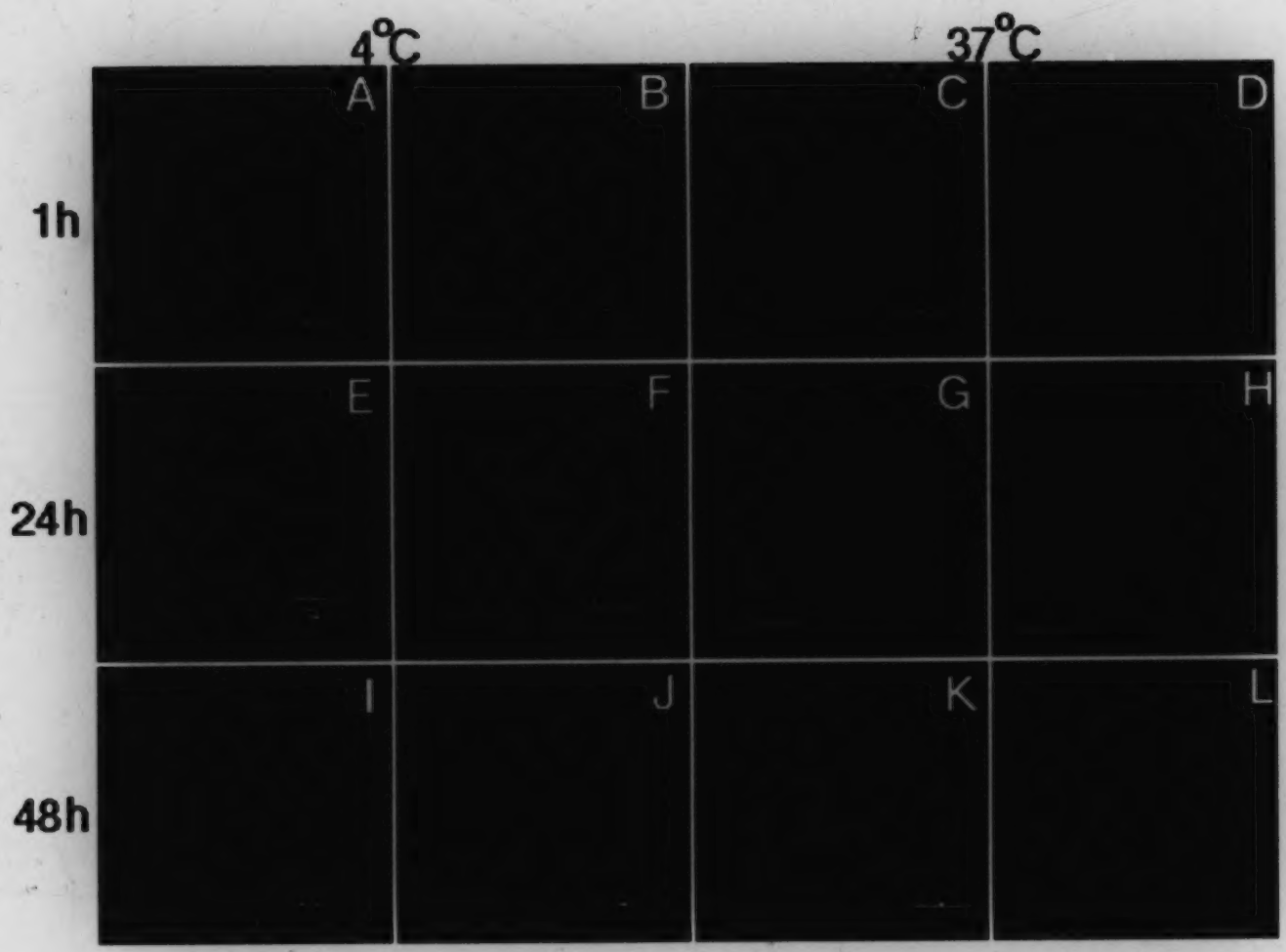
4°C
37°C
A
B
C
D
1h
E
F
G
H
24h
I
J
K
L
48h

Cells that were incubated at 37°C, showed increased intracellular accumulation of DXR-SIL[anti-CD19] with time (Fig. 3.9H,K,L). At early times, DXR-SIL[anti-CD19] appeared mainly on the cell exterior with some diffuse occurrence of drug in the cytoplasm, but not in the nucleus (Fig. 3.9D). The appearance of nuclear staining was evident only after 24 h, and at 48 h, the amount of DXR within the cells (cytoplasm + nuclei) was comparable to that seen with the free DXR treatment (Fig. 3.5A *vs.* 3.9H,L).

3.4.8 Measurement of doxorubicin-induced apoptosis.

DNA levels in cells were measured by flow cytometry using the DNA dye propidium iodide, following treatment with free DXR or liposomal DXR. Untreated Namalwa or H9 cells show a characteristic DNA profile, representing the G0/G1, S, G2/M phases of the cell cycle (Fig. 3.10A-a and B-a). From the untreated cell profile, the position, M2, of the diploid peak was set, so as to make comparisons of the DNA levels in treated cells, i.e., hypodiploid and apoptotic (M1) cells, diploid (M2), dividing (S-phase, M3) or G2/M phase (M4) (Fig. 3.10). Untreated controls resulted in cells with <5 % hypodiploid content. Namalwa (Fig. 3.10A) or H9 (Fig. 3.10B) cells were treated with free DXR, DXR-SL, DXR-SIL[anti-CD19] or the isotype-matched control liposomes DXR-NSIL[IgG2a] at 20 μg DXR/ml for 24 h at 37°C. Exposure of cells to free DXR or liposomal DXR treatments for 1 h was insufficient to demonstrate any differences in the cellular DNA profiles. For this reason we incubated cells with treatments for 24 h, washed the cells and incubated them for an additional 48 h to allow cells to be exposed to the intracellular drug at all phases of the cell cycle. This protocol allowed for substantial drug accumulation into cells (Fig. 3.9) as well as time for the drug to elicit its action.

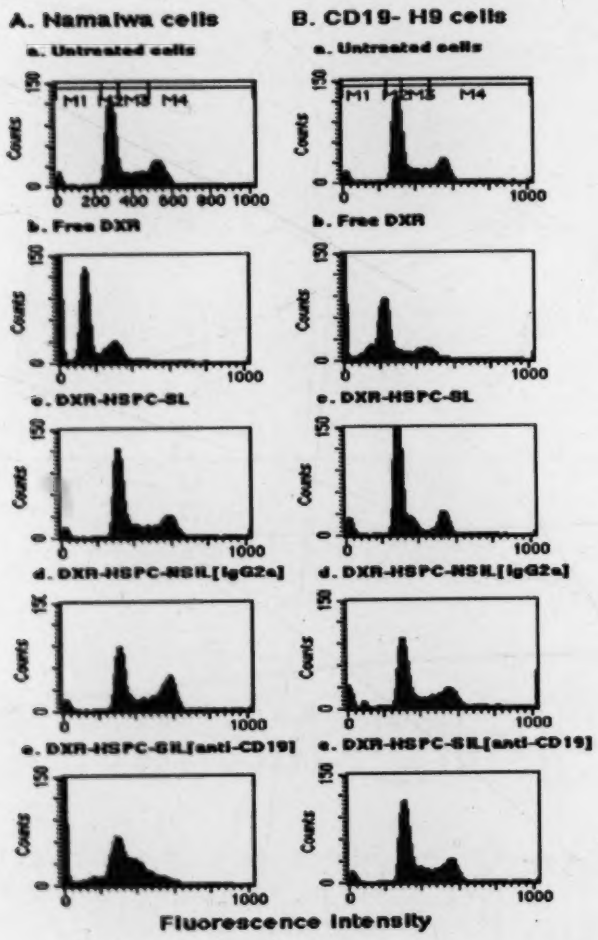

Figure 3.10. Cytotoxicity of liposomal doxorubicin to Namalwa cells compared to H9 cells. Cells ($1x10^6$ cells/well) were incubated with either free DXR or various formulations of liposomes at a final DXR concentration of 20 μg/ml. The cytotoxicity of DXR to Namalwa cells was determined by DNA content analysis using the DNA stain propidium iodide. DNA histograms of a typical experiment are illustrated. **Panels: A. Namalwa cells: a.** Untreated control; **b.** Free DXR; **c.** DXR-SL (no Ab); **d.** DXR-NSIL[IgG2a]; **e.** DXR-SIL[anti-CD19]. **B. H9 cells: a.** Untreated control; **b.** Free DXR; **c.** DXR-SL; **d.** DXR-NSIL[IgG2a]; **e.** DXR-SIL[anti-CD19]. Markers (M1-M5) inserted in panel **a** apply to all panels **a-e**. Markers illustrate apoptotic and hypodiploid DNA (**M1**), Diploid, Go/G1 cells (**M2**), S-phase (**M3**) and dividing quadruploid cells, G2/M phase (**M4**).

Using this experimental design, free DXR induced DNA strand breaks. Figure 3.10 is a representative from three independent experiments. Seventy-four percent of the Namalwa cells and 66 % of the T cells were hypodiploid and apoptotic (M1) (Fig. 3.10A-b). This demonstrates the non-specific activity of the free DXR against both Namalwa and H9 cells (Fig. 3.10A-b,B-b). Neither DXR-SL nor DXR-NSIL[IgG2a] altered the DNA profile of either cell line to any significant degree (Fig. 3.10A-c,d and Fig. 3.10B-c,d), the DNA profile remaining mainly diploid, with only a small fraction of cells (<10 %) being hypodiploid and apoptotic (M1). In contrast, DXR-SIL[anti-CD19] was selectively apoptotic to Namalwa cells (25 % apoptotic and hypodiploid, M1, Fig. 3.10A-e), but not to the H9 cell line (4 % apoptotic and hypodiploid, M1, Fig. 3.10B-e). In addition, DXR-SIL[anti-CD19] appeared to reduce the percentage of actively dividing cells in the G2/M phase of the cell cycle, resulting in these cells showing higher S-phase accumulation (Fig. 3.10A-e, marker M3 *vs.* M4). These results indicate that the DXR released from targeted DXR-SIL[anti-CD19] induces apoptosis after endocytosis of liposomes *in vitro.*

3.5 DISCUSSION

We have studied the binding, internalization and cellular trafficking of free DXR, non-targeted and targeted liposomal doxorubicin in a human B lymphoma cell line. We have previously demonstrated that radiolabeled SIL[anti-CD19] can specifically bind $CD19^+$ Namalwa cells *in vitro*, and that the interaction of SIL[anti-CD19] can saturate all CD19 sites on Namalwa cells (Chapter 2). The affinity of SIL[anti-CD19] was however, slightly reduced compared to that of free antibody (Chapter 2). In this study, the binding

of the SIL[anti-CD19] to $CD19^+$ Namalwa cells was studied using a fluorescent lipid label, NBD, and flow cytometry. NBD-lipid tags have been previously used to study intracellular trafficking (i.e., lipid fusion and endocytosis) in cells (333). These fluorophores are excellent tools to study liposome-cell interactions, as they are reported to be non-exchangeable between cell membranes (333). In our experience, these NBD lipid label was not suitable for confocal imaging, as the fluorophore appeared to bleach upon extended laser excitation during cell slicing. This photobleaching was of little significance using flow cytometry, as the short duration of dye excitation did not appear to interfere with determination of total lipid association.

After cell binding of immunoliposomes, liposome-encapsulated drug can enter cells number of ways (90); namely, (1) binding of liposomes to the target epitope with drug released locally at the cell surface and taken into the cell as free drug (no internalization of liposomes); (2) fusion of liposomes with the cell membrane with the drug contents introduced directly into the cytoplasm (334); or (3) internalization of liposomes *via* the endocytotic machinery of the cell and intracellular release of the drug (335). We were able to differentiate between some of these mechanisms experimentally. CD19 is a signalling receptor, and binding of complementary antibodies has been shown to trigger endocytosis (309, 310). A common pathway in the endocytotic process involves the processing of the receptor-Ab complex, *via* a series of acidification stages from early endosomes to lysosomes (pH 4 - 6) (336, 337). The end stage results in the dismantling of the Ab-receptor complex, with possible recycling of the receptor (336, 338). Our HPTS experiments suggest that coupling of HPTS-SIL[anti-CD19] to the CD19 receptor

may route liposomes *via* a similar receptor-mediated endocytotic pathway to deliver liposomes into lysosomes, as the pH sensed by HPTS delivered *via* SIL[anti-CD19] dropped to pH 6.1. Arguably, SIL bound to the outer surface of the cells may be subject to an acidic microenvironment as a result of proton excretion when some cell surface receptors are activated by ligands (339). This could perhaps have caused the observed drop in pH seen for the targeted liposomes. However, neither non-targeted SL nor NSIL[IgG2a] experienced any significant pH change, and the transfer of SIL[anti-CD19] to acidic endosomes/lysosomes was inhibited at 4°C or by metabolic inactivators like sodium azide, suggesting a metabolic requirement for internalization, indicative of endocytotic processes (336, 340).

Liposome-mediated endocytosis of liposomal drug was also supported by the observation of punctate intracellular fluorescence by confocal microscopy (Fig. 3.5 and 3.9). Targeted DXR-SIL[anti-CD19] were able to deliver higher drug levels to Namalwa cells compared to non-targeted DXR-SL. It is not known how rapidly DXR delivered to the lysosomal apparatus is able to leave these compartments. Weak amines, including DXR, acquire a net positive charge at low pH, and the rate of translocation of protonated molecules across lysosomal membranes will depend on the equilibrium between the charged and uncharged molecules (341). Neutral molecules will cross membranes. Thus, negatively-charged carboxyfluorescein entrapped in liposomes, upon liposome internalization and subsequent neutralization of dye in the lysosomes, appears to rapidly enter into the cell cytoplasm (335, 342). In our confocal results with DXR-SIL[anti-CD19] we observed punctate cytosolic fluorescence and only minimal diffuse fluorescence

of DXR at early time points (1 h), consistent with very little DXR present in the uncharged form. Even if DXR was escaping out of lysosomes, it is possible that the fluorescence of any DXR reaching the nucleus is quenched as a result of intercalation with DNA (343). Only when the amounts of DXR reaching the nucleus are in excess of that bound to DNA would the nuclear fluorescence of DXR become apparent (Fig. 3.9, 37°C, 48 h). Similarly, confocal imaging done with SIL[anti-CD19], entrapping the high-affinity charged DNA dye propidium iodide, which gives enhanced fluorescence upon intercalation with nucleic acids (344), was unable to demonstrate any nuclear staining up to 24 h after internalization (Fig. 3.8).

Currently, the mechanism by which the drug gets from the lysosomes into the cytoplasm and then the nucleus is unknown. There are several barriers and possible routes by which DXR inside liposomes has to overcome before reaching the nucleus, i.e., degradation of liposomes and PEG bilayers, dissolution of DXR out of the precipitate, gradient collapse, and translocation of neutral drug molecules across the lysosomal membrane. Some reports have suggested the role of certain membrane transporters in the translocation of aromatic amino acids across the lysosomes (345). It is not known whether the aromatic cyclic ring structure of DXR may be a substrate for these transporters. Our experiments have shown that continuous exposure to DXR-SIL[anti-CD19] results in steady accumulation of drug in cells, which is not seen in the case of the DXR-SL. We speculate this may be a result of the degradation of liposomes by lysosomal enzymes (346) and subsequent dismantling of lysosomes to release the drug, at which point the receptors may then be recycled to the cell surface to participate in further binding

(309, 310, 336, 338). An alternative explanation is fusion of liposomes with lysosomal and/or endosomal membranes (347, 348) to deliver the drug into the cytoplasm. The kinetics of the drug binding to its nuclear target was shown to be a time-dependent event (Fig. 3.9). Confocal imaging with DXR-SIL[anti-CD19] demonstrates that this happens only after exposure of the cells to liposomes in excess of 24 h. It is possible that exposure of cells to cytotoxic concentrations of DXR for long incubation times may cause a loss of cell membrane integrity characteristic of cells undergoing apoptosis (349). Under these conditions, any free DXR from the media, or associated with intracellular compartments may be able to easily reach the nucleus.

Using flow cytometry, the binding of NBD-SIL[anti-CD19] to Namalwa cells was found to be 3 to 10-fold higher than non-targeted SL (no Ab), while immunoliposome binding to H9 cells was negligible. The results using the lipid label, i.e., NBD, confirm those previously obtained with radiolabelled SIL[anti-CD19] (Chapter 2). When liposome contents, i.e., DXR determined by HPLC were used as a measure of determining liposome uptake by cells, similar increases in cellular uptake of SIL[anti-CD19] were observed for fluid and rigid liposome compositions (Fig. 3.4). However, the experiments measuring the total cell-associated contents (i.e., DXR fluorescence) using flow cytometry showed a significantly higher fluorescence for fluid PC40 liposomes compared to their rigid (HSPC) counterparts (Fig. 3.3e *vs.* f). DXR is quenched in liposomes, and leakier PC40 liposomes, in which the drug is released and dequenched will have higher fluorescence in cells (350) than the less leaky HSPC liposomes in flow cytometry experiments.

In leakage experiments (Fig. 3.1), a small fraction of the drug (<15 % in 24 h) was

released from HSPC-SL in 25 % human plasma, compared to 40 % plasma-induced DXR leakage for PC40-SL after 24 h. This is likely due to the interaction of PC40-liposomes with serum proteins, resulting in a greater release of drug from the lower phase transition temperature PC40-liposomes compared to more rigid HSPC-liposomes (72, 111, 351). Drug released from the liposomes at the cell surface, as well as any liposomal drug endocytosed and subsequently released inside the cell, will contribute to the increased DXR fluorescence within cells. To differentiate between these two processes, studies with liposome-encapsulated DXR were done by co-incubating the liposomes and cells with the cation exchange resin, Dowex (331, 332). Free DXR present in the media was rapidly taken up by the Dowex beads, resulting in 18-fold higher IC_{50} compared to IC_{50} of DXR in the absence of Dowex (Table 3.3). Similarly, the IC_{50} of DXR-SL was increased > 4-fold with the Dowex treatment (Table 3.3). However, there was only a 3-fold increase in IC_{50} of DXR-SIL[anti-CD19] against Namalwa cells in the presence of Dowex (see Table 3.3). This suggests that the cytotoxicity of DXR-SIL[anti-CD19] has a larger component which is dependent on endocytosis of the immunoliposome-drug package by the Namalwa cells, than for DXR-SL.

Our previous work and that of others has shown immunoliposomes to be more effective than their non-targeted counterparts, and in some cases more cytotoxic than the free drug (147, 165, 202, 324, 352). Several factors are responsible for the increased cytotoxicity observed in our experiments: the characteristics of the target CD19 antigen on the cancer cell, the targeting ligand (monoclonal antibody), and composition of the liposomal delivery system. The relationship between the binding efficiency of antibody-

targeted liposomes and the targeted receptor has been shown to be closely dependent on the abundance of the target receptor and the density of the ligand present on liposomes (284). For immunoliposomes to be selective for tumour cells, it is necessary that the antigen be either differentially expressed (i.e., higher on malignant cells than normal tissues) or present exclusively on tumour cells (16). Targeting highly expressed antigens or receptors (e.g., CD19, MUC-1 (185), folate (202), Her2 (165)) with high affinity ligands not only increases the probability of the immunoliposomes to find their target cells, but also strengthens the association of the liposome-receptor complex.

The processes of receptor internalization, lysosomal handling of the drug and the kinetics of passage of drug to its nuclear target still remain unclear. This study shows that long circulating PEG-immunoliposomes directed to an internalizing CD19 receptor are effectively endocytosed, and can deliver cytotoxic drug levels to specific target cell populations. We are continuing to investigate the mechanisms by which internalized liposomal drugs reach their site of action in the nucleus. Understanding these mechanisms could lead to improved designs for liposomal drug delivery systems.

We have shown that DXR-SIL[anti-CD19] is more cytotoxic than non-targeted DXR-SL to CD19-expressing B cells *in vitro*. We have also tested the effectiveness of our immunoliposomal formulations in a model of human CD19-expressing B cell lymphoma (Namalwa cell line) xenograft in SCID mice and have shown that targeted formulations are significantly more effective than free drug or non-targeted liposomal drug (Chapter 2). This therapeutic strategy may be effective in the treatment of hematological B-cell malignancies, where selective eradication of malignant B cells in a heterogenous

population of blood cells *in vivo* could improve the selective toxicity and therapeutic effectiveness of doxorubicin and other anticancer drugs.

CHAPTER 4

Selective targeting of immunoliposomal doxorubicin against human multiple myeloma *in vitro* and *ex vivo*

4.1 ABSTRACT

This study investigated the applicability of long circulating immunoliposomal doxorubicin (DXR) against $CD19^+$ human multiple myeloma cells. *In vitro* binding studies and flow cytometry with the $CD19^+$ multiple myeloma cell line ARH77 demonstrated that anti-CD19 immunoliposomes (SIL[anti-CD19]) specifically bound to ARH77 cells. Formulations of DXR-SIL[anti-CD19] showed a higher association with and cytotoxicity against ARH77 cells compared to their respective non-targeted DXR-SL or isotype-matched DXR-NSIL[IgG2a]. A leakier low phase transition formulation, DXR-PC40-SIL[anti-CD19], was significantly more cytotoxic than a higher phase transition formulation, DXR-HSPC-SIL[anti-CD19]. Experiments with the pH-sensitive fluorophore, HPTS, with confocal laser scanning microscopy and the use of metabolic inhibitors supported endocytosis of the SIL[anti-CD19] into endosomes and/or lysosomes.

Antitumour activity of free DXR *versus* liposomal DXR formulations was evaluated in an i.p. model of ARH77 cells implanted in SCID-beige mice. Free DXR was able to substantially delay tumour growth of ARH cells in SCID-beige mice. The mean survival times of mice treated with either DXR-HSPC-SIL[anti-CD19] or non-targeted DXR-SL were similar, and not different to that of free DXR. Treatments of DXR-PC40-SIL[anti-CD19], or free anti-CD19 given in conjunction with DXR-HSPC-SIL[anti-CD19] were superior to DXR-HSPC-SIL[anti-CD19], DXR-HSPC-SL, or untreated controls. These results suggest that although targeting and cytotoxicity was achieved in *in vitro*, effective *in vivo* therapy may be dependent upon the receptor density of CD19 receptors on cells, which were low on ARH77 cells.

Binding, internalization and cytotoxicity experiments were conducted with human peripheral blood mononuclear cells (PBMC) isolated from multiple myeloma patients. MM B cells expressed high levels of CD19, and binding studies and confocal imaging demonstrated that fluorescent SIL[anti-CD19] was able to selectively target $CD19^+$ B cells, in a heterogenous mixture of human blood cells *ex vivo*. The specific cytotoxicity of targeted DXR-SIL[anti-CD19] was studied with two-color ELITE flow cytometry and DAPI staining for DNA content. PBMC treated with free DXR resulted in random cytotoxicity to both B and T cells, which could be quantitated experimentally by their reduced DAPI binding. Non-targeted liposomes were only minimally cytotoxic to either B- or T-cell populations. In comparison, targeted DXR-SIL[anti-CD19] demonstrated selective apoptosis to B cells, but not T cells, in mixed populations of blood cells.

The evidence presented in Chapter 4 indicates that targeted DXR-SIL[anti-CD19] against internalizing CD19 antigens may be an effective therapy for selectively eradicating malignant B cells in multiple myeloma patients.

4.2 INTRODUCTION

Multiple myeloma (MM) is a malignancy of the immune system, characterized by bone marrow infiltration of terminally differentiated neoplastic plasma cells (247). Most patients initially respond to conventional chemotherapy, but nearly all relapse within 1-2 years. Aggressive combination chemotherapy, or high-dose chemotherapy followed by a bone marrow transplant improves relapse-free intervals, but for most patients the disease recurs and is refractory to further treatment (247, 248, 267). Recent reports have

described a circulating population of monoclonal $CD19^+$ B cells with extensive DNA aneuploidy (255), and displaying traits consistent with the invasive progenitors of plasma cells (257, 260-262). These malignant B cells, express functional plasma membrane transporters, like P-glycoprotein (P-gp) (258, 270), which has been implicated in drug resistance and correlated with most chemotherapeutic failures (271, 272). Current therapies of MM have focussed on eradicating the malignant plasma cells in bone marrow, but these therapies have been largely unsuccessful (257, 267, 271). Malignant B cells in MM persist despite chemotherapy and patient relapse is suggested to occur as these malignant B cells repopulate the bone marrow (255, 257, 263, 271).

A possible approach to the eradication of malignant B cells in blood is the use of immunoliposomal anticancer drugs targeted against the CD19 receptor on the B cells. Highly invasive and possibly regenerative malignant B cells resident in blood of MM patients may be a distinct target for immunoliposomal therapy. Highly expressed, internalizing CD19 receptors have been identified on malignant clonotypic B cells and are restricted to the B-cell lineage (287, 288). CD19 is a signaling receptor, and binding of monoclonal antibody (mAb) anti-CD19 has been shown to trigger a cascade of intracellular messages, committing cells to differentiate, and/or undergo cell-cycle arrest or apoptosis (309, 310). This receptor has been a target for a number of antibody-based therapies and is currently in preclinical and clinical trials in the treatment of a variety of B-cell cancers, as either immunotoxins, radiolabelled mAbs or free mAb therapies (9, 288-293). Anti-CD19 antibodies coupled to long-circulating immunoliposomes encapsulating anticancer drugs may have some advantages. With liposomal drug delivery systems, higher

drug to antibody ratios can be achieved, and liposome-mediated changes in the drug pharmacokinetics may allow the drug to be maintained in circulation for longer times for effective targeting of diseased cells within the vasculature (16, 185, 216).

Immunoliposomal therapy has proved effective against several solid tumour models (16, 146, 147, 185, 201, 324) and in the treatment of murine hematological models of human B-cell lymphoma (Chapter 2), but its applicability in multiple myeloma has not yet been explored. This strategy may allow selective eradication of the malignant $CD19^+$ B cell population, with minimal toxicities to normal tissues, including T cells, thereby not interfering with any of the T-cell mediated immune responses. Selective elimination of the malignant blood B-cell population may prevent dissemination of B cells to bone marrow and extra-skeletal tissues, attenuating the symptoms of myeloma and hence improving patient survival. An additional advantage of this targeting approach would be in relapsed MM, where endocytosis of drug-loaded immunoliposomes could possibly bypass the multidrug transporter to deliver high levels of the cytotoxic agent to resistant cells (271).

To test our hypothesis, we examined the targeting and cytotoxicity of immunoliposomal doxorubicin to human B lymphocytes from multiple myeloma patients *ex vivo,* and to a human multiple myeloma cell line (ARH77) *in vitro.* Survival studies were also performed in a SCID-beige mouse xenograft model using ARH77 cells. In this study, we examined two formulations of DXR-SIL, prepared with different phase transition temperature phospholipids and compared their binding, intracellular trafficking and cytotoxicity to $CD19^+$ myeloma cells.

4.3 MATERIALS AND METHODS

4.3.1 Chemicals.

Poly(ethyleneglycol), molecular weight 2000, covalently linked to distearoylphosphatidylethanolamine (PEG_{2000}-DSPE), hydrazide-derivatized PEG-DSPE (Hz-PEG-DSPE), hydrogenated soy phosphatidylcholine (HSPC) and partially hydrogenated egg phosphatidylcholine with an iodine number 40 (PC40), were generous gifts from SEQUUS Pharmaceuticals, Inc. (Menlo Park, CA) (123, 168, 325). Cholesterol (CHOL) and 12-[N-(nitrobenz-2-oxa-1,3-diazol-4-yl)amino]dodecanoyl phosphatidylethanolamine (NBD-PE) were purchased from Avanti Polar Lipids (Alabaster, AL). 1-hydroxypyrene-3,6,8-trisulfonic acid (HPTS) was obtained from Molecular Probes (Eugene, OR). Sephadex G50, Sepharose CL-4B, and Ficoll-Paque were obtained from Pharmacia Biotech (Baie d' Urfé, Quebec). N-acetyl-methionine (NAM), sodium periodate, 4,6-diamidino-2-phenylindole (DAPI) and 3-[4,5-dimethylthiazol-2-yl]-2,5,-diphenyltetrazolium bromide (MTT), were purchased from Sigma Chemical Co. (St. Louis, MO). Doxorubicin (DXR, Adriamycin RDF) was obtained from Adria Laboratories Inc. (Mississauga, ON). RPMI 1640 media without phenol red, penicillin-streptomycin, and fetal bovine serum (FBS) were purchased from Gibco BRL (Burlington, ON). Cholesteryl-[1,2- ^{3}H-(N)]-hexadecyl ether ([^{3}H]CHE), 1.48-2.22 TBq/mmol, was purchased from New England Nuclear (Mississauga, ON). Scintillation fluor/ aqueous counting scintillant (ACS) was from Amersham Canada Ltd. (Oakville, ON). Polycarbonate filtration membranes, Nuclepore^{R} (pore sizes: 0.4 μm, 0.2 μm, 0.1 μm and 0.08 μm), were obtained from Corning Costar (Kennebunk, ME). All

other chemicals were of analytical grade purity.

4.3.2 Antibodies, human cells and cell lines.

Murine mAb anti-CD19 (IgG2a) (from FMC63 murine CD19 hybridoma) and isotype-matched control IgG2a (IAG.11) were obtained from Dr. H. Zola (Adelaide, Australia) (295, 313). MAbs anti-CD19 (IgG1), anti-CD22 (IgG1) and isotype matched control (IgG1) were a generous gift from Dr. E. Vitetta (University of Texas Southwestern Medical Centre, Dallas). Anti-CD45-phycoerythrin (anti-CD45-PhE) was mAb 17G10 from Dr. J. Wilkins, University of Manitoba. Mouse monoclonal antibodies, as follows, specific for human leukocyte differentiation antigens were prepared in one of our laboratories, or purchased from Coulter (Hialiah, FL) or Becton Dickinson (San Jose, CA): CD4, CD8, CD20, CD21, CD22, CD24, CD29, CD34, CD38, PCA-1, CD44, CD45, CD45RA, CD45RB. The concentrations of all laboratory mAbs were determined by spectrophotometry (λ=280 nm) and BioRad^R protein assays, and purity was assessed by SDS-PAGE. Reactivities of mAb were checked prior to use by indirect immunofluorescence using fluorescein isothiocyanate (FITC)-labelled goat anti-mouse Ab and fluorescence activated cell sorting (FACS) (Becton Dickinson, San Jose, CA) against appropriate cell lines, and compared to appropriate FITC or PhE-conjugated isotype-matched controls.

Human peripheral blood mononuclear cells (PBMC) from multiple myeloma patients were obtained, after informed consent, by Dr. A.R. Belch (Department of Oncology, Cross Cancer Institute, University of Alberta). Patients in this study were chosen at random during routine checkup, and were either newly diagnosed or undergoing

chemotherapy. PBMC were isolated *via* Ficoll-Paque density gradient centrifugation (Pharmacia). Briefly, blood obtained from MM patients were diluted with 1:1 with phosphate buffered saline (PBS) and carefully layered on 20 ml Ficoll-Paque in a 50 ml polypropylene tube. The tubes were centrifuged for 25 minutes at 1800 rpm. After centrifugation, PBMC were collected from the interface, washed with PBS and finally resuspended at a density of $1x10^7$ cells/ml in RPMI 1640 media containing 10 % FBS prior to experimental use. The cell viability was assessed by eosin dye exclusion and counted using a haemocytometer.

The human multiple myeloma cell line ARH77 (ATCC CRL1621) was obtained from American Type Culture Collection (Rockville, MD). ARH77 cells were grown as suspension cultures in RPMI 1640 with no phenol red, supplemented with 10 % heat-inactivated FBS and 1 % penicillin-streptomycin (10,000 unit/ml penicillin G and 10,000 µg/ml streptomycin sulfate). Cells were maintained at 37°C in a 90 % humidified incubator containing 5 % CO_2. All experiments were performed on mycoplasma-free cell lines. For in *vitro* experiments, only cells in exponential growth phase were utilized.

4.3.3 Mice.

SCID-beige (female, 4 weeks of age) were obtained from Dr. L.-J. Chang (Department of Medical Microbiology and Infectious Disease, University of Alberta). All SCID mice (including, C.B.-17/Icr-Tac- SCID (Taconic Farms, NY) and SCID-NOD (Cross Cancer Vivarium, Univ. of Alberta)) were housed in sterile enclosures under specific virus antigen-free conditions. SCID mice were kept on a specified diet with trimethoprim-sulphamethoxazole in their drinking water. Mice were used when they were

4-5 weeks old. All animal experiments were approved by the Animal Welfare Committee (University of Alberta).

4.3.4 Immunophenotyping of the ARH77 cell line.

The human multiple myeloma cell line (ARH77) was phenotyped with antibodies against the following lymphocyte differentiation antigens (CD19, CD20, CD21, CD22, CD24) using flow cytometry. Antibodies were either purified mAbs, or conjugated to FITC or PhE. ARH77 cells ($1x10^6$ cells) were incubated with 10 µg mAb/10^6 ARH cells at 4°C for 30 min in the dark in a total volume adjusted to 50 µl with PBS. After incubation, cells were washed three times with immunofluorescence buffer (IF buffer: PBS-containing 1 % FBS and 0.1 % sodium azide) and analysed by flow cytometry. For indirect staining, after staining with the primary Ab, and washing, cells were incubated with 50 µl of 1:20 dilution of goat anti-mouse-FITC (Sigma) IgG in PBS at 4°C for 30 min. In some cases, cells were fixed with 1 % formalin in PBS. Cell-associated fluorescence was analysed on Becton Dickinson FACScan using LYSIS II software (Becton Dickinson, San Jose, CA). FITC and PhE fluorescent markers were excited with an argon laser (488 nm) and the emitted fluorescence was detected through 530 nm (FL1 for FITC) and 560 nm (FL2 for PhE) band pass filters, respectively.

4.3.5 Preparation of liposomes.

Liposomes were composed of either HSPC:CHOL:$mPEG_{2000}$-DSPE at a 2:1:0.1 molar ratio, or PC40:CHOL:Hz-PEG_{2000}-DSPE (2:1:0.1 molar ratio). In some preparations, [^{3}H]CHE was added as a non-exchangeable, non-metabolizable lipid tracer (296, 297). Fluorescent-labelled liposomes were prepared by incorporating NBD-PE (1

mol %) into the lipid mixture. Briefly, dried lipid films were hydrated in 25 mM HEPES, 140 mM NaCl buffer, pH 7.4 and sequentially extruded (Lipex Biomembranes Extruder, Vancouver, BC) through a series of polycarbonate filters of pore size ranging from 0.4 down to 0.08 μm, to produce primarily unilamellar vesicles 95-110 nm in diameter (34). Liposome size was characterized by dynamic light scattering using a Brookhaven B190 submicron particle size analyser (Brookhaven Instruments Corp., Holtsville, NY). Phospholipid concentrations were determined by either the specific activity counts of [^{3}H]CHE tracer or by the Bartlett colorimetric assay (298). The number of liposomes in the liposome dispersion was estimated at 7.7×10^{12} liposomes/μmol PL (Chapter 2). This was calculated using the following assumptions: the liposomes were monodisperse, spherical, with a mean particle diameter of 100 nm and containing a single phospholipid bilayer. The values for bilayer thickness, molecular areas of lipid and cholesterol molecules were obtained from the literature, and were used to calculate the number of liposomes/μmol PL dispersion (18).

Doxorubicin (DXR) was remote-loaded *via* an ammonium sulphate gradient method (42) previously described (284). The liposome-encapsulated DXR was separated from the free DXR over a Sephadex G-50 column equilibrated with 123 mM sodium citrate (pH 5.5). The concentration of the liposome-entrapped DXR was determined by spectrophotometry (λ= 480 nm in methanol). The amount of DXR loaded in liposomes was 150 μg DXR/μmol PL (0.26 μmol DXR/μmol PL).

Antibodies were coupled to the terminus of pre-formed Hz-PEG-DSPE liposomes *via* the hydrazide coupling method described in references (53, 169). The amount of anti-

CD19 on liposomes was calculated from the radioactive counts of the ^{125}I-labeled anti-CD19 liposomes in comparison to the specific activity of the ^{125}I-anti-CD19 label incorporated during coupling. This gave a coupling of 40 μg anti-CD19/μmol PL (or 25 antibodies/liposome, taking 7.7 x10^{12} liposomes/μmol PL).

4.3.6 *In vitro* cell binding/recognition experiments.

ARH77 cells were plated at 1x10^6 cells/100 μl RPMI 1640 supplemented with 10 % FBS in 48-well tissue culture plates. Various formulations of ^{3}H-CHE-labelled liposomes, with or without coupled anti-CD19, were added to each well (50-1600 nmol/ml) and maintained at 37°C in a humidified atmosphere containing 5 % CO_2 in air in a total volume of 200 μl. After 1 h incubation, the cells were washed three times with cold PBS, pH 7.4, and the amount of ^{3}H-CHE-liposomes associated with the cells was determined by scintillation counting in a Beckmann LS-6800 counter. The amount of bound liposomes, in nmol PL, was calculated from the initial specific activity of ^{3}H-CHE-lipid suspension before extrusion.

In some experiments, immunoliposomes were labelled with a fluorescent lipid marker, NBD-PE (1 mol %), and liposome-cell recognition was determined using flow cytometry. Various formulations of NBD-PE-labelled liposomes were incubated with 1x10^6 ARH77 cells, at a final PL concentration of 400 nmol/ml for 1 or 24 h at 37°C in a humidified incubator containing 5 % CO_2. In competition experiments, targeted NBD-SIL[anti-CD19] liposomes were incubated with 3-fold excess free anti-CD19 (6.4 x 10^{-4} μmol anti-CD19). Cells were washed three times with IF buffer and fixed with 1 % formalin prior to analysis on the flow cytometer. Cell debris was excluded by appropriate

gating on forward *versus* side angle scatter profiles. Files were collected of 5000-20000 events and later analysed using the LYSIS II software program (Becton Dickinson, San Jose, CA). For two-colour immunofluorescence experiments with PBMC from MM patients, in addition to fluorescent liposomes, cells were labelled with either anti-CD20-PhE (B cell marker) or a combination of anti-CD4-PhE and anti-CD8-PhE (CD4,8-PhE, T cell markers) to identify the individual lymphocyte populations.

4.3.7 Uptake of DXR by ARH77 cells using flow cytometry.

To determine the association of DXR with ARH77 cells using flow cytometry, cells were incubated with either free DXR or various liposomal DXR at concentrations of drug ranging from 0.1 - 100 μg/ml for 1, 4 or 24 h at 37°C. Post-incubation, cells were washed with cold IF buffer and immediately run on a Becton Dickinson FACScan (Becton Dickinson, San Jose, CA). DXR molecules associated with cells were excited with an argon laser (488 nm) and the emitted fluorescence was detected through 560 nm (FL2) band pass filters. Files were collected of 20,000 ungated events and later analysed using the LYSIS II software program (Becton Dickinson, San Jose, CA). Cell debris was excluded by appropriate gating during analysis on forward *versus* side angle scatter profiles.

4.3.8 Internalization experiments using the pH-sensitive fluorophore HPTS.

Internalization of liposomes by ARH77 cells was studied using an encapsulated pH-sensitive fluorescent probe HPTS (pyranine) described elsewhere (329, 330). Cells, plated at 1 x 10^6 cells, were incubated with various formulations of HPTS-liposomes at a final PL concentration of 400 nmol/ml for 1 or 24 h at 37°C. After incubation, cells were then

washed three times with PBS, and the cell-associated fluorescence spectrum determined by scanning the excitation spectra from 320 to 500 nm, keeping the emission wavelength fixed at 510 nm. The excitation spectra of the HPTS molecules were obtained and were used to sense the pH of the liposome environment upon interaction with ARH77 cells. The pH environment of the liposomal HPTS was determined from a previously prepared standard curve of the free HPTS probe in various pH solutions (pH range from 5-9).

4.3.9 Intracellular distribution of liposomes using confocal laser scanning microscopy.

ARH77 cells or PBMC from MM patients were plated at 1 x 10^6 cells/well in a total volume of 100 µl RPMI 1640 supplemented with 10 % FBS. Cells were incubated with either free DXR, or liposomal formulations of DXR (20 µg/ml, in a total volume of 500 µl media) for 1 h at 37°C. After incubation, cells were washed with cold PBS and stained for 30 min with anti-CD19-FITC. Cells were allowed to adhere onto poly-l-lysine-coated slides prior to mounting with PermaFluor (Lipshaw Immunon, Pittsburgh, PA.). Cells were then visualized on the confocal laser scanning microscope system consisting of a Leitz Aristoplan Fluorescence Microscope illuminated by a 100W HBO mercury burner for direct observation and an argon-krypton laser with major emissions at 488, 568, and 647 nm for scanning. Cells were optically sectioned over a random field of cells. Acquired images (512 x 512 pixel) acquired were stored on optical disks for further analyses using Leica Lasertechnick GmbH (Heidelberg, Germany) software. All instrumental parameters pertaining to fluorescence illumination, detection, and image analyses were held constant: 100/1.32 oil-immersion objective lens, pinhole 100, off-sets -

29/-30, KP590 short-pass excitation filter, neutral beam-splitter, barrier long-pass filter OG 590, and a photomultiplier gain of 790 volts.

4.3.10 *In vitro* cytotoxicity experiments.

Comparisons of the *in vitro* cytotoxicity of various liposomal formulations were performed on $CD19^+$ ARH77 cells with an *in vitro* proliferation assay utilizing the tetrazolium dye, MTT (299). Groups included free DXR; DXR-PC40/HSPC-SL; or DXR-PC40/HSPC-SIL[anti-CD19] or DXR-HSPC-NSIL[IgG2a] with or without free mAb anti-CD19 or isotype-matched control IgG2a. The IC_{50} was determined as previously described (Chapter 2).

4.3.11 *In vitro* cytotoxicity using DNA content analysis.

Cytotoxicity of DXR or liposomal DXR to the B lymphocyte population in eight myeloma PBMC patient samples was evaluated using the DNA-binding dye DAPI (4,6-diamidino phenylindole) (353, 354). Treatment groups were assigned to each patient sample, depending upon the number of PBMC isolated from individual patients. PBMC ($2x10^6$ cells/well) were incubated with either DXR or different formulations of liposomal DXR for 24 h at 37°C. After incubation, cells were washed, re-plated, and incubated for an additional 48 h at 37°C in RPMI 1640 media, supplemented with 10 % FBS. At the end of the assay, cell viability was assessed using eosin dye exclusion. Myeloma PBMC were stained with the appropriate mAbs for detecting B (anti-CD19-FITC) or T cells (anti-CD4,8-PhE), and with DAPI for DNA content. DAPI staining was done on ethanol-permeabilized (70 % ethanol at 4°C) and RNAase-treated cells at a final DAPI concentration of 1.5 µg/ml. Chicken red blood cells (cRBC), which have a three-fold

lower DNA content compared to cellular DNA in humans, were used as an internal standard. The positions of the B- and T- cell diploid peaks were set relative to the cRBC peak. Samples were immediately run on the Elite flow cytometer (Coulter, Hialeah, FL) with both FITC and PhE excited at 488 nm by the argon laser and simultaneous UV excitation of DAPI at 353 nm by the water-cooled laser. Files of 10,000-40,000 events were collected, and were ungated to prevent exclusion of any drug-induced apoptotic cells. Files were later analysed by listmode using the ELITE software (Coulter). Electronic gates were set for B cells or T cells to evaluate individual DAPI profiles, against appropriate FITC or PhE isotype-matched mAb controls. B cells, which consisted of all CD19 positive, CD4,8 negative cells. Cell doublets were excluded during analyses by appropriate gating on DAPI intensity *versus* DAPI peak. The histogram profiles of DAPI staining of T cells were first analysed to identify the position of the diploid peak (2N number of chromosomes), and was set relative to the cRBC internal standard. The diploid peak marker was set at twice the standard deviation, to include untreated cells within this marker with a 95 % confidence interval. Relative to the diploid peak (2N), appropriate statistical markers were selected to determine populations considered as either hypodiploid (<2N), severely apoptotic (cells with extremely low DAPI staining), or dividing cells, i.e., S-phase and tetraploid cells (4N).

4.3.12 Therapeutic experiments.

ARH77 cells were passaged i.p. in SCID-beige mice to develop a more virulent subclone with reproducible tumour takes. The selected cell line was grown in tissue culture and cells were harvested in sterile PBS. Cell viability was assessed for dye

exclusion using trypan blue staining prior to implantation. Mice were injected i.p. with $1x10^7$ ARH77 cells per mouse in 0.2 ml sterile PBS.

From some mice, blood samples were taken by tail vein bleeding and the blood lymphocytes were separated using Ficoll-Paque gradients. In order to detect tumour cells in the tissues, samples of liver, spleen, lung, heart, kidney, bone marrow and solid tumours were dissociated with pronase and collagenase treatment and, following labelling with both anti-CD19-FITC and anti-CD45-PhE, were analysed by FACS. Euthanized animals were also subjected to a gross histopathological examination to detect tumour dissemination.

In therapeutic experiments, SCID-beige mice (5/group), implanted i.p. with 1×10^7 ARH77 cells were treated 24 hours post-implantation with single i.p. doses of 2 mg/kg DXR as either free DXR, DXR-HSPC-SL (no Ab), DXR-HSPC-SIL[anti-CD19] or DXR-PC40-SIL[anti-CD19] or DXR-HSPC-NSIL[IgG2a]. SCID-beige mice given 2 mg/kg free DXR showed no signs toxicities (or weight loss), and this dose was close to the MTD of free drug in SCID-beige mice. Mice were monitored routinely for weight loss, and survival times were noted.

4.3.13 Statistical analyses.

All linear regression analyses were done using Quattro Pro 4.0 (Borland Inc., Scotts Valley, CA). Unless stated, two-tailed Student's t-test was used to measure statistical significance, assuming equal variances with 95 % confidence interval using INSTAT (GraphPAD software, version 1.11a). Multiple comparisons of various groups in cytotoxic assays were evaluated using one-way analysis of variance also performed on

INSTAT. Post-tests comparing the various treatment means were done using Bonferroni's test. Data was considered statistically significant at p values < 0.05. Data were reported as mean ± standard deviation (S.D.).

4.4 RESULTS

4.4.1 Phenotyping of ARH77 multiple myeloma cell line using flow cytometry.

The expression of selected antigens on ARH77 cells was compared to control staining with the appropriate isotype-matched IgG1 or IgG2a antibodies conjugated to FITC or PhE (Table 4.1). ARH77 cells expressed the following leukocyte differentiation antigens: CD19, CD20, CD21, CD22, CD24, CD38, CD45, CD45RA, CD45RO. The ranking of levels of expression of the B-cell epitopes was CD20 > CD21 = CD22 = CD24 > CD19 (Table 4.1). Antibodies to CD4 and CD8 were negative on ARH77 cells, and B-cell mAbs tested were not found to cross-react with the control T cell line, H9.

Using anti-CD19-FITC, the number of CD19 receptors on ARH77 cells was estimated using flow cytometry, by comparison to the mean fluorescence intensity (MFI) of the human B lymphoma cell (Namalwa), which expresses approximately 40,000 CD19 receptors (312-314). From the binding curves of free anti-CD19-FITC to ARH77 cells and Namalwa cells (at saturation binding), the relative density of CD19 receptors on ARH77 cells was estimated to be approximately 3000 sites per cell.

4.4.2 Binding of immunoliposomes to ARH77 cells.

Binding experiments on the $CD19^+$ multiple myeloma cell line ARH77 were done using ^{3}H[CHE]-labelled liposomes (Fig. 4.1). SIL[anti-CD19] showed a 2- to 3-fold

Table 4.1. Immunophenotyping of ARH77 cell line using flow cytometry.

The human multiple myeloma cell line ARH77 was incubated with appropriate mAbs (10 μg mAb/10^6 cells) at 4°C for 30 min. Cell surface markers were evaluated by immunostaining with specific Abs, by either direct or indirect immunofluorescent staining methods (see methods). Cells were washed with IF buffer and cell-associated fluorescence was analysed on a Becton Dickinson FACScan.

Marker	Expression[1]
CD4 (T cell)	-
CD8 (T cell)	-
CD19	+½
CD20	+++
CD21	++
CD22	++
CD24	++
CD29 (β)	++
CD34 (haematopoietic stem cell)	-/+
CD38	+½
CD45	+++
CD45RA	++
CD45RO	++
PCA-1 (plasma cell antigen)	+
IgG1(control)	-
IgG2a (control)	-

[1] The reactivities of mAbs are presented in terms of relative mean intensity of fluorescent (MFI) staining on Namalwa cells. ++++ MFI 10^4 (very high); +++ MFI 10^3 (high); ++ MFI 10^2 (moderate); + MFI 10^1 (dim/low); +/- MFI $10^{0.5\text{-}1}$ (very low); - MFI $<10^{0.5}$ (negative). Control unstained cells were set at $<10^{0.5}$ MFI.

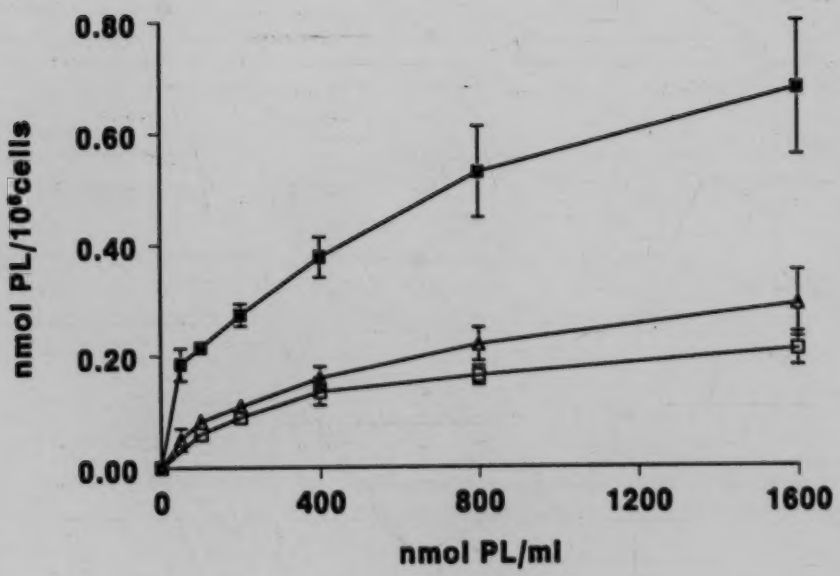

Figure 4.1. Binding of [^{3}H]CHE-labelled liposomes by ARH77 cells as a function of liposome concentration.
Liposomes, 104 nm in diameter, were composed of HSPC:CHOL:PEG_{2000}-DSPE, 2:1:0.1 ± mAb anti-CD19 or isotype-match control mAb IgG2a at approximately 50 μg mAb/μmol phospholipid. SL (□), SIL[anti-CD19] (■) or NSIL[IgG2a] (△) were incubated with 10^6 ARH77 cells for 1 h at 37°C. Data are expressed as nmol PL ± S.D. per 10^6 cells (n=3).

higher binding to ARH77 cells compared to either non-targeted SL, or the isotype-matched control liposomes NSIL[IgG2a].

From the binding data, at the maximum liposome binding at 1600 nmol PL, there were approximately, 6.9 $x10^{-4}$ μmol PL binding sites/10^6 cells for SIL[anti-CD19] and 2.1 $x10^{-4}$ μmol PL binding sites/10^6 cells for SL, respectively. The dissociation constant K_D for the SIL[anti-CD19] was estimated at 220 μM, and was 2-fold lower than that for SL.

Similar experiments were done using fluorescent NBD-PE-labelled liposomes and flow cytometry (Fig. 4.2). ARH77 cells specifically bound free anti-CD19-FITC, compared to isotype-matched staining with irrelevant IgG2a-FITC or autofluorescence of untreated cells (Fig. 4.2A-a). The association of SL or NSIL[IgG2a] to ARH77 cells after 1 h incubation at 37°C was non-specific and low (MFI = 4) (Fig. 4.2A-b). SIL[anti-CD19] was found to have a 2-fold higher recognition to ARH77 cells compared to non-targeted liposome controls (MFI = 9) (Fig. 4.2A-b *vs.* c). Competition with excess free anti-CD19 was able to inhibit the binding of SIL[anti-CD19] with ARH77 cells (MFI = 4), indicating specificity of SIL[anti-CD19] with CD19 receptors (Fig. 4.2A-c).

In addition, we compared the recognition of two formulations of liposomes, a rigid formulation composed of HSPC, and a more fluid formulation composed of the phospholipid PC40 (Fig. 4.2B) as a function of time up to 24 h at 37°C. After 1 h or 24 h incubation at 37°C, both SIL formulations demonstrated approximately 2-fold higher binding (or MFI) to ARH77 cells over an irrelevant NSIL formulation (Fig. 4.2B-c *vs.* a,d *vs.* b). There was no difference between binding of NBD-PC40-SIL[anti-CD19] or NBD-

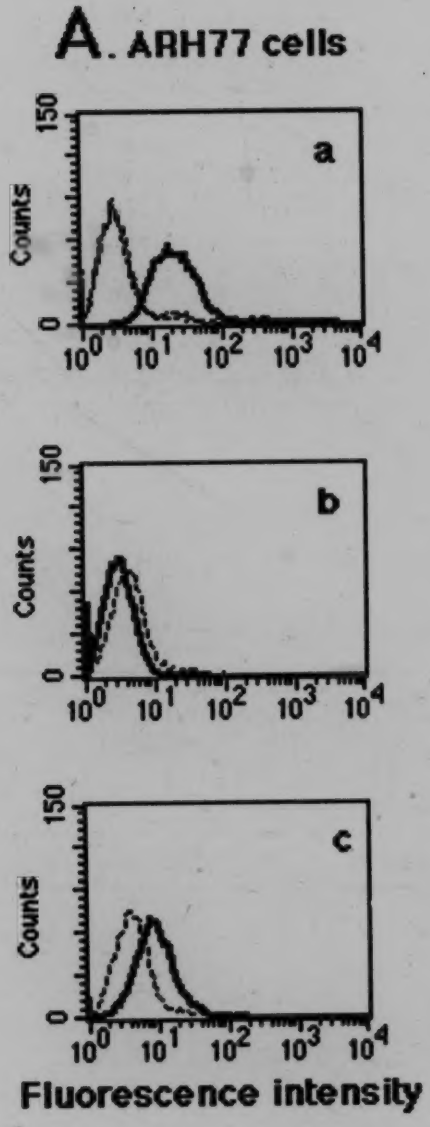
A. ARH77 cells
a
b
c
Counts
150
0
10^0 10^1 10^2 10^3 10^4
Fluorescence intensity

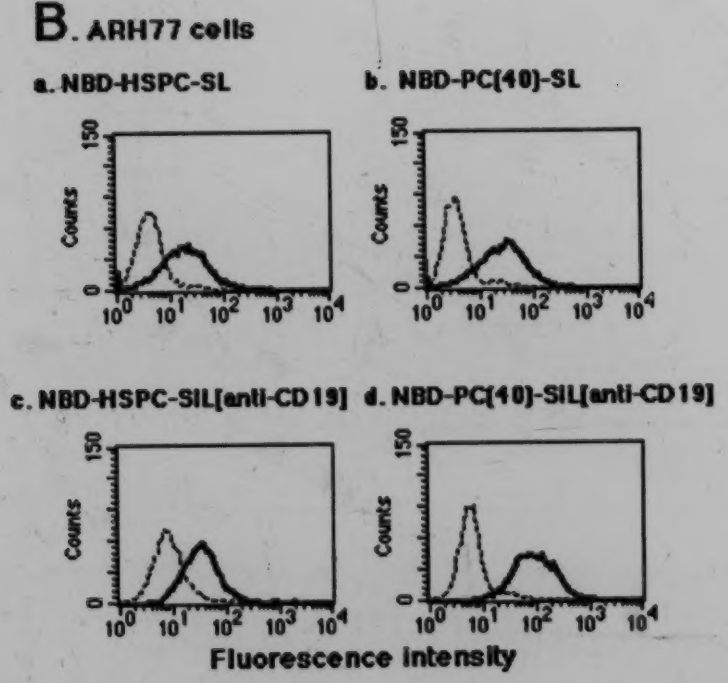

Figure 4.2. ***In vitro*** **binding of fluorescent NBD-labeled liposomes to ARH77 cells using flow cytometry.** NBD-labelled liposomes (0.1 mol %) were composed of HSPC:CHOL:Hz-PEG-DSPE or PC40:CHOL:Hz-PEG-DSPE, 2:1:0.1 molar ratio (105 nm in diameter) ± mAb anti-CD19 or isotype-matched control IgG2a. ARH77 cells were incubated with various formulations of liposomes at a final lipid concentration of 400 nmol/ml for 1 or 24 h at 37°C. Excitation was 480 nm (argon laser) and emission at 510 nm (FL1). Overlayed histogram panels illustrate: **(A) a.** Unstained cells (dotted), or cells treated with irrelevant antibody IgG2a-FITC (dashed) or anti-CD19-FITC (bold line); **b.** NBD-HSPC-SL (dotted) or NBD-HSPC-NSIL[IgG2a] (bold line); **c.** Free anti-CD19 + NBD-HSPC-SIL[anti-CD19] (dashed) or NBD-HSPC-SIL[anti-CD19] (bold line). **(B) a.** NBD-HSPC-SL at 1 h (dashed) and 24 h (bold line); **b.** NBD-PC40-SL at 1 h (dashed) and 24 h (bold line); **c.** NBD-HSPC-SIL[anti-CD19] at 1 h (dashed) and 24 h (bold line); **d.** NBD-PC40-SIL[anti-CD19] at 1 h (dashed) and 24 h (bold line).

HSPC-SIL[anti-CD19] to ARH77 cells after 1 h treatment at 37°C (Fig. 4.2B-c *vs.* d). After 24 h incubation at 37°C, there was a 5-fold higher non-specific association of HSPC-SL, and a 10-fold higher association of PC40-SL with ARH77 cells (Fig. 4.2B-a,b) compared to the binding at 1 h. The corresponding increase in binding at 24 h for HSPC- and PC40-SIL[anti-CD19] was 6- and 15-fold, respectively (Fig. 4.2A-c,d).

4.4.3 Association of free doxorubicin (DXR) or liposomal DXR with ARH77 cells *in vitro* using flow cytometry.

ARH77 cells ($1x10^6$ cells/well) were incubated with free DXR or liposomal DXR at a DXR concentration of 20 μg DXR/ml for 1 and 24 h at 37°C. The relative cell-associated DXR was analysed using flow cytometry with excitation at 488 nm; the emission of the drug could be detected at 560 nm (FL2).

Free DXR rapidly accumulated in ARH77 cells after 1 h at 37°C (Fig. 4.3b). The two targeted formulations (Fig. 4.3e,f) had a 3-fold higher association of DXR compared to non-targeted DXR-HSPC-SL (Fig. 4.3c) or isotype-matched liposomes DXR-NSIL[IgG2a] (Fig. 4.3d). The cellular uptake of DXR resulting from either of the DXR-SIL[anti-CD19] treatments was significantly lower (5-8 fold) than that seen for free DXR (Fig. 4.3e,f, *vs.* b). Incubation of cells with various treatments for 24 h, increased the amount of DXR associated with the cells (Fig. 4.3). At 24 h DXR-HSPC-SIL[anti-CD19] showed a 2-fold higher accumulation of DXR into ARH77 cells (Fig. 4.3e), compared to non-targeted DXR-SL (Fig. 4.3c) or DXR-NSIL[IgG2a] (Fig. 4.3d). DXR-PC40-SIL[anti-CD19] demonstrated 1.5-fold levels of cellular DXR than DXR-HSPC-SIL[anti-CD19], (Fig. 4.3e *vs.* 4.3f).

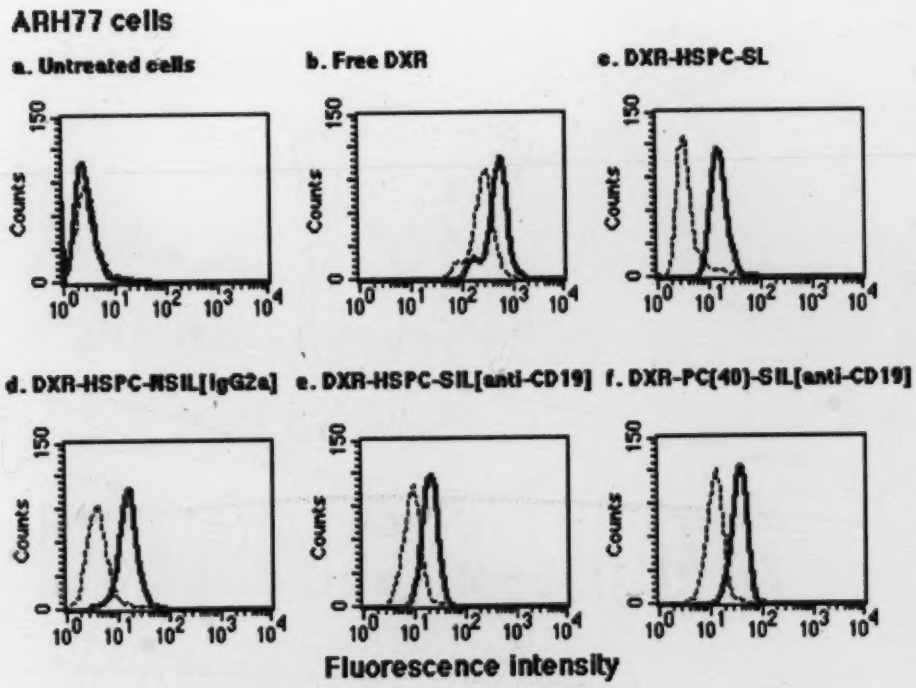

Figure 4.3. Flow cytometric analyses for the association of free DXR or liposome-encapsulated DXR with ARH77 cells.
ARH77 cells ($1x10^6$ cells/well) were incubated with either free DXR or various formulations of liposomes, 108 nm in diameter, at a final DXR concentration of 20 μg/ml for 1 (dotted line) or 24 h (bold line) at 37°C. Cells were washed and cell-associated DXR was evaluated using flow cytometry. **a.** Untreated cells; **b.** Free DXR; **c.** DXR-SL (no mAb); **d.** DXR-NSIL[IgG2a]; **e.** DXR-HSPC-SIL[anti-CD19]; **f.** DXR-PC40-SIL[anti-CD19].

4.4.4 Spectrofluorimetric measurement of immunoliposomal internalization using liposome-encapsulated HPTS.

To ascertain if the interaction of targeted SIL[anti-CD19] liposomes with CD19 receptors on ARH77 cells triggers internalization, we examined this process using a spectrofluorimetric assay described previously (329, 330). Incubation at 37°C for 1 h of ARH77 with HSPC-SIL[anti-CD19] or PC40-SIL[anti-CD19], containing entrapped HPTS, was associated with a drop in pH from 7.3 to pH 6.5-6.6 ($p<0.01$). No pH change was observed for the control $CD19^-$ T cell line, H9. The pH drop for either of the formulations of SIL[anti-CD19] was similar ($p>0.05$). The drop in pH was more apparent after the liposomes were allowed to incubate with cells for 24 h (Fig. 4.4C). This drop in pH could be inhibited by incubations at 4°C or by metabolic inhibitors like 0.1 % sodium azide (Fig. 4.4A and D), suggesting acidification of HPTS-liposomes was an event requiring metabolic active cells. These results support the involvement of receptor-mediated endocytosis in the cellular uptake of liposomes. No pH drop was observed for non-targeted SL or isotype-matched control liposomes, NSIL[IgG2a] ($p>0.05$), consistent with non-specific absorption of liposomes at the cell surface (Fig. 4.4).

4.4.5 Interaction of liposomes with ARH77 cells by confocal microscopy.

The mechanism of association of various formulations of liposomal DXR incubated with ARH77 cells for 1 h at 37°C was also studied using confocal laser scanning microscopy. DXR fluoresces red, and is entrapped in liposomes at concentration which result in approximately 10-fold quenching of the fluorescent signal. ARH cells express CD19, and the epitopes on the surface of cells were stained with anti-CD19-FITC,

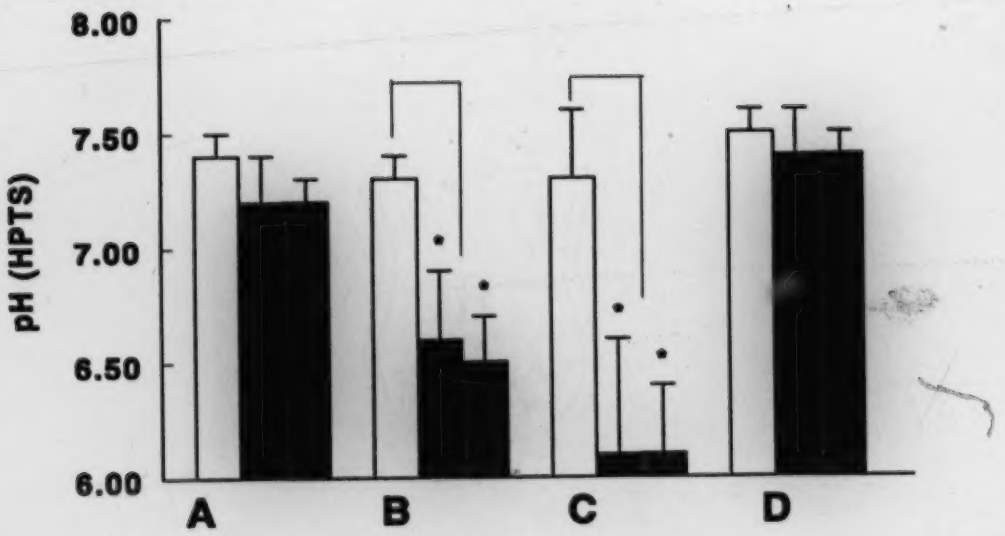

Figure 4.4. Internalization of liposomes by CD19$^+$ multiple myeloma cell line ARH77 using a pH-sensitive fluorophore, HPTS.
Liposomes, 109 nm in diameter, were composed of HSPC:CHOL:Hz-PEG$_{2000}$-DSPE or PC40:CHOL:Hz-PEG$_{2000}$-DSPE ± mAb anti-CD19 at a 2:1:0.1:0.002 molar ratio (50 μg anti-CD19/ μmol PL) and containing encapsulated HPTS. ARH77 cells were plated in 48-well plates (1 x 10^6 cells/well) and incubated with either HPTS-SL (empty bars), HPTS-HSPC-SIL[anti-CD19] (solid bars) or HPTS-PC40-SIL[anti-CD19] (hatched bars) with indicated treatments. After incubation, cells were washed with cold PBS and the fluorescence excitation spectra were scanned from λ=325-500 nm, keeping the emission wavelength fixed at λ=510 nm. Measuring the ratio of the excitation peaks, 403/413 nm and 450/413 nm, the pH environment of the liposomes (in cells) was determined (n=3). **(A)** 4°C, 1 h; **(B)** 37°C, 1 h; **(C)** 37°C, 24 h or **(D)** sodium azide-treated ARH77 at 37°C, 1 h. * student's t-test $p<0.01$.

and fluoresce green.

Free DXR rapidly diffused into cells and brightly stained the cell nuclei of ARH77 cells (Fig. 4.5A). Cellular DXR fluorescence for non-targeted liposomes, DXR-HSPC-SL (Fig. 4.5B) or non-specific, isotype-matched DXR-NSIL[IgG2a] (Fig. 4.5C) was minimal. The DXR fluorescence for the targeted formulations (Fig. 4.5D,E), although higher compared to non-targeted formulations, was significantly lower than that seen for the free DXR at 1 h incubation (Fig. 4.5A). Cells incubated with targeted liposomes appeared to contain punctate red fluorescent dots within the cytosol, with some DXR fluorescence associated with the outer cell membrane (Fig. 4.5D and E). There appeared to be minimal diffuse DXR fluorescence (from released drug) in the cytoplasm after 1 h at 37°C. This suggests that, at early times, the drug may be localised to the cell surface or sequestered in the endosomes and/or lysosomes in ARH77 cells, with no nuclear staining.

No difference in binding and internalization between DXR-HSPC-SIL[anti-CD19] and DXR-PC40-SIL[anti-CD19] (Fig. 4.5D *vs.* E) was observed at 1 h. The binding of targeted DXR-SIL[anti-C19] could be competitively inhibited by excess free anti-CD19, resulting in lower levels of DXR fluorescence associated with cells (Fig. 4.5F).

In another experiment to determine if targeted liposomes are able to internalize and traffic the drug from the lysosomes to the nuclear compartment, experiments were conducted with an aqueous, charged, fluorescent nuclear stain, propidium iodide (red) encapsulated within liposomes. Intact cell membranes are impermeable to free propidium iodide (Fig. 4.6A), but will stain the nuclei of ethanol-permeabilized cells (Fig. 4.6B).

Figure 4.5. Confocal laser scanning micrographs of ARH77 cells treated with free DXR or various formulations of liposomal doxorubicin.
Liposomes (104 nm in diameter) were composed of HSPC:CHOL:Hz-PEG-DSPE or PC40:CHOL:PEG_{2000}-DSPE at a 2:1:0.1 molar ratio ± mAb anti-CD19 or isotype-match control mAb IgG2a. ARH77 cells ($1x10^6$ cells) were incubated with either free DXR or various DXR formulations of liposomes at DXR concentration of 20 μg DXR/ml, for 1 h at 37°C. Post-incubation of liposomes, cells were washed and stained with anti-CD19-FITC. **(A)** Free DXR; **(B)** DXR-HSPC-SL; **(C)** DXR-HSPC-NSIL[IgG2a]; **(D)** DXR-HSPC-SIL[anti-CD19]; **(E)** DXR-PC40-SIL[anti-CD19]; **(F)** DXR-HSPC-SIL[anti-CD19] + excess free anti-CD19.

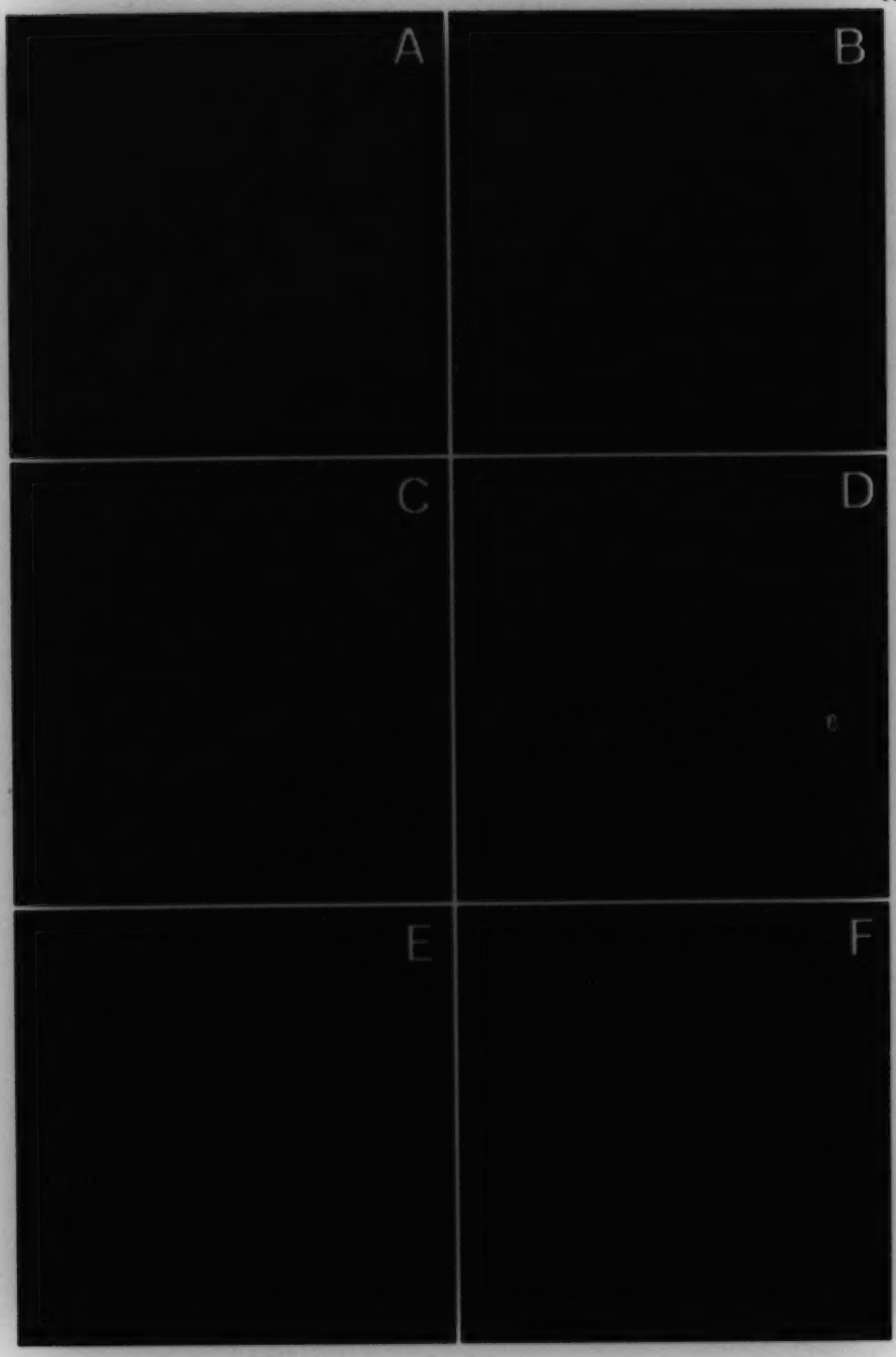
A
B
C
D
E
F

Figure 4.6. Confocal laser scanning micrographs of ARH77 cells treated with liposomal propidium iodide.
Liposomes (104 nm in diameter) were composed of HSPC:CHOL:PEG_{2000}-DSPE, 2:1:0.1 molar ratio ± mAb anti-CD19, and encapsulating propidium iodide. ARH77 cells ($1x10^6$ cells) were incubated with either free propidium iodide or liposomal propidium iodide for 1 h at 37°C. Post-incubation, cells were washed and stained with anti-CD19-FITC. **(A)** Free propidium iodide, 1µg/ml; **(B)** cells permeabilized with 70 % ethanol and then stained with 1 µg/ml propidium iodide **(C)** SL containing propidium iodide; **(D)** DXR-SIL[anti-CD19] containing propidium iodide.

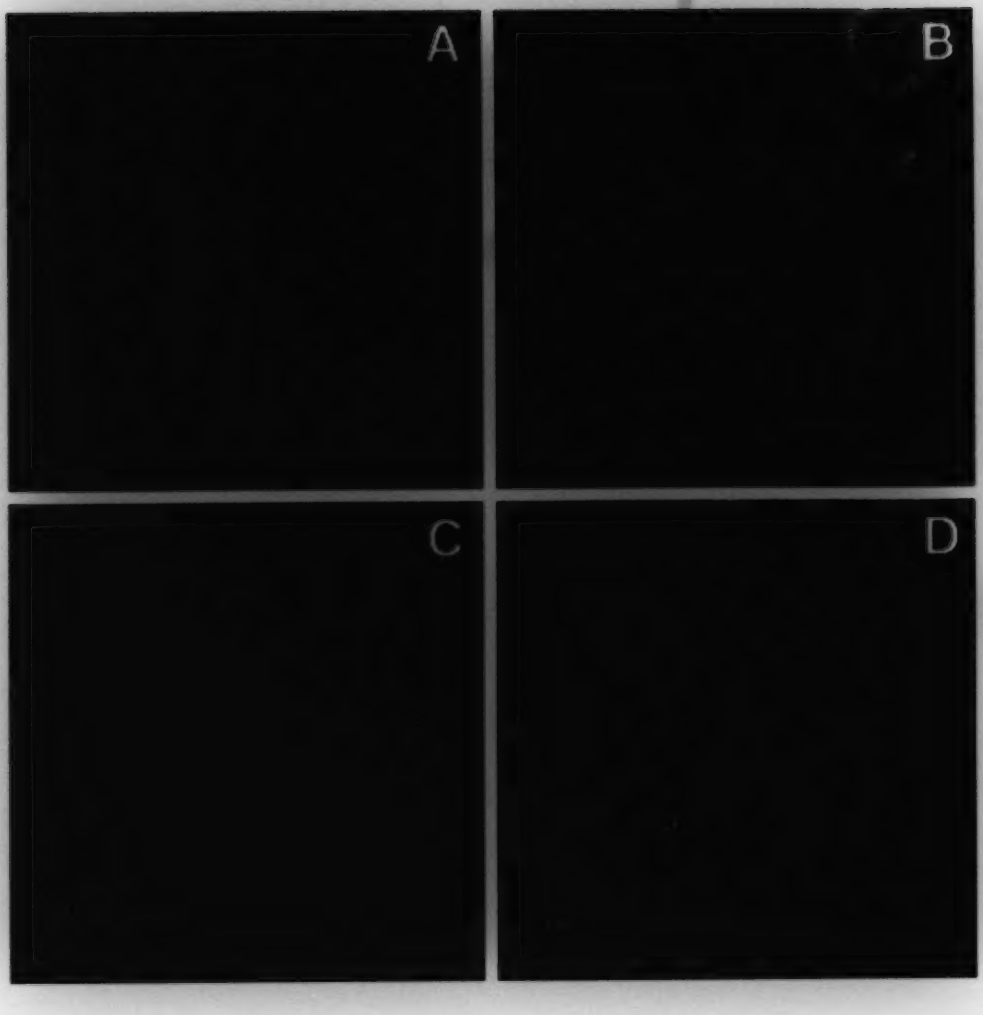
A
B
C
D

Propidium iodide released from liposomes at the cell surface would not be expected to cross intact cell membranes. Targeted SIL[anti-CD19] containing propidium iodide gave higher levels of propidium iodide fluorescence (red) in ARH77 cells compared to non-targeted SL, but none of this fluorescence was associated with the nucleus (Fig. 4.6D *vs.* C). This indicates that the liposomal drug may be endocytosed, but access of the drug to the cytoplasm and the nucleus will depend on the chemical nature of the entrapped drug, and/or the existence of transporters or other mechanisms for drug release.

4.4.6 *In vitro* cytotoxicity of SIL[anti-CD19] to ARH77 cells.

Targeted DXR-HSPC-SIL[anti-CD19] or DXR-PC40-SIL[anti-CD19] were more cytotoxic to ARH77 cells than were DXR-HSPC-SL ($p<0.01$) or DXR-PC40-SL ($p<0.01$), or the isotype-matched control DXR-HSPC-NSIL[IgG2a] ($p<0.001$) (Table 4.2). The IC_{50} of DXR-PC40-SIL[anti-CD19] was lower than that of DXR-HSPC-SIL[anti-CD19] ($p<0.001$) and was equivalent to the cytotoxicity of free DXR ($p>0.05$) after 1 h incubation at 37°C (Table 4.2). Twenty-four incubations lowered the IC_{50}s of all DXR-formulations ($p<0.01$) (Table 4.2). At 24 h, DXR-PC40-SIL[anti-CD19] were more cytotoxic than free DXR ($p<0.001$), DXR-HSPC-SIL[anti-CD19] ($p<0.001$) or non-targeted DXR-PC40-SL ($p<0.05$). HSPC-SIL[anti-CD19] were 17- to 27-fold more cytotoxic than DXR-HSPC-SL or DXR-HSPC-NSIL[IgG2a] at 1 h, and 8- to 11-fold more cytotoxic at 24 h (Table 4.2), suggesting that at later times non-specific association of liposomes and leakage may contribute to the cytotoxicity of non-targeted liposomes. For comparisons, at the IC_{50} for DXR-SIL[anti-CD19], i.e., 9.97 μM, the relative amount of anti-CD19 coupled was equivalent to a mAb concentration of 10 nM, which was

Table 4.2. Cytotoxicity data (IC_{50} μM) for free mAbs, doxorubicin (DXR), or various liposome-encapsulated DXR formulations against ARH77 cells.
ARH77 cells ($5x10^5$ /well) were incubated with various treatments, shown in Table below. Cells were incubated for 1 or 24 h at 37°C in an atmosphere of 95 % humidity and 5 % CO_2. At the time points indicated, cells were washed and each well replaced with fresh media. At 48 h, the plates were then centrifuged and the tetrazolium dye MTT solution (25 μg/well) was added to each well and the plates were further incubated for 4 h at 37°C. The colored formazan product was dissolved using 100 μl of acid-isopropanol and the plates were read on a Titertek Multiskan Plus (Flow Laboratories Inc., Mississauga, Ont.) at dual wavelengths 570 and 650 nm. Data represent mean of n= 2-4, ± S.D. for n=3 -4.

Treatment	IC_{50}, 1 h	IC_{50}, 24 h
Drug-free SIL[anti-CD19] (μM PL)	>1500	580
Free DXR (μM DXR)	1.28 ± 0.16	0.47 ± 0.03
DXR-HSPC-SL (μM DXR)	265.85 ± 31.98	10.39 ± 0.62
DXR-HSPC-NSIL[IgG2a] (μM DXR)	165.78 ± 17.21	7.90 ± 2.24
DXR-HSPC-SIL[anti-CD19] (μM DXR)	9.97 ± 2.29	0.98 ± 0.02
DXR-PC40-SL (μM DXR)	2.75 ± 0.30	0.33 ± 0.06
DXR-PC40-SIL[anti-CD19] (μM DXR)	1.06 ± 0.29	0.16 ± 0.05
Free anti-CD19 (μM mAb)	>1.28	>1.28
Free IgG2a isotype match (μM mAb)	>1.28	>1.28
anti-CD19 + Free DXR (μM DXR)	1.06 ± 0.40	0.09 ± 0.02
anti-CD19 + DXR-HSPC-SL (μM DXR)	248.97 ± 59.83	75.64 ± 37.76
anti-CD19 + DXR-HSPC-SIL[anti-CD19] (μM DXR)	235.21 ± 32.38	23.72 ± 2.66
IC_{50} ratio, DXR-HSPC-SL:DXR-HSPC-SIL[anti-CD19]	26.7:1	10.6:1
IC_{50} ratio, DXR-PC40-SL:DXR-PC40-SIL[anti-CD19]	2.6:1	2.1:1
IC_{50} ratio, anti-CD19+DXR-SL:anti-CD19+DXR-SIL[anti-CD19]	1.1:1	3.2:1

greater than 130-fold the IC_{50} of free anti-CD19 (not cytotoxic at 1.28 μM, Table 4.2). Empty SIL[anti-CD19] without loaded drug, at comparable antibody densities, showed low cytotoxicity to ARH77 cells compared to DXR-SIL[anti-CD19] (Table 4.2).

To determine if the free anti-CD19 sensitizes cells to DXR, we repeated the cytotoxicities by co-incubating cells and DXR or liposomal DXR formulations with 3.2 x 10^{-7} μmoles free anti-CD19, i.e., to saturate all CD19 sites on ARH77 cells (Table 4.2). Free anti-CD19 and the isotype-match non-specific IgG2a were not cytotoxic in the concentration range tested (Table 4.2). Comparing the IC_{50} after 1 h incubation, there was no difference between the cytoxicities of either free DXR or free DXR combined with anti-CD19 ($p>0.05$). The cytotoxicity of DXR-SL plus anti-CD19 was comparable to that of DXR-SL alone ($p>0.05$) (Table 4.2). Combination of free anti-CD19 with DXR-SIL[anti-CD19] increased the IC_{50} of the liposomes by 24-fold ($p<0.001$), to a value similar to that of the non-targeted DXR-SL ($p>0.05$). This indicates that free anti-CD19 competitively inhibits the binding of DXR-SIL[anti-CD19] to ARH77 cells, whereas the cytotoxicity of free DXR or DXR-SL was independent of the association of anti-CD19 with its receptor.

At 24 h, an increased cytotoxicity was observed when free anti-CD19 was incubated with free DXR ($p<0.001$) (Table 4.2). However this effect was not seen with the free anti-CD19, used in combination with non-targeted DXR-HSPC-SL ($p>0.05$).

4.4.7 Specific binding, and recognition of immunoliposomes to PBMC from MM patients.

The population of B cells present in the PBMC from different multiple myeloma

patients ranged from 4-20 %, determined by staining with anti-CD19-FITC and/or anti-CD20-Phycoerythrin (PhE) (Table 4.3). As the radiolabelled liposome binding assays do not discriminate between B cells and other cells in mixed populations of cells, we used two-colour immunofluorescence experiments and FACS to determine if SIL[anti-CD19] specifically bound target B cells in heterogenous populations of PBMC from MM patients (Fig. 4.7).

Fluorescent liposomes containing NBD-PE were incubated with PBMC, and individual populations of B- and T-cells were identified by staining with fluorescent markers anti-CD20-PhE (for B cells) or anti-CD4,8-PhE (for T cells). Individual cell populations were identified, against appropriate control FITC- or PhE-conjugated isotype-matched IgG1 or IgG2a mAbs cell staining. B cells were stained with anti-CD20-PhE instead of anti-CD19-PhE, as binding of SIL[anti-CD19] to CD19 receptors was found to inhibit labelling of B cells with free anti-CD19 (see Fig. 4.2A-c,Fig. 4.5F). Identification of B lymphocytes with CD20 staining may preclude identification of a subset of $CD19^+$ $CD20^-$ B lymphocytes, and thus underestimate the total B cell count. Hence, patient samples were tested for their absolute B and T cell percentages by dual labelling with both CD19 and CD20, and to T-cell subsets with both CD4 and CD8. This confirmed the $CD19^+$, $CD20^+$ phenotype on B cells, and allowed accurate determination of any B-cell subsets that would be $CD19^+$ and yet be $CD20^-$.

Figure 4.7 shows a representative experiment, for the association of NBD-labelled liposomes with individual B- or T- cell populations stained with either CD20-PhE or CD4,8-PhE. By staining with anti-CD19-FITC or anti-CD4,8-PhE the percentages of B

Table 4.3. Specific binding of liposomes to either B or T cells in a heterogenous mixture of PBMC from multiple myeloma patients.
PBMC from MM patients were purified using Ficoll gradients. The percentage of B and T cells in PBMC isolated from each MM patient blood sample was determined by immunofluorescent staining with anti-CD19-FITC or anti-CD4-PhE plus anti-CD8-PhE followed by two-color flow cytometric analysis. For an accurate determination of the percentage of B cells, PBMC were stained with both anti-CD19-FITC and anti-CD20-PhE. B and T lymphocytes in MM patient PBMC ranged from 4-20 % B cells and 25-70 % T cells (n=10). Staining of individual cell populations was compared against relevant fluorescent isotype-matched control antibodies.

PBMC were incubated with various formulations of liposomes (400 nmol PL/ml) in RPMI 1640 media supplemented with 10 % FBS. Liposomes, with or without coupled mAb anti-CD19 or isotype-matched control mAb IgG2a were composed of HSPC:CHOL:Hz-PEG-DSPE (2:1:0.1 molar ratio, 100-112 nm in diameter) and contained 1 mol % fluorescent lipid marker NBD-PE (green). Specific labeling of individual cell populations by liposomes was determined by identification of cells with either anti-CD20-PhE (B cells) or anti-CD4,8-PhE (T cells) (see Fig. 4.7). Cells were appropriately gated to exclude debris, and files of 10,000 gated events were collected. Files were later analyzed and the percentages of liposomes labeling individual cell populations was determined by quadrant statistics. Data represents mean ± S.D.

Liposome formulation	Specific labeling of B or T cells by liposomes			
	% of $CD20^+$ B cells binding liposomes	% of Non-B cells binding liposomes	% of $CD4^+$ and $CD8^+$ T cells binding liposomes	% of Non-T cells binding liposomes
SL (no Ab), n= 10 patients	8.3 ± 5.3	0.9 ± 0.80	2.6 ± 4.2	1.6 ± 2.2
NSIL[IgG2a], n= 3 patients	6.7 ±1.8	0.5 ± 0.4	1.1 ± 0.3	0.4 ± 0.1
SIL[anti-CD19], n= 10 patients	72.0 ± 20.5	2.7 ± 1.9	5.3 ± 4.7	13.6 ± 12.1

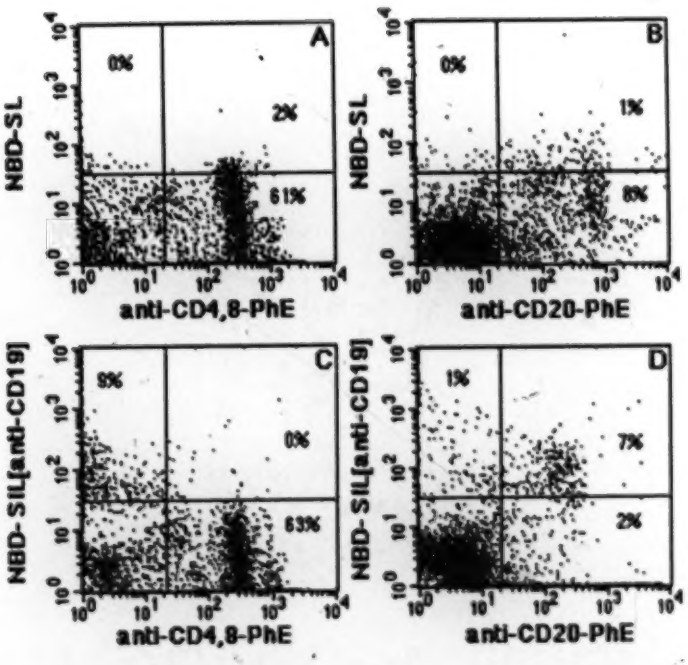

Figure 4.7. Two-colour flow cytometry of the binding of immunoliposomes by B cells in PBMC from a representative multiple myeloma patient.
Liposomes were composed of HSPC:CHOL:PEG_{2000}-DSPE (2:1:0.1 molar ratio, 107 nm) ± mAb anti-CD19 coupled by the hydrazide method and were labelled with 1 mole% NBD-PE . PBMC from a MM patient was incubated with either NBD-SIL[anti-CD19] or NBD-SL, and stained with either anti-CD20-PhE (B1RD1, a B cell marker) or both anti-CD4-PhE + anti-CD8-PhE (T cell markers). **(A)** NBD-SL and anti-CD4-PhE + anti-CD8-PhE,**(B)** NBD-SL and anti-CD20-PhE, **(C)** NBD-SIL[anti-CD19] and anti-CD4-PhE + anti-CD8-PhE, **(D)** NBD-SIL[anti-CD19] and anti-CD20-PhE.

and T lymphocytes in the patient sample were found to be 9 % B cells and 63 % T cells.

NBD-SIL[anti-CD19] selectively bound to B cells (7 % cells dual-labelled, Fig. 4.7D, i.e., 78 % specific labelling), with little or no labelling of the T cell population (0 % dual-labelled, Fig. 4.7C). Sixty-three percent of the cells stained with CD4,8-PhE (Fig. 4.7C), and are presumably T cells. From Fig. 4.7C, it is also observed that 9 % of non-T cells were labelled with NBD-SIL[anti-CD19] are presumably B cells. The association of NBD-SL (Fig. 4.7A,B) to PBMC cells was significantly lower. In this case, only 1 % of cells were positive for both NBD and anti-CD20, and 2 % of T cells with both NBD-SL and anti-CD4,8.

A summary of the results for 10 patients is presented in Table 4.3, normalized for the percentages of B and T cells in individual patient samples. The average percentage of B cells in patient samples was 9.5 ± 5.1 % and for T cells was 43.3 ± 18.3 % (n= 10), non-specific labelling of B cells was comparatively higher (marginally significant at $p<0.05$) (Table 4.3). SIL[anti-CD19] displayed a specific affinity for B cells (72 % labelled) compared to T cells (5 % labelled) ($p<0.001$). The specific labelling of B cells by SIL[anti-CD19] was significantly higher than either SL (8 %) ($p<0.001$) or the isotype-matched control NSIL[IgG2a] (7 %) ($p<0.001$) (Table 4.3). There was no significant difference between the association of non-targeted SL or NSIL[IgG2a] ($p>0.05$) to either B or T cells (Table 4.3).

4.4.8 Confocal microscopy of uptake of DXR-SIL[anti-CD19] by PBMC.

Targeting and intracellular distribution of liposome-encapsulated DXR in PBMC from MM patients was examined using fluorescent confocal laser scanning microscopy

(Fig. 4.8). PBMC were incubated with liposome-encapsulated DXR for 1 h at 37°C *in vitro*. Individual B and T cells were identified using anti-CD19-FITC for B cells and anti-CD4 plus anti-CD8-FITC for T cells. Free DXR rapidly stained the nuclei of both T cell (identified with anti-CD4,8-FITC) and non-T cells (Fig. 4.8A). Similarly, B cells (identified with anti-CD19-FITC) and non-B cells were found to rapidly accumulate free DXR (Fig. 4.8B). Neither non-targeted DXR-SL (Fig. 4.8C,D) nor isotype-matched non-specific DXR-NSIL[IgG2a] (Fig. 4.8E,F) showed accumulation of DXR into either T (Fig. 4.8C,E, respectively) or B cells (Fig. 4.8D,F, respectively). DXR-SIL[anti-CD19] incubated with PBMC did not associate with T cells (Fig. 4.8G), but did associate with a non-T population of cells, presumably the B cells. The identity of these cells was determined by staining PBMC with anti-CD19-FITC (Fig. 4.8H). In this case, DXR-SIL[anti-CD19] was found to co-localize with anti-CD19-FITC, confirming that targeted DXR-SIL[anti-CD19] bind to $CD19^+$ B lymphocytes. B cells appeared to internalize DXR-SIL[anti-CD19], while DXR-SIL[anti-CD19] did not associate with non-B cells, which were not fluorescently labelled, and hence not identified in the confocal image.

4.4.9 Cytotoxicity of DXR-SIL[anti-CD19] to B cells in PBMC from MM patients.

The cytotoxicity of DXR-SIL[anti-CD19], free DXR, DXR-SL or DXR-NSIL[IgG2a] to PBMC isolated from MM patient blood was evaluated at concentrations of 1, 5 and 25 μM DXR. Evaluation was by two-colour immunofluorescence and DAPI staining for DNA content as an indicator of cell death. The cytotoxicity results for individual samples from eight MM patients are presented in Table 4.4. A typical experiment for Patient 6 (Table 4.4, #6) is illustrated in Figure 4.9. Using this

Figure 4.8. Confocal microscopy of the interaction of liposome-encapsulated DXR with PBMC from MM patients.
Liposomes were composed of HSPC:CHOL:Hz-PEG_{2000}-DSPE, 2:1:0.1 molar ratio (108 nm in diameter) ± mAb anti-CD19 or isotype-matched control mAb IgG2a, and contained encapsulated DXR. PBMC from MM patients ($2x10^6$ cells) were incubated with either free DXR or various liposomal formulations of DXR at 20 μg DXR/ml, for 1 h at 37°C. After incubation with liposomes, cells were washed and stained with anti-CD19-FITC or anti-CD4-FITC plus anti-CD8-FITC. **(A)** Free DXR and anti-CD4,8-FITC; **(B)** Free DXR and anti-CD19-FITC; **(C)** DXR-SL and anti-CD4,8-FITC; **(D)** DXR-SL and anti-CD19-FITC; **(E)** DXR-NSIL[IgG2a] and anti-CD4,8,-FITC; **(F)** DXR-NSIL[IgG2a] and anti-CD19-FITC **(G)** DXR-SIL[anti-CD19] and anti-CD4,8-FITC; **(H)** DXR-SIL[anti-CD19] and anti-CD19-FITC.

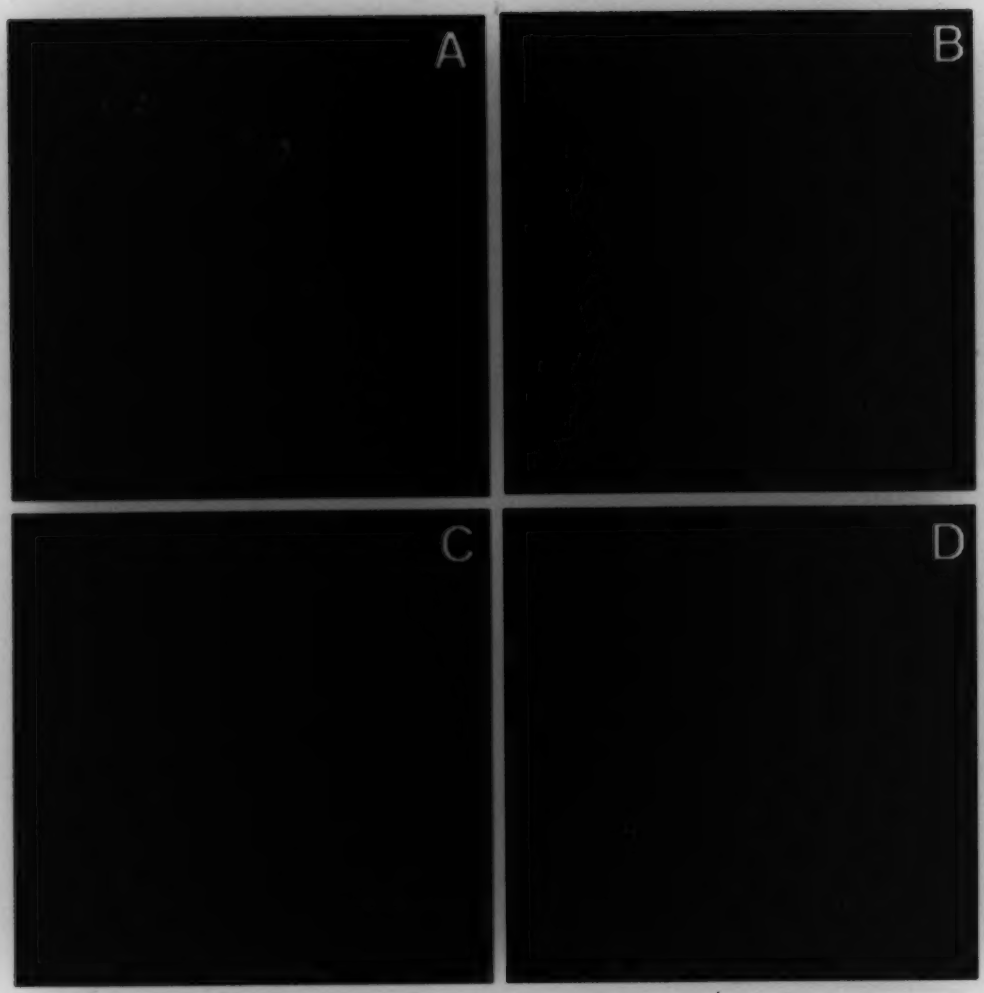
A
B
C
D

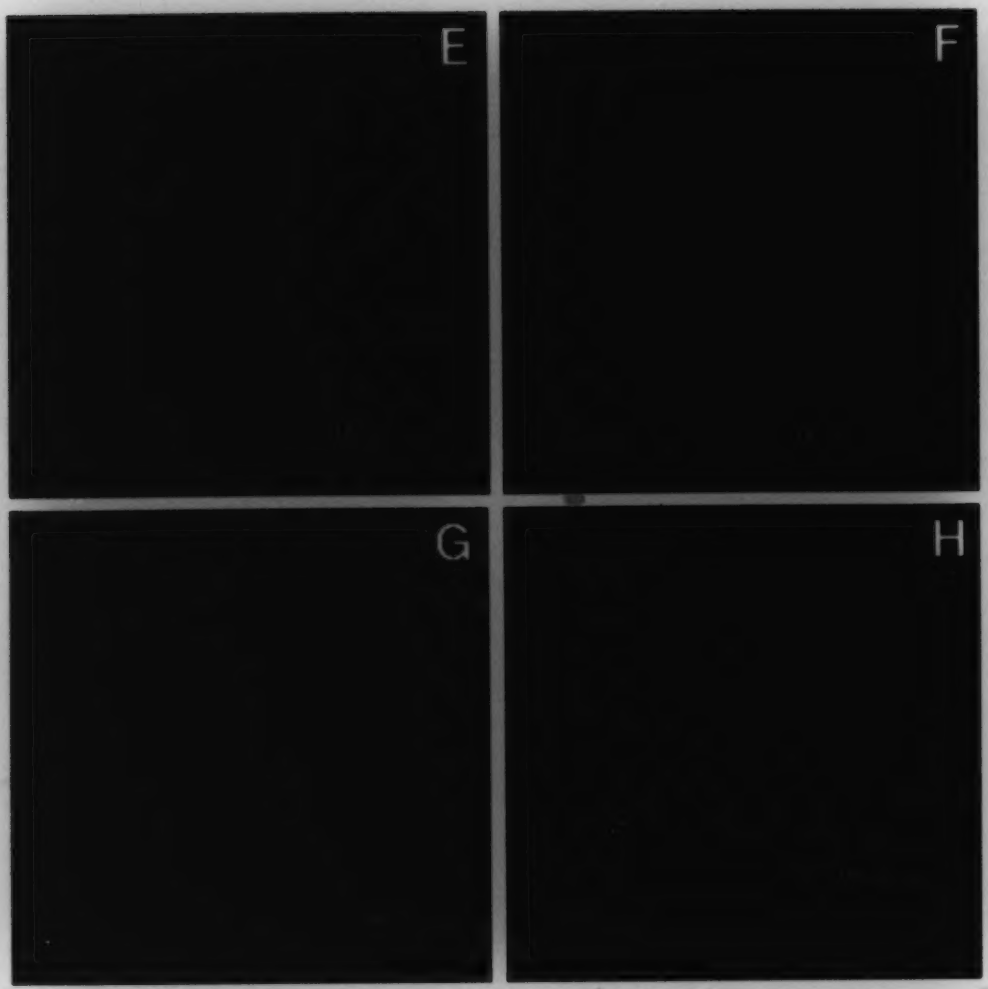
E
F
G
H

experimental design, untreated PBMC from MM patient samples had from 7-40 % hypodiploid and apoptotic cells (Fig. 4.9, Table 4.4). T cells showed a DNA content approximately three times that of the cRBC controls consistent with normal diploid cells (G0/G1, marker M3) (Fig. 4.9A). MM B cells displayed a slightly higher DNA peak (excess DNA) corresponding to an aneuploid B-cell clone speculative of a malignant clone described elsewhere (Fig. 4.9A) (255). Hypodiploid (marker M2), diploid (marker M3) and hyperdiploid cells (>2N, seen as a shoulder over the diploid peak), tetraploid cells (G2/M, 4N) and low percentage of B cells in S-phase (marker M4) were observed (Fig. 4.9A) (255). As seen in Fig. 4.9B, free DXR results in random apoptosis of both B and T cell populations, as indicated by a reduced staining with DAPI. The majority of the B cells (70 %) and T cells (54 %) were hypodiploid (hypodiploid + apoptotic DNA content), i.e., cells with very low DAPI binding, implying low DNA content in the marker M1 (Fig. 4.9B). Non-targeted DXR-SL (5 μM DXR) displayed minimal cytotoxicity to either B or T cells (i.e., <6 % hypodiploid + apoptotic B or T cells) (Fig. 4.9C). DXR-SIL-[anti-CD19] (5 μM DXR) was selectively cytotoxic to B cells (47 % hypodiploid, 33 % apoptotic), with the T cell population remaining mostly diploid (89 % diploid, 9 % hypodiploid, 1 % apoptotic) (Fig. 4.9D).

A free DXR concentration of 5 μM appeared to be a minimal concentration required for achieving toxicity against both B and T cells. This however varied amongst the patient samples, e.g. patient 5 and 6 showed different sensitivities to the free DXR treatment (Table 4.4), and may be related to the drug resistant status of the cells. Lower concentrations (1 μM either free or liposomal DXR) did not result in significant

Figure 4.9. ***In vitro*** **cytotoxicity assay of free DXR or various liposomal DXR formulations on PBMC obtained from a MM patient using the DAPI assay.** Gated populations of B (solid line) or T cells (dotted line) were selected by appropriate staining with either anti-CD19-FITC (B cells) or anti-CD4,8-PhE (T cells) and each of these populations was analysed independently for their DAPI content. Histogram panels **A-D** illustrate DAPI profiles of Patient 6 (Table 4.4-6). **(A)** Untreated B- or T cells, and internal cRBC control (dashed line), **(B)** 5 μM free DXR, **(C)** Non-targeted DXR-SL (5 μM DXR), and **(D)** DXR-SIL-[anti-CD19] (5 μM DXR).

Selective cytotoxicity of DXR-SIL[anti-CD19] to CD19⁺ B cells in PBMC from MM patients

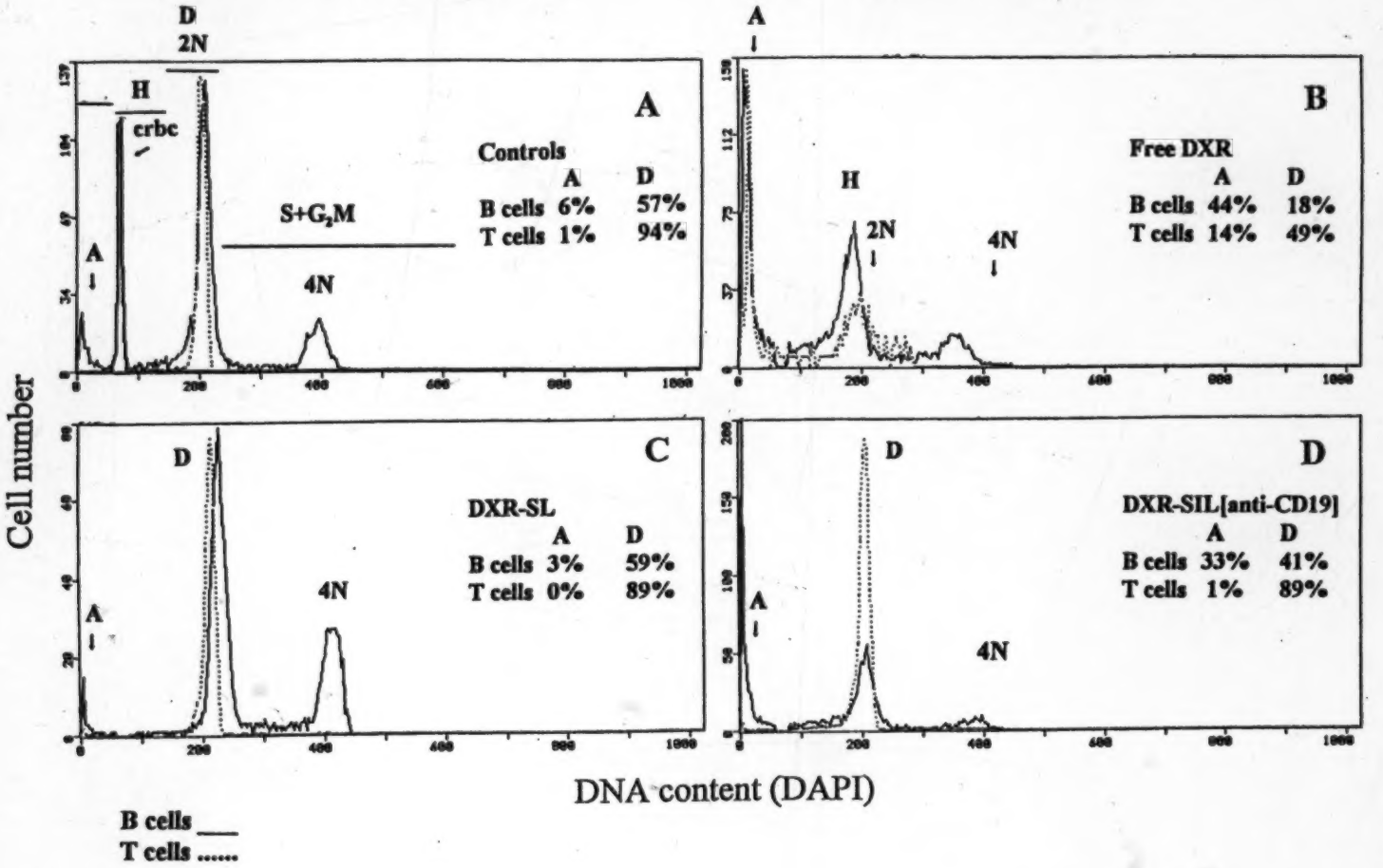

Table 4.4. Cytotoxicity of free DXR or various formulations of liposomal DXR on PBMC from MM patients.
PBMC from MM patients isolated *via* Ficoll gradients were untreated or treated with free DXR or various liposomal DXR (equivalent to 5 μM DXR). After incubation, cells were stained with anti-CD19-FITC, anti-CD4-PhE plus anti-CD8-PhE, and DAPI. Files were gated for either B ($CD19^+$) or T ($CD4,8^+$) cells, and their DAPI profiles were plotted as DNA histograms (Fig. 4.9). The relative ploidy levels of cells were determined from the position of the diploid (2N) DNA peak of B and T cells, against a cRBC internal standard (Fig. 4.9A). Hypodiploid cells were defined as those having <2N DNA and severely apoptotic cells were those with extremely low DNA content (determined from their reduced DAPI binding). Samples were characterized as dividing if they had >2N DNA content (this included tetraploid cells of 4N DNA content).

Patient	Treatment	B cells				T cells			
		% apoptotic (<< 2N)	% hypodiploid (< 2N)	% diploid (2N)	% dividing (4N)	% apoptotic (<< 2N)	% hypodiploid (< 2N)	% diploid (2N)	% dividing (4N)
1	Untreated	20.1 ± 3.8	21.3 ± 2.9	49.9 ± 6.6	8.3 ± 0.2	7.8 ± 2.7	4.5 ± 0.1	86.0 ± 1.0	2.2 ± 2.1
	DXR-SL	18.8	23.6	44	13.4	5.1	2.2	94.1	0
	DXR-SIL	19.6	42.9	31.8	4.7	0.7	0.7	93.8	4.8
2	Untreated	17.5 ± 2.3	12.1 ± 1.1	70.0± 2.6	0.4 ± 0.2	5.1 ± 3.1	6.8 ± 1.4	87.9 ± 5.2	0.6 ± 0.2
	Free DXR	53.9 ± 25.3	37.4 ± 18.2	2.1 ± 0.5	2.6 ± 3.2	64.1 ± 11.4	20.2 ± 1.2	13.2 ± 8.9	2.2 ± 1.2
	DXR-SL	17.3	22.3	60.8	0.9	12.2	6.2	80.3	0.4
	DXR-SIL	64.3 ± 6.2	30.0 ± 6.1	2.1 ± 0.5	3.2 ± 1.1	11.3 ± 3.4	3.6 ± 1.5	84.4 ± 4.2	0.7 ± 0.1
3	Untreated	6.7	29.1	49.3	11.7	1.2	8.9	89.4	0.3
	Free DXR	69	19	3	0	49	32	14	0
	DXR-SL	9	38	39	13	2	17	81	0
	DXR-SIL	53	30	10	1	2	32	64	1

Patient	Treatment	B cells				T cells			
		% apoptotic (<< 2N)	% hypodiploid (< 2N)	% diploid (2N)	% dividing (4N)	% apoptotic (<< 2N)	% hypodiploid (< 2N)	% diploid (2N)	% dividing (4N)
4	Untreated	22.5	15	49.3	12.6	20.2	10.4	62.8	0.3
	DXR-SL	22.6	12.9	52.5	11.5	22	7.2	67.3	0.3
	DXR-SIL	51.6	11.8	20.8	14.9	28.3	12.9	57.8	0.4
	Empty SIL	22.5	15.4	48.6	12.8	24.5	7.4	61	0.7
5	Untreated	8.6 ± 3.8	7.4 ± 0.4	55.1 ± 0.9	25.3 ± 1.0	3.9 ± 1.5	0.5 ± 0.4	94.2 ± 2.7	1.6 ± 0.9
	Free DXR	89	4.7	5.2	0.9	68.2	29.6	2.8	0
	DXR-SL	3.7 ± 2.2	14.6 ± 1.7	64.5 ± 5.9	17.9 ± 2.5	3.3 ± 1.8	11.9 ± 6.5	70.6 ± 7.9	4.1 ± 1.3
	DXR-SIL	16.3 ± 16.2	53.8 ± 22.3	16.5 ± 10.8	8.5 ± 3.8	2.0 ± 1.7	15.6 ± 9.8	80.9 ± 9.3	1.1 ± 0.4
	DXR-NSIL	4.4	10.8	77.8	5.7	3.4	5.7	90.9	0
	Empty SIL	2.1	3.3	59.1	35.5	3.9	1.4	93.6	1.2
6	Untreated	5.8	9.8	57.1	22.9	0.6	5.2	93.8	0.7
	Free DXR	43.5	27.6	17.6	12	13.2	40.9	48.9	0.3
	DXR-SL	2.9	2.6	58.8	35.9	0.2	3.1	89.3	9.2
	DXR-SIL	32.6	14	40.7	12.9	0.8	8.2	89.1	2.5
	DXR-NSIL	2.6	2.1	58.7	36.6	0.8	5.2	92.5	1.6

Patient	Treatment	B cells				T cells			
		% apoptotic (<< 2N)	% hypodiploid (< 2N)	% diploid (2N)	% dividing (4N)	% apoptotic (<< 2N)	% hypodiploid (< 2N)	% diploid (2N)	% dividing (4N)
7	Untreated	3.1	4.5	68.8	23.6	1.4	6.1	91.5	0.9
	Free DXR	39.8	37.6	17.9	5.1	28.7	26.5	44.2	0.7
	DXR-SL	7.2	9.3	56.6	27	3.9	6.5	87.9	1.7
	DXR-SIL	17.4	26.1	44.5	11.7	4	6	87.4	2.7
	DXR-NSIL	4	4.8	58.1	33.2	2.7	4.6	91.4	1.4
8	Untreated	3.8	3.7	70.4	22.2	1	1	97.1	0.9
	Free DXR	20.2	65.8	6.6	7.5	38.5	25.1	39.3	0.1
	DXR-SL	5.6	7.2	57.4	35.4	0.5	3.5	94.8	1.2
	DXR-SIL	22.3	9.5	43.6	30.1	0.5	4.4	94.8	0.4
	DXR-NSIL	4.5	6.7	64.1	25.7	0.3	7	92.6	0.4
Aggregate data set, n=2-8	Untreated	11.0 ± 7.8	12.9 ± 8.1	58.7 ± 8.9	15.9 ± 8.4	5.2 ± 6.2	5.4 ± 3.2	87.8 ± 10.0	0.9 ± 0.6
	Free DXR	52.6 ± 22.0	32.0 ± 18.9	5.1 ± 3.8	4.7 ± 4.1	43.6 ± 19.3	29.1 ± 6.5	27.1 ± 17.6	0.6 ± 0.8
	DXR-SL	10.9 ± 7.0	16.3 ± 10.6	54.2 ± 8.1	19.4 ± 11.6	6.2 ± 7.0	7.2 ± 4.7	83.2 ± 9.6	2.1 ± 3.0
	DXR-SIL	34.6 ± 17.8	27.3 ± 14.5	26.3 ± 15.2	10.9 ± 8.6	6.2 ± 9.0	10.4 ± 9.4	81.6 ± 12.7	1.7 ± 1.4
	DXR-NSIL	3.8 ± 0.8	6.1 ± 3.2	64.7 ± 8.0	25.3 ± 11.9	1.8 ± 1.3	3.4 ± 2.2	91.9 ± 0.7	0.9 ± 0.7
	Empty SIL	12.3	9.2	53.9	24.2	14.2	4.4	77.3	1

Data represent single measurement or mean of 2 -4 replicates for an individual patient sample. S.D. indicated only for 3-4 replicates.

cytotoxicity to either B or T cell populations, and higher concentrations (25 μM DXR or liposomal DXR) were extremely cytotoxic to both cell populations.

An aggregate data set for all patient eight samples in presented in Table 4.4. In all patient samples, free DXR (5 μM) was equally cytotoxic to both B and T cell populations ($p>0.05$), observed experimentally as a decrease in percent diploid cells, and a concomitant increase in cells with reduced DNA content (Table 4.4). In comparison, DXR-SIL[anti-CD19] was more selectively cytotoxic to $CD19^+$ B cells, and displayed a relatively low cytotoxicity to T cells ($p<0.001$, Table 4.4). DXR-SIL[anti-CD19] increased the percent hypodiploid cells by 1.5 to 4-fold that of cells treated with non-targeted DXR-SL, or untreated controls ($p<0.001$, Table 4.4). The percent hypodiploid resulting from DXR-SIL[anti-CD19] treatment were not significantly different from that of free DXR ($p>0.05$). Non-targeted DXR-SL or isotype-matched NSIL[IgG2a] showed minimal cytotoxicity to both B and T cells ($p>0.05$, Table 4.4), resulting in only a marginally increase in percent hypodiploid cells compared to untreated controls ($p>0.05$, Table 4.4). Empty SIL[anti-CD19] were not cytotoxic at equivalent mAb and lipid doses of drug-loaded liposome formulations (Table 4.4, Patients 4 and 5).

4.4.10 *In vivo* therapeutics of ARH77 cells in SCID-beige mice.

ARH77 cells were not transplantable i.p. or i.v. either into either BALB/C nude or SCID-Tac/Icr mice (0/5 mice). SCID-NOD mice were able to engraft ARH77 cells *via* the i.p. route but not *via* the i.v. route. The tumour takes (2/5 mice) and time for tumour development (mean survival time, 47 ± 14 days) were not reproducible. Excised tumours developed in SCID-NOD mice were selected for $CD19^+CD45^+$ ARH77 cells by Coulter

Elite cell-sorting (Coulter, Hialiah, FL). These cells were grown in culture and passaged into SCID-beige mice.

Xenografting of passaged ARH77 cells i.p. into SCID-beige mice resulted in 100 % transplantation success (10/10 mice) and the mean survival time of mice was 36 ± 4 days. Mice showed distinct signs of abdominal distention, characteristic of ascitic tumour growth. The majority of the tumour cells were detected in the peritoneal cavity, along with some solid tumours in lymph nodes, particularly the mesenteric and inguinal lymph nodes. Some ARH77 cells were found to infiltrate certain organs, namely spleen, liver, kidney capsule, and ovaries. There was no histological evidence of ARH77 cells infiltrating the bone marrow in any of the necropsied mice. From histology, single cells or clusters of ARH77 cells were detected in the peritoneal cavity.

To confirm the presence of ARH77 cells and expression of target CD19 receptors on ARH77 cells implanted in SCID-beige mice, representative control mice were necropsied, and cells dissociated from tissues were detected by immunophenotyping for CD19 using flow cytometry. Isolated cells from selected tissues, PBMC (recovered *via* Ficoll gradients) and cells from ascites fluid lavaged from i.p. tumours were stained for both CD19 and CD45 (human common leukocyte antigen). This allowed for identification of human cells, in SCID-beige mice. Flow cytometry could not detect any tumour cells in the liver, spleen, lung, heart, kidney, or bone marrow, perhaps due to the low tumour-cell involvement in these tissues (confirmed using histology). A large fraction of the cells isolated from solid tumours and ascites (Fig. 4.10) was found to be ARH77 cells and to retain expression of CD19.

The antitumour effect of DXR-SIL[anti-CD19] was tested against ARH77 cells xenografted i.p. into SCID-beige mice. SCID-beige mice were injected i.p. with $1x10^7$ ARH77 cells and treatments were commenced i.p. on day 1 with either free DXR, DXR-SL, DXR-HSPC-SIL[anti-CD19], DXR-PC40-SIL[anti-CD19] or free anti-CD19 given in conjunction with DXR-SIL[anti-CD19]. The results of this therapeutic study are shown in Figure 4.11. Control mice were injected with PBS had a mean survival time (MST) of 36 days. ARH77 cells were extremely sensitive to free DXR *in vitro* (see Table 4.4.2), and consequently, free DXR was able to substantially delay tumour growth in tumour-implanted mice compared to controls (free DXR, MST 130 ± 41 days, $p<0.01$). There was no statistically significant difference ($p>0.05$) in effectiveness between either free DXR, DXR-SL (MST 83 ± 29 days) or DXR-HSPC-SIL[anti-CD19] (MST 66 ± 13 days). However, each of these treatments was significantly better than PBS controls. Treatment with either DXR-PC40-SIL[anti-CD19] (MST 3/5 mice= 66 ± 3 days; LTS 2/5) or free anti-CD19 given in conjunction with DXR-HSPC-SIL[anti-CD19] (MST 2/5 mice= 73 ± 6 days; LTS 3/5) was able to significantly increase survival times of ARH77-implanted mice, resulting in some long-term survivors (LTS> 250 days).

4.5 DISCUSSION

In Chapter 2, on the use of immunoliposomal DXR to treat human B lymphoma we suggested that this treatment may be applicable to other B-cell malignancies. In MM, malignant B cells are present as individual cells or small clusters of cells in blood, or in close access to the circulatory system (247, 248, 255, 276). This may make MM more

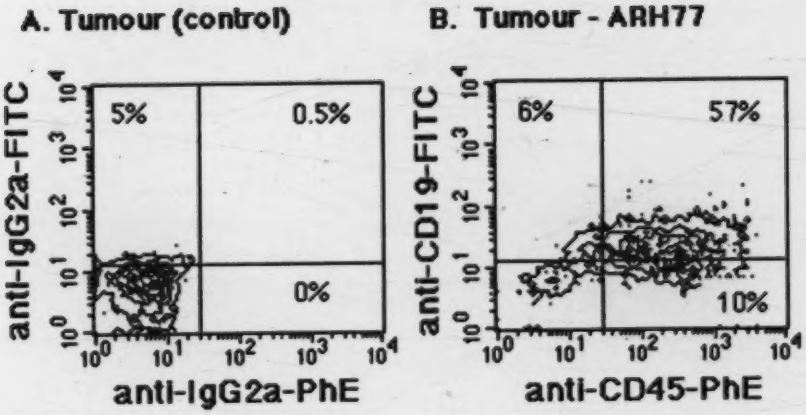

Figure 4.10. Two-colour flow cytometry to examine the expression of CD19 on ARH77 cells after i.p. implantation in SCID-beige mice.
Cells retrieved from peritoneal cavity were stained with both anti-CD19-FITC (B cell marker) and anti-CD45-PhE (common leucocyte antigen marker) and run on the flow cytometer. Panel illustrate, **(A)** Control ascitic tumour cells from peritoneum stained with isotype-matched antibodies; **(B)** tumour cells stained with anti-CD19-FITC and anti-CD45-PhE.

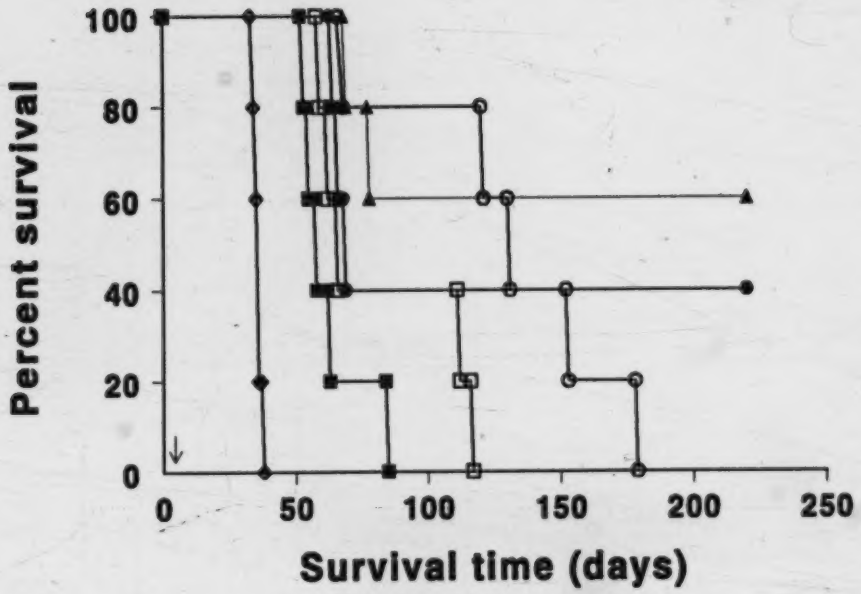

Figure 4.11. ***In vivo*** **therapeutics of free DXR and various liposomal DXR in SCID-beige mice.** SCID-beige mice (5/group) were implanted i.p. with $5x10^7$ ARH77 cells. Treatments were commenced 24 h after inoculation of cells with a single i.p. injection of PBS (◆) or 2 mg/kg DXR as either free DXR (○), DXR-SL (□), DXR-PC40-SIL[anti-CD19] (●), DXR-HSPC-SIL[anti-CD19] (■) or DXR-HSPC-SIL[anti-CD19] in conjunction with 10 μg free anti-CD19 (▲). Individual mice received approximately 0.27 μmol PL and 14 μg mAb in 0.2 ml. Data are reported as % survival *vs.* days survived.

amenable to treatment with targeted carriers, which are resident in the blood for prolonged times (139). The studies presented in this paper focus on the applicability of targeted liposomes in hematological cancers, specifically multiple myeloma. This work demonstrates that some selectivity of targeting of DXR-SIL[anti-CD19] can occur against the human $CD19^+$ multiple myeloma cell line ARH77 *in vitro,* and against $CD19^+$ B lymphocyte populations of peripheral blood mononuclear cells from MM patients *ex vivo.*

Our binding studies reveal that SIL[anti-CD19] rapidly associate with the ARH77 cells. At maximal binding, approximately 5300 SIL[anti-CD19] or 1600 SL were bound per ARH77 cell. This translates into approximately 3700 specific SIL[anti-CD19] binding sites per ARH77 cell, which is similar to the estimated 3000 CD19 sites determined on ARH77 cells by flow cytometry. The fact that equilibrium binding was not completely attained at 1 h at liposome concentrations as high as 1600 μmol PL/ml suggests that SIL[anti-CD19] bound to the surface of ARH77 cells may be continually endocytosed and CD19 may recycle to the cell surface to participate in further binding. It has been previously shown that free anti-CD19 binds CD19 with a high affinity (295, 313) and hence, it is unlikely that the binding process (see Fig. 4.1) is a result of weak or low affinity interaction. At a mAb coupling density of 25 antibodies/liposome and assuming a single antibody interaction with a single CD19 site, the relative K_D of the anti-CD19 mAb coupled to liposomes was calculated as 2.2×10^{-3} μM. The K_D of the liposome-coupled anti-CD19 was similar to that seen for the Namalwa cell line (1.8×10^{-3} μM), and 9-fold lower than the K_D of free anti-CD19 to Daudi cells (B cell line) $K_D = 2.5 \times 10^{-4}$ μM (i.e., 4×10^9 M^{-1}) (313). The slight decrease in affinity of the mAb may be due to oxidative

modification of the antibody prior to coupling to liposomes (53, 168, 169). It is also possible that anchoring of the mAb to the PEG polymer terminus *via* the Fc portion of the mAb could result in decreased rotational freedom of anti-CD19, or that the mAbs affinity may be decreased by the effects of coupling to PEG chains (315).

We observed a high *in vitro* cytotoxicity of SIL[anti-CD19] to ARH77 cells. However, unlike our observations with the human B lymphoma model (Chapter 2), this did not translate into a significant antitumour activity *in vivo*. At the maximum tolerated DXR dose (2 mg/kg), mice showed no signs of free drug toxicity, and both targeted and non-targeted liposomes had pronounced antitumour activity in the i.p. xenografts of ARH77 cells in SCID-beige mice. ARH77 cells express low levels of CD19, i.e, 3000 sites/cell. In our therapeutic experiments, mice were dosed at 2 mg DXR/kg, which was approximately 0.27 μmol PL (or 2.1×10^{12} liposomes). As i.p. treatments were initiated at 24 h (after approximately one doubling time of these cells), this means that there were potentially 6×10^{10} total CD19 sites available to bind DXR-SIL[anti-CD19]. Mice were injected with 35-fold higher number of liposomes relative to the total CD19 receptor sites on ARH77 cells, and yet this did not translate into a significant antitumour effect *in vivo* compared to non-targeted controls. Implanted ARH77 cells in SCID-beige mice are mainly present mainly as single cells or small clusters of cells within the peritoneal cavity, and hence cytotoxicity of DXR-SIL[anti-CD19] to cells may be directly dependent upon the association of liposomes to cells within this compartment. We have previously shown that the transit of SL from the peritoneal cavity into blood occurs with an half life of approximately 0.6 h (311). As DXR-SIL[anti-CD19] were able saturate all CD19

receptor sites on ARH77 cells, the rate at which the receptor internalizes and recycles to the cell surface may determine the effectiveness of DXR-SIL[anti-CD19]. In addition, the passage of liposomes out of the peritoneal cavity into blood (284) or uptake by peritoneal monocytes and macrophages may contribute to the poor antitumour response (311, 355).

Our binding results indicate that fluid PC40 liposomes bound more readily to ARH77 cells than did their rigid HSPC counterparts (Fig. 4.2B). This was consistent with the increased DXR from DXR-PC40-SIL[anti-CD19] associated with ARH77 cells, compared to their HSPC counterparts (Fig. 4.3e *vs.* 4.3f). It is possible that portion of the drug entering cells may come from any free drug released in the media, or at the cell surface after drug leakage from liposomes in peritoneal fluid. Hence, the enhanced antitumour activity of DXR-PC40-SIL[anti-CD19] may be due to a high local release rate of drug from these liposomes (Chapter 3).

Numerous studies have utilized free antibodies in targeting B cell tumours, and it has been suggested that anti-CD19 signals a series of intracellular messages leading to B-cell differentiation, cell arrest or apoptosis (4, 289, 312). It is likely that the *in vivo* cytotoxicity of free anti-CD19 is a result of a variety of host immune factors, acting after binding of the mAb to CD19 (4), and may result from mechanisms involving CD19-mediated signalling, antibody-dependent cellular cytotoxicity, activation of immune system (mediated *via* monocytes, macrophages or natural killer (NK) cells) or complement-mediated processes (4, 289, 312, 356, 357). This is reasonable given that SCID mice, although lacking functional B and T cells, possess a residual immune system comprising monocyte, macrophage, NK cells, and complement-activity (358, 359), and this lack of an

immune system may be responsible in part for the cytotoxic action of the free anti-CD19.

We were unable to observe any effect of free anti-CD19 in our *in vitro* cytotoxicity assays up to a concentration of 1 μM. In the cytotoxicity studies reported here, anti-CD19 did not induce any increased sensitivity of ARH77 cells to free DXR or liposomal DXR. In fact at 1 h, free anti-CD19 in conjunction with targeted DXR-SIL[anti-CD19] competively inhibited the action of DXR-SIL[anti-CD19], giving cytotoxicities equivalent to non-targeted liposomes. However, a cytotoxic effect of anti-CD19 in combination with DXR-SIL[anti-CD19] was observed at 24 h, suggesting that recycling of the receptor in the continued presence of the DXR-SIL[CD19] may be involved in the observed cytotoxicity (Chapter 3). We have previously reported that the free mAb has an additive effect when given in conjunction with DXR-SIL[anti-CD19] *in vivo* therapeutics of human B-cell lymphoma (Namalwa) in SCID mice (Chapter 2). Similar to these results, the free anti-CD19 plus DXR-SIL[anti-CD19] therapy appeared to be by far the most successful treatment for ARH77 cells in SCID-beige mice (Fig. 4.11). It is likely that, although both anti-CD19 and DXR-SIL[anti-CD19] compete for the same membrane receptor, they may subsequently have cytotoxic effects *via* independent pathways, i.e., anti-CD19 signalling of apoptosis (4, 289, 312, 356, 357) or DXR-induced DNA strand breaks in cells (341). The antitumour effects of DXR-PC40-SIL[anti-CD19] in the i.p. model (Fig. 4.11) were in agreement with our *in vitro* results, and may be due to specific binding and internalization of liposomes, together with the cytotoxic effect of any free drug released in liposomes within the peritoneal cavity.

In myeloma peripheral blood cells we observed a variable cytotoxicity of free DXR

(quantified experimentally using DAPI staining), giving anywhere from hypodiploid to apoptotic DNA profiles in B and T cells from different patient samples (Table 4.4). DXR-SIL[anti-CD19] was able to selectively target and result in selective cytotoxic to a large fraction of malignant $CD19^+$ B cells in MM blood *ex vivo* (Fig. 4.9, Table 4.4). Differences in the cytotoxicity of DXR or DXR-SIL[anti-CD19] to human B cells from different MM patients blood may be due to several patient factors. In this study we did not correlate cytotoxic outcomes with patient factors, such as, the disease stage (newly diagnosed, remission, or relapsed), the treatment schedule of the patient, or the multidrug resistant (MDR) status of MM B cells. $CD19^+$ B cells in relapsed MM have been shown to express functional P-gp, and the expression of the pump has been implicated in multidrug resistance (258, 270). Drugs like DXR, which are substrates for the multidrug resistance transport protein, would be actively pumped out of the cytoplasm in P-gp-expressing cells (269, 317, 360), leading to low intracellular drug levels.

Our confocal data shows that interaction of B cells with targeted DXR-SIL[anti-CD19] results in perinuclear, punctate DXR fluorescence throughout the cytoplasm. These observations are consistent with cellular uptake of DXR-SIL[anti-CD19] by receptor-mediated endocytosis into possible endosome and/or lysosomal structures (206, 361). This mechanism may be responsible for the improved selective toxicity to B cells *versus* T cells, relative to free DXR or DXR-SL. Routing of drug through receptor-mediated endocytotic processes may bypass the P-gp pump mechanism, to deliver high DXR concentrations directly into the cytoplasm. Experiments to test this hypothesis are underway.

MM still remains largely incurable. Current therapeutic interventions, i.e., conventional chemotherapy, or radiotherapy, including, bone marrow transplants, have resulted in limited therapeutic success (247, 267, 362). Although these therapies are able to eliminate the plasma cells from the bone marrow, $CD19^+$ malignant B cells in blood still persist, and presumably have regenerative potential, despite treatment (255, 257, 259). Considerable evidence now implicates this invasive population of blood B cells, which are often multidrug resistant, in disease spread (255, 263). Relapse has been suggested to occur as these blood B cells continuously differentiate into end-stage plasma cells which migrate to the bone marrow (255, 257). Treatment with DXR-SIL[anti-CD19] may eradicate the malignant clone of circulatory B cells, preventing these cells from repopulating the bone marrow and hence decreasing the likelihood of relapse.

As both normal and malignant B cells express CD19 (287, 288), the lack of specificity of treatment with DXR-SIL[anti-CD19] to the malignant B-cell compartment over the normal B-cell clone may lead to deletion of both normal and malignant B-cell populations, causing patients to become immunocompromised. Normal B-cell numbers in MM are generally depressed, and hence this issue may be of little significance (316). Moreover, the target CD19 antigen is present only on a certain lineage of B cells, and is absent on progenitor B cells, which could allow CD19-negative B-cell precursors and hematopoietic stem cells to regenerate the B-cell population from normal precursor cells (287, 288). Due to the selectivity of immunoliposomal treatment, T cell-mediated immunity should not be not be compromised.

The success of immunoliposomal therapy relies on tumour cells expressing their

target antigen. Modulation or down-regulation of CD19 epitopes during the normal cell-growth cycle, differentiation stages, or during the process of therapy may limit this approach (4, 15, 16, 288, 310). Highly expressed, internalizing antigens, like CD19, may be ideal target epitopes for such antibody-based therapies (4, 287, 288). Surface phenotyping of ARH77 cells (Table 4.1), reveal that this cell line resembles an end-stage B-, or lymphoplasmacytoid cell phenotype. The observations that ARH77 cells have a lower CD19 expression, and thus lower capacity for endocytosis of SIL[anti-CD19] compared to malignant B cells from MM patients, and may account for the differences in targeting and cytotoxicity observed between ARH77 cells *in vivo* therapeutics, and MM patient $CD19^+$ B lymphocytes *ex vivo*.

This strategy is dependent on the ability of the malignant B cells to retain CD19. End-stage plasma cells do not express (or express low levels) of CD19, and hence this targeting strategy precludes treatment of the plasma cell component of the disease. In cases where the receptor is downregulated or lost during cell differentiation, it may be necessary to identify a different cell surface antigen for targeting immunoliposomes. An attractive approach could be the use of a combination of several different immunoliposomes, including CD19 (9), CD20 (10), CD22 (363), and/or CD38, that would target both the malignant blood B cells and plasma cell components of this disease.

CHAPTER 5

Summarizing discussion and conclusions

The use of liposomes as drug carriers has been extensively investigated, and this has led to the development of a number of liposomal drugs that are being used in humans or in clinical trials (48, 50, 55, 60). Amongst the first of the liposomal therapies to be approved were the liposomal anthracyclines doxorubicin (DXR) and daunorubicin (48, 54, 55). Encapsulation of DXR in liposomes, has led to significant pharmacokinetic and pharmacodynamic improvements over the free drug (47, 51, 86, 364). The engrafting of hydrophilic polymers on liposomes (SL) inhibits the *in vivo* adsorption of plasma proteins, reducing their recognition by cells of the mononuclear phagocyte system (MPS), thus allowing longer circulation times for SL (123, 130, 282). As a consequence of the circulation longevity, SL have been shown to "passively" localize into solid tumours which develop leaky capillaries during the process of angiogenesis accompanying tumour growth (47, 51, 81, 365). This mechanism of "passive" targeting may not be appropriate for hematological cancers, where angiogenesis is not a predominant feature. In hematological malignancies, individual cells or clusters of cells are present in the blood, lymph and bone marrow. Since SL lack the means of attaching to malignant cells, an approach that would selectively deliver the drug to the target cells *via* targeted liposomes may result in improved therapy.

In this thesis, we examined the applicability of antibody-targeted, long-circulating liposomes in the treatment of hematological diseases, like B-cell lymphoma and multiple myeloma (MM). In these diseases, target cells are present in the blood stream or in close proximity to the circulatory system, and are easily accessible by injected immunoliposomal drugs. The premise of this approach relies on the ability of targeted liposomes to

specifically bind tumour cells and to internalize the targeted liposome-drug package. As a result, the high intracellular drug levels achieved in this way would augment the cytotoxicity of the entrapped agent.

B cells express a variety of surface antigens, like CD19, CD20 and CD22, and have been targets for a variety of immunotherapies (4, 5). CD19 antigens are present on 90 % of human B-cell malignancies and are internalizing receptors. In our experiments, targeting of liposomes was achieved with high affinity anti-CD19 monoclonal antibodies (mAbs) (295, 313) directed against the highly expressed leukocyte differentiation antigen CD19 on B cells (287, 288, 308-310). MAb anti-CD19 was coupled to the terminus of Hz-PEG-DSPE *via* a hydrazone bond (168). In this coupling procedure, the Ab was immobilized by an oxidized carbohydrate on the Fc portion of the Ab so as to expose the binding regions, allowing it to recognize CD19 epitopes on B cells (169). In chapter 2, we showed that targeted SIL[anti-CD19] rapidly bound Namalwa or ARH77 cells *in vitro*, and the binding was specifically mediated through the interactions of the coupled anti-CD19 with the CD19 receptors on B cells.

As the interaction of liposomes with cells depends primarily upon random collisions, the number of productive collisions would be affected by the density of target epitopes and/or the number of ligands coupled to liposomes. High affinity ligands interacting with highly specific receptors could increase the strength of binding to target cells (165, 199). The association of liposomes with cells may be enhanced by multivalent interactions of more than one Ab with one or more target epitopes on cells.

In our system, liposomes were actively loaded with DXR *via* an ammonium

sulphate gradient, which results in the precipitation of DXR as DXR-sulphate increasing its latency in liposomes. The free DXR has a large volume of distribution, and after i.v. injection is rapidly cleared from blood (51). Drugs, with large volumes of distribution, and with low latency in liposomes may not reach target cells due to rapid release and distribution *in vivo* (Fig. 5.1). Conversely, drugs with high latency in liposomes may be retained within liposomes, and may not release their drug contents.

Liposomes may specifically or non-specifically associate with cells. Non-specific association of liposomes with cells may result in diffusion of released DXR away from the cell and inefficient uptake of drug into the cell (195, 201, 324, 366). Specific interactions may be mediated *via* binding of targeted liposomes to either internalizing or non internalizing receptors. In the case of non-internalizing receptors, liposomes bound to the surface may result in diffusion-mediated uptake of only a portion of drug into cells and diffusion and redistribution of the remainder of the released drug into blood and tissues (Fig. 5.1) (151, 185, 324, 342). In comparison, in our model interaction of SIL[anti-CD19] with CD19 on B cells triggered rapid internalization of the liposomal drug package into cells *via* receptor-mediated internalization. And as a result, higher levels of DXR was found to accumulate in target cells treated with DXR-SIL[anti-CD19] compared to non-targeted DXR-SL, which are not internalized (Fig. 5.1).

Our results from Chapter 3, indicate that SIL[anti-CD19] are sequestered in compartments of low pH, providing evidence of endosomal and/or lysosomal trafficking (schematized in Fig. 5.1). The cytotoxicity of the drug, will depend upon its stability within the acidic pH of the endosomes (198, 367) and its release from this compartment to

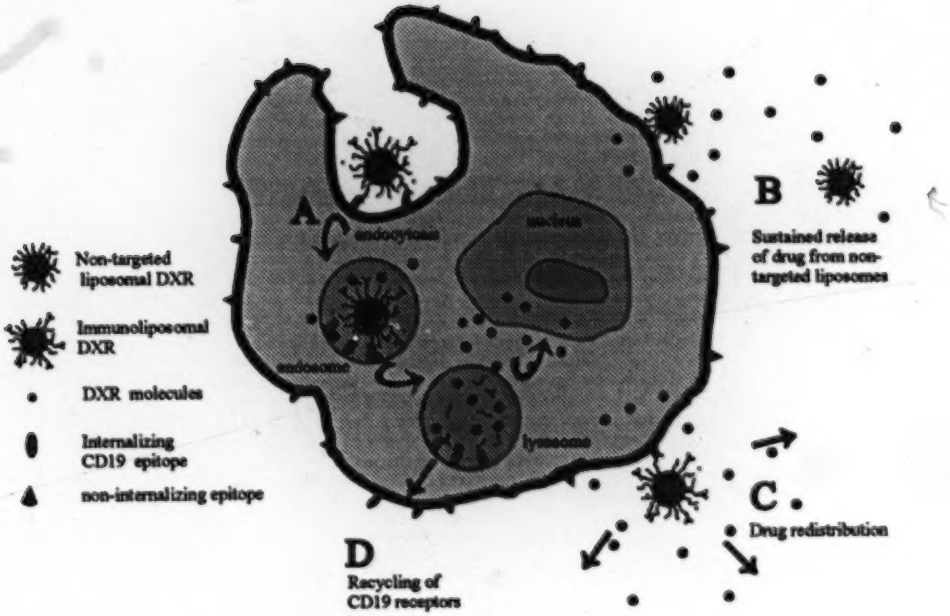

Figure 5.1. Proposed mechanism of action of immunoliposomes.
Binding of SIL[anti-CD19] to target CD19 receptors results in receptor-mediated endocytosis of liposomes into endosome and/or lysosomes (A). Non-targeted liposomes non-specifically associate with cells, to release drug in close proximity to cells (B). Immunoliposomes targeted to non-internalizing receptors, specifically bind to cells and release drug at the cell surface, but are not internalized (C). Processing of internalized immunoliposomes in the acid-labile, enzyme-enriched environment of lysosomes, results in disintegration of liposomes in the lyososomes. Neutral drug species that are resistant to the acid environment of the lyososomes may traffic across the lysosomal membranes into the cytoplasm. Drugs released in the cytoplasm may be accessible to intracellular targets, like the nucleus. The receptors engaged in binding immunoliposomes may be recycled to the surface to participate in further binding events (D).

its site of action in the nucleus. The release of drug from the endosomes depends upon the dismantling of liposomes within the lysosomes (336). In stable liposomes, such as those used in these experiments, drug may not easily be released from the liposomes and may be sequestered for many hours within the endosome and/or lysosomes. In chapter 3, we demonstrated that the translocation of DXR molecules from DXR-SIL[anti-CD19] across the lysosomal membranes into the cytoplasm was a time dependent event, and probably determined by the rate of charge neutralization of the cationic form of the drug (335, 341, 342). Negatively charged drugs like carboxyfluorescein encapsulated in liposomes, will translocate across the lysosomal membranes, after liposome internalization and subsequent charge neutralization within acidic lysosomal compartment (335, 342). On the other hand, drugs like DXR which are protonated at acid pH may be sequestered within the lysosomes, and entry of the drug into the cell cytoplasm may depend upon the rate of generation of uncharged molecules. In chapter 3, we showed that the internalization, and intracellular release of DXR from DXR-SIL[anti-CD19] after translocation across the lysosomal membranes led, after 24 to 48 h, to appearance of DXR into the nucleus of cells and cell kill.

B cells have inherent endocytosing capacity, where antigens processed by cells within the endosome may be presented to cell surface *via* MHC class II molecules (368). Analogous to this mechanism, it is possible that immunoliposomes endocytosed within the lysosomes could be regurgitated out of cells after liposome-receptor internalization, with some of the drug lost to the cell interior (309). This would apply in the case of recycling receptors such as the CD19 receptor, but not in cases where the receptors are degraded

within the lysosomes (336). There was no evidence of this phenomenon in our experiments from either the pH-sensitive fluorophore HPTS or confocal imaging. Possibly, breakdown of the hydrazide linker at low pH results in release of the anti-CD19 from the liposome and preserves the liposomes within the lysosomal compartments (172). In other words, the use of cleavable polymers or acid-labile coupling chemistry may prevent the immunoliposomes from being dragged back to the cell surface along with the receptor-complex during recycling (369, 370). In chapter 3 and 4, we showed that DXR-SIL[anti-CD19] were able to elicit nuclear strand breaks in B cells, confirming that DXR released from DXR-SIL[anti-CD19] within the lysosomes was able to translocate across the lysosomal membranes and bind to nuclear DNA.

In our work, free DXR treatment was cytotoxic *in vitro* to Namalwa, ARH77 or H9 cells, i.e., it demonstrated non-selective cytotoxicity to both B and T cells. DXR-SIL[anti-CD19], on the other hand, was selectively cytotoxic to $CD19^+$ Namalwa and ARH77 cells *in vitro*, and had low cytotoxicity to the control T cell line (H9). The specificity of targeting of SIL[anti-CD19] to B cells was also demonstrated in a heterogenous mixture of PBMC from MM patients *ex vivo*. In all MM patient samples *ex vivo*, DXR-SIL[anti-CD19] was selectively apoptotic to B cells, with relatively low cytotoxicity to T cells. Non-targeted liposomes, on the other hand, showed low cytotoxicity to both B and T cells from MM patients. These results suggest that the DXR-SIL[anti-CD19] may be an effective strategy for the selective eradication of malignant B cells in blood of MM patients.

Immunoliposomes having circulation times of sufficient length to allow binding

of the liposomes to their target B cells within the circulation (53, 171, 371) were necessary to achieve the therapeutic results described in the preceding chapters. Following i.v. administration, the susceptibility of liposomes to opsonization and rapid clearance by the MPS is related to the composition of immunoliposomes, particularly the presence of sterically stabilizing components such as PEG, and the density of antibodies on the liposomes (372, 373). There is an inverse relationship between the number of antibodies on liposomes and their circulation half life (53). The development of long circulating liposomes, and improved methods for the attachment of antibodies (53), have increased the potential for targeting liposomes to diseased cells (16, 175, 216). Sites easily accessible from the vasculature are obvious targets for immunoliposomes, and our results demonstrate the utility of this approach.

In Chapter 2, we showed that SIL[anti-CD19] with approximately 50 μg mAb/μmol PL retained long-circulation times, consistent with the pharmacokinetics of Ab-free SL (53, 71, 123). In tumour-bearing mice implanted i.p. with Namalwa cells, the kinetics were found to be remarkably different from that seen in naive mice. SIL[anti-CD19] were rapidly eliminated from circulation, probably because of their binding to tumour cells in blood and the peritoneal cavity, which were detected from histological evidence. Evaluation of the levels of liposomes in solid tumours of the lymph nodes indicated that the accumulation of SL was significantly more than SIL[anti-CD19]. We hypothesize that SIL[anti-CD19] can readily bind to individual tumour cells or small clusters of cells, accessible from the vasculature, but the penetration of SIL[anti-CD19] into large solid tumours may be restricted by the "binding site barrier" to cells at the

tumour periphery (Fig. 5.2) (174). In the case of SL, the penetration of SL into solid tumours may be less restricted, as it depends primarily on the presence of discontinuities in the capillaries of the blood vessels in the solid tumours (80, 81).

The antitumour effectiveness of targeted liposomal therapy was demonstrated in the models of human B lymphoma (Namalwa) and multiple myeloma (ARH77) growing in SCID mice. Treatment effectiveness of DXR-SIL[anti-CD19] in the Namalwa model depended upon the drug formulation, dose and dosing schedule. SIL[anti-CD19] therapy resulted in a significantly increased mean survival times of mice implanted with Namalwa cells, compared to non-targeted liposomes or free DXR. Treatment of the i.p. implanted tumour with the immunoliposomal drug was more effective than treatment of the i.v. implanted tumour. In the case of the i.p. model, cells were mainly confined within the i.p cavity as individual cells or small clusters of cells. We observed no ascitic tumour growth in mice with i.p. treatments of DXR-SIL[anti-CD19] when the tumour cells were implanted i.p., but observed some solid tumours in the peritoneum of DXR-SIL[anti-CD19]-treated mice. This suggests that DXR-SIL[anti-CD19] may readily target single cells or small clusters of cells in the peritoneum, however, DXR-SIL[anti-CD19] was unable to kill cells once they extravasated out of circulation and established themselves as multicellular tumours. Initiation of DXR-SIL[anti-CD19] treatment at 1h, while cells were still in circulation, or at lower tumour burdens, resulted in the most successful therapy, yielding some cures in mice implanted with the B-cell tumour. The success of this treatment schedule, indicated that DXR-SIL[anti-CD19] were readily able to target and destroy tumour cells which are circulating in blood. Multiple treatments of

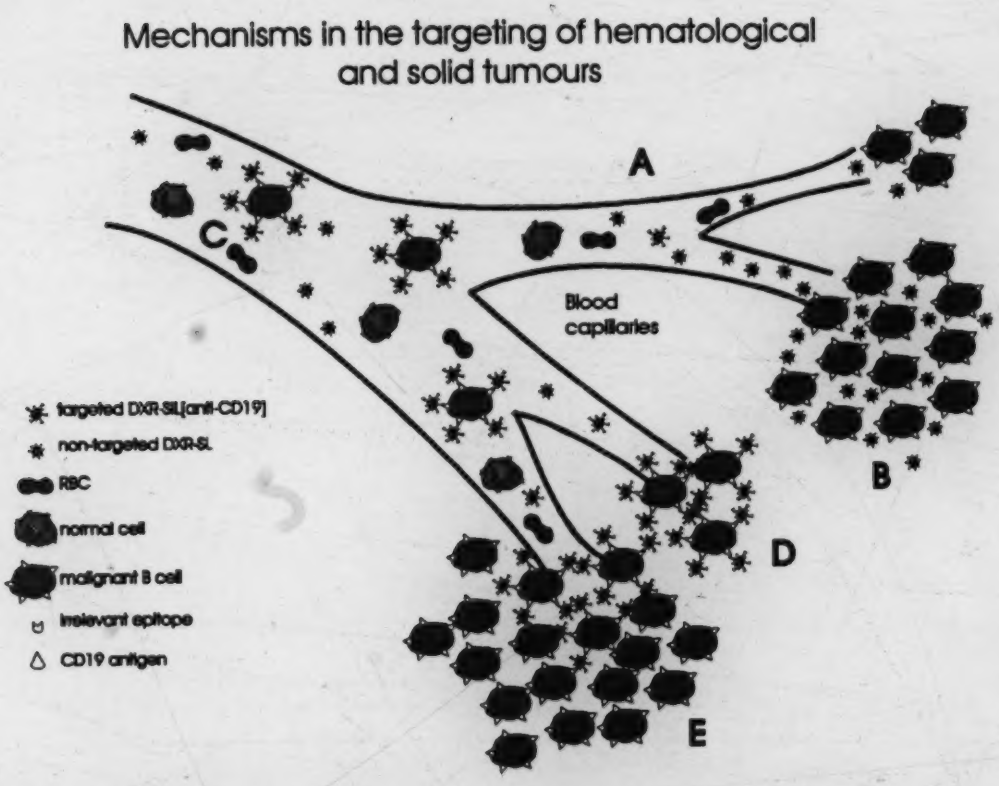

Figure 5.2. Schematic illustrating the interaction of targeted and non-targeted liposomes *in vivo*.
Non-targeted SL do not associate with individual blood cells to a significant extent (A) and are able to passively localize into solid tumours (B). The distribution of SL is however, dependent upon the vascular permeability of capillaries, particularly enhanced in areas of solid tumour growth. Passive accumulation of liposomes into the solid tumour may release drug over time. Immunoliposomes can interact with individual cells in blood or small clusters of cells in blood (C), or as micrometastatic tumours (D) contiguous to the capillary lining. The binding of SIL[anti-CD19] to target $CD19^+$ B cells in blood may lead to the removal of SIL[anti-CD19]-cell complexes *via* recognition and uptake by macrophages in liver and spleen. The penetrability of SIL[anti-CD19] into large solid tumours may be restricted by the "binding site barrier", where liposomes would first bind to cells on the outer limits of the tumour mass, preventing further penetration of SIL[anti-CD19] into the tumour interior (E).

DXR-SIL[anti-CD19] were able to slightly increase the survival times of mice implanted with Namalwa cells over single treatments. This may be due to the fact that at later treatment doses, the cells begin to grow as multicellular tumours, or at sites not readily accessible to immunoliposomes circulating in the blood.

Clinical applications of immunoliposomes in humans may require repeated administration of liposomes to achieve maximum therapeutic benefit. Some studies in mice have shown that repeated administration of injected immunoliposomes may induce an immune response, leading to the rapid clearance of subsequent injections of immunoliposomes (171, 201). Most antibodies that are currently in clinical trials are of murine origin (4). The possible immunogenicity of liposomes bearing murine Abs remains a concern when liposomes are to be injected into humans (4, 176-180). Antibody-based therapies may become ineffective or dangerous because of immune responses to the foreign protein (171, 177, 374). In clinical studies, murine monoclonal antibodies or immunoconjugates have led to the development of human anti-mouse antibodies (HAMA) (4, 176, 179, 180). HAMA (anti-idiotypic antibodies to the injected antibody) can lead to rapid elimination of the injected Ab-based therapeutic, significantly reducing its *in vivo* targeting and hence its therapeutic effectiveness. To alleviate some of these problems, antibody fragments, chimeric or humanized antibodies with lower immunogenic potential have been developed and are being investigated in association with immunoliposomes (165, 183, 184, 295, 313, 375, 376). From the pharmaceutical standpoint there are a variety of issues that have to be addressed for human applications of immunoliposomes. These include, the quality of the monoclonal antibody (affinity, purity), the linker

chemistry (and coupling efficiency), and the sterility and pyrogenicity of the immunoliposomal therapeutic.

One of the major problems in the treatment of most B cell diseases is the development of resistance to drugs upon continuous exposure to chemotherapeutics, like DXR (271, 272). For DXR the expression of the multidrug resistant glycoprotein pump (P-gp), or the multidrug resistant protein, MRP, is responsible for one form of resistance in which there is the efflux of drugs from cancer cells (269, 317, 360). P-gp expression has been correlated with shorter patient remissions and higher relapse rates in B-cell lymphoma and MM patients treated with vincristine and DXR. Agents such as verapamil and cyclosporin A (CsA) (360), that work as specific blockers of P-gp, have been shown to reverse drug resistance. The clinical effectiveness of these P-gp blockers may be limited, because of potential toxicities of these agents in clinically effective doses. The use of P-gp blockers not only sensitize resistant cancer cells but also sensitize the normal tissues which express P-gp to the effects of DXR. Antibody-targeted liposomes may be applicable as an alternative mode of treatment, where the mechanism of action of DXR-SIL may be independent of the drug efflux pumps. Such therapies could directly deliver the drug, *via* endosome and/lysosomes, into the cell interior, delivering high intracellular drug levels to target cells in excess of the capacity of the P-gp pump to flush the drug out of the cell.

Efforts at improving the effectiveness of chemotherapeutic regimens may rely upon combination drug therapy in the treatment of B-cell malignancies. New therapeutic protocols using combinations of drugs with non-overlapping toxicities have demonstrated

increasing success in terms of toxicity and overall patient response rates. In spite of these efforts, patients with B cell malignancies or MM relapse, or become resistant to chemotherapy. Recent reports have suggested combining a variety of antibodies and/or immunotoxins with a variety of cytotoxic agents to obtain synergistic responses (377). The free anti-CD19 on its own is a signalling antibody and is known to induce cell cycle arrest and apoptosis (4, 289, 312). In this thesis, we established that combining free mAb with free DXR, DXR-SL, or DXR-SIL[anti-CD19], resulted in an additive action. The combination of two therapeutic agents which may act on the same receptor but by different mechanisms may be an interesting therapeutic application that remains to be investigated.

Recently, with the development of long circulating liposomes, and strategies for coupling of targeting moieties to liposomes, possibilities exist for targeting drugs within the vasculature or to sites outside the MPS (165, 167, 199, 201, 283, 318, 378). The successful development of DXR-SIL[anti-CD19] for targeting malignant B cells requires the identification of appropriate targets on the B cells, the accessibility of DXR-SIL[anti-CD19] to target cells, and the use of high affinity antibodies against internalizing epitopes. To date, there have been few reports of targeting of immunoliposomes to specific cell populations *in vitro* or *in vivo*. The results in this thesis are an important step towards realizing the goal of selective toxicity for anticancer drugs, i.e. magic bullets. We have shown that targeted liposomal anticancer drugs can selectively increase cellular drug levels in target cells, decreasing toxicities to normal tissues. This has led to an increase in the therapeutic index of the encapsulated drug, DXR.

In conclusion, the studies presented in this thesis have important clinical applications. We establish that targeted long-circulating immunoliposomes are an effective therapy for the treatment of murine models of human B cell lymphoma, and for the eradication of malignant B cells in MM *ex vivo*. This strategy may be generally applicable to other blood dyscrasias of B or T cell origin, or for other therapeutic applications within the vascular system, and may be helpful in overcoming multidrug resistance in cancer patients.

REFERENCES

1. Ehrlich, P. The relations existing between chemical constitution, distribution and pharmacological action, *In*: Ehrlich, P. (ed.) Collected studies on immunity. pp. 404-442. New York: John Wiley and Sons, Ltd, 1906.
2. Korngold, L. and Pressman, D. The localization of antilymphosarcoma antibodies in the Murphy lymphosarcoma of the rat, Cancer Res. *14:* 96-99, 1954.
3. Kohler, G. and Milstein, C. Continuous cultures of fused cells secreting antibody of predetermined specificity, Nature (London). *256:* 495-497, 1975.
4. Vitetta, E. S. and Uhr, J. W. Monoclonal antibodies as agonists: an expanded role for their use in cancer therapy, Cancer Res. *54:* 5301-5309, 1994.
5. Waldmann, T. A. Monoclonal antibodies in diagnosis and therapy, Science. *252:* 1657-1662, 1991.
6. Gaber, M. H., Hong, K., Huang, S. K., and Papahadjopoulos, D. Thermosensitive sterically stabilized liposomes: formulation and in vitro studies on mechanism of doxorubicin release by bovine serum and human plasma, Pharmaceut. Res. *12:* 1407-1416, 1995.
7. Trail, P. A., Willner, D., Lasch, S. J., Henderson, A. J., Hofstead, S., Casazza, A. M., Firestone, R. A., Hellstrom, I., and Hellstrom, K. E. Cure of xenografted human carcinomas by BR96-doxorubicin immunoconjugates, Science. *261:* 212-215, 1993.
8. Grossbard, M. L., Press, O. W., Appelbaum, F. R., Bernstein, R., and Nadler, L. M. Monoclonal antibody-based therapies in leukemia and lymphoma, Blood. *80:*

863-878, 1992.

9. Grossbard, M. L., Freedman, A. S., Ritz, J., Coral, F., Goldmacher, V. S., Eliseo, L., Spector, N., Dear, K., Lambert, J. M., Blattler, W. A., Taylor, J. A., and Nadler, L. M. Serotherapy of B-cell neoplasms with anti-B4-blocked ricin: A phase I trial of daily bolus infusion, Blood. *79:* 576-585, 1992.

10. Kaminski, M. S., Zasadny, K. R., Francis, I. R., Milik, A. W., Ross, C. W., Moon, S. D., Crawford, S. M., Burgess, J. M., Petry, N. A., Butchko, G. M., Glenn, S., D. , and Wahl, R. L. Radioimmunotherapy of B-cell lymphoma with [131I]anti-B1 (anti-CD20) antibody, New Engl. J. Med. *329:* 459-465, 1993.

11. Ghetie, V. and Vitetta, E. Immunotoxins in the therapy of cancer: from bench to clinic, Pharmacol. Therapeutics. *63:* 209-234, 1994.

12. Tyle, P. and Ram, B. P. Monoclonal antibodies, immmunoconjugates, and liposomes as targeted therapeutic systems, Targeted Diagn. Ther. *3:* 3-22, 1990.

13. Saltzman, W. M. Antibodies for treating and preventing diseases: the potential role of polymeric controlled release., Crit. Rev. Therap. Drug Carrier Systems. *10:* 111-142, 1993.

14. Larson, S. M., Macapinlac, H. A., Scott, A. M., and Divgi, C. R. Recent achievements in the development of radiolabelled monoclonal antibodies for diagnosis, therapy and biological characterization of human tumours, Acta Oncologica. *32:* 709-715, 1993.

15. Allen, T. M., Hansen, C. B., and Stuart, D. D. Targeted sterically stabilized liposomal drug delivery. *In,* D. Lasic and D. Papahadjopoulos (eds). Medical

Applications of Liposomes, pp. 297-323. Amsterdam: Elsevier Science Publishers, 1998.

16. Park, J. W., Hong, K., Kirpotin, D. B., Papahadjopoulos, D., and Benz, C. C. Immunoliposomes for cancer treatment, Adv. Pharmacol. *40:* 399-435, 1997.

17. Bangham, A. D., Standish, M. M., and Watkins, J. C. Diffusion of univalent ions across the lamellae of swollen phospholipids, J. Mol. Biol. *13:* 328-252, 1965.

18. Lasic, D. D. Liposomes: from physics to applications, Amsterdam: Elsevier Science Publishers B.V., 1993.

19. Papahadjopoulos, D., Jacobson, K., Nir, S., and Isac, T. Phase transition of phospholipid vesicles; fluorescence polarization and permeability measurements concerning the effect of temperature and cholesterol, Biochim. Biophys. Acta. *311:* 330-348, 1973.

20. McIntosh, T. J. The effect of cholesterol on the structure of phosphatidylcholine bilayers, Biochim. Biophys. Acta. *513:* 43-58, 1978.

21. Allen, T. M., Austin, G. A., Chonn, A., Lin, L., and Lee, K. C. C. Uptake of liposomes by cultured mouse bone marrow macrophages: influence of liposome composition and size, Biochim. Biophys. Acta. *1061:* 56-64, 1991.

22. Chonn, A., Semple, S. C., and Cullis, P. R. Association of blood proteins with large unilamellar liposomes in vivo. Relation to circulation lifetimes, J. Biol. Chem. *267:* 18759-18765, 1992.

23. Gregoriadis, G. Liposome technology: liposome preparation and related techniques, Vol. 1. Boca Raton, FL.: CRC Press, 1993.

24. Kirby, C. and Gregoriadis, G. Dehydration-rehydration vesicles (DRV): a new method for high yield drug entrapment in liposomes, Biotechnology. *2:* 979-984, 1984.

25. Mayer, L. D., Hope, M. J., Cullis, P. R., and Janoff, A. S. Solute distributions and trapping efficiencies observed in freeze-thawed multilamellar vesicles, Biochim Biophys Acta. *817:* 193-196, 1985.

26. Batzri, S. and Korn, E. D. Single bilayer liposomes prepared without sonication, Biochim Biophys Acta. *16:* 1015-1019, 1973.

27. Talsma, H., Ozer, A. Y., Van Bloois, L., and Crommelin, D. J. A. The size reduction of liposomes with high pressure homogenizer (microfluidizer). Characterization of prepared dispersion and comparison of conventional methods, Drug Dev. Ind. Pharm. *15:* 197-207, 1989.

28. Barenholz, Y., Amselem, S., and Lichtenberg, D. A new method for the preparation of phospholipid vesicles (liposomes) French Press, FEBS Lett. *99:* 210-213, 1979.

29. Huang, C. H. Studies on phosphatidylcholine vesicles: formation and physical characteristics, Biochemistry. *8:* 344-352, 1969.

30. Szoka, F. and Papahadjopoulos, D. Procedure for preparation of liposomes with large internal aqueous space and high capture by reverse-phase evaporation, Proc. Natl. Acad. Sci. USA. *75:* 4194-4198, 1978.

31. Phillipot, J. R. and Liautard, J. P. A very mild method allowing the encapsulation of very high amounts of macromolecules into very large (1000 nm) unilamellar

liposomes. *In:* G. Gregoriadis (ed.) Liposome technology: liposome preparation and related techniques, Vol. 1, pp. 81-98. Boca Raton, FL.: CRC Press, 1993.

32. Hope, M. J., Bally, M. B., Mayer, L. D., Janoff, A. S., and Cullis, P. R. Generation of multilamellar and unilamellar phospholipid vesicles, Chem. Phys. Lipids. *40:* 89-96, 1986.

33. Olson, F., Hunt, C. A., Szoka, F. C., Vail, W. J., and Papahadjopoulos, D. Preparation of liposomes of defined size distribution by extrusion through polycarbonate membranes, Biochim. Biophys. Acta. *557:* 9-23, 1979.

34. Mayer, L. D., Hope, M. J., and Cullis, P. R. Vesicles of variable sizes produced by a rapid extrusion procedure, Biochim. Biophys. Acta. *858:* 161-168, 1986.

35. Hope, M. J., Bally, M. B., Webb, G., and Cullis, P. R. Production of large unilamellar vesicles by a rapid extrusion procedure. Characterization of size distribution, trapped volume and ability to maintain a membrane potential., Biochim. Biophys. Acta. *812:* 55-65, 1985.

36. Gregoriadis, G. The carrier potential of liposomes in biology and medicine. Part 1, New Engl. J. Med. *295:* 704-710, 1976.

37. Defrise-Quertain, F., Chatelain, P., Delmelle, M., and Ruysschaert, J. Model studies for drug entrapment and liposome stability, Vol. 2, pp. 1-17. Boca Raton, FL: CRC Press, Inc., 1984.

38. Allen, T. M., Hansen, C. B., and Peliowski, A. Subcutaneous administration of sterically stabilized (Stealth) liposomes is an effective sustained release system for 1-ß-D-arabinofuranosylcytosine, Drug Delivery. *1:* 55-60, 1993.

39. Perez-Soler, R., Francis, K., Baker , S., Pilkiewicz , F., and Khokhar , A. R. Preparation and characterization of liposomes containing a lipophilic cisplatin derivative for clinical use, J. Microencap. *11:* 41-54, 1994.

40. Mayer, L. D., Bally, M. B., and Cullis, P. R. Uptake of adriamycin into large unilamellar vesicles in response to a pH gradient, Biochim. Biophys. Acta. *857:* 123-126, 1986.

41. Haran, G., Cohen, R., Bar, L. K., and Barenholz, Y. Transmembrane ammonium sulfate gradients in liposomes produce efficient and stable entrapment of amphipathic weak bases, Biochim. Biophys. Acta. *1151:* 201-315, 1993.

42. Bolotin, E. M., Cohen, R., Bar, L. K., Emanuel, S. N., Lasic, D. D., and Barenholz, Y. Ammonium sulphate gradients for efficient and stable remote loading of amphipathic weak bases into liposomes and ligandosomes, J. Liposome Res. *4:* 455-479, 1994.

43. Forssen, E., Coulter, D., and Proffitt, R. Selective in vivo localization of daunorubicin small unilamellar vesicles in solid tumours, Cancer Res. *52:* 3255-3261, 1992.

44. Boman, N. L., Masin, D., Mayer, L. D., Cullis, P. R., and Bally, M. B. Liposomal vincristine which exhibits increased drug retention and increased circulation longevity cures mice bearing P388 tumours, Cancer Res. *54:* 2830-2833, 1994.

45. Allen, T. M., Newman, M. S., Woodle, M. C., Mayhew, E., and Uster, P. S. Pharmacokinetics and anti-tumour activity of vincristine encapsulated in sterically stabilized liposomes, Int. J. Cancer. *62:* 199-204, 1995.

46. Duzgunes, N., Paiement , J., Freeman, K. B., Lopez, N. G., Wilschut , J., and Papahadjopoulos, D. Modulation of membrane fusion by ionotropic and thermotropic phase transitions, Biochemistry. *23:* 3486-94, 1984.

47. Gabizon, A., Shiota, R., and Papahadjopoulos, D. Pharmacokinetics and tissue distribution of doxorubicin encapsulated in stable liposomes with long circulation times, J. Natl. Cancer Inst. *81:* 1484-1488, 1989.

48. Gill, P. S., Espina, B. M., Muggia, F., Cabriales, S., Tulpule, A., Esplin, J. A., Liebman, H. A., Forssen, E., Ross, M. E., and Levine, A. M. Phase I/II clinical and pharmacokinetic evaluation of liposomal daunorubicin, J. Clin. Oncol. *13:* 996-1003, 1995.

49. Gabizon, A., Meshorer, A., and Barenholz, Y. Comparative long-term study of the toxicities of free and liposome-associated doxorubicin in mice after intravenous administration, J. Natl. Cancer Inst. *77:* 459-469, 1986.

50. Lopez-Berestein, G., Fainstein, V., Hopfer, R., Mehta, K., Sullivan, M. P., Keating, M., Rosenblum, M. G., Mehta, R., Luna, M., Hersh, E. M., Reuben, J., Juliano, R. L., and Bodey, G. P. Liposomal amphotericin B for the treatment of systemic fungal infections in patients with cancer: A preliminary study, J. Infect. Dis. *151:* 704-710, 1985.

51. Gabizon, A., Catane, R., Uziely, B., Kaufman, B., Safra, T., Cohen, R., Martin, F., Huang, A., and Barenholz, Y. Prolonged circulation time and enhanced accumulation in malignant exudates of doxorubicin encapsulated in polyethylene-glycol coated liposomes, Cancer Res. *54:* 987-992, 1994.

52. Bakker-Woudenberg, I. A. J. M., Lokerse, A. F., ten Kate, M. T., Woodle, M. C., and Storm, G. Liposomes with prolonged blood circulation and selective localization in Klebsiella pneumonia-infected lung tissue, J. Infect. Dis. *168:* 164-171, 1993.

53. Hansen, C. B., Kao, G. Y., Moase, E. H., Zalipsky, S., and Allen, T. M. Attachment of antibodies to sterically stabilized liposomes: evaluation, comparison and optimization of coupling procedures, Biochim. Biophys. Acta. *1239:* 133-144, 1995.

54. Northfelt, D. W., Dezube, B. J., Thommes, J. A., Levine, R., Von Roenn, J. H., Dosik, G. M., Rios, A., Krown, S. E., DuMond, C., and Mamelok, R. D. Efficacy of pegylated-liposomal doxorubicin in the treatment of AIDS-related Kaposi's sarcoma after failure of standard chemotherapy, J. Clin. Oncol. *15:* 653-659, 1997.

55. Cowens, J. W., Creaven, P. J., Greco, W. R., Brenner, D. E., Tung, Y., Osto, M., Pilkiewicz, F., Ginsberg, R., and Petrelli, N. Initial clinical (phase I) trial of TLC D-99 (doxorubicin encapsulated in liposomes), Cancer Res. *53:* 2796-2802, 1993.

56. Mayer, L. D., Gelmon, K., Cullis, P. R., Boman, N., Webb, M. S., Embree, L., Tolcher, T., and Bally, M. B. Preclinical and clinical studies with liposomal vincristine. *In:* S. Hirota (ed.) Progress in Drug Delivery, Vol. 4, pp. 151-161. Tokyo: Biomedical Research Foundation, 1995.

57. Fidler, I. J. and Kleinerman, E. S. Clinical application of phospholipid liposomes containing macrophage activators for therapy of cancer metastasis, Adv. Drug Del. Rev. *13:* 325-340, 1994.

58. Tollemar, J., Hockersted, K., Ericzon, B. C., Jalanko, H., and Ringden, O. Liposomal amphotericin B prevents invasive fungal infections in liver transplant recipients: a randomized, placebo controlled study, Transplantation. *59:* 45-50, 1995.

59. Sundar, S. and Murray, H. W. Cure of antimony-unresponsive Indian visceral leishmaniasis with amphotericin B lipid complex, J. Infect. Dis. *173:* 762-765, 1996.

60. Russo, R., Nigro, L. C., Minniti, S., Montineri, A., Gradoni, L., Caldeira, L., and Davidson, R. N. Visceral leishmaniasis in HIV infected patients: treatment with high dose liposomal amphotericin B (AmBisome), J. Infect. *32:* 133-137, 1996.

61. Heinemann, V., Kahry, B., Debus, A., Wachholz, K., and Jehn, U. Pharmacokinetics of liposomal amphotericin B (AmBisome) versus other lipid based formulations, Bone Marrow Transplant. *14:* S8-S9, 1994.

62. Alving, C. R. Liposomes as carriers of antigens and adjuvants, J. Immunol. methods. *140:* 1-13, 1991.

63. Felgner, J. H., Kumar, R., Sridhar, C. N., Wheeler, C. J., Tsai, Y. J., Border, R., Ramsey, P., Martin, M., and Felgner, P. L. Enhanced gene delivery and mechanism studies with a novel series of cationic lipid formulations, J. Biol. Chem. *269:* 2550-2561, 1994.

64. Presant, C. A., Proffitt, R. T., Turner, A. F., Willlians, L. E., Winsor, D., Werner, J. L., Kennedy, P., Wiseman, C., Gala, K., McKenna, R. J., Smith, J. D., Bouzalou, S. A., Callahan, R. A., Baldeschwieler, J., and Crossley, R. J.

Successful imaging of human cancer with Indium-111- labelled phospholipid vesicles, Cancer. *62:* 905-911, 1988.

65. Mezei, M. Liposomes in the topical application of drugs. A review. *In:* G. Gregoriadis (ed.) Liposomes as drug carriers. pp. 663-678, N.Y.: John Wiley and Sons Ltd., 1988.

66. Meisner, D. and Mezei, M. Liposome ocular delivery systems, Adv. Drug Del. Rev. *16:* 75-93, 1995.

67. McCalden, T. A. and Levy, M. Retention of topical liposomal formulations on the cornea, Experimentia. *46:* 713-715, 1990.

68. Mezei, M. Liposomes and the skin. *In:* G. Gregoriadis and A.T. Florence (eds) Liposomes in Drug Delivery, pp. 125-135. Chur, SW: Harwood Academic, 1993.

69. Niven, R. W., Speer, M., and Schreir, H. Nebulization of liposomes: II The effect of size and modelling on solute release profile, Pharm. Res. *8:* 217-221, 1991.

70. Handjani-Vila, R. M., Ribier, A., and Vanlerberghe, G. Liposomes in cosmetic industry. *In:* G. Gregoriadis (ed.) Liposomal technology, Vol. 2. pp. 201-214. Boca Raton, FL.: CRC Press, 1993.

71. Allen, T. M. and Hansen, C. B. Pharmacokinetics of Stealth versus conventional liposomes: effect of dose, Biochim. Biophys. Acta. *1068:* 133-141, 1991.

72. Scherphof, G., Roerdink, F., Waite, M., and Parks, J. Disintegration of phosphatidylcholine liposomes in plasma as a result of interaction with high-density lipoproteins, Biochim. Biophys. Acta. *542:* 296-307, 1978.

73. Devine, D. V., Wong, K., Serrano, K., Chonn, A., and Cullis, P. R. Liposome-

complement interactions in rat serum: implications for liposome survival studies, Biochim. Biophys. Acta. *1191:* 43-51, 1994.

74. Wassef, N. M., Matyas, G. R., and Alving, C. R. Complement-dependent phagocytosis of liposomes by macrophages: suppressive effects of "Stealth" lipids., Biochem. Biophys. Res. Commun. *176:* 866-874, 1991.

75. Chonn, A., Semple, S. C., and Cullis, P. R. Separation of large unilamellar liposomes from blood components by a spin column procedure: towards identifying plasma proteins which mediate liposome clearance in vivo, Biochim. Biophys. Acta. *1070:* 215-222, 1991.

76. Moghimi, S. M. and Patel, H. M. Serum factors that regulate phagocytosis of liposomes by Kupffer cells, Biochem. Soc. Trans. *21:* 128S, 1993.

77. Allen, T. M. Interactions of drug carriers with the mononuclear phagocyte system. *In:* G. Gregoriadis (ed.) Liposomes as Drug Carriers, pp. 37-50. New York: John Wiley & Sons, 1988.

78. Scherphof, G. L., Damen, J., and Wilschut, J. Interactions of liposomes with plasma proteins, Vol. III, p. 205-224. Boca Raton: CRC Press, 1984.

79. Devine, D. V. and Marjan, J. M. The role of immunoproteins in the survival of liposomes in the circulation, Crit. Rev. Ther. Drug. Carrier Syst. *14:* 105-131, 1997.

80. Jain, R. K. Transport of molecules across tumour vasculature, Cancer Metastasis Rev. 559-593, 1987.

81. Wu, N. Z., Da, D., Rudoll, T. L., Needham, D., Whorton, A. R., and Dewhirst, M.

W. Increased microvascular permeability contributes to preferential accumulation of stealth liposomes in tumour tissue, Cancer Res. *53:* 3765-3770, 1993.

82. Zu, N. Z., Da, D., Rudoll, T. L., Needham, D., Whorton, A. R., and Dewhirst, M. W. Increased microvascular permeability contributes to preferential accumulation of Stealth liposomes in tumour tissue, Cancer Res. *53:* 3765-3770, 1993.

83. Unezaki, S., Maruyama, K., Hosoda, J.-I., Nagae, I., Koyanayi, Y., Nakata, M., Ishida, O., Iwatsuru, M., and Tsuchiya, S. Direct measurement of the extravasation of polyethyleneglycol-coated liposomes into solid tumour tissue by in vivo fluorescence microscopy, Int. J. Pharmaceut. *144:* 11-17, 1996.

84. Rosenecker, J., Zhang, W., Hong, K., Lausier, J., Geppetti, P., Yoshihara, S., Papahadjopoulos, D., and Nadel, J. A. Increased liposome extravasation in selected tissues: effect of substance P, Proc. Natl. Acad. Sci. U S A. *93:* 7236-7241, 1996.

85. Huang, S. K., Mayhew, E., Gilani, S., Lasic, D. D., Martin, F. J., and Papahadjopoulos, D. Pharmacokinetics and therapeutics of sterically stabilized liposomes in mice bearing C-26 colon carcinoma, Cancer Res. *52:* 6774-681, 1992.

86. Papahadjopoulos, D., Allen, T. M., Gabizon, A., Mayhew, E., Matthay, K., Huang, S. K., Lee, K. D., Woodle, M. C., Lasic, D. D., Redemann, C., and Martin, F. J. Sterically stabilized liposomes: improvements in pharmacokinetics and antitumour therapeutic efficacy, Proc. Natl. Acad. Sci. USA. *88:* 11460-11464, 1991.

87. Vaage, J., Donovan, D., Loftus, T., Uster, P., and Working, P. Prophylaxis and therapy of mouse mammary carcinomas with doxorubicin and vincristine encapsulated in sterically stabilised liposomes, Eur. J. Cancer. *31(A):* 367-372, 1995.

88. Vaage, J. and Barbera, E. Tissue uptake and therapeutic effects of Stealth doxorubicin. *In:* D. Lasic and F. Martin (eds) Stealth Liposomes, pp.149-172, Boca Raton: CRC Press, Inc., 1995.

89. Vaage, J., Donovan, D., Mayhew , E., Abra, R., and Huang, A. Therapy of human ovarian carcinoma xenografts using doxorubicin encapsulated in sterically stabilized liposomes, Cancer. *72:* 3671-3675, 1993.

90. Pagano, R. E. and Weinstein, J. N. Interactions of liposomes with mammalian cells, Ann. Rev. Biophys. Bioeng. *7:* 435-468, 1978.

91. Forssen, E. and Willis, M. Ligand-targeted liposomes, Adv. Drug Del. Rev. *29:* 249-271, 1998.

92. Van Renswonde, A. J. B. M. and Hoekstra, D. Cell-induced leakage of liposomal contents, Biochemistry. *20:* 540-548, 1981.

93. Abra, R. M., Bosworth, M. E., and Hunt, C. A. Liposome disposition in vivo: effects of pre-dosing with liposomes, Res. Commun. Chem. Path. Pharmacol. *29:* 349-360, 1980.

94. Liu, D. Biological factors involved in the blood clearance of liposomes by liver, Adv. Drug Del. Rev. *24:* 201-213, 1997.

95. Mauk, M. R. and Gamble, R. C. Stability of lipid vesicles in tissues of the mouse:

A gamma-ray perturbed angular correlation study, Proc. Natl. Acad. Sci. USA. *76:* 765-769, 1979.

96. Abra, R. M. and Hunt, C. A. Liposome disposition in vivo. III. Dose and vesicle-size effects, Biochim. Biophys. Acta. *666:* 493-503, 1981.

97. Hwang, K. J. Liposome pharmacokinetics, *In*: M.J. Ostro (ed.), Liposomes: from biophysics to therapeutics. pp. 109-156. New York, NY: Marcel Dekker, 1987.

98. Semple, S. C., Chonn, A., and Cullis, P. R. Influence of cholesterol on the association of plasma proteins with liposomes, Biochemistry. *35:* 2521-2525, 1996.

99. Senior, J. H. Fate and behaviour of liposomes in vivo: a review of controlling factors, Crit. Rev. Ther. Drug Carrier Sys. *3:* 123-193, 1987.

100. Alving, C. R., Steck, E. A., Chapman, W. L. J., Waits, V. B., Hendricks, L. D., Swartz, G. M. J., and Hanson, W. L. Therapy of leishmaniasis: superior efficacies of liposome-encapsulated drugs, Proc. Natl. Acad. Sci. USA. *75:* 2959-2963, 1978.

101. Fidler, I. J. Systemic activation of macrophages by liposomes containing muramyltripeptide phosphatidylethanolamine for therapy of cancer metastases, J. Liposome Res. *1:* 461-468, 1990.

102. Forssen, E. A. The design and development of DaunoXome^{R} for solid tumour targeting in vivo, Adv. Drug Del. Rev. *24:* 133-150, 1997.

103. Illum, L., Hunneyball, I. M., and Davis, S. S. The effect of hydrophilic coatings on the uptake of colloidal particles by the liver and by peritoneal macrophages, Intl. J.

Pharmacol. *29:* 53-65, 1986.

104. Bally, M. B., Nayar , R., Masin, D., Hope, M. J., Cullis, P. R., and Mayer, L. D. Liposomes with entrapped doxorubicin exhibit extended blood residence times, Biochim. Biophys. Acta. *1023:* 133-139, 1990.

105. Allen, T. M. Toxicity of drug carriers to the mononuclear phagocyte system, Adv. Drug Del. Rev. *2:* 55-67, 1988.

106. Poste, G. Liposome targeting in vivo: problems and opportunities, Biol. Cell. *47:* 19-38, 1983.

107. Allen, T. M. The use of glycolipids and hydrophilic polymers in avoiding rapid uptake of liposomes by the mononuclear phagocyte system, Adv. Drug Del. Rev. *13:* 285-309, 1994.

108. Juliano, R. L. and Stamp, D. Effects of particle size and charge on the clearance of liposomes and liposome-encapsulated drugs, Biochim. Biophys. Acta. *1113:* 651-658, 1975.

109. Allen, T. M. and Everest, J. M. Effect of liposome size and drug release properties on pharmacokinetics of encapsulated drug in rats, J. Pharmacol. Exp. Ther. *226:* 539-544, 1983.

110. Allen, T. M. A study of phospholipid interactions between high-density lipoproteins and small unilamellar vesicles, Biochim. Biophys. Acta. *640:* 385-397, 1981.

111. Allen, T. M. and Cleland, L. G. Serum-induced leakage of liposome contents, Biochim. Biophys. Acta. *597:* 418-426, 1980.

112. Moghimi, S. M. and Patel, H. M. Tissue specific opsonins for phagocytic cells and their different affinity for cholesterol-rich liposomes, FEBS Lett. *233:* 143-147, 1988.

113. Allen, T. M. and Chonn, A. Large unilamellar liposomes with low uptake into the reticuloendothelial system, FEBS Lett. *223:* 42-46, 1987.

114. Gabizon, A. and Papahadjopoulos, D. Liposome formulations with prolonged circulation time in blood and enhanced uptake by tumours, Proc. Natl. Acad. Sci. USA. *85:* 6949, 1988.

115. Park, Y. S., Maruyama, K., and Huang, L. Some negatively charged phospholipid derivatives prolong the liposome circulation in vivo, Biochim. Biophys. Acta. *1108:* 257-260, 1992.

116. Schroit, A. J., Tanaka, Y., Madsen, H., and Fidler, I. J. The recognition of red blood cells by macrophages: role of phosphatidylserine and possible implications of membrane phospholipid asymmetry, Bio. Cell. *51:* 227-238, 1984.

117. Gabizon, A. and Papahadjopoulos, D. The role of surface charge and hydrophilic groups on liposome clearance in vivo, Biochim. Biophys. Acta. *1103:* 94-100, 1992.

118. Clark, M. R. and Shohet, S. B. Red cell senescence, Clin. Haematol. *14:* 223-257, 1985.

119. Allen, T. M., Hansen , C., and Rutledge , J. Liposomes with prolonged circulation times: factors affecting uptake by reticuloendothelial and other tissues, Biochim. Biophys. Acta. *981:* 27-35, 1989.

120. Klibanov, A. L., Maruyama, K., Torchilin, V. P., and Huang, L. Amphipathic polyethyleneglycols effectively prolong the circulation time of liposomes, FEBS Lett. *268:* 235-237, 1990.

121. Blume, G. and Cevc , G. Molecular mechanism of the lipid vesicle longevity in vivo, Biochim. Biophys. Acta. *1146:* 157-168, 1993.

122. Woodle, M. C., Newman, M., Collins, L., Redemann, C., and Martin, F. Improved long circulating (Stealth^{R}) liposomes using synthetic lipids, Proceed. Intern. Symp. Control. Rel. Bioact. Mater. *17:* 77, 1990.

123. Allen, T. M., Hansen, C. B., Martin, F., Redemann, C., and Yau-Young, A. Liposomes containing synthetic lipid derivatives of poly(ethylene glycol) show prolonged circulation half-lives *in vivo*, Biochim. Biophys. Acta. *1066:* 29-36, 1991.

124. Papahadjopoulos, D., Allen, T. M., Gabizon, A., Mayhew, E., Matthay, K., Huang, S. K., Lee, K. D., Woodle, M. C., Lasic, D. D., Redemann, C., and Martin, F. J. Sterically stabilized liposomes: pronounced improvements in blood clearance, tissue disposition, and therapeutic index of encapsulated drugs against implanted tumours, Proc. Natl. Acad. Sci. USA. *88:* 11460-11464, 1991.

125. Maruyama, K., Yuda, T., Okamoto, A., Ishikura, C., Kojima, S., and Iwatsura, M. Effect of molecular weight in amphipathic polyethyleneglycol on prolonging the circulation time of large unilamellar liposomes, Chem. Pharm. Bull. *39:* 1620-1622, 1991.

126. Abuchowski, A., Van Es, T., Palczuk, N. C., and Davis, F. F. Alterations on

immunological properties of bovine serum albumin by covalent attachment of polyethylene glycol, J. Biol. Chem. *252:* 3578-3581, 1977.

127. Davis, S. S., Hunneyball, I. M., Illum, L., Ratcliffe, J. H., Smith, A., and Wilson, C. G. Recent advances in the use of microspheres for targeted therapy, Exper. Clin. Res. *11:* 633-640, 1985.

128. Pain, D., Das, P. K., Ghosh, P. C., and Bachhawat, B. K. Increased circulatory half-life of liposomes after conjugation with dextran, J. Biosci. *6:* 811-816, 1984.

129. Sunamoto, J. Application of polysaccaride-coated liposomes in chemotherapy and immunotherapy. *In:* Y. Yagi (ed.), Medical Applications of Liposomes, pp. 121-131. Tokyo: Japan Scientific Society Press, 1986.

130. Torchilin, V. P., Omelyanenko, V. G., Papisov, M. I., Bogdanov, A. A., Trubetskoy, V. S., Herron, J. N., and Gentry, C. A. Poly(ethylene glycol) on the liposome surface: on the mechanism of polymer coated liposome longevity, Biochim. Biophys. Acta. *1195:* 11-20, 1994.

131. Needham, D., Kristova, K., McIntosh, T. J., Dewhirst, M., Wu, N., and Lasic, D. D. Polymer-grafted liposomes, Physical basis for the "Stealth" property, J. Liposome Res. *2:* 411-430, 1992.

132. Lasic, D. D., Woodle, M. C., and Papahadjopoulos, D. On the molecular mechanism of steric stabilization of liposomes in biological fluids, J. Liposome Res. *2:* 335-353, 1992.

133. Torchilin, V. P., Shtilman, M. I., Trubetskoy, V. S., Whitman, K., and Milstein, A. M. Amphiphilic vinyl polymers effectively prolong liposome circulation time *in*

vivo, Biochim. Biophys. Acta. *1195:* 181-184, 1994.

134. Zalipsky, S., Hansen, C. B., Oaks, J. M., and Allen, T. M. Evaluation of blood clearance and biodistribution of poly(2-oxazoline)-grafted liposomes, J. Pharm. Sci. *85:* 133-137, 1996.

135. Maruyama, K., Okuizumi, S., Ishida, O., Yamauchi, H., Kikuchi, H., and Iwatsuru, M. Phosphatidyl polyglycerols prolong liposome circulation in vivo, Int. J. Pharmaceutics. *111:* 103-107, 1994.

136. Myers, C. E. and Chabner, B. A. Anthracyclines. *In:* B. A. Chabner and J. M. Collins (eds.), Cancer chemotherapy: principles and practice, pp. 356-380. Philadelphia: Lippencott, 1990.

137. Young, R. C., Ozols, R. F., and Myers, C. E. The anthracycline antineoplastic drugs, New Engl. J. Med. *305:* 139-142, 1981.

138. Ross, W. A., Glaubiger, D. L., and Kohn, K. W. Protein-associated DNA breaks in cells treated with adriamycin and ellipticine, Biochim. Biophys. Acta. *519:* 23-30, 1978.

139. Allen, T. M. and Stuart, D. Liposome pharmacokinetics: classical, sterically stabilized, cationic liposomes and immunoliposomes. *In:*.A. Janoff (ed.) Liposomes: Rational Design. New York: Marcel Dekker, Inc., 1998 (in press).

140. Gabizon, A., Catane, R., Uziely, B., Kaufman, B., Safra, T., Barenholz, Y., and Huang, A. A pilot study of doxorubicin encapsulated in long-circulating (Stealth^{R}) liposomes (S-DOX) in cancer patients, Proc. Am. Soc. Clin. Oncol. *11:* 124, 1992.

141. Working, P. K., Newman, M. S., Huang, S. K., Mayhew, E., Vaage, J., and Lasic,

D. D. Pharmacokinetics, biodistribution and therapeutic efficacy of doxorubicin encapsulated in stealth(TM) liposomes (Doxil), J. Liposome Res. *4:* 667-687, 1994.

142. Northfelt, D. W., Martin, F. J., Working, P., Volberding, P. A., Russell, J., Newman, M., Amantea, M. A., and Kaplan, L. D. Doxorubicin encapsulated in liposomes containing surface-bound polyethylene glycol: pharmacokinetics, tumour localization, and safety in patients with AIDS-related Kaposi's sarcoma, J. Clin. Pharmacol. *36:* 55-63, 1996.

143. Urdal, D. L. and Hakomori, S. Tumour-associated ganglio-N-triosylceramide: target for antibody-dependent, avidin-mediated drug killing of tumour cells, J. Biol. Chem. *255:* 10509-10516, 1980.

144. Loughrey, H., Bally, M. B., and Cullis, P. R. A non-covalent method of attaching antibodies to liposomes, Biochim. Biophys. Acta. *901:* 157-160, 1987.

145. Abeywardena, M. Y., Allen , T. M., and Charnock , J. S. Lipid-protein interactions of reconstituted membrane-associated adenosinetriphosphatases. Use of a gel-filtration procedure to examine phospholipid-activity relationships, Biochim. Biophys. Acta. *729:* 62-74, 1983.

146. Ahmad, I., Longenecker, M., Samuel, J., and Allen, T. M. Antibody-targeted delivery of doxorubicin entrapped in sterically stabilized liposomes can eradicate lung cancer in mice, Cancer Res. *53:* 1484-1488, 1993.

147. Ahmad, I. and Allen, T. M. Antibody-mediated specific binding and cytotoxicity of liposome-entrapped doxorubicin to lung cancer cells *in vitro*, Cancer Res. *52:*

4817-4820, 1992.

148. Loughrey, H. C., Choi, L. S., Cullis, P. R., and Bally, M. B. Optimized procedures for the coupling of proteins to liposomes, J. Immunol. Methods. *132:* 25-35, 1990.

149. Loughrey, H. C., Choi, L. S., Wong, K. F., Cullis, P. R., and Bally, M. B. Preparation of streptavidin-liposomes for use in ligand specific targeting applications. *In:* G. Gregoriadis (ed.) Liposome Technology 2nd ed., Vol. III, pp. 163-178. Boca Raton: CRC Press, 1993.

150. Corley, P. and Loughrey, H. C. Bonding of biotinylated-liposomes to streptavidin is influenced by liposome composition, Biochim. Biophys. Acta. *1195:* 149-156, 1994.

151. Longman, S. A., Cullis, P. R., Choi, L., de Jong, G., and Bally, M. B. A two-step targeting approach for delivery of doxorubicin-loaded liposomes to tumour cells in vivo, Cancer Chemother. Pharmacol. *36:* 91-101, 1995.

152. Trubetskoy, V. S., Berdichevsky, V. R., Efremov, E. E., and Torchilin, V. P. On the possibility of the unification of drug targeting systems. Studies with liposome transport to the mixtures of target antigens, Biochem. Pharmacol. *36:* 839-842, 1987.

153. Martin, F. J., Hubbell, W. l., and Papahadjopoulos, D. Immunospecific targeting of liposomes to cells: a novel and efficient method for covalent attachment of Fab' fragments via disulfide bonds, Biochemistry. *20:* 4229-4238, 1981.

154. Heath, T. D. Covalent attachment of proteins to liposomes, Methods Enzymol. *149:* 111-119, 1987.

155. Weiner, A. L. Chemistry and biology of immunotargeted liposomes. *In:* P. Tyle and B.P. Ram (eds) Targeted Therapeutic Systems, pp. 305-336. New York: Marcel Dekker, Inc., 1990.

156. Torchilin, V. P. and Klibanov, A. L. Coupling of ligands with liposome membranes, Drug Target Del. *2:* 227-238, 1993.

157. Leserman, L. D., Barbet, J., Kourilsky, F., and Weinstein, J. N. Targeting to cells of fluorescent liposomes covalently coupled with monoclonal antibody or protein A, Nature. *288:* 602-604, 1980.

158. Martin, F. J. and Papahadjopoulos, D. Irreversible coupling of immunoglobulin fragments to preformed vesicles. An improved method for liposome targeting, J. Biol. Chem. *257:* 286-288, 1982.

159. Maruyama, K., Kennel, S. J., and Huang, L. Lipid composition is important for highly efficient target binding and retention of immunoliposomes, Proc. Natl. Acad. Sci. USA. *87:* 5744-5748, 1990.

160. Maruyama, K., Mori, A., Bhadra, S., and Ravi Subbiah, M. T. Proteins and peptides bound to long-circulating liposomes, Biochim. Biophys. Acta. *1070:* 246-252, 1991.

161. Litzinger, D. and Huang, L. Biodistribution and immunotargetability of ganglioside-stabilized dioleoylphosphatidylethanolamine liposomes, Biochim. Biophys. Acta. *1104:* 179-187, 1992.

162. Torchilin, V. P., Klibanov, A. L., Huang, L., O'Donnell, S., Nossiff, N. D., and Khaw, B. A. Targeted accumulation of polyethylene glycol-coated

immunoliposomes in infarcted rabbit myocardium, FASEB J. *6:* 2716-2719, 1992.

163. Mori, A., Klibanov, A. L., Torchilin, V. P., and Huang, L. Influence of the steric barrier of amphipathic poly(ethyleneglycol) and ganglioside GM_1 on the circulation time of liposomes and on the target binding of immunoliposomes *in vivo*, FEBS Lett. *284:* 263-266, 1991.

164. Mori, A. and Huang, L. Immunoliposome targeting in a mouse model: optimization and therapeutic application. *In:* G. Gregoriadis (ed.) Liposome Technology, 2nd edition, Vol. 3, pp. 153-162. Boca Raton: CRC Press, 1992.

165. Park, J. W., Hong, K., Carter, P., Asgari, H., Guo, L. Y., Keller, G. A., Wirth, C., Shalaby, R., Kotts, C., Wood, W. I., Papahadjopoulos, D., and Benz, C. C. Development of anti-$p185^{HER2}$ immunoliposomes for cancer therapy, Proc. Natl. Acad. Sci. USA. *92:* 1327-1331, 1995.

166. Uster, P. S., Allen, T. M., Daniel, B. E., Mendez, C. J., Newman, M. S., and Zhu, G. Z. Insertion of poly(ethylene glycol) derivatized phospholipid into preformed liposomes results in prolonged in vivo circulation time, FEBS Lett. *386:* 243-246, 1996.

167. Blume, G., Cevc, G., Crommelin, M. D., Bakker-Woudenberg, L. A., Kluft, C., and Storm, G. Specific targeting with poly(ethylene glycol)-modified liposomes: coupling of homing devices to the ends of the polymeric chains combines effective target binding with long circulation times, Biochim. Biophys. Acta. *1149:* 180-184, 1993.

168. Zalipsky, S. Synthesis of end-group functionalised polyethylene glycol-lipid

conjugates for preparation of polymer-grafted liposomes, Bioconjugate Chem. *4:* 296-299, 1993.

169. Zalipsky, S., Hansen, C. B., Lopes de Menezes, D. E., and Allen, T. M. Long-circulating polyethylene glycol-grafted immunoliposomes, J. Control. Rel. *39:* 153-161, 1996.

170. Zalipsky, S., Puntambekar, B., Bolikas, P., Engbers, C. M., and Woodle, M. C. Peptide attachment to extremities of liposomal surface grafted PEG chains: Preparation of the long-circulating form of laminin pentapetide, YIGSR, Bioconj. Chem. *6:* 705-708, 1995.

171. Harding, J. A., Engbers, C. M., Newman, M. S., Goldstein, N. I., and Zalipsky, S. Immunogenicity and pharmacokinetic attributes of poly(ethyleneglycol)-grafted immunoliposomes, Biochim. Biophys. Acta. *1327:* 181-192, 1997.

172. Allen, T. M., Agrawal, A. K., Ahmad, I., Hansen, C. B., and Zalipsky, S. Antibody-mediated targeting of long-circulating (Stealth®) liposomes, J. Liposome Res. *4:* 1-25, 1994.

173. Regimbald, L. H., Pilarski, L. M., Longenecker, B. M., Reddish, M. A., Zimmermann, G., and Hugh, J. C. The breast mucin MUC1 as a novel adhesion ligand for endothelial intercellular adhesion molecule 1 in breast cancer, Cancer Res. *56:* 4244-4249, 1996.

174. Weinstein, J. N. and van Osdol, W. Early intervention in cancer using monoclonal antibodies and other biological ligands: micropharmacology and the "binding site barrier", Cancer Res. *52:* 2747-2751, 1992.

175. Allen, T. M. and Moase, E. H. Therapeutic opportunities for targeted liposomal drug delivery, Adv. Drug Del. Rev. *21:* 117-133, 1996.

176. Berkower, I. The promise and pitfalls of monoclonal antibody therapeutics, Curr. Opin. Biotechnol. *7:* 622-628, 1996.

177. Phillips, N. C. and Dahman, J. Immunogenicity of immunoliposomes: reactivity against species-specific IgG and liposomal phospholipids, Immunol. Lett. *45:* 149-152, 1995.

178. Phillips, N. C., Gagne, L., Tsoukas, C., and Dahman, J. Immunoliposome targeting to murine $CD4^+$ Leucocytes is dependent on immune status, J. immunol. *152:* 3168-3174, 1994.

179. Courtenay-Luck, N. S., Epenetos, A. A., Moore, R., Larche, M., Pecatasides, D., and Ritter, M. A. Development of primary and secondary immune responses to mouse monoclonal antibodies used in the diagnosis and therapy of malignant neoplasms, Cancer Res. *46:* 6489-6493, 1986.

180. Schroff, R. W., Foon, K. A., Beatty, S. M., Oldham, R. K., and Morgan, A. C. Human anti-mouse immunoglobulin responses in patients receiving monoclonal antibody therapy, Cancer Res. *48:* 879-885, 1985.

181. Shek, P. N. and Heath, T. D. Immune response mediated by liposome-associated protein antigens. III. Immunogenicity of bovine serum albumin covalently coupled to vesicle surface, Immunology. *50:* 101-106, 1983.

182. Brewer, J. M., Richmond, J., and Alexander, J. The demonstration of an essential role for macrophages in the in vivo generation of IgG2a antibodies, Clin. Exp.

Immunol. *97:* 164-171, 1994.

183. de Kruif, J., Storm, G., van Bloois, L., and Logtenberg, T. Biosynthetically lipid-modified human sc Fv fragments from phage display libraries as targeting molecules for immunoliposomes, FEBS Lett. *399:* 232-236, 1996.

184. Winter, G. and Harris, W. J. Humanized antibodies, Trends Pharmacol. Sci. *14:* 139-143, 1993.

185. Allen, T. M., Ahmad, I., Lopes de Menezes, D. E., and Moase, E. H. Immunoliposome-mediated targeting of anti-cancer drugs *in vivo*, Biochem. Soc. Trans. *23:* 1073-1079, 1995.

186. Truneh, A., Mishal, Z., Barbet, J., Machy, P., and Leserman, L. D. Endocytosis of liposomes bound to cell surface proteins measured by flow cytometry, J. Biochem. *214:* 189-194, 1983.

187. Matthay, K. K., Abai, A. M., Cobb, S., Hong, K., Papahadjopoulos, D., and Straubinger, R. M. Role of ligand in antibody-directed endocytosis of liposomes by human T-leukemia cells, Cancer Res. *49:* 4879-4886, 1989.

188. Petty, H. R. and McConnell, H. M. Cytochemical study of liposome and lipid vesicle phagocytosis, Biochim. Biophys. Acta. *735:* 77-85, 1983.

189. Collins, D., Maxfield, F., and Huang, L. Immunoliposomes with different acid sensitivities as probes for the cellular endocytotic pathway, Biochim.. Biophys.. Acta. *987:* 47-55, 1989.

190. Hege, K., Daleke, D. L., Waldman, T. A., and Matthay, K. K. Comparison of anti-Tac and anti-transferrin receptor-conjugated liposomes for specific drug delivery

to adult T-cell leukemia, Blood. *6:* 2043-2052, 1989.

191. Machy, P., Truneh, A., Gennaro, D., and Hoffstein, S. Endocytosis and de novo expression of major histocompatibility complex encoded class I molecules: kinetic and ultrastructure studies, European J. Cell Biol. *45:* 126-136, 1987.

192. Ohta, S., Igarashi, S., Honda, A., Sato, S., and Hanai, N. Cytotoxicity of adriamycin-containing immunoliposomes targeted with anti-ganglioside monoclonal antibodies, Anticancer Res. *13:* 331-336, 1993.

193. Huwyler, J., Wu, D., and Pardridge, W. M. Brain drug delivery of small molecules using immunoliposomes, Proc. Natl. Acad. Sci. USA. *93:* 14164-14169, 1996.

194. Maruyama, K., Takahashi, N., Tagawa, T., Nagaike, K., and Iwatsuru, M. Immunoliposomes bearing polyethyleneglycol-coupled Fab' fragment show prolonged circulation time and high extravasation into targeted solid tumours *in vivo*, FEBS Lett. *413:* 177-180, 1997.

195. Scherphof, G. L., Kamps, J. A. A. M., and Koning, G. A. In vivo targeting of surface-modified liposomes to metastatically growing colon carcinoma cells and sinusoidal endothelial cells in the rat liver, J. Liposome Res. *7:* 419-432, 1997.

196. Rosenberg, M. B., Breakefield, X. O., and Hawrot, E. Targeting of liposomes to cells bearing nerve growth factor receptors mediated by biotinylated nerve growth factor, J. Neurochem. *48:* 865-875, 1987.

197. Suzuki, H., Zelphati, O., Hildebrand, G., and Leserman, L. CD4 and CD7 molecules as targets for drug delivery from antibody bearing liposomes, Exp. Cell Res. *193:* 112-119, 1991.

198. Connor, J. and Huang, L. pH-sensitive immunoliposomes as an efficient and target-specific carrier for antitumour drugs, Cancer Res. *46:* 3431-3435, 1986.

199. Bloemen, P. G. M., Henricks, P. A. J., van Bloois, L., van den Tweel, M. C., Bloem, A. C., Nijkamp, F. P., Crommelin, D. J. A., and Storm, G. Adhesion molecules: a new target for immunoliposome-mediated drug delivery, FEBS Lett. *357:* 140-144, 1995.

200. De Kruif, J., Storm, G., Vanbloois, L., and Logtenberg, T. Biosynthetically lipid modified human scFv fragments from phage display libraries as targeting molecules for immunoliposomes, FEBS Lett. *399:* 232-236, 1996.

201. Mori, A., Kennel, S. I., Waalkes, M. V. B., Scherphof, G. L., and Huang, L. Characterization of organ-specific immunoliposomes for delivery of 3', 5'-O-dipalmitoyl-5-fluoro-2'-deoxyuridine in a mouse lung-metastasis model, Cancer Chemother. Pharmacol. *35:* 447-456, 1995.

202. Lee, R. J. and Low, P. S. Folate-mediated tumour cell targeting of liposome-entrapped doxorubicin *in vitro*, Biochim. Biophys. Acta. *1233:* 134-144, 1995.

203. Wang, S., Lee, R. J., Cauchon, G., Gorenstein, D. G., and Low, P. S. Delivery of antisense oligodeoxyribonucleotides against the human epidermal growth factor receptor into cultured KB cells with liposomes conjugated to folate via polyethylene glycol, Biochemistry. *92:* 3318-3322, 1995.

204. Suzuki, S., Uno, S., Fukuda, Y., Aoki, Y., Masuko, T., and Hashimoto, Y. Cytotoxicity of anti-c-erbB-2 immunoliposomes containing doxorubicin on human cancer cells, Br. J. Cancer. *72:* 663-668, 1995.

205. Emanuel, N., Kedar, E., Bolotin, E. M., Smorodinsky, N. I., and Barenholz, Y. Targeted delivery of doxorubicin via sterically stabilized immunoliposomes: pharmacokinetics and biodistribution in tumour-bearing mice, Pharm. Res. *13:* 861-868, 1996.

206. Kirpotin, D., Park, J. W., Hong, K., Zalipsky, S., Li, W.-L., Carter, P., Benz, C. C., and Papahadjopoulos, D. Sterically stabilized anti-HER2 immunoliposomes: design and targeting to human breast cancer cells *in vitro*, Biochemistry. *36:* 66-75, 1997.

207. Nassander, U. K., Steerenberg, P. A., De Jong, W. H., Van Overveld, W. O. M., Te Boekhorst, C. M. E., Poels, L. G., Jap, P. H. K., and Storm, G. Design of immunoliposomes directed against human ovarian carcinoma, Biochim. Biophys. Acta. *1235:* 126-139, 1995.

208. Lundberg, B., Hong, K., and Papahadjopoulos, D. Conjugation of apolipoprotein B with liposomes and targeting to cells in culture, Biochim. Biophys. Acta. *1149:* 305-312, 1993.

209. Vidal, M., Sainte-Marie, J., Philippot, J. R., and Bienvenue, A. LDL-mediated targeting of liposomes to leukemic lymphocytes in vitro, EMBO J. *4:* 2461-2467, 1985.

210. Spanjer, H. H., van Berkel, T. J., Scherphof, G. L., and Kempen, H. J. The effect of a water-soluble tris-galactoside terminated cholesterol derivative on the in vivo fate of small unilamellar vesicles in rats, Biochim. Biophys. Acta. *816:* 396-402, 1985.

211. Medda, S., Das, N., Bachhawat, B. K., Mahato, S. B., and Basu, M. K. Targeting of plant glycoside-bearing liposomes to specific cellular and subcellular sites, Biotechnol. Appl. Biochem. *12:* 537-543, 1990.

212. Murahashi, N., Sasaki, A., Higashi, K., Morikawa, A., and Yamada, H. Relationship between the anchor structure of the galactosyl ligand for liposome modification and accumulation in the liver, Biol. Pharm. Bull. *18:* 82-88, 1995.

213. Schreier, H., Moran, P., and Caras, I. W. Targeting of liposomes to cells expressing CD4 using glycosylphosphatidylinositol-anchored gp120. Influence of liposome composition on intracellular trafficking, J. Biol. Chem. *269:* 9090-9098, 1994.

214. Hara, T., Aramaki, Y., Takada, S., Koike, K., and Tsuchiya, S. Receptor mediated transfer of psv2cat DNA to mouse liver cells using asialofetuin labelled liposomes, Gene Ther. *2:* 784-788, 1995.

215. Ishii, Y., Aramaki, Y., Hara, T., Tsuchiya, S., and Fuwa, T. Preparation of EGF labelled liposomes and their uptake by hepatocytes, Biochem. Biophys. Res. Commun. *160:* 732-736, 1989.

216. Vingerhoeds, M. H., Storm, G., and Crommelin, D. J. Immunoliposomes *in vivo*, Immunomethods. *4:* 259-272, 1994.

217. Torchilin, V. P., Narula, J., Halpern, E., and Khaw, B. A. Poly(ethylene glycol)-coated anti-cardiac myosin immunoliposomes: factors influencing targeted accumulation in the infarcted myocardium, Biochim. Biophys. Acta. *1279:* 75-83, 1996.

218. Khaw, B.-A., Torchilin, V. P., Vural, I., and Narula, J. Plug and seal: prevention of hypoxic cardiocyte death by sealing membrane lesions with antimyosin-liposomes, Nature Med. *1:* 1195-1198, 1995.

219. Briscoe, P., Caniggia, I., Graves, A., Benson, B., Huang, L., Tanswell, A. K., and Freeman, B. A. Delivery of superoxide dismutase to pulmonary epithelium via pH-sensitive liposomes, Am. Physiol. Society. *268:* L374-L380, 1995.

220. Bankert, R. B., Yokota, S., Ghosh, S. k., Mayhew, E., and Jou, Y. H. Immunospecific targeting of cytosine arabinonucleoside-containing liposomes to the idiotype on the surface of a murine B-cell tumour in vitro and in vivo, Cancer Res. *49:* 301-308, 1989.

221. Lin, A. Y. and Tucker, M. A. Epidemiology of Hodgkin's disease and non-Hodgkin's lymphoma. *In:* G. P. Canellos, T. A. Lister, and J. L. Sklar (eds.), The Lymphomas. pp. 43-61 Philadelphia: W.B. Saunders Co., 1998.

222. Kincade, P. W. and Gimble, J. M. B lymphocytes. *In:* W. E. Paul (ed.) Fundamental immunology, 3 rd edition, pp. 43-74. N.Y.: Raven Press, Ltd., 1993.

223. Sprent, J. T lymphocytes and the thymus. *In:* W. E. Paul (ed.) Fundamental immunology, 3 rd edition, pp. 75-110. N.Y.: Raven Press, Ltd., 1993.

224. von Boehmer, H., Teh, H. S., and Kisielow, P. The thymus selects the useful, neglects the useless and destroys the harmful, Immunol. Today. *10:* 57-61, 1989.

225. Banchereau, J. and Rousset, F. Human B lymphocytes: phenotype, proliferation and differentiation, Adv. Immunol. *52:*125-262, 1992.

226. Paynes, J. R. Molecular biology and function of CD4 and CD8, Adv. Immunol. *44:*

265-311, 1988.

227. Hood, L., Kronenberg, M., and Hunkapiller, T. T-cell antigen receptors and immunoglobulin supergene family, Cell. *40:* 225-229, 1985.

228. Hodgkin, P. D. and Basten, A. B-cell activation, tolerance and antigen-presenting functions, Curr. Opinion Immunol. *7:*121-129, 1995.

229. Townsend, A. and Bodmer, M. Antigen recognition by class I-restricted T lymphocytes, Annu. Rev. Immunol. *7:* 601-624, 1989.

230. Rothbard, J. B. and Gefler, M. L. Interaction between immunogenic peptides and MHC proteins, Annu. Rev. Immunol. *1991:* 527-565, 1991.

231. Cooper, M. D. B lymphocytes. Normal development and function, New Engl. J. Med. *317:* 1452-1456, 1987.

232. Jacobsen, K., Tepper, J., and Osmond, D. G. Early B-lymphocyte precursor cells in mouse bone marrow: subosteal localization of B220 and cells during post-irradiation regeneration, Exp. Hematol. *18:* 304-310, 1990.

233. Chen, J. and Alt, F. W. Gene rearrangement and B cell development, Curr. Opinion Immunol. *5:* 194-200, 1993.

234. Cambier, J. C., Pleiman, C. M., and Clark, M. R. Signal transduction by the B-cell antigen receptor and its coreceptors, Annu. Rev. Immunol. *12:* 457-486, 1994.

235. Hokland, P., Ritz, J., Schlossman, S. F., and Nadler, L. M. Orderly expression of B-cell antigens during the in vitro differentiation of non-malignant human pre-B cells, J. Immunol. *135:*1746-1751, 1985.

236. Bradbury, L. E., Kansas, G. S., Levy, S., Evans, R. L., and Tedder, T. F. The

CD19/CD21 signal transducting complex of human B-lymphocytes includes the target of antiproliferative antibody-1 and leu-13 molecules, J. Immunol. *149:* 2841-2850, 1992.

237. Tedder, T. F., Zhou, L.-J., and Engel, P. The CD19/CD21signal transduction complex of B lymphocytes, Immunol. Today. *15:* 437-442, 1994.

238. Clark, E. A. CD22, a B-cell-specific receptor, mediates adhesion and signal transduction, J. Immunol. *150:* 4715-4718, 1993.

239. Kansas, G. S. and Tedder, T. F. Transmembrane signals generated through MHC class II, CD19, CD20, CD39, and CD40 antigens induce LFA-1-dependent and -independent adhesion in human B cells through a tyrosine kinase-dependent pathway, J. Immunol. *147:* 4094-4102, 1991.

240. Justement, L. B., Campbell, K. S., Chien, N. C., and Cambier, J. C. Regulation of B-cell antigen receptor signal transduction and phosphorylation by CD45, Science (Washington, DC). *252:* 1839-1842, 1991.

241. Fearon, D. T. The CD19-CR2-TAPA-1 complex, CD45 and signalling by the antigen receptor of B-lymphocytes, Curr. Opin. Immunol. *5:* 341-348, 1993.

242. Van Noesel, C. J. M., Lankester, A. C., van Schijndel, G. M. W., and Van Lier, R. A. W. The CR2/CD19 complex on human B-cells contains the src-family kinase lyn, Int. Immunol. *5:* 699-705, 1993.

243. Gaidano, G. and Dalla-Favera, R. Lymphomas. *In:* V. T. DeVita, S. Hellman, and S. A. Rosenberg (eds.), Cancer: principles and practice of oncology, Vol. 2, pp. 2131-2145. Philadelphia: Lippincott-Raven, 1997.

244. Shipp, M. A., Mauch, P. M., and Harris, N. L. Non-Hodgkin's lymphomas. *In:* V. T. DeVita, S. Hellman, and S. A. Rosenberg (eds.), Cancer: principles and practice of oncology, Vol. 2, pp. 2165-2220. Philadelphia: Lippincott-Raven, 1997.

245. Weinstein, H. J., Cassady, J. R., and Levey, R. Long-term results of the APO protocols (vincristine, doxorubicin and prednisone) for treatment of mediastinal lymphoblastic lymphoma, J. Clin. Oncol. *1:* 537-542, 1983.

246. Link, M. P., Donaldson, S. S., Berard, C. W., Shuster, J. J., and Murphy, S. B. Results of treatment of childhood localized non-Hodgkin lymphoma with combination chemotherapy with or without radiation, N. Engl. J. Med. *322:* 1169-1175, 1990.

247. Griepp, P. R. Advances in the diagnosis and management of myeloma, Sem. Hematol. *29:* 24-45, 1992.

248. Osserman, E. F., Giampaolo, M., and Butler, V. P. Multiple myeloma and related plasma cell dyscrasias, JAMA. *258:* 2930-2937, 1987.

249. Barlogie, B., Epstein, J., Selvanayagam, P., and Alexanian, R. Plasma cell myeloma: new biological insights and advances in therapy, Blood. *73:* 865-879, 1989.

250. Blattner, W. A. Epidemiology of multiple myeloma and related plasma cell disorders: An analytic review. *In:* M. Potter (ed.) Progress in Myeloma, pp. 1-65. Amsterdam: Elsevier Science Publishers, 1980.

251. Bergsagel, D. E. Epidemiology and incidence of plasma cell neoplasms. *In:* G. Gahrton and B. G. M. Durie (eds.), Multiple myeloma, pp. 12-21. N.Y.: Oxford

University Press, Inc., 1996.

252. Caligaris-Cappio, F. and Gregoretti, M. G. Basic concepts - the plasma cell in multiple myeloma. *In:* G. Gahrton and B. G. M. Durie (eds.), Multiple Myeloma pp. 22-35. N.Y.: Oxford University Press, 1996.

253. Epstein, J., Xiao, H., and He, X. Y. Markers of multiple hematopoietic-cell lineages in multiple myeloma, New Engl. J. Med. *322:* 664-669, 1990.

254. MacLennan, I. C. M. In which cells does neoplastic transformation occur in myelomatosis?, Curr. Topics in Microbiol. Immunol. *182:* 209-213, 1992.

255. Pilarski, L. M., Masellis-Smith, A., Szczepek, A., Mant, M., J., and Belch, A. R. Circulating clonotypic B cells in the biology of myeloma: speculations on the origins of multiple myeloma, Leukemia Lymphoma. *18:* 179-187, 1995.

256. MacKenzie, M. R. and Lewis, J. P. Cytogenetic evidence that the malignant event in multiple myeloma occurs in a precursor lymphocyte., Cancer Genet. Cytogenet. *17:* 13-20, 1985.

257. Pilarski, L. M. and Jensen, G. S. Monoclonal circulating B cells in multiple myeloma: a continuously differentiating, possible invasive, population as defined by expression of CD45 isoforms and adhesion molecules, Hematol. Oncol. Clin. North America. *6:* 297-322, 1992.

258. Pilarski, L. M. and Belch, A. R. Circulating monoclonal B cells expressing P-glycoprotein may be a reservoir of multi-drug resistant disease in multiple myeloma, Blood. *83:* 724-736, 1994.

259. Bergsagel, P. L., Smith, A. M., Szczepek, A., Mant, M. J., Belch, A., and Pilarski,

L. M. In multiple myeloma, clonotypic B lymphocytes are detectable among CD19+ peripheral blood cells expressing CD38, CD56, and monotypic lg light chain, Blood. *85:* 436-447, 1995.

260. Jensen, G. S., Belch, A. R., Mant, M. J., Ruether, B. A., Yacyshyn, B. R., and Pilarski, L. M. Expression of multiple beta-1 integrins on circulating monoclonal B cells in patients with multiple myeloma., Am. J. Hematol. *43:* 29-39, 1992.

261. Jensen, G. S., Mant, M. J., Belch, A. R., Berensen, J. R., Ruether, B. A., and Pilarski, L. M. Selective expression of CD45 isoforms defines CALLA+ monoclonal B lineage cells in peripheral blood from myeloma patients as late stage B cells, Blood. *78:* 711-719, 1991.

262. Masellis-Smith, A., Belch, A. R., Mant, M. J., and Pilarski, L. M. Adhesion of multiple myeloma peripheral blood B cells to bone marrow fibroblasts: a requirement for CD44 and α4β7, Cancer Res. *57:*930-936, 1997.

263. Szczepek, A. K., Bergsagel, P. L., Axelsson, L., Brown, C. B., Belch, A. R., and Pilarski, L. M. CD34+ cells in the blood of patients with multiple myeloma express CD19 and IgH mRNA and have patient-specific IgH VDJ gene rearrangements, Blood. *89:* 1824-1833, 1997.

264. Samson, D. Principles of chemotherapy and radiotherapy. *In:* G. Gahrton and B. G. M. Durie (eds.), Multiple myeloma. N.Y.: Oxford University Press, 1996.

265. Bishoff, J. R. and Samuel, C. E. Mechanism of interferon action, J. Biol. Chem. *260:* 8237-8239, 1985.

266. Westin, J., Rodjer, S., Turesson, I., Cortelezzi, A., Hjorth, M., and Zador, G.

Interferon alfa-2b versus no maintenance therapy during the plateau phase in multiple myeloma: a randomized study., Br. J. Haematol. *89:* 561-568, 1995.

267. Barlogie, B. and Gahrton, G. Bone marrow transplantation in multiple myeloma, Bone Marrow Transplant. *7:* 71-79, 1991.

268. Gottesman, M. M. and Pastan, I. Biochemistry of multidrug resistance mediated by the multidrug transporter, Ann. Rev. Biochem. *62:* 385-427, 1993.

269. Bradley, G. and Ling, V. P-glycoprotein, multidrug resistance and tumour progression, Cancer and Metastasis Rev. *13:* 223-233, 1994.

270. Pilarski, L. M., Cass, C. E., Tsuro, T., and Belch, A. R. Multidrug resistance of a continuously differentiating monoclonal B lineage in the blood and bone marrow of patients with multiple myeloma, Current Topics In Microbiol. Immunol. *182:* 177-185, 1992.

271. Pilarski, L. M. and Belch, A. R. Intrinsic expression of the multidrug transporter, P-glycoprotein 170, in multiple myeloma: implications for treatment, Leukemia Lymphoma. *17:* 367-374, 1995.

272. Grogan, T. M., Spier, C. M., Salmon, S. E., Matzner, M., Rybski, J., Weinstein, R. S., Scheper, R. J., and Dalton, W. S. P-glycoprotein expression in human plasma cell myeloma: correlation with prior chemotherapy, Blood. *81:* 490-495, 1993.

273. Sonneveld, P., Schoester, M., and De Leeuw, K. Clinical modulation of multidrug resistance in multiple myeloma: effect of cyclosporine on resistant tumour cells, J. Clin. Oncol. *72:* 7584-7597, 1994.

274. Dalton, W. S., Grogan, T. M., Meltzer, P. S., Scheper, R. J., Durie, B. G., Taylor,

C. W., Miller, T. P., and Salmon, S. E. Drug-resistance in multiple myeloma and non-Hodgkin's lymphoma: detection of P-glycoprotein and potential circumvention by addition of verapamil to chemotherapy, J. Clin. Oncol. *7:* 415-424, 1989.

275. Dalton, W. S., Crowley, J. J., Salmon, S. S., Grogan, T. M., Laufman, L. R., Weiss, G. R., and Bonnet, J. D. A phase III randomized study of oral verapamil as a chemosensitizer to reverse drug resistance in patients with refractory myeloma. A Southwest Oncology Group study, Cancer. *75:* 815-820, 1995.

276. Foon, K. A. and Todd, R. F. III. Immunologic classification of leukemia and lymphoma, Blood. *68:* 1-31, 1986.

277. Magrath, I. T. and Ziegler, J. L. Bone marrow involvement in Burkitt's lymphoma and its relationship to acute B-cell leukemia, Leukemia Res. *4:* 33-59, 1979.

278. Hakomori, S. Aberrant glycosylation on cancer cell membranes as focussed on glycolipids: overview and perspectives., Cancer Res. *45:* 2405-2414, 1985.

279. Waldmann, T. A. Immune receptors: targets for therapy of leukemia/lymphoma, autoimmune diseases and for the prevention of allograft rejection, Ann. Rev. Immunol. *10:* 675-704, 1992.

280. Allen, T. M., Mehra, T., Hansen, C. B., and Chin, Y. C. Stealth liposomes: an improved sustained release system for 1-β-D-arabinofuranosylcytosine, Cancer Res. *52:* 2431-2439, 1992.

281. Allen, T. M., Hansen, C. B., and Lopes de Menezes, D. E. Pharmacokinetics of long circulating liposomes, Adv. Drug Del. Rev. *16:* 267-284, 1995.

282. Woodle, M. C., Matthay, K. K., Newman, M. S., Hidayat, J. E., Collins, L. R.,

Redemann, C., Martin, F. J., and Papahadjopoulos, D. Versatility in lipid compositions showing prolonged circulation with sterically stabilized liposomes, Biochim. Biophys. Acta. *1105:* 193-200, 1992.

283. Maruyama, K., Takizawa, T., Yuda, T., Kennel, S. J., Huang, L., and Iwatsuru, M. Targetability of novel immunoliposomes modified with amphipathic poly(ethylene glycol)s conjugated at their distal terminals to monoclonal antibodies, Biochim. Biophys. Acta. *1234:* 74-80, 1995.

284. Allen, T. M., Brandeis, E., Hansen, C. B., Kao, G. Y., and Zalipsky, S. A new strategy for attachment of antibodies to sterically stabilized liposomes resulting in efficient targeting to cancer cells, Biochim. Biophys. Acta. *1237:* 99-108, 1995.

285. Hughes, B. J., Kennel, S., Lee, R., and Huang, L. Monoclonal antibody targeting of liposomes to mouse lung *in vivo*, Cancer Res. *49:* 6214-6220, 1989.

286. Yuan, F., Leunig, M., Huang, S. K., Berk, D. A., Papahadjopoulos, D., and Jain, R. K. Microvascular permeability and interstitial penetration of sterically stabilized (stealth) liposomes in a human tumour xenograft, Cancer Res. *54:* 3352-3356, 1994.

287. de Rie, M. A., Schumacher, T. N., van Schijndel, G. M., van Lier, R. A., and Miedema, F. Regulatory role of CD19 molecules in B-cell activation and differentiation, Cell. Immunol. *118:* 368-381, 1989.

288. Uckun, F. M., Jaszcz, W., Ambrus, J. L., Fauci, A. S., Gajl-Peczalska, K., Song, S. W., Wick, M. R., Myers, D. E., Waddick, K., and Ledbetter, J. A. Detailed studies on expression and function of CD19 surface determinant by using B43

monoclonal antibody and the clinical potential of anti-CD19 immunotoxins, Blood. *71:* 13-29, 1988.

289. Ghetie, M. A., Picker, L. J., Richardson, J. A., Tucker, K., Uhr, J. W., and Vitetta, E. S. Anti-CD19 inhibits the growth of human B-cell tumour lines in vitro and of Daudi cells in SCID mice by inducing cell cycle arrest, Blood. *83:* 1329-1336, 1994.

290. Pizer, B. L. and Kemshead, J. T. The potential of targeted radiotherapy in the treatment of central nervous system leukemia, Leukemia Lymphoma. *15:* 281-289, 1994.

291. Vervoordeldonk, S. F., Merle, P. A., van Leeuwen, E. F., von dem Borne, A. E., and Slaper-Cortenbach, I. C. Preclinical studies with radiolabeled monoclonal antibodies for treatment of patients with B-cell malignancies, Cancer. *73:*1006-1011, 1994.

292. Stone, M. J., Sausville, E. A., Fay, J. W., Headlee, D., Collins, R. H., Figg, W. D., Stetler Stevenson, M., Jain, V., Jaffe, E. S., Solomon, D., Lush, R. M., Senderowicz, A., Ghetie, V., Schindler, J., Uhr, J. W., and Vitetta, E. S. A phase I study of bolus versus continuous infusion of the anti-CD19 immunotoxin, IgG-HD-37-dgA, in patients with B-cell lymphoma, Blood. *88:* 1188-1197, 1996.

293. Hekman, A., Honselaar, A., Vuist , W. M., Sein, J. J., Rodenhuis, S., Bokkel Huinink, W. W., Somers, R., Rumke, P., and Melief, C. J. Initial experience with treatment of human B cell lymphoma with anti-CD19 monoclonal antibody, Cancer Immunol. Immunother. *32:* 364-372, 1991.

294. Sommerman, E. F., Pritchard, P. H., and Cullis, P. R. ^{125}I labelled inulin: a convenient marker for deposition of liposomal contents *in vivo*, Biochem. Biophys. Res. Commun. *122:* 319-324, 1984.

295. Zola, H., Macardle, P. J., Bradford, T., Weedon, H., Yasui, H., and Kurosawa, Y. Preparation and characterization of a chimeric CD19 monoclonal antibody., Immunol. and Cell Biol. *69:* 411-422, 1991.

296. Derksen, J. T., Morselt, H. W., and Scherphof, G. L. Processing of different liposomal markers after *in vitro* uptake of immunoglobulin-coated liposomes by rat liver macrophages, Biochim. Biophys. Acta. *931:* 33-40, 1987.

297. Pool, G. L., French, M. E., Edwards, R. A., Huang, L., and Lumb, R. H. Use of radiolabelled hexadecyl cholesterol ether as a liposome marker, Lipids. *17:* 445-452, 1982.

298. Bartlett, G. R. Phosphorus assay in column chromatography, J. Biol. Chem. *234:* 466-468, 1959.

299. Mosmann, T. Rapid colorimetric assay for cellular growth and survival: application to proliferation and cytotoxicity assays, J. Immunol. Methods. *65:* 55-63, 1983.

300. Allen, T. M. Stealth liposomes: avoiding reticuloendothelial uptake, *In:* G. Lopez-Berestein and I. Fidler (eds) Liposomes in the Therapy of Infections Disease and Cancer Vol. 3, pp. 205-224. Boca Raton, FL: CRC Press, 1984.

301. Ishiwata, H., Vertut-Doi, A., Hirose, T., and Miyajima, K. Physical chemistry characteristics and biodistribution of poly(ethyleneglycol)-coated liposomes using poly(oxyethylene) cholesteryl ether, Chem. Pharm. Bull. *43:* 1005-1011, 1995.

302. Huang, C. and Mason, J. T. Geometric packing constraints in egg phosphatidylcholine vesicles, Proc. Natl. Acad. Sci. *75:* 308-310, 1978.

303. Blaurock, A. E. Evidence for bilayer structure and of membrane interactions from X-ray diffraction analysis, Biochim. Biophys. Acta. *650:* 167-207, 1982.

304. Kenworthy, A. K., Simon, S. A., and McIntosh, T. J. Structure and phase behaviour of lipid suspensions containing phospholipids with covalently attached poly(ethylene glycol), Biophys. J. *68:* 1903-1920, 1995.

305. Miyajima, K., Lee, T., and Nakagaki, M. Micelle formation of polyoxyethylene cholesteryl ether in water, Chem. Pharm. Bull. *32:* 3670-3673, 1984.

306. Moore, M. S., Mahaffey, D. T., Brodsky, F. M., and Anderson, R. G. Assembly of clathrin-coated pits onto purified plasma membranes, Science. *236:* 558-563, 1987.

307. Wolff, B. and Gregoriadis, G. The use of monoclonal anti-Thy1 IgG1 for the targeting of liposomes to AKR-A cells in vitro and in vivo, Biochim. Biophys. Acta. *802:* 259-273, 1984.

308. Tedder, T. F. and Isaacs, C. M. Isolation of cDNA encoding the CD19 antigen of human and mouse B lymphocytes. A new member of the immunoglobulin superfamily, J. Immunol. *143:* 712-717, 1989.

309. van Oosterhout, Y. V. J. M., van den Herik-Oudijk, I. E., Wessels, H. M. C., de Witte, T., van de Winkel, J. G. J., and Preijers, F. W. M. B. Effect of isotype on internalization and cytotoxicity of CD19-ricin A immunotoxins, Cancer Res. *54:* 3527-3532, 1994.

310. Press, O. W., Farr, A. G., Borroz, K. I., Andersen, S. K., and Martin, P. J. Endocytosis and degradation of monoclonal antibodies targeting human B-cell malignancies, Cancer Res. *49:* 4906-4912, 1989.

311. Allen, T. M., Hansen, C. B., and Guo, L. S. Subcutaneous administration of liposomes: a comparison with the intravenous and intraperitoneal routes of injection, Biochim. Biophys. Acta. *1150:* 9-16, 1993.

312. Goulet, A. C., Goldmacher, V. S., Lambert, J. M., Baron, C., Roy, D. C., and Kouassi, E. Conjugation of blocked ricin to an anti-CD19 monoclonal antibody increases antibody-induced cell calcium mobilization an CD19 internalization, Blood. *90:* 2364-2375, 1997.

313. Nicholson, I. C., Lenton, K. A., Little, D. J., DeCorso, T., Lee, F. T., Scott, A. M., Zola, H., and Hohmann, A. W. Construction and characterisation of a functional CD19 specific single chain Fv fragment for immunotherapy of B lineage leukemia and lymphoma, Mol. Immunol., *34:* 1157-1165, 1998.

314. Lambert, J. M., Goldmacher, V. S., Collinson, A. R., Nadler, L. M., and Blattler, W. A. An immunotoxin prepared with blocked ricin: a natural plant toxin adapted for therapeutic use, Cancer Res. *51:* 6236-6242, 1991.

315. Torchilin, V. P. and Papisov, M. I. Why do polyethylene glycol-coated liposomes circulate so long? molecular mechanism of liposome steric protection with polyethylene glycol: role of polymer chain flexibility, J. liposome Res. *4:* 725-739, 1994.

316. Pilarski, L. M., Mant, M. J., Reuther, B. A., and Belch, A. R. Severe deficiency of

B lymphocytes in peripheral blood from multiple myeloma patients, J. Clin. Invest. *74:* 1301-1305, 1984.

317. Sumizawa, T., Chuman, Y., Sakamoto, H., Iemura, K., Almquist, K., C., Deeley, R. G., Cole, S. P., and Akiyama, S. Non-P-glycoprotein-mediated multidrug resistant human KB cells selected in medium containing adriamycin, cepharantine and mezerein, Somatic Cell Molec. Genetics. *20:* 423-435, 1994.

318. Crommelin, D. J. A., Scherphof, G., and Storm, G. Active targeting with particulate carrier systems in the blood compartment, Adv. Drug Del. Rev. *17:* 49-60, 1995.

319. Allen, T. M. Stealth liposomes: avoiding reticuloendothelial uptake, *In:* G. Lopez-Berestein (ed.), Liposomes in the Therapy of Infectious Diseases and Cancer, Vol. 89, pp. 405-415. New York: Alan R. Liss, Inc., 1989.

320. Huang, S. K., Martin, F. J., Friend, D. S., and Papahadjopoulos, D. Mechanism of stealth liposome accumulation in some pathological tissues. *In:* D. Lasic and F. Martin (eds.), Stealth Liposomes, pp. 119-125. Boca Raton, Fla: CRC Press, 1995.

321. Mayer, L. D., Bally, M. B., Loughrey, H., Masin, D., and Cullis, P. R. Liposomal vincristine preparations which exhibit decreased drug toxicity and increased activity against murine L1210 and P388 tumours, Cancer Res. *50:* 575-9, 1990.

322. Allen, T. M., Hansen, C. B., and Zalipsky, S. Antibody-targeted Stealth® liposomes, *In:* D. Lasic and F. Martin (eds.), Stealth Liposomes, pp. 193-202. Boca Raton, FL: CRC Press, Inc., 1995.

323. Maruyama, K., Holmber, E., Kennel, S. J., Klibanov, A., Torchilin, V., and Huang, L. Characterization of in vivo immunoliposome targeting to pulmonary endothelium, J. Pharm. Sci. *79:* 978-984, 1990.

324. Nassander, U. K., Steerenberg, P. A., Poppe, H., Storm, G., Poels, L. G., de Jong, W. H., and Crommelin, D. J. A. In vivo targeting of OV-TL 3 immunoliposomes to ascitic ovarian carcinoma cells (OVCAR-3) in athymic nude mice, Cancer Res. *52:* 646-653, 1992.

325. Lang, J., Vigo-Pelfrey, C., and Martin, F. Liposomes composed of partially hydrogenated egg phosphatidylcholines: fatty acid composition, thermal phase behaviour and oxidative stability, Chem. Phys. Lipids. *53:* 91-101, 1990.

326. Andersen, A., Warren, D. J., and Slørdal, L. A sensitive and simple high-performance liquid chromatographic method for the determination of doxorubicin and its metabolite in plasma, Ther. Drug Monit. *15:* 455-461, 1993.

327. Zhang, Y., Sweet, K. M., Sognier, M. A., and Belli, J. A. An enhanced ability for transforming adriamycin into a noncytotoxic form in a multidrug-resistant cell line (LZ-8), Biochem. Pharmacol. *44:* 1869-1877, 1992.

328. Gabizon, A. A., Barenholz, Y., and Bialer, M. Prolongation of the circulation time of doxorubicin encapsulated in liposomes containing a polyethylene glycol-derivatized phospholipid: pharmacokinetic studies in rodents and dogs, Pharm. Res. *10:* 703-708, 1993.

329. Daleke, D. L., Hong, K., and Papahadjopoulos, D. Endocytosis of liposomes by macrophages: binding, acidification and leakage of liposomes monitored by a new

fluorescence assay, Biochim. Biophys. Acta. *1024:* 352-366, 1990.

330. Straubinger, R. M., Papahadjopoulos, D., and Hong, K. Endocytosis and intracellular fate of liposomes using pyranine as a probe, Biochem. *29:* 4929-4939, 1990.

331. Storm, G., van Bloois, L., Brouwer, M., and Crommelin, D. J. A. The interaction of cytostatic drugs with adsorbents in aqueous media. The potential implications for liposomes preparation, Biochim. Biophys. Acta. *818:* 343-351, 1985.

332. Amselem, S., Gabizon, A., and Barenholz, Y. Optimization and upscaling of doxorubicin-containing liposomes for clinical use., J. Pharm. Sci. *79:* 1045-1052, 1990.

333. Hoekstra, D., Babia, T., Zegers, M., Zaal, K., Arts, E. G. J. M., and Kok, J. W. Dynamic properties of membranes: application of fluorescent lipid analogs. *In:* M. C. Pedroso De Lima, N. Duzgunes, and D. Hoekstra (eds.), Trafficking of intracellular membranes: from molecular sorting to membrane fusion, Vol. 91. pp. 11-33. Berlin: Springer-Verlag, 1995.

334. Weinstein, J. N., Yoshikami, S., Henkart, P., Blumenthal, R., and Hagins, W. A. Liposome-cell interaction: transfer and intracellular release of trapped fluorescence marker, Science. *195:* 489-492, 1977.

335. Straubinger, R. M., Hong, K., Friend, D. S., and Papahadjopoulos, D. Endocytosis of liposomes and intracellular fate of encapsulated molecules: encounter with a low pH compartment after internalization in coated vesicles, Cell. *32:* 1069-1079, 1983.

336. Brown, V. I. and Greene, M. I. Molecular and cellular mechanisms of receptor-mediated endocytosis, DNA and Cell Biol. *10:* 399-409, 1991.

337. Mellman, I., Fuchs, R., and Helenius, A. Acidification of the endocytic and exocytic pathways, Annu. Rev. Biochem. *55:* 663-700, 1986.

338. Schmid, S. L., Fuchs, R. M., Male, P., and Mellman, I. Two distinct subpopulations of endosomes involved in membrane recycling and transport to lysosomes, Cell. *52:* 73-83, 1988.

339. Renschler, M. F., Wada, H. G., Fok, K. S., and Levy, R. B-lymphoma cells are activated by peptide ligands of the antigen binding site receptor or by anti-idiotypic antibody to induce extracellular acidification, Cancer Res. *55:* 5642-47, 1995.

340. Pastan, I. and Willingham, M. C. Endocytosis. *In:* I. Pastan and M. C. Willingham (eds.), Endocytosis, pp. 1-44. London, U.K.: Plenum Press, 1985.

341. Gianni, L., Corden, B., and Myers, C. The biochemical basis of anthracycline toxicity and antitumour action, Rev. Biochem. Toxicol. *5:* 1-82, 1983.

342. Suzuki, S., Watanabe, S., Uno, S., Tanaka, M., Masuko, T., and Hashimoto, Y. Endocytosis does not necessarily augment the cytotoxicity of adriamycin encapsulated in immunoliposomes, Biochim. Biophys. Acta. *1224:* 445-453, 1994.

343. Gigli, M., Doglia, S. M., Millot, J. M., Valentini, L., and Manfait, M. Quantitative study of doxorubicin in living cell nuclei by microspectrofluorometry, Biochim. Biophys. Acta. *950:* 13-20, 1988.

344. Arndt-Jovin, D. J. and Jovin, T. M. Fluorescent labeling and microscopy of DNA, Meth. Cell Biol. *30:* 417-448, 1989.

345. Lloyd, J. B. Metabolic efflux and influx across the lysosome membrane, *In:* J.B. Lloyd and F. Mason (eds.), Subcellular Biology: Biology of the Lysosome,Vol. 27, pp. 361-386. N.Y.: Plenum Press, 1996.

346. Yoshimura, T., Shono, M., Imai, K., and Hong, K. Kinetic analysis of endocytosis and intracellular fate of liposomes in single macrophages, J. Biochem. *117:* 34-41, 1995.

347. Lee, R. J. and Low, P. S. Folate-targeted liposomes for drug delivery, J. Liposome Res. *7:* 455-466, 1997.

348. Duzgunes, N., Straubinger, R. M., Baldwin, P. A., Friend, D. S., and Papahadjopoulos, D. Proton-induced fusion of oleic acid-phosphatidylethanolamine liposomes, Biochemistry. *24:* 3091-3098, 1985.

349. Carson, D. A. and Ribeiro, J. M. Apoptosis and disease, Lancet. *341:* 1251-1254, 1993.

350. Forssen, E. A., Male-Brune, R., Adler-Moore, J. P., Lee, M. J. A., Schmidt, P. G., Kraieva, T. B., Shimizu, S., and Tromberg, B. J. Fluorescence imaging studies for the disposition of daunorubicin liposomes (DaunoXome) in tumour tissue, Cancer Res. *56:* 2066-2075, 1996.

351. Hoekstra, D. and Scherphof, G. Effect of fetal calf serum and serum protein fractions on the uptake of liposomal phosphatidylcholine by rat hepatocytes in primary monolayer culture, Biochim. Biophys. Acta. *551:* 109-121, 1979.

352. Vingerhoeds, M. H., Steerenberg, P. A., Hendriks, J. J. G. W., Kekker, L. C., van Hoesel, Q. G. C. M., Crommelin, D. J. A., and Storm, G. Immunoliposome-

mediated targeting of doxorubicin to human ovarian carcinoma *in vitro* and *in vivo*, Br. J. Cancer. *74:* 1023-1029, 1996.

353. Coleman, A. W., Maguire, M. J., and Coleman, J. R. Mithramycin and 4,6-diamidino-2-phenylindole (DAPI)-DNA staining for fluorescence microspectrophotometric measurement of DNA nuclei, plastids and virus particles, J. Histochem. Cytochem. *29:* 959-968, 1981.

354. Hedley, D. W., Friedlander, M. L., and Taylor, i. W. Application of DNA flow cytometry to paraffin-embedded archival material for the study of aneuploidy and its clinical significance, Cytometry. *6:* 327-333, 1985.

355. Scherphof, G. L. *In vivo* behaviour of liposomes: Interactions with the mononuclear phagocyte system and implications for drug targeting, *In:* R.L. Juliano (ed.) Handbook of Experimental Pharmacology: Targeted Drug Delivery, Vol. 100, pp. 285-310, 1991.

356. Bruggemann, M., Williams, G. T., Bindon, C. I.,. Comparison of the effector functions of human immunoglobulins using a matched set of chimeric antibodies, J. Exp. Med. *166:* 127-142, 1987.

357. Steplewski, Z., Sun, L. K., Shearman, C. W., Ghrayeb, J., Daddona, P., and Koprowski, H. Biological activity of human-mouse IgG1, IgG2, IgG3 and IgG4 chimeric monoclonal antibodies with antitumour specificity, Proc. Natl. Acad. Sci. *85:* 4852-4856, 1988.

358. Custer, R. P., Bosma, G. C., and Bosma, M. J. Severe combined immunodeficiency (SCID) in the mouse: pathology, reconstitution, neoplasms,

Am. J. Pathol. *120:* 464-471, 1985.

359. Dorshkind, K., Keller, G. M., Phillips, R. A., Miller, R. G., Bosma, G. C., O'Toole, O., and Bosma, M. J. Functional status of cells from lymphoid and myeloid tissues in mice with severe combined immunodeficiency disease, J. Immunol. *132:* 1804-1808, 1984.

360. Gottesman, M. M. How cancer cells evade chemotherapy, Cancer Res. *53:* 747-754, 1993.

361. Lee, R. J. and Low, P. S. Delivery of liposomes into cultured KB cells via folate receptor-mediated endocytosis, J. Biol. Chem. *269:* 3198-3204, 1994.

362. Bergsagel, D. E. Treatment of plasma cell myeloma, Ann. Rev. Med. *30:* 431-433, 1979.

363. Vitetta, E. S., Stone, E., Amlot, P., Fay, J., May, R., Till, M., Newman, J., Clark, P., Collins, R., Cunningham, D., Ghetie, V., Uhr, J. W., and Thorpe, P. E. Phase I immunotoxin trial in patients with B-cell lymphoma, Cancer Res. *51:* 4052-4058, 1991.

364. Gabizon, A., Lossos, A., and Siegal, T. Selective tumour accumulation of doxorubicin encapsulated in long-circulating liposomes on brain and lung murine tumours, Proc. Am. Assoc. Cancer Res. *34:* 365, 1993.

365. Folkman, J. Angiogenesis in cancer, vascular, rheumatoid and other disease, Nature Med. *1:* 27-31, 1995.

366. Vingerhoeds, M. H., Haisma, H. J., Belliot, S. O., Smit, R. H. P., Crommelin, D. J. A., and Storm, G. Immunoliposomes as enzyme carriers (immuno enzymosomes)

for antibody directed enzyme prodrug therapy (ADEPT): optimization of prodrug activating capacity, Pharmaceut. Res. *13:* 604-610, 1996.

367. Huang, A., Kennel, S. J., and Huang, L. Interactions of immunoliposomes with target cells, J. Biol. Chem. *258:* 14034-14040, 1983.

368. Aragnol, D., Malissen, B., Schiff, C., Piron, M.-A., and Leserman, L. Endocytosis of MHC molecules by B cell-B lymphoma and B-cell T lymphoma hybrids, J. Immunol. *137:* 3347-3353, 1986.

369. Kirpotin, D., Hong, K., Mullah, N., Papahadjopoulos, D., and Zalipsky, S. Liposomes with detachable polymer coating: destabilization and fusion of dioleoylphosphatidylethanolamine vesicles triggered by cleavage of surface-grafted poly(ethylene glycol), FEBS Lett. *388:* 115-118, 1996.

370. Thompson, D. H., Gerasimov, O. V., Wheeler, J. J., Rui, Y. J., and Anderson, V. C. Triggerable plasmalogen liposomes: improvement of system efficiency, Biochim. Biophys. Acta. *1279:* 25-34, 1996.

371. Maruyama, K., Takizawa, T., Takahashi, N., Tagawa, T., Nagaike, K., and Iwatsuru, M. Factors influencing longevity and target binding of PEG-immunoliposomes conjugated antibodies at PEG's terminals, J. Liposome Res. *6:* 206-207, 1996.

372. Aragnol, D. and Leserman, L. Immune clearance of liposomes inhibited by an anti-Fc receptor antibody in vivo, Proc. Natl. Acad. Sci. USA. *83:* 2699-2703, 1986.

373. Debs, R. J., Heath, T. D., and Papahadjopoulos, D. Targeting of anti-Thy 1.1

monoclonal antibody conjugated liposomes in Thy 1.1 mice after intravenous administration, Biochim. Biophys. Acta. *901:* 183-190, 1987.

374. Phillips, N. C. and Emili, A. Immunogenicity of immunoliposomes, Immunol. Lett. *30:* 291-296, 1991.

375. Pietersz, G. A., Wenjun, L., Sutton, V. R., Burgess, J., McKensie, I. F. C., Zola, H., and Trapani, J. A. *In vitro* and *in vivo* antitumor activity of a chimeric anti-CD19 antibody, Cancer immunol. Immunother. *41:* 53-60, *1995*.

376. Nassander, U. K., Steerenberg, P. A., De Jong, W. H., Van Overveld , W. O., Te Boekhorst , C. M., Poels, L. G., Jap, P. H., and Storm, G. Design of immunoliposomes directed against human ovarian carcinoma, Biochim. Biophys. Acta. *1235:* 126-139, 1995.

377. Flavell, D. J., Noss, A., Pulford, K. A. F., Ling, N., and Flavell, S. U. Systemic therapy with 3BIT, a triple combination cocktail of anti-CD19, -CD22, and -CD38-saponin immunotoxins, is curative of human B-cell lymphoma in severe combined immunodeficient mice., Cancer Res. *57:* 4824-4829, 1997.

378. Torchilin, V. P. Targeting of drugs and drug carriers within the cardiovascular system, Adv. Drug Del. Rev. *17:* 75-101, 1995.